

ISSN 1681-9004 (Print)
ISSN 2500-302X (Online)

Russian Academy of Sciences
Ural Branch
A.N. Zavaritsky Institute of Geology and Geochemistry

LITHOSPHERE (RUSSIA)

Volume 18 No. 5A 2018 September–October

Founded in 2001
Issued 6 times a year

Lithosphere (Russia), 2018. Volume 18, No. 5A

Scientific journal. Issued 6 times a year
Founded in 2001

Founder: Federal State Budgetary Scientific Institution A.N. Zavaritsky Institute of Geology and Geochemistry, Ural Branch of Russian Academy of Sciences (IGG, UB of RAS)

The journal aims to develop scientific knowledge in the field of a wide range of problems of the solid Earth: the structure and dynamics of the development of the lithosphere in space and time; processes of sedimentation, lithogenesis, magmatism, metamorphism, mineral genesis and ore formation; creation of effective methods for prospecting and exploration of minerals; geophysical features of the Earth; development of modern technologies for researching and monitoring the state of the environment, forecasting and preventing natural and technogenic catastrophic phenomena; development of geoanalytical techniques

Editors-in-chief **Viktor A. Koroteev, Sergei L. Votyakov**

Deputy Editor-in-chief **Valerii V. Murzin**

Secretary **Gunar A. Mizens**

IGG, UB of RAS, Ekaterinburg, Russia

Editorial board: Valerii P. Alekseev (Ural State Mining University, Ekaterinburg, Russia); Anna I. Antoshkina (Institute of Geology, Komi SC UB of RAS, Syktyvkar, Russia); Vsevolod N. Anfilogov (Institute of Mineralogy, UB of RAS, Miass, Russia); Tamara B. Bayanova (Geological Institute, Kola SC RAS, Apatity, Russia); Fernando Bea (University of Granada, Spain); Nikolai S. Bortnikov (Institute of Geology of Ore Deposits, Petrography, Mineralogy and Geochemistry, RAS, Moscow, Russia); Valerii A. Vernikovskii (Institute of Oil Geology and Geophysics, SB of RAS, Novosibirsk, Russia); Giorgio Garuti (University of Leoben, Austria); Vladimir Davydov (Permian Research Institute, Boise State University, Department of Geosciences, Boise, ID, USA); Reimar Seltmann (Natural History Museum, London, Great Britain); Efim S. Kontar' (Ural State Mining University, Ekaterinburg, Russia); Vladimir Kutcherov (Royal Institute of Technology, Department of Energy, Stockholm, Sweden); Mikhail G. Leonov (Geological Institute, RAS, Moscow, Russia); Petr S. Martyshko (Institute of Geophysics, UB of RAS, Ekaterinburg, Russia); Valerii V. Maslennikov (Institute of Mineralogy, UB of RAS, Miass, Russia); Andrei V. Maslov (IGG, UB of RAS, Ekaterinburg, Russia); Fancang Meng (Institute of Geology, Chinese Academy of Geologic Sciences, China); Viktor M. Necheukhin (IGG, UB of RAS, Ekaterinburg, Russia); Viktor N. Puchkov (IGG, UB of RAS, Ekaterinburg, Russia); Sergei D. Sokolov (Geological Institute, RAS, Moscow, Russia); Rafael H. Sungatullin (Kazan Federal University, Institute of Geology and Petroleum Technologies, Kazan, Russia); Valerii N. Udachin (Institute of Mineralogy, UB of RAS, Miass, Russia); Richard Herrington (Natural History Museum, London, Great Britain); Il'ya I. Chaikovskii (Mining Institute, UB of RAS, Perm, Russia); Richard Ernst (Department of Earth Sciences, Carleton University, Ottawa, Canada); Viktor L. Yakovlev (Mining Institute, UB of RAS, Ekaterinburg, Russia)

Editorial council: Albert V. Zubkov (Mining Institute, UB of RAS, Ekaterinburg, Russia); Kirill S. Ivanov (IGG, UB of RAS, Ekaterinburg, Russia); Sergei N. Kashubin (All-Russian Geological Institute, St.Petersburg, Russia); Sergei V. Kornilkov (Mining Institute, UB of RAS, Ekaterinburg, Russia); Artur A. Krasnobaev (IGG, UB of RAS, Ekaterinburg, Russia); Kreshimir N. Malitch (IGG, UB of RAS, Ekaterinburg, Russia); Vitalii N. Ogorodnikov (Ural State Mining University, Ekaterinburg, Russia); Evgenii V. Pushkarev (IGG, UB of RAS, Ekaterinburg, Russia); Aleksandr G. Talalai (Ural State Mining University, Ekaterinburg, Russia); Vladimir V. Holodnov (IGG, UB of RAS, Ekaterinburg, Russia); Valerii V. Chernykh (IGG, UB of RAS, Ekaterinburg, Russia)

Editorial address: 15 Akad. Vonsovsky St., Zavaritsky Institute of Geology and Geochemistry, Ekaterinburg 620016, Russia
Tel. (343) 287-90-45, Tel./fax (343) 287-90-12

E-mail: lithosphere@igg.uran.ru

Website: <http://lithosphere.ru>

© Institute of Geology and Geochemistry

© Authors of articles

Contents

Volume 18, No. 5A, 2018

SPECIAL ISSUE

MAGMATISM AND MANTLE-CRUST INTERACTION IN THE GEOLOGICAL HISTORY OF EARTH

Devoted to G. B. Fershtater

Foreword	4
Early evolution of Earth and beginning of its geological history: how and when granitoid magmas appeared <i>M. I. Kuzmin, V. V. Yarmolyuk, A. B. Kotov</i>	5
Murzinka massif in the Middle Urals as an example of an interformational granite pluton: magmatic sources, geochemical zonation, peculiarities of formation <i>G. B. Fershtater, N. S. Borodina</i>	20
Plume-related granite-rhyolite magmatism <i>V. N. Puchkov</i>	37
Ancient age of zircons and issues associated with the genesis of dunites from gabbro-ultrabasite complexes of orogenic areas and central-type platform massifs <i>V. N. Anfilogov, A. A. Krasnobaev, V. M. Ryzhkov</i>	48
Xenocrysts and megacrysts of alkaline olivine-basalt-basanite-nephelinite association Makhtesh Ramon (Israel): interaction with carrier magmas and crystallographic transformations <i>Z. Yudalevich, Ye. Vapnik</i>	57
Geo-petrological model for the formation of diamond-bearing fluid-explosive breccia structures (ural type) <i>L. N. Sharpenok, L. I. Lukianova, O. V. Petrov</i>	78
U-Pb dating of niobium minerals from the pyrochlore group (Ilmeny-Vishnevogorsky carbonatite-miaskite complex, South Urals) <i>I. L. Nedosekova, V. A. Koroteev, B. V. Belyatsky, V. V. Sharygin, E. N. Lepechina, S. V. Pribavkin</i>	90

Subscription

The current and preceding issues of the Journal can be ordered at
15 Akad. Vonsovsky St., A.N. Zavaritsky Institute of Geology and Geochemistry, Ekaterinburg 620016, Russia.
Tel.: (343) 287-90-45, Tel./fax: (343) 287-90-12. E-mail: lithosphere@igg.uran.ru

FOREWORD

This special issue of the journal covers the problems of magmatic petrology, concerning the processes of mantle-crust interaction in the geological history of Earth. Various issues pertaining to the nature and conditions of magma generation, the evolution and interaction of melts associated with mantle and crustal sources remain among the most important topics of modern geology and continue to attract the interest of leading specialists in petrology. It is the interaction between the earth's mantle and crust at different stages in the geological evolution of the planet under various geotectonic conditions that determined the nature and composition of the lithosphere itself, its structure and the patterns of distribution of various magmatic formations and related minerals, including strategic ones.

The present issue includes articles examining problems associated with magma formation under crustal conditions. It opens with an article by M.I. Kuzmin et al., which analyses the causes, nature and time of the emergence of the first granitoid melts, as well as the evolution of granite formation in the history of Earth – the phenomenon that determines its fundamental difference from the other planets of the Solar system. The article by V.N. Puchkov covers the formation of silicic igneous rocks (granites and rhyolites) constituting derivatives of various types of plumes: large igneous provinces (LIPs) and silicic LIPs (SLIPs); as well as their relationship with the type of crust and the role of continental crust melting in the formation of plume-related granite-rhyolite magmatism. Drawing on detailed petrological and geochemical studies of the Murzinka interformational granite pluton in the Urals, G.B. Fershtater and N.S. Borodina trace the changes in the composition of granite rocks derived from the anatectic melting of the sialic crust of different compositions and ages, formed during a single tectonic-magmatic stage in the Late Paleozoic. Using the example of upper mantle, lower and upper crustal xenoliths from the rocks of an Early Cretaceous olivine-basalt-basanite-nephelinite association (Makhtesh Ramon, Izrael), Z. Yudalevich and E. Vapnik consider the interaction of magmatic melt with various xenoliths, as well as their reaction products. The article by L.N. Sharpenok et al. covers diamond-bearing fluid-explosive breccias. The authors give petrographic and mineralogical characteristics of the clastic, protomagmatic and newly formed fluideo-

genic material; characterise the intrusion sequence of rock varieties and the differences in diamond content associated with it; as well as propose the assessment criteria for the diamond potential of newly identified fluid-bearing breccia formations. The issues associated with the genesis of dunites from gabbro-ultrabasite complexes of orogenic areas and central-type platform massifs, the aspects of formation and interpretation of the age of zircon contained in them are solved by the team of authors (V.N. Anfilogov, A.A. Krasnobaev, V.M. Ryzhkov) drawing on the experimental study of phase equilibrium in the system MgO-SiO₂-ZrO₂. I.L. Nedosekova and her colleagues present new data on the age of pyrochlore group minerals from the rare-metal deposits of the Ilmeny-Vishnevogorsky complex (South Urals) indicating the multi-stage formation of rare-metal niobium mineralisation. The early stage in mineralisation is associated with the concluding stages in the crystallisation of alkaline-carbonatite magmatic system (D₃), whereas the late ore-forming stages are associated with the remobilisation and redeposition of rare-metal substance during the post-collisional evolution of carbonatite complexes (T₃).

The idea of this special issue belongs to German Borisovich Fershtater – the initiator of holding the scientific conference ‘Granites and Earth evolution: mantle and crust in granite formation’ in Ekaterinburg, in 2017. German Fershtater always considered the Urals to be a standard example of epioceanic orogens, an orogenic belt of mafic type, which is a natural testing ground for studying the mechanisms underlying mantle-crust interaction. The range of his scientific interests went far beyond granite petrology: they included all the most important types of Ural igneous rocks, which served as the basis for creating a special volume of the journal. It so happened, that having begun working on the issue, German Fershtater, who was full of new research ideas and plans, suddenly died. He was a remarkable person; bright and talented scientist; kind, sympathetic, considerate and principled colleague; as well as a friend and a mentor. On the 30th of September 2018 German Borisovich Fershtater – Doctor in Geology and Mineralogy, Professor, Honored Worker of Science, a leading petrologist of the Urals, a scientist known all over the world – would have turned 85 years old.

This issue is devoted to his blessed memory.

T.A. Osipova

EARLY EVOLUTION OF EARTH AND BEGINNING OF ITS GEOLOGICAL HISTORY: HOW AND WHEN GRANITOID MAGMAS APPEARED

Mikhail I. Kuzmin¹, Vladimir V. Yarmolyuk², Alexander B. Kotov³

¹*Institute of Geochemistry SB RAS, 1A Favorsky St., Irkutsk 664033, Russia, e-mail: mikuzmin@igc.irk.ru*

²*Institute of Geology of Ore Deposits, Petrography, Mineralogy and Geochemistry (IGEM RAS),
35 Staromonetny lane, Moscow 119017, Russia*

³*Institute of Precambrian Geology and Geochronology, Russian Academy of Sciences (IGGD RAS),
2 Makarova quay, St.Petersburg 199034, Russia*

Received 17.11.2017, accepted 11.01.2018

Earth has a number of differences from the planets of the Solar System, as well as other stellar-planetary systems, which were acquired during its formation and geological history. The early *Chaotian* aeon was marked by Earth's accretion, the differentiation of its primary material into a mantle and a core, as well as the by formation of its satellite (Moon). Earth's geological history began 4500 million years ago in the Hadean aeon. At that time, the endogenous processes on Earth were largely controlled by meteorite and asteroid bombardments, which caused large-scale melting and differentiation of its upper layers. In magmatic chambers, differentiation proceeded until the appearance of granitoid melts. The Hadean continental crust was almost completely destroyed by meteorite bombardments, with the last heavy bombardment occurring at the end of the Hadean aeon (4000–3900 Ma). Conclusions about the geological situation of this aeon can be drawn only from the preserved Hadean zircons. In particular, their geochemical features indicate that Earth had an atmosphere. The Hadean aeon was replaced by the Archaean one, starting from which the processes of self-organisation were predominant on Earth. At that time, a crust composed of komatiite-basalt and tonalite-trondhjemite-granodiorite (TTG) rock series was forming. Its formation was driven by sagduction processes – vertical growth of the crust over rising mantle plumes. Thus, the lower basaltic crust subsided into the mantle, eclogitised and melted, which led to the appearance of sodium TTG rocks series. At the end of the Archaean aeon (3.1–3.0 Ga), lid tectonics, which determined the structure and development of the Archaean crust, was replaced by small-plate tectonics that later evolved into modern plate tectonics combined with mantle plume tectonics.

Keywords: *Chaotian and Hadean aeons, Archaean period, lid tectonics, plume tectonics, sagduction, mantle convection*

INTRODUCTION

Earth is different from other terrestrial planets of the Solar System. What is more, it has no analogues among the planets of 600 stellar-planetary systems that have been discovered in recent decades. It is not a coincidence that the authors of the article “Born from the chaos” [S. Batygin et al., 2016] called Earth a black sheep. An outstanding geologist K. Condi identified a number of characteristics inherent to Earth [Condie, 2011], which allowed it to become the cradle of humankind. The characteristic features of our planet, including its size and mass, a near-circular orbit, existence of a satellite (Moon), were acquired during the birth of the Solar System and then during the Chaotian aeon [Goldblatt et al., 2010]. Earth acquired its other important characteristics, such as the division of Earth's interior into a number of layers, during its subsequent history. The above-mentioned layers include the continental crust containing a significant amount of granitoids, as well as the atmosphere and hydrosphere. The first granites on Earth appeared in the Hadean aeon, while granitoids, well-preserved to our days, were already fairly widespread in the Archaean aeon. The Earth's birth, its formation as a planet, as well as possible mechanisms for the development of the first granitoid rocks in the

Hadean and Archaean aeons will be discussed in this work.

Knowing when the tectonics of lithospheric plates got started is of great importance for understanding the geological history of our planet. The mechanisms of endogenous processes stipulated by this theory are well studied. They describe the formation of basic geological structures, such as continents, oceans, orogens. Not coincidentally, in 2008 following a corresponding conference the Geological Society of America published a special issue, which contained articles by a number of prominent geologists covering the onset of plate tectonics on Earth. In his article published in this issue K. Condi writes: “It is unlikely that plate tectonics began on Earth as a single global ‘event’ at a distinct time, but rather it is probable that it began locally and progressively became more widespread from the early to the late Archaean”. However, even today, such well-known Japanese geologists as S. Maruyama and his colleague [Maruyama, Ebisuzaki, 2017], establish the exact start date of plate tectonics (4.37–4.20 Ga) when proposing a new model of the Earth's formation (ABEL). Similar start dates of the plate tectonics on Earth are proposed in the works of other geologists. In the same issue published by the Geological Society of America, R. Stern wrote more cautiously and prudent-

ly about the significance of the early tectonic style on Earth saying that we will not be able to understand the current system until we know when the current tectonic style began and what preceded it [Stern, 2008].

ORIGIN OF THE SOLAR SYSTEM AND EARLY STAGES OF ITS EVOLUTION

The solar system originated 4568 million years ago in a massive dust and gas cloud. The reason for the formation of this protosolar nebula, which must have included a large variety of chemical elements along with various short- and long-lived isotopes, is of the essence here. This cloud (nebula) could have originated from the explosion of a supernova in the vicinity of the future Solar System. Due to nuclear reactions, the explosion of a massive star brought about the synthesis (nucleosynthesis) and, naturally, the appearance of various elements, in particular, radioactive isotopes. This explosion could have induced the condensation of interstellar matter resulting from gravitational compression. Short-lived isotopes and their decay products help to identify a number of fea-

tures associated the formation of the Solar System and Earth in particular.

The calculations of astronomers and planetary scientists show that a star (proto-Sun) appeared in the centre of the nebula under the influence of gravity in less than 100 thousand years. The proto-Sun was surrounded by a wide disk of gas and dust – a protoplanetary disk [Lin, 2008], which served as the building material for the planets of the Solar System. When moving, particles of dust and gas collided and slowed down, with many of them spiralling onto the proto-Star. Upon collision, solid particles heated, whereas water and other volatiles having a low boiling point evaporated. This resulted in a natural boundary between the areas of the protoplanetary disk, with the predominance of solid particles in one part and volatiles in the other. This boundary (a region between the orbits of Mars and Jupiter) is referred to as the snow line, dividing the Solar System into the inner region, where the terrestrial planets were formed, and the outer one, where the gas giant planets were located [Batygin et al., 2016]. This separation occurred 2 million years after the onset of the Solar System formation (Fig. 1).

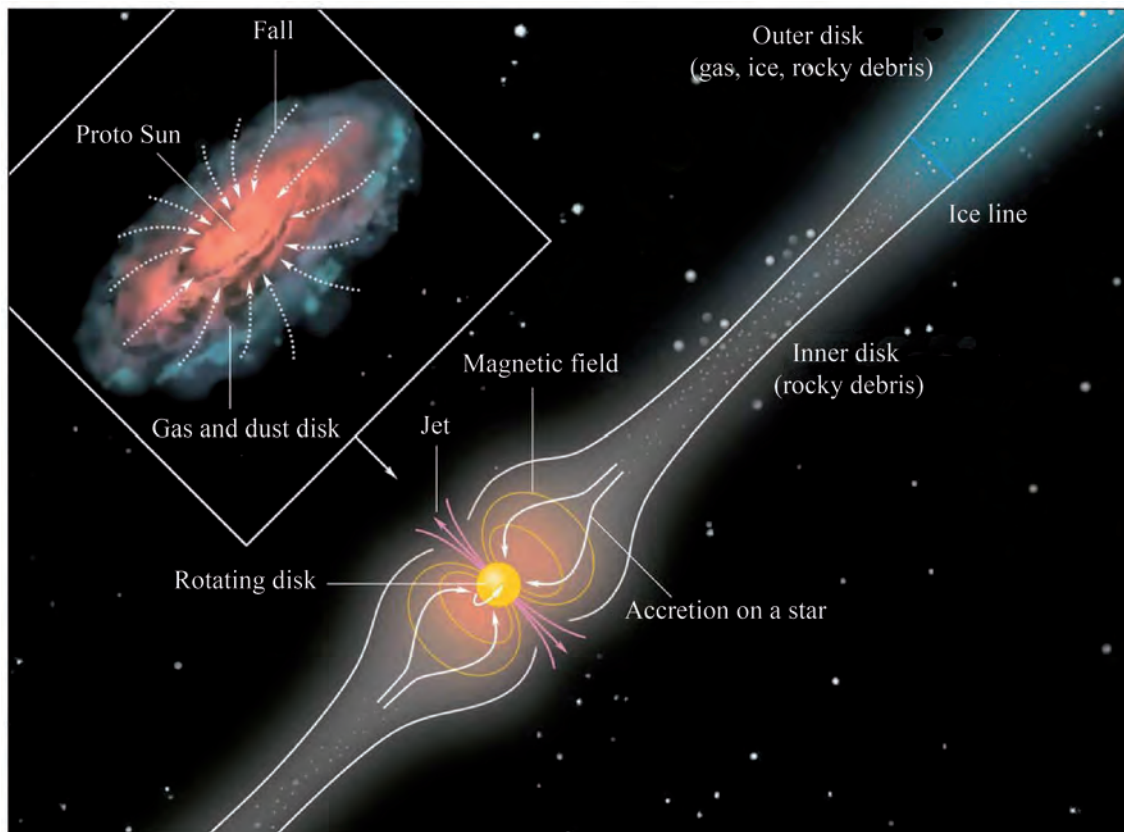


Fig. 1. Initial stage of the Solar System's evolution 4568 Ma ago [Batygin et al., 2016].

The beginning of the Chaotian aeon of the Solar System; birth of the proto-Sun; formation of the internal area consisting of stony fragments; snow lines – internal border of the external gas-ice region, where giant planets Saturn and Jupiter were formed 2 million years after the birth of the Solar System.

Thus, in the first 2 million years of the Solar System's history, numerous planetary embryos (planetesimals), as well as giant planets beyond the snow line (Jupiter and Saturn) were formed. In this respect, the Solar System is very different from other planetary systems, where similar giants are located much closer to the sun. According to K. Batygin and his colleagues [2016], such features of the Solar System are products of its youth, which included more drama and chaos. The complex interaction of giant peripheral planets constituted an important part of the primary chaos. For the first time, this was noted in the computer model of F. Masset and M. Snellgrove [Masset, Snellgrove, 2001], who described the simultaneous evolution of Saturn's and Jupiter's orbits in the protoplanetary disk. These studies showed that due to inward migration, the giant planets acquired a certain mutual configuration, due to which they were able to influence the protoplanetary disk. The established balance of forces (gravity, angular momentum, the gravitational influence of the outer belt of comets, etc.) changed the motion of both planets.

Developing these ideas, K. Batygin and his colleagues [2016] demonstrated that a change in the motion direction of the giant planets (tacking) mainly resulted in the attack of Jupiter and Saturn on the 'population' of the primary inner planets of the Solar System, i.e. terrestrial planets. Even when migrating towards the Sun, the giants affected the motion of small bodies, which shattering in collisions formed swarms of debris. The mass of debris that could fall on the Sun over hundreds of thousands of years is comparable to any super-Earth (planet exceeding the Earth in mass). As the former super-Earths were driven into the Sun, they had to leave behind a gap in a protoplanetary nebula. It is assumed that, before changing the tack, Jupiter migrated towards the Sun to the current position of Mars. In doing so, Jupiter pushed accumulations of ice, evidently along with solid material, having a mass of more than 10 Earth's masses towards the inner region of the Solar System, thus enriching it with water and other volatile substances. The proto-planets forwarded to the inner parts of the Solar System changed the orbital angular momentum of both Jupiter and Saturn, which resulted in their outward migration. The building material brought by the giant planets ensured a fairly large mass of Earth and Venus.

Gradually, the migrating planets stabilised their orbits, which was facilitated by their interaction with other giant planets (Neptune and Uranus), as well as the outer Kuiper Belt. It is assumed that the stabilisation of their orbits resulted in sending another swarm of debris into the inner region of the Solar System, thus causing powerful asteroid bombardments of the inner planets. The asteroid bombardments left their mark in the form of craters on the surface of the Moon, Mercury and Mars, whereas on Earth they led to the almost complete destruction of the Hadean continental crust – the

first crust in the geological history of our planet. Approximately 3.9 billion years ago, the giant planets settled down. Thus, the Solar System acquired its current structure [Batygin et al., 2016].

Astronomers distinguish a chaotic period in the Solar System's development (beginning of Earth's formation to 4.0–3.9 billion years). In the geological literature, this period is divided into two aeons: Chaotian (4568–4500 Ma) and Hadean (4500–4000 / 3900 Ma) [Goldblatt et al., 2010].

EARLY STAGES OF EARTH'S FORMATION AND EVOLUTION

Chaotian Eon (4568–4500 Ma)

The accretion of Earth took place in this period. As little as 11 million years after the onset of its formation, Earth acquired 63% of its current mass, in 30 million years amounting to 93% [Wood, 2011]. During this period, accreted Earth underwent differentiation into a liquid iron-nickel core and a silicate mantle, accompanied by the formation of the Earth's satellite (Moon) resulting from the collision of a large space body with proto-Earth.

Data on the composition of the protosolar nebula, from which the Sun and the planets of the Solar System were formed, are of great importance for calculating the composition of the Earth's layers. It has been established that the composition of the Sun is similar to that of the nebula from which this whole system originated [Kuzmin, 2014]. Carbonaceous chondrites correspond to this composition. With the exception of hydrogen and helium, they have the same composition as the Sun, which can be observed from the diagram (Fig. 2) comparing the relative abundances of elements on the Sun's surface and in carbonaceous chondrites [Wood, 2011]. The composition of carbonaceous chondrites differs from that of the Sun in the content of lithium that is destroyed by thermonuclear reactions in the Sun. In addition, meteorites are characterised by reduced content of three volatile components – N, C, O. This is quite understandable, as in the initial period of the Solar System's formation (first 2 million years) these gases were driven into its outer part, where they were used, among other things, to form gas giant planets. As can be seen from this diagram, Fe, O, Mg, Si and Ni account for 95% of the Solar System's mass (that is not H and He) and, naturally, the terrestrial planets, with 9 more elements – Cu, Al, S, Cr, Ni, Mn, P, Ti and Co – bringing the total to over 99% [Lauretta, 2011].

Considering the geochemical properties of the elements, as well as the composition of the Earth's silicate mantle, data on the composition of the material (carbonaceous chondrites) from which Earth was formed allows us to estimate the composition of Earth's core [Allègre et al., 1995; McDonough, Sun, 1995]. In this

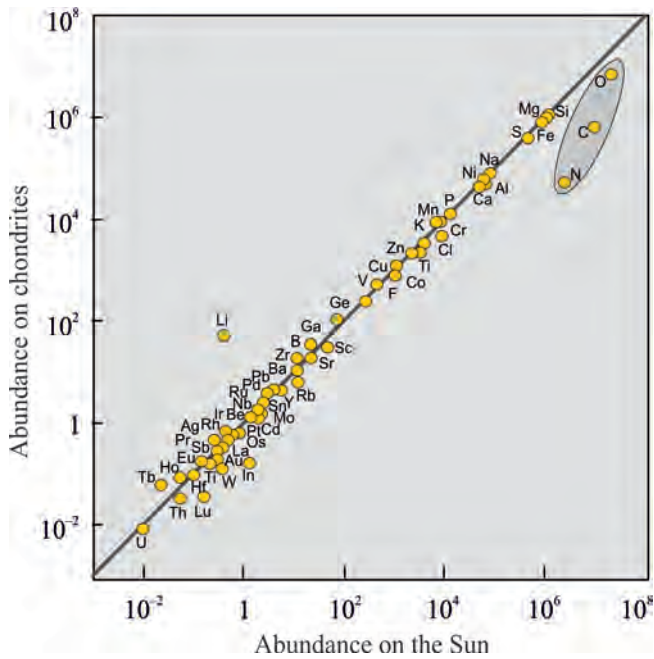


Fig. 2. Comparison of elemental abundances in carbonaceous chondrites (CI) and on the Sun's surface according to [Wood, 2011].

The general content of the petrogenic and rare elements in the Sun and carbonaceous meteorites (CI) is the same with the exception of Li which is destroyed on the Sun in the course of nuclear reactions. The content of volatile components (N, C, O) in meteorites is less than in the Sun, since in the first 1–2 Ma most of these volatile elements were involved in the formation of gas giant planets in the outer part of the Solar System.

connection, knowing the properties of individual elements in terms of their affinity with iron, silicate and volatile elements is of great importance [Allègre et al., 1995; Kuzmin, 2014]. According to the analysis, silicate Earth (i.e. mantle) contains the same amount of refractory lithophile elements (Zr, Al, Sc, rare-earth elements, Ti, Ca, Mg) as carbonaceous chondrites, whereas the content of siderophile elements in the mantle is low as compared to chondrites, as they accumulate in the core. Silicate Earth has the lowest content of highly-siderophile elements (Pd, Pt, Re, Os, etc.), whose concentration is maximum in the core. However, judging by the mantle xenoliths found in kimberlites, a slightly higher content of these elements in the mantle is occasionally observed, which may have been caused by the meteorite shower that hit the Earth after most of the core had already been formed [Wood, Halliday, 2010].

The time of the Earth's core formation can be estimated using the data on the distribution of products of short-lived isotope systems (Fig. 3), whose parent and daughter isotopes could have different geochemical properties, in the silicate layer of Earth. As a result, they behaved differently in the course of the Earth's differentiation into layers. In this respect, the most interest-

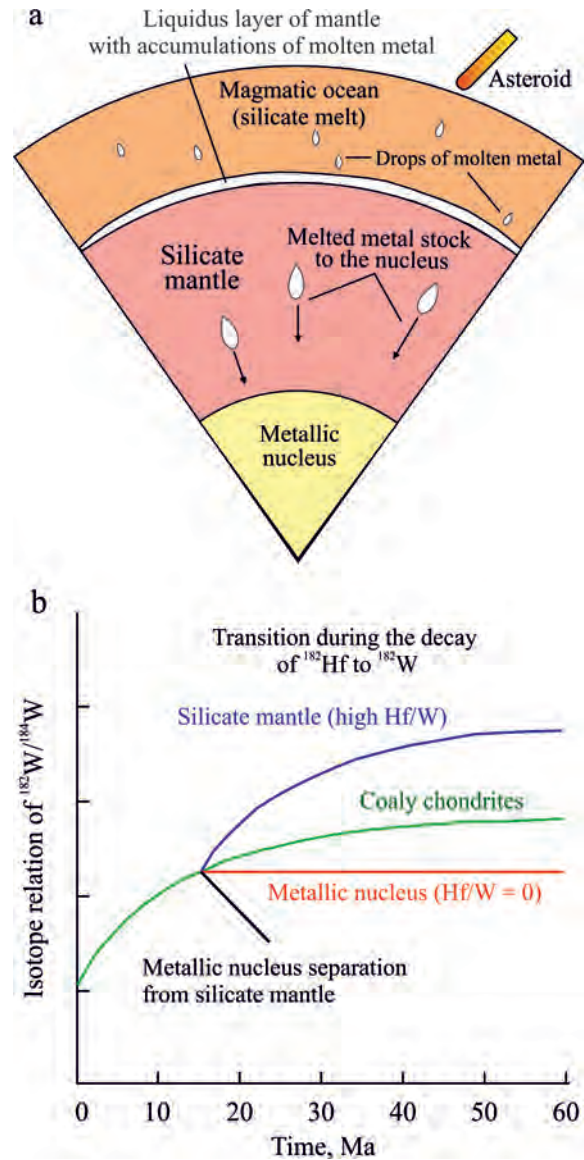


Fig. 3. Model of Earth's differentiation in the course of accretion according to [Wood, 2011].

a. Formation of the mantle and the core under the asteroid and meteorite bombardments of proto-Earth. The energy produced by asteroids colliding with Earth led to the formation of large magmatic basins reaching a depth of 400–700 km. Drops of siderophile elements formed during the melting of the iron-stone material of asteroids (meteorites) and were submerged to the bottom of the magmatic basin, where they formed accumulations of molten metal, which plunged through the lower mantle, thus increasing the core. b. Time of the core's formation determined using $^{182}\text{Hf} \rightarrow ^{182}\text{W}$ system; $T_{1/2} = 8.9$. The diagram shows changes in the $^{182}\text{W}/^{184}\text{W}$ ratio depending on the system (iron core, carbonaceous chondrites, silicate mantle) according to [Wood, 2011]. They indicate that the core was mostly formed in about 20 Ma, with almost the entire core being formed in 50 Ma.

ing results were produced by the $^{182}\text{Hf} \rightarrow ^{182}\text{W}$ system. Its parent isotope ^{182}Hf having a half-life of about 9 million years almost disappeared during the first 50 mil-

lion years of the Earth's history. Unlike the siderophile daughter isotope ^{182}W , hafnium is a lithophile element. In the course of the planet's differentiation into the iron core and the silicate mantle, ^{182}W headed towards the core, whereas ^{182}Hf remained in the mantle (see Fig. 3). If the core had formed immediately following accretion, the daughter isotope would have remained with the parent isotope in the mantle and would have corresponded to the composition of chondrites. As compared to chondrites, the mantle is depleted of tungsten ($\text{Hf} / \text{W} = 19$ and 1.1 , respectively), which indicates that the core formed at a certain interval of geological time during which tungsten along with iron was partially redistributed to the nucleus. Judging by the tungsten isotopic composition of the Earth's mantle, the minimum time (following the onset of Earth's accretion) required for the core to form is estimated at 34 ± 7 Ma [Kostitsyn, 2012].

Thus, the Earth's differentiation began almost from the moment of its formation. Collisions of the emerging planet with large asteroids, as well as the heat of radioactive decay (primarily of short-lived isotopes) resulted in the melting of its silicate layer to the extent that magma oceans were formed. At a high temperature and pressures of 20–23 hPa, magma was divided into silicate and iron melts [Wood, 2011]. After the first 5–8 Ma, the volume of Earth was already half of its present size. Collisions with large asteroids could result in the formation of magma basins reaching up to 400 km in depth. Iron melts, as the heavier ones, accumulated at the bottom and then fell through it, thus increasing the core [Wood, 2011].

The Moon's formation (Fig. 4) – which took place approximately 30 million years after the birth of the Solar System – is of great importance for Earth. Different scenarios for its formation were proposed: fission of proto-Earth; joint formation of Earth and Moon; capture of an independent space body by Earth. The available facts are most consistent with the impact origin of the Moon. The Moon was formed as a result of a Mars-sized body Theia (about 0.14% of Earth's mass) colliding with Earth at a velocity of about 5 km/s [Condie, 2011]. By that time, the Earth's core was largely formed and separated from the mantle; Earth had an atmosphere similar to that of Venus (this example shows what the Earth's atmosphere would have been like if it had not been affected by such a large collision).

In the course of discussing the first models of the impact Moon formation, some questions were raised [Cameron, 1986; Hartmann, 1986] which prevented the proposed model to be conclusively accepted. The above-mentioned questions were primarily related to the composition of the cosmic body with which proto-Earth had collided. The determination of the lunar soil composition solved this issue. Lunar rocks have the same isotopic composition of oxygen as those of Earth. They are also characterised by a deficiency of siderophile elements. This fact suggests that the cos-

mic body called Theia was formed in the inner part of the Solar System along with other terrestrial planets. Hence, like proto-Earth, Theia had a formed core and mantle. A computer simulation carried out in 1989 [Newsom, Taylor, 1989] revealed that, as a result of the impact, the silicate (mantle) part of this cosmic body, together with the Earth's mantle, turned into the impact-generated melt and dust cloud, whereas the iron core of this cosmic body sank into the core of proto-Earth merging with it. Figure 4a shows some modelled images of Earth's collision with Theia. According to H. Newsom and S. Taylor [1989], the formation of the Moon was completed in no more than first hundreds of years.

Figure 4b shows a scheme of Theia colliding with proto-Earth and the resulting formation of the Moon from the melt and dust cloud generated by the impact. This cloud consisted of molten mantle silicates from the colliding bodies, silicate dust particles, and, possibly, the gases of proto-Earth's atmosphere. Most likely, this cloud was stretching in the direction of the Earth's collision with the cosmic body. The core of Theia penetrated into that of Earth, increasing it. On the periphery of the cloud, the Moon began to accrete from its molten part. A comparative geochemical analysis of the silicate parts of Earth and the Moon [Condie, 2011] reveals that lunar rocks are enriched in refractory oxides (according to K. Condie's classification) (Ca, Sc, Ti, Th). In addition, volatile lithophile (Na, K, Rb, Sr) and especially siderophile (Co, Ni) elements are shown to be depleted in the lunar mantle, as compared to that of Earth. Such geochemical characteristics are quite explicable. The Moon crystallised from the inner part of the molten silicate disc of the impact cloud; therefore, it was slightly enriched with refractory elements, whereas Earth's rocks were enriched with lithophile (volatile, according to [Condie, 2011]) elements having lower condensation temperatures. As for siderophile elements, they were concentrated in the cores of two planetary bodies during accretion and initial differentiation. Volatile components (proto-Earth's atmosphere) appeared into the Earth's atmosphere after it cooled down, which is confirmed by the presence of oxygen in the Earth's atmosphere at the beginning of the Hadean aeon.

Considering the crystallisation of the Moon's and Earth's magma oceans (on Earth it reached about 700 km in depth and maybe more), all these events ended by 4520–4505 Ma, given that 4,500 Ma ago the Moon and Earth were already solid, which is evidenced by the traces of meteorite bombardments on the Moon's surface.

Hadean aeon

The Hadean aeon was proposed in the 1980s when zircons dated at 4376 Ma were found in metamorphosed sedimentary rocks outcropping in the Jack

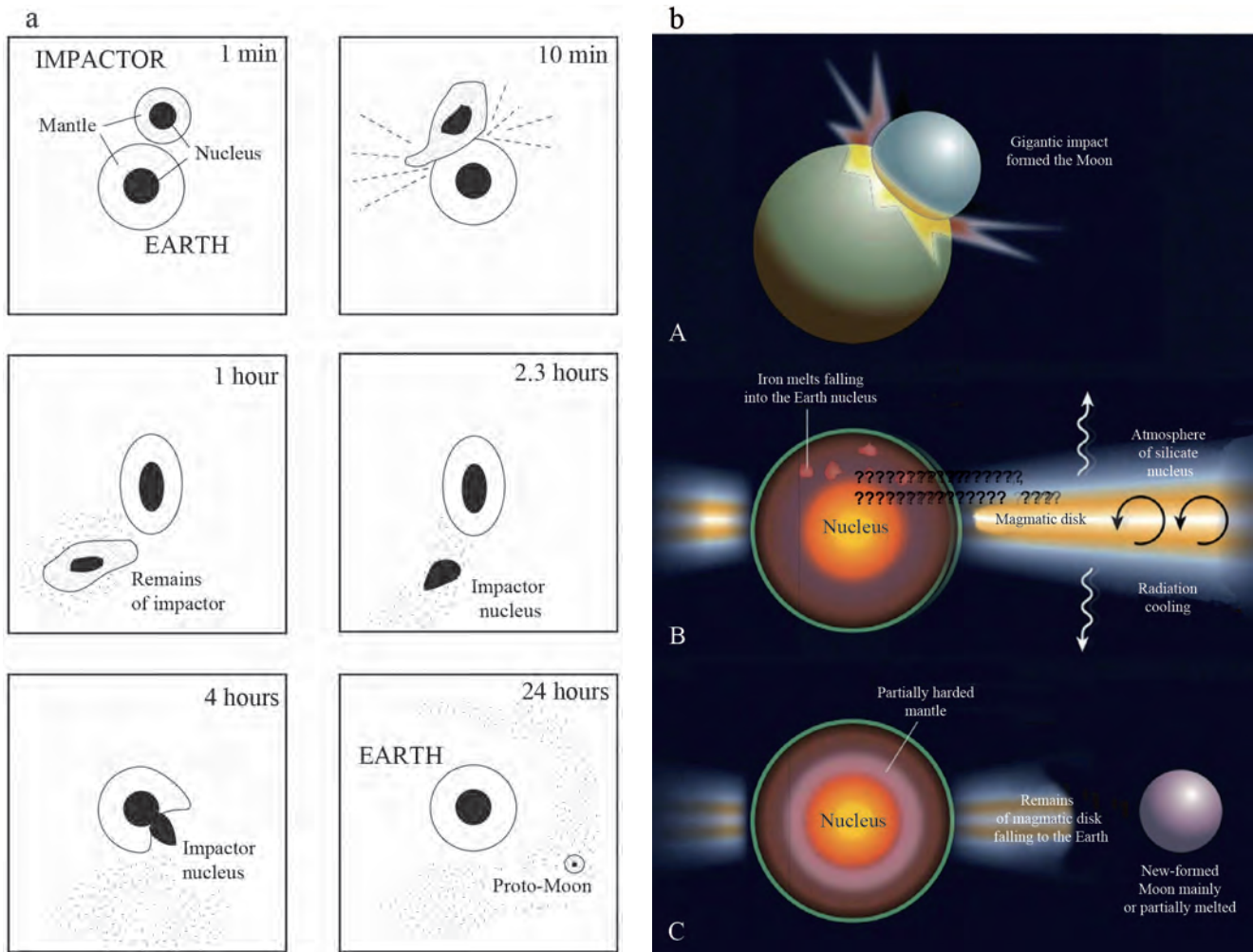


Fig. 4. Formation of the Moon as a result of the cosmic body (Theia) colliding with Earth.

a. Computer simulation of Theia colliding with Earth and the resulting formation of the Moon according to [Newsom, Taylor, 1989].

According to the model, the birth of the moon took 24 h. The authors of the model believe that the Moon's formation took no more than hundreds of years following the collision.

b. Model of the Moon's formation [Condie, 2011].

A. A planetary embryo (Theia) colliding with almost formed Earth.

B. Following the collision, a melt-dust disc was formed stretching in the direction of the location where the Moon was formed.

C. The Moon formed on the periphery of the disc; the mantle crystallised around the Earth's core.

Hills of Western Australia [Myers, 1988]. This period marks the beginning of the Earth's geological history. At first, there were great doubts whether it was possible to uncover the conditions for the formation of the first rocks on Earth, relying on such scarce materials as accessory minerals preserved from those rocks. However, due to the development of modern analytical research methods, tangible results were obtained in as early as the 21st century, which allow us to understand the geological situation on Earth in the Hadean aeon.

The results of detailed studies on Hadean zircons are given in [Nebel et al., 2014]. In addition, recent data on the geological situation in the Hadean aeon are presented in [Kuzmin, 2014; Kuzmin, Yarmolyuk, 2016; and

etc.]. The first results on the content of rare elements in Hadean zircons were obtained by R. Maas and his colleagues [Maas et al., 1992]. The results showed that the content of Hf in these zircons reached 0.86–1.30 wt %, with $Zr / Hf = 30\text{--}57$. In addition, fractional distribution of REE (high ratio of HREE / LREE), exhibited both positive Ce and negative Eu anomalies. The same researchers discovered inclusions of potassium feldspar, quartz, plagioclase, monocyte and apatite in zircons, which allowed the authors to conclude the granite composition of the Hadean zircon source.

Studies on the oxygen isotopic composition of zircons were of great importance for uncovering the conditions for their crystallisation in the Hadean aeon. It should be pointed out that oxygen isotopes can frac-

tionate during magmatic differentiation. The isotopic composition of primary rocks can be significantly changed in the course of weathering when weathering products are enriched with a heavy oxygen isotope. Respective changes in the oxygen isotopic composition were detected in the Hadean zircons, which led to the following conclusions: 1) weathering processes, similar to modern ones, were active during the Hadean aeon; 2) granitoid melts were formed under near-surface conditions [Nebel et al., 2014].

The discovery of zircons on the Moon played a great role in understanding the geological processes in the Hadean aeon as well. Hadean zircons [Nebel et al., 2014], as well as the ones found on the Moon [Taylor et al., 2009], are dated at 4.0–4.4 Ga; however, their formation temperatures differ: the Hadean zircons crystallised at $\approx 700^\circ\text{C}$ [Harrison et al., 2008], whereas the lunar ones did at $975\text{--}1150^\circ\text{C}$ [Taylor et al., 2009]. Normalised graphs showing REE distribution in the lunar (Fig. 5a) and Hadean (Fig. 5b) zircons are similar and characterised by the predominance of

HREE over LREE. At the same time, lunar zircons differ from the Hadean ones in the absence of a positive Ce anomaly; hence, they were formed in a reducing environment. An important conclusion on the crystals of lunar zircon was made when studying the zircon microstructure [Grange et al., 2013]. The study of the zircon microstructure revealed local areas of recrystallisation, localised amorphous areas, plastic crystal deformations and faults, cracks, i.e. typical traces of impact structures.

Considering the proximity between the Moon and Earth on a cosmic scale, it is clear that these two bodies were simultaneously subjected to meteorite and asteroid bombardments. While on the Moon, these bombardments resulted in numerous meteorite craters; on Earth, these bombardments continuously destroyed the continental crust being created, plunging into the mantle where it melted. Nonetheless, refractory zircon crystals were preserved and as a result of mantle plumes poured onto the surface together with the new portions of the primary mantle magma. On the surface,

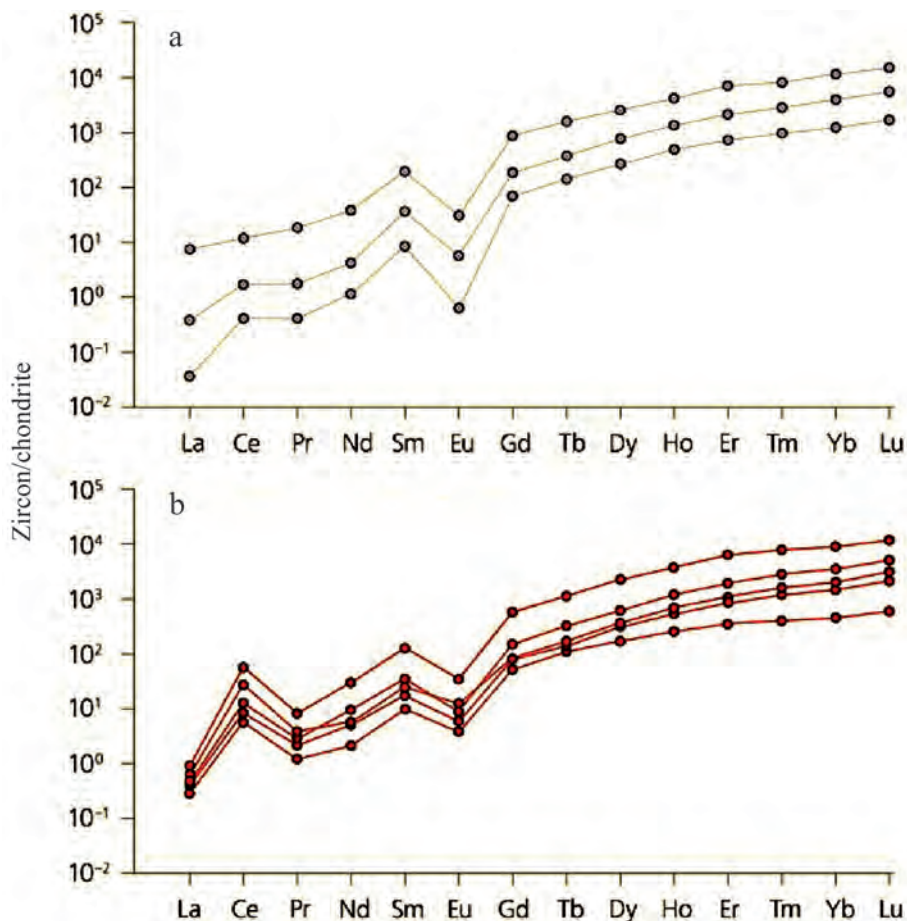


Fig. 5. Chondrite-normalised graphs showing the content of rare-earth elements in the lunar (a; according to [Taylor et al., 2009]) and Hadean (b; according to [Maas et al., 1992]) zircons.

Age of the lunar and Hadean zircon is estimated at 4.0–4.4 Ga. Lunar and Hadean zircons formed at $975\text{--}1150^\circ\text{C}$ [Taylor et al., 2009] and $\approx 700^\circ\text{C}$ [Harrison et al., 2008], respectively.

they underwent differentiation, while zonal zircons crystallised from small volumes of granitoid melts. This served as a sort of recycling for the Hadean continental crust, as evidenced by the zonal Hadean zircons [Nebel et al., 2014].

Despite the heavy bombardment of the terrestrial planets, which was caused, as mentioned above, by the stabilisation of the giant planets' orbits (Saturn and Jupiter), a small part of the Hadean primary crust was preserved, discovered and described in detail in [O'Neil et al., 2012]. These most ancient rocks of Earth were recently discovered in the Nuvvuagittuq Greenstone Belt on the northeast coast of the Hudson Bay (Canada). Its central part (Ujaraaluk unit) is composed of basic and ultrabasic volcanic and intrusive rocks. The age of rocks was estimated by the ratio of decay products of short-lived ($^{146}\text{Sm} \rightarrow ^{142}\text{Nd}$; $T_{1/2} = 68 \text{ Ma}$) and long-lived ($^{147}\text{Sm} \rightarrow ^{143}\text{Nd}$; $T_{1/2} = 106 \text{ Ga}$) isotope systems, amounting to about 4,400 Ma. The obtained results indicate that these rocks belong to the oldest crust of Earth, which developed following the Moon's formation. Age determination of the Hadean rocks is shown in Fig. 6 [O'Neil et al., 2012].

A small rock unit (Idiwhaa) outcropping 4.03 Ga Hadean granitoids was recently discovered among the rocks of the Nuvvuagittuq Greenstone Belt [Reimink et al., 2014]. These granitoids occur among typical Archaean TTG (tonalite-trondhjemite-granodiorite) rocks in the Acasta Gneiss Complex (Canada). The identified granitoids from the Idiwhaa unit form thin interlayers in amphibolites and gneisses with a thickness ranging from several centimetres to a decimetre. The constituent minerals of tonalites include plagioclase, quartz, hornblende and biotite. Their composition comprises 57.9–66.9 wt % of SiO_2 with a low content of Al_2O_3 (13.8–14.1 wt %), high content of total iron ΣFeO (8.6–15.2 wt %) and a low magnesian coefficient Mg\# (13–18 wt %). Unlike Archaean TTG rocks, the Hadean tonalites have a completely different distribution of normalised REEs (Fig. 7). While Archaean TTG rocks are enriched with LREEs, which indicates their formation during the partial melting of the mantle substance in the presence of garnet, the Hadean tonalites originated at shallower depths during the partial melting of the hydrous basalt crust in the presence of plagioclase, which contributed to the development of a negative Eu anomaly.

Hadean granitoid rocks of such genesis were obviously formed at various points in time. 4.2 Ga zircon xenocrystals were found in Archaean TTG rocks dated at 3.9 Ga [Iizuka et al., 2006]. An example of such xenocrystal, located in the centre of a magmatic zircon dated at approximately 3.9 Ga, is shown in Fig. 8a. In this case, magma that generated Archaean TTG rocks must have been smelted from the residual magmatic reservoir of the Hadean time. It could have been a partially melted remnant of the Hadean crust which was immersed in the mantle as a result of a meteorite bom-

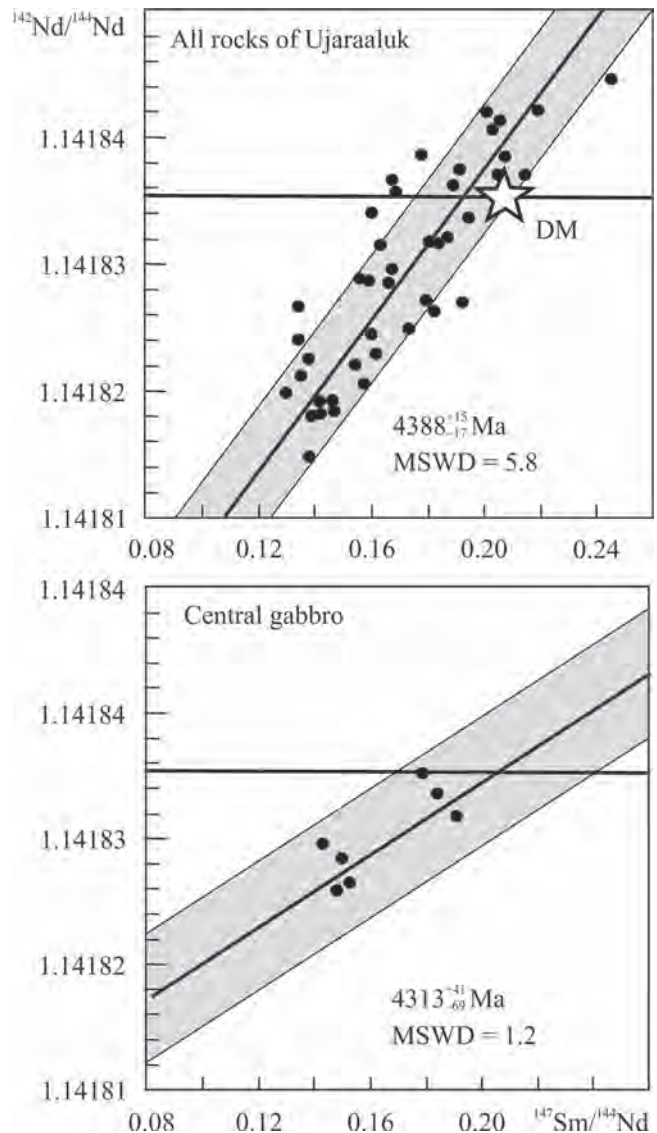


Fig. 6. Age of the Ujaraaluk series obtained using two isotopic pairs $^{147}\text{Sm} \rightarrow ^{143}\text{Nd}$ ($T_{1/2} = 106 \text{ Ga}$) and $^{146}\text{Sm} \rightarrow ^{142}\text{Nd}$ ($T_{1/2} = 68 \text{ Ma}$) according to [O'Neil et al., 2012].

Perhaps this is the only part of the Hadean crust left after the giant impact that formed the Moon. The site was preserved after the last heavy bombardment of Earth, which destroyed the Hadean crust.

bombardment. Figure 8b shows the distribution of normalised REEs in Hadean zircons dated at approximately 4.2 Ga. In terms of the REE distribution, these zircons are comparable to Hadean zircons found in Austria. It should be pointed out that zircon xenocrystals of the Hadean time were found in various cratons, which indicates a wide distribution of the Hadean continental crust on Earth.

Among all else, available data on a possible mechanism for the formation of Hadean zircon melt suggest that granitoid melts could have been formed in the

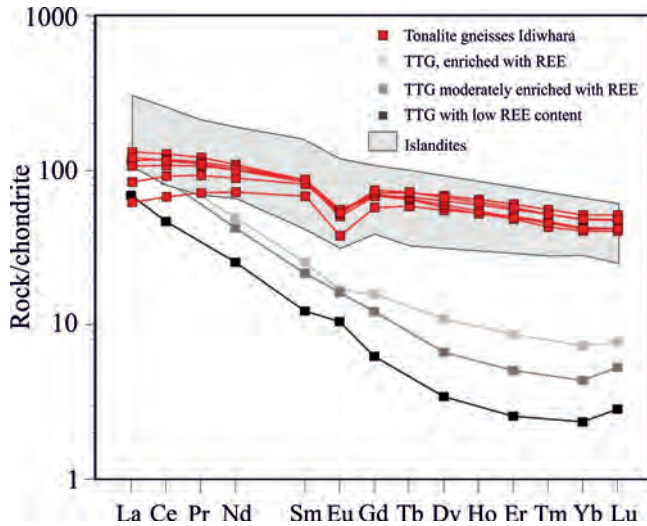


Fig. 7. Normalised distribution of rare-earth elements in the tonalite gneisses of the Idiwhaa site (4.03 Ga) and in Archaean TTG rock series according to [Reimink et al., 2014].

Hadean aeon in various ways, but in shallow chambers and usually in an oxidising environment when the hydrous basalt crust was melting.

In concluding the analysis of the Hadean geological history, we consider it necessary to draw attention to one important factor observed in [Jackson et al., 2017]. The authors of this work noted high values of the $^3\text{He}/^4\text{He}$ ratio in some basalts, which was shown to be related to hot plumes, namely Hawaiian and Icelandic. In these basalts, the value of the $^3\text{He}/^4\text{He}$ ratio was 30–50 times higher than its atmospheric values. It was suggested that this could be due to the presence of non-degassed reservoirs in the mantle, which have survived to the present. It is likely, that such reservoirs had high density, so they were not mixed in the course of mantle convection. The authors of this article refer to the Oligocene basalts (Baffin Island, West Greenland) associated with the proto-Iceland plume, which are plotted between the 4.55 Ga and 4.45 Ga geochrons in lead isotope diagrams, as shown in [Jackson et al., 2010]. However, basalts from a number of hot spots not having high $^3\text{He}/^4\text{He}$ ratios, as well as basalts from mid-oceanic ridges, are plotted in the same area of this diagram (in terms of the lead isotope ratio), which does not allow basalts having a high $^3\text{He}/^4\text{He}$ ratio to be clearly identified as the products of ancient non-degassed mantle reservoirs. At the same time, it is known that volatiles, in particular He and H, can form compounds with metals (He – metal of high density). It is likely, that some of them got into the core in the course of the Earth’s accretion and the formation of its core [Gilat, Vol, 2012]. Subsequently, these elements (or compounds) concentrated in the outer core, whose density is lower than that of the inner core; then they could get into the D” layer, which according to geo-

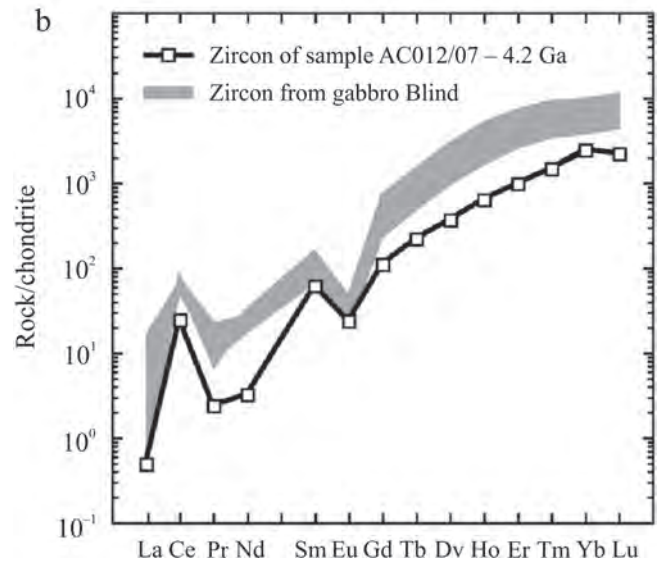
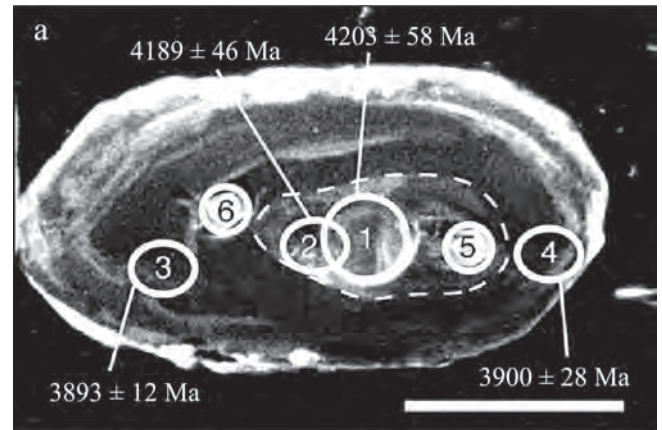


Fig. 8. Comparison of Hadean xenocrystals with Archaean zircon from the rocks of the Acasta Gneiss Complex (Canada) according to [Iizuka et al., 2012].

- a. Position of xenocrystals in the zircon host and their age characteristics.
- b. Normalised distribution of chondrite-normalised contents of rare-earth elements in zircon xenocrysts. The distribution of REE in gabbro is given for comparison.

physicists, comprises ultrahigh velocity zones [Garnero, McNamara, 2008], probably, represented by magmatic chambers feeding mantle plumes. Obviously, research in this direction should be continued, since it will help solve a number of issues related to the early evolution of Earth.

**ARCHAEOAN TTG ROCKS:
PRESERVED PRIMORDIAL CONTINENTAL
CRUST OF EARTH**

The Archaean aeon was marked by the preservation of the continental crust represented by the tonalite-trondhjemite-granodiorite (TTG) rock association. There are marked petrochemical and geochemical dif-

ferences between early Archaean TTG rocks (grey gneisses) and Phanerozoic granitoids [Condie, 2011].

TTG rocks are notably different (petrochemically and geochemically) from the late Archaean, Proterozoic and Phanerozoic rocks. It can be seen in Figure 9a that TTGs are typical sodic rocks plotted at the Na-apex of the ternary Na–K–Ca diagram. It is quite clear that the ancient mantle of Earth – which has not yet parted with most of the lithospheric elements used in the formation of the Earth’s continental crust – served as the parent material for TTG rocks [Kuzmin, Yarmolyuk, 2017]. Post-Archaean calc-alkaline rocks, usually confined to subduction zones, exhibit a sig-

nificantly higher potassium content, since the lithosphere together with the continental crust served as the basis for their genesis. The rocks are even more contrasted in terms of the rare element content (Fig. 9b). Firstly, TTG rocks are strongly enriched with LREEs. This is obviously due to the considerable depth at which partial melting of the Archaean basaltic crust immersed in the mantle took place. The Archaean basaltic crust must have been enriched with lithophile elements, as compared to the Phanerozoic MORB (mid-ocean ridge basalts), whose ancient basic rocks represented by proto-ophiolites were identified in 1977 [Glukhovskii et al., 1977]. A distinct prevalence of

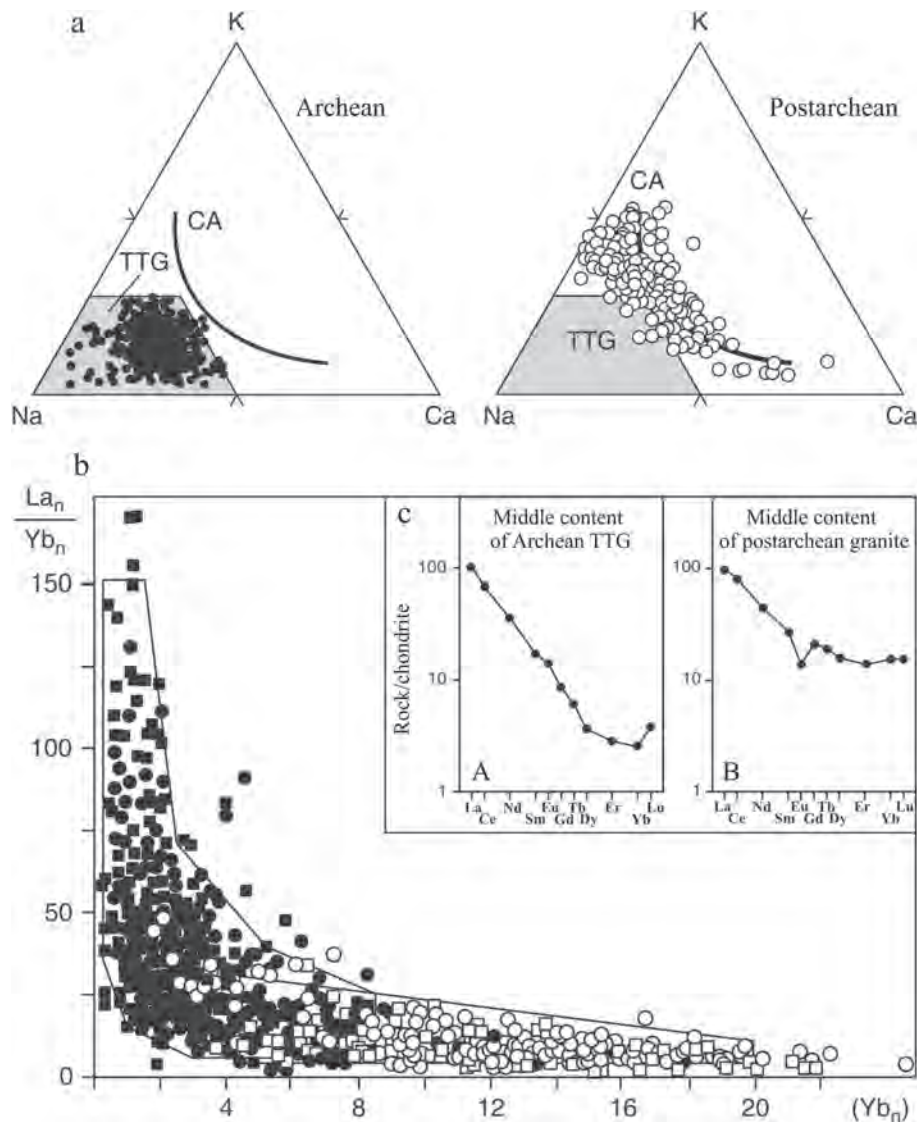


Fig. 9. Comparison of the rock formations of the Archaean tonalite-trondhjemite-granodiorite series (A) and the post-Archaean granites (B) according to [Condie, 2011].

a. K–Na–Ca diagrams show differences determined mainly by the sodium composition of TTG series and by the calc-alkaline composition of the post-Archaean volcanites and granites, according to [Condie, 2011].

b. Distribution of normalised REE contents, as well as the La/Yb ratio on the La/Yb–Yb_{norm} plot in the TTG and post-Archaean rocks. The TTG rocks are enriched with light REE, as compared to heavy REE.

LREE in TTG rocks can be observed in Figure 9c. Post-Archaean granitoids and calc-alkaline volcanites also exhibit high contents of LREEs, as compared to HREEs; however, they are not as predominant, which may indicate that Phanerozoic volcanites were formed at shallower depths.

Summarising the data on the TTG composition, it is clear that these preserved Archaean continental rocks are of mantle genesis considering the published data on the isotopic composition of TTG rocks, obtained from the U–Th–Pb, Sm–Nd, Rb – Sr and Re–Os systems, many of which are given in the monograph [Condie, 2011]. It has been established that TTG rocks were formed during the melting of highly hydrolysed basalts at sufficiently high pressures, at which the garnet remained stable in refractory residue [Reimink et al., 2014], which indicates eclogite paragenesis. At the same time, the increased values of incoherent elements in the source basalts indicate that the composition of TTG rocks is comparable with the island-arc rocks of the Phanerozoic time. However, no traces of subductions occurring in the course of TTG formation were detected. It can be assumed that basic and ultrabasic mantle magmas derived from Archaean plumes were responsible for the formation of a thick basaltoid crust. Having been formed from these magmas, Archaean basaltoids were enriched with lithophile elements, as compared to Phanerozoic MORBs.

The upper mantle derived from rising plumes was saturated with fluids, whereas crustal basalts were saturated with incoherent elements. Under the weight of a massive basaltoid crust, basalts sagged, being immersed into the mantle. This process involving vertical motions [Hain, 2003] is called sagduction.

The most ancient (3.9–3.8 Ga) TTG rocks originated from protoliths or the Hadean crustal matter during the formation of primary magmas for Archaean TTG rocks. Drawing on the study of Lu–Hf and U–Pb isotopes in gneisses, the work of A. Bauer and his colleagues [Bauer et al., 2017] provides detailed evidence of the Hadean mantle source (age > 4.0 Ga) being involved in the formation of Archaean gneissic TTG rocks (Canada). Figure 10 shows the distribution of isotopic characteristics exhibited by the tonalites (TTG) of the Acasta Gneiss Complex (Canada) for the two above-mentioned isotopic series. In terms of the subchondritic $^{177}\text{Lu}/^{177}\text{Hf}$ ratio, they are connected by two ratio values 0.015 and 0.022; whereas in terms of age, five rock groups are distinguished: 3.96–3.94 Ga (group A), 3.74–3.72 Ga (B), 3.66–3.58 Ga (C), \approx 3.4 Ga (D) and 2.9 Ga (E). As shown in [Bauer et al., 2017], these TTG rocks are obviously derived from two Hadean igneous protoliths originating at different times. The rocks of groups A, B and partly C (the lower part of this group in Fig. 10) are linked to the subchondritic $^{177}\text{Lu}/^{177}\text{Hf}$ isotope ratio of 0.015, whereas groups D and E, as well as the upper part of group C, are linked to the subchondritic ratio of the same isotopes equal to 0.022. As rightly noted in [Bauer et al., 2017], this is due to the different depths to which the remnants of the Hadean crust originating at different times sank into the mantle as a result of meteorite bombardments. This Hadean crust was melted and mixed with the mantle material. Subsequently, this material served as a protolith for magmas that gave rise to Archaean TTG rocks. The protolith (source of younger rocks) could have formed at great depths; thus later it was involved in magma formation.

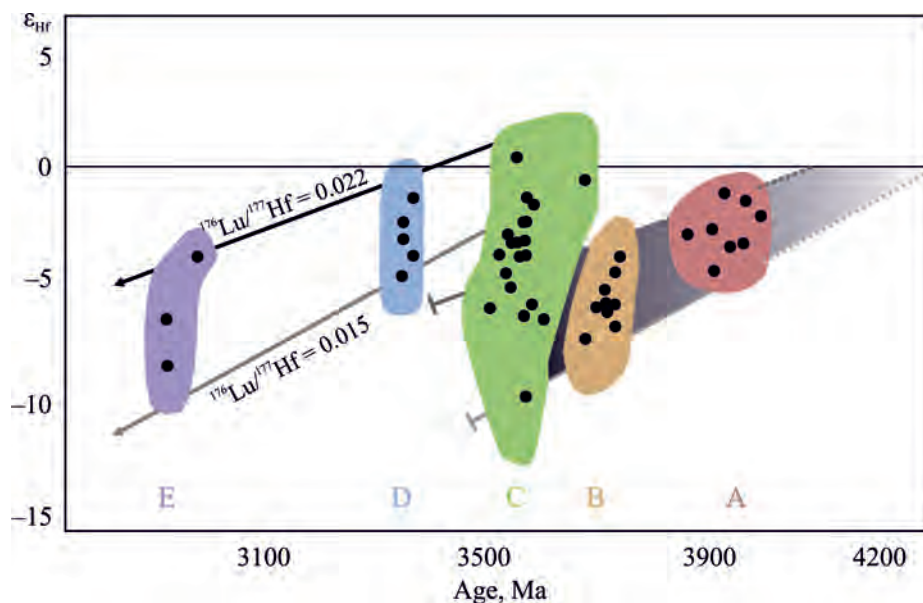


Fig. 10. Model Lu/Hf age of TTG sources from the Acasta Gneiss (Canada) according to [Bauer et al., 2017].

Judging by the presented data, the gneiss source of groups A and B is less radioactive than the magma source of younger gneisses.

In [Bauer et al., 2017], the authors also studied Archaean rocks from Greenland and Central Africa using a similar method: they established close age groups having slightly different subchondritic Lu/Hf isotope ratios. These observations indicate a wide distribution of the Hadean crust on Earth.

In his work [Bédard, 2006], J. Bédard gives a detailed consideration of a sagduction model drawing from a detailed petrological and geochemical study of a greenstone belt (Superior Province, Canada). The greenstone belt in question comprises volcanites of basalt-komatiite composition, which are associated with the rocks of the tonalite-trondhjemite series (Fig. 11). The model is as follows: basaltoid volcanic series of high-thickness crust are intruded by magmas generated by a rising plume. As a result, the volcanites are partially melted and restites subside, whereas granitoid (tholeiitic) magmas rise from the lower crust to its upper levels. The formation of TTG series consists of multiple stages. In the proposed model, it includes at least 3-4 stages. To some extent, this model can be applied to the formation of oceanic plateaus. It is evident that the drilling of modern oceanic plateaus, which, like Archaean TTG series, occur above mantle plumes, will give a better understanding of this process. The formation of granitoid rocks is in many ways similar to the formation of calc-alkaline series of subduction-related volcanites and granitoids. Unlike subduction, the sagduction process in-

volves vertical subsidence of basaltoid rocks into the depths of the mantle.

In 2011–2016, an international program aimed at studying the Archaean magmatism of Earth was carried out. The results of these studies were published as a collective work [Halla et al., 2017]. In the course of work, Archaean granitoid formations in North Atlantic, Fennoscandian, Indian and Ukrainian shields were studied.

The researches working on the program came to the following conclusions.

The formation of tonalite-trondhjemite-granodiorite rock associations (called grey gneisses in Russia) from the studied cratons is dated at 3.9–3.6–3.4–3.1 Ga. Granitoid massifs – including batholiths – younger than 3.1 Ga were replaced by potassium calc-alkaline granitoids (sanukitoids, monzogranites enriched with rare elements and quartz monzonites).

According to the authors of [Halla et al., 2017], a change in the Earth's dynamics triggered plate tectonics.

It is assumed [Halla et al., 2017] that during the formation of K granitoids dated at 3.1–2.5 Ga, some Precambrian cratons, which previously constituted a single supercontinent, were divided into a series of smaller ones separated by oceanic basins.

Thus, lid tectonics, the tectonics of mantle overturns and deep mantle plumes of ultrabasic-basic composition lasted until 3.1 Ga.

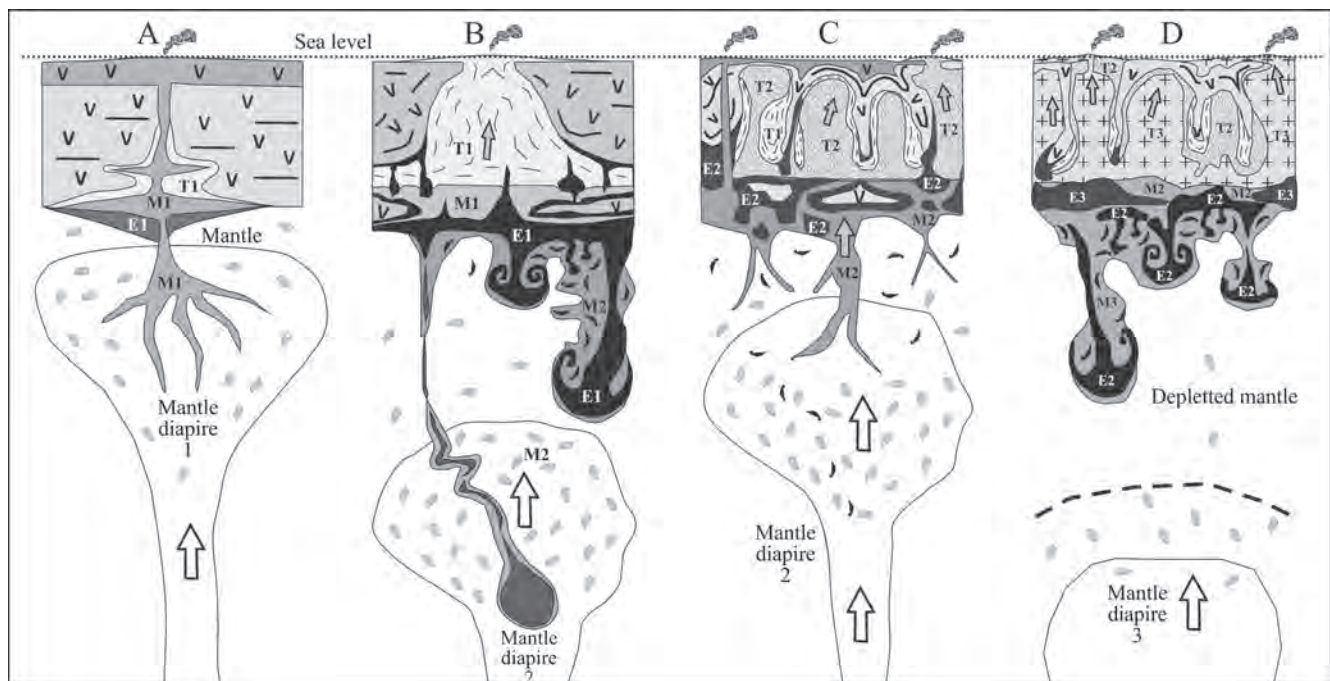


Fig. 11. Model of sagduction describing the generation of 3.9–3.1 Ga TTG rocks [Bédard, 2006].

The Archaean crust of high thickness subsides into the mantle to a depth at which garnet remains in restite after melting. Under the influence of high mantle temperatures, the TTG rocks are melted from the eclogitised Archaean basaltoid, which intrude into the main Archaean crust, forming the preserved first continental crust. J.H. Bédard noted that there could be 3–4 such stages.

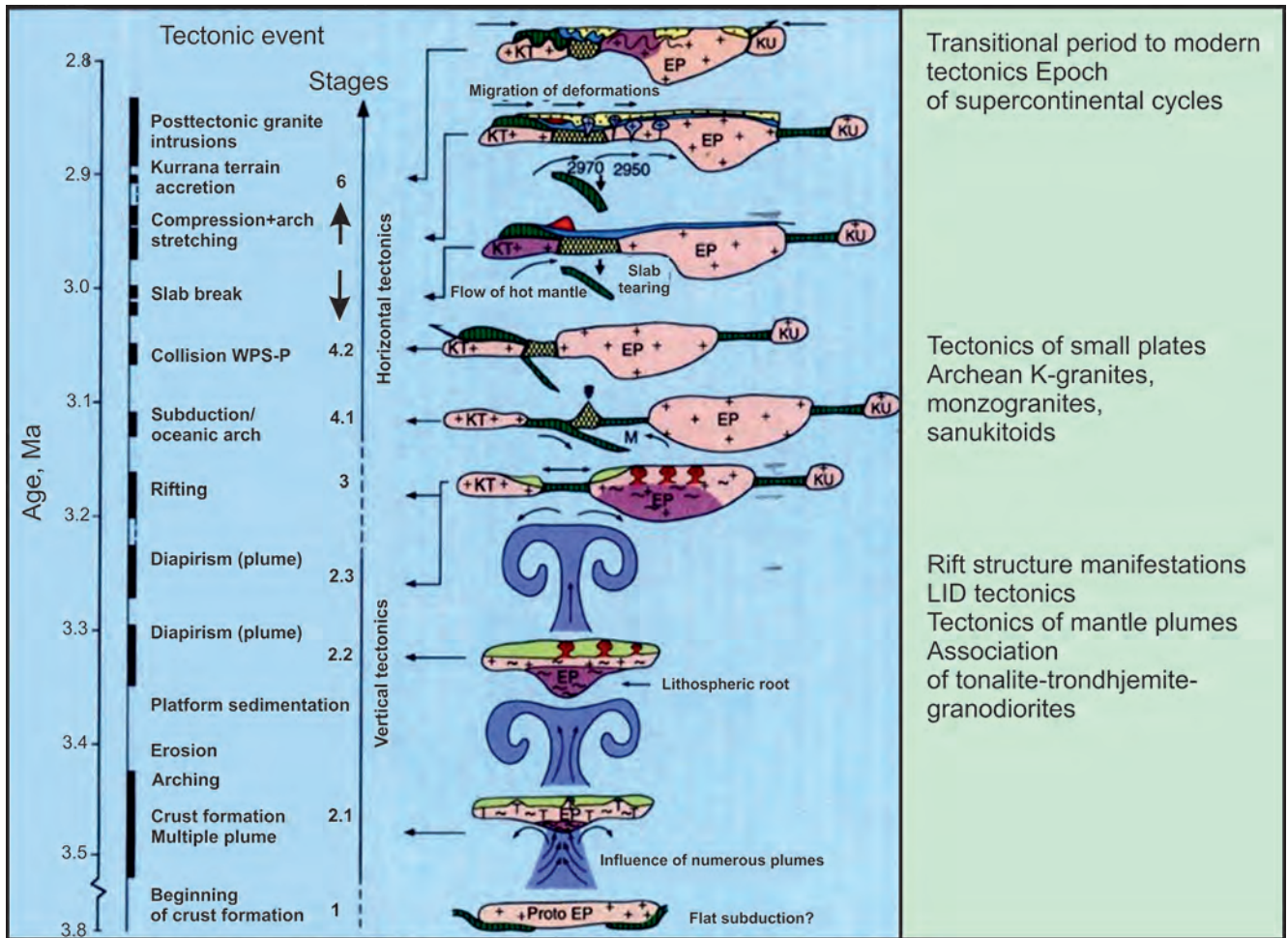


Fig. 12. Diagram showing tectonic-magmatic events involved in the formation of the geological structure of Pilbara Craton (Australia) according to [Pease et al., 2008] with additions.

We believe that the time interval of 3.1–2.7 Ga included a period of small-plate tectonics, whereas the interval of 2.7–2.0 Ga constituted a transitional period from the small-plate tectonics to modern-style tectonics. At that time, all the Earth’s inner layers were formed [Kuzmin, Yarmolyuk, 2016, 2017]. The changes of tectonic movements, as well as the types of tectonic structures, that took place from the beginning of the Archaean aeon to the onset of plate tectonics, can be illustrated by a diagram (Fig. 12) containing the authors’ additions.

CONCLUSION

Studying the early stages of the Earth’s evolution constitutes the basis for understanding its further geological history. The Chaotian aeon was marked by cosmic events that determined the initial development of our planet. At that time (4568–4500 Ga), the Earth formed as a result of planetesimal accretion and cosmic factors determined all the processes occurring on Earth: differentiation into the core and the mantle, for-

mation of the Earth’s satellite – the Moon. At the same time, the evolution of the Solar System itself determined its division into rocky inner and gas-water outer parts, in which the terrestrial planets were located closer to the Sun, whereas its outer part was occupied by giant gas-ice planets. The early history of the giant planets, as well as the intensity with which the terrestrial planets were bombarded by meteorites, greatly contributed to the delivery of building material to the inner part of the system.

Heavy meteorite bombardments of the Earth continued in the Hadean aeon as well. At the time, the first crust of the Earth began to form; however it was practically destroyed at the end of the Hadean aeon when the giant planets settled in their orbits and the main meteorite material was accreted by the terrestrial planets, with a significant part of it being absorbed by the Sun. Despite the fact that the Hadean aeon is seen as the beginning of the Earth’s geological history, it was dominated by cosmic events. In particular, Earth, like other planets of the terrestrial group, was constantly subjected to meteorite and asteroid bombardments. Figure 13

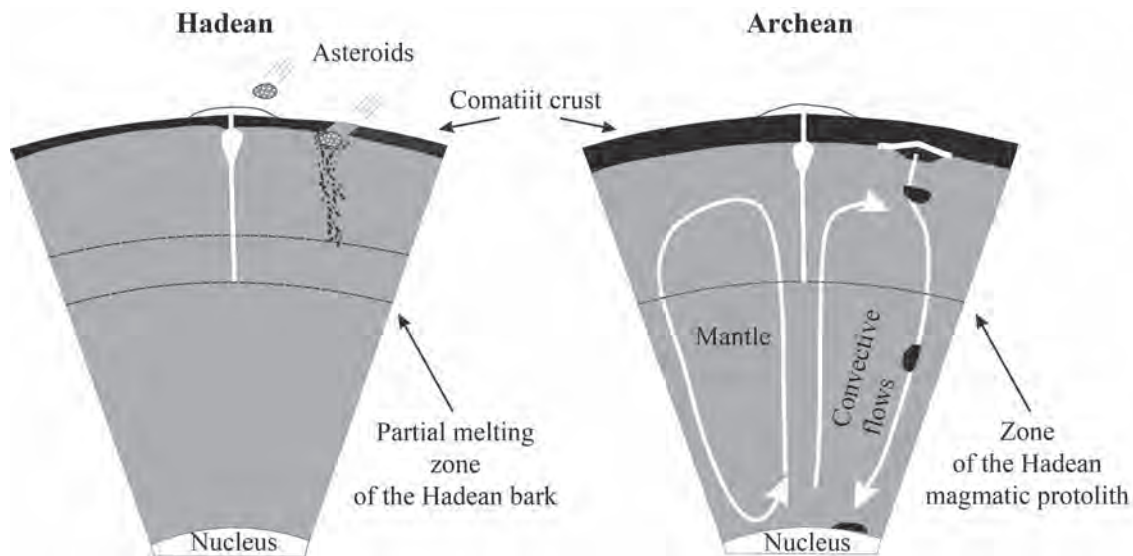


Fig. 13. Models of possible endogenous processes in the Hadean aeon and the Eoarchean era.

In the Hadean aeon, a thin crust was formed by mantle magmas, whose eruptions were induced by asteroid bombardments. The bombardments destroyed the crust that subsided into the upper part of the mantle forming the Hadean protolith for subsequent magma generation. Whole-mantle convection began in the Archean aeon, which also involved the Hadean protolith in melting. The melting of the lower crust under the influence of mantle magmas caused the appearance of melts forming TTG complexes. The residue of the lower crust descended into the lower mantle (see the text for explanation).

shows a model of the manifested endogenous processes characteristic of the Hadean time. A high temperature of the Hadean mantle, on the one hand, resulted from recently crystallised hot mantle ocean produced by the Moon-forming impact and, on the other, from the presence of a great number of short-lived isotope systems releasing a large amount of energy during the radioactive decay of parent isotopes. In this connection, whole-mantle convection most likely did not exist in the Hadean aeon. A flat stagnated surface of Earth was hit by cosmic asteroids or large meteorites destroying the planet's surface represented by rocks formed during the outpouring and differentiation of basic mantle magmas. The fragments of surface rocks subsided into the mantle, melting and mixing with the mantle material. This material subsequently formed the protoliths of the late-Hadean and Archean magmas, which could contain refractory zircon crystals. New portions of the basic and komatiitic mantle magmas poured into the destroyed parts of the Hadean Earth's surface, which were restored by the subsequent crystallisation of magma and damaged again during the next bombardment. Thus, the Earth's endogenous activity in the Hadean aeon was completely affected by space processes.

At the end of the Hadean aeon, the mantle temperature was lowered due to the loss of a large amount of endogenous energy following the last heavy meteorite bombardment, as well as to the cessation of the radioactive decay of short-lived isotopes, which marked the beginning of the Archean period of the Earth's geological history.

It can be assumed that due to the beginning of the whole-mantle convection (see Fig. 13), a decrease in mantle temperature did not affect the thermal state of the Earth's core. Consequently, Earth became a self-organised unit, which led to the manifestation of deep tectonic processes, i.e. endogenous activity of the planet itself, whereas cosmic impact on Earth decreased significantly. The Earth's surface remained flat and stagnated, i.e. the operation of lid tectonics continued; however it was torn apart by rising deep plumes carrying magmas of ultrabasic-basic composition, which formed a thick crust of the basic (basaltoid) composition at the exit points. The surface layer of Earth could not withstand the load of the upper layer, which, undergoing sagduction, subsided forming granitoid magmas, subsequently producing rocks of the TTG series. Pouring onto the surface, magmas formed the Archean granitoid continental crust that has been preserved to date.

With its thickness gradually increasing, the continental crust started to break and sink into the mantle: marking the onset of small-plate tectonics, which due to the formation of the Earth's inner layers [Condie, 2011; Kuzmin, Yarmolyuk, 2017] further evolved into the modern-style tectonics combining plate tectonics and plume tectonics.

Surely, this general view of our planet's evolution is largely speculative and needs to be further revised, which in turn requires detailed comprehensive geological studies.

REFERENCES

- Allègre C.J., Poirier J.P., Humler E., Hofmann A.W. (1995) The Chemical-Composition of the Earth. *Earth Planet. Sci. Lett.*, **134**(3-4), 515-526. [http://dx.doi.org/10.1016/0012-821X\(95\)00123-T](http://dx.doi.org/10.1016/0012-821X(95)00123-T)
- Batygin K., Laflin G., Morbidelli A. (2016) Born from the chaos. *V mire nauki*, (7), 16-27. (In Russian)
- Bauer A.M., Fisher C.M., Vervoort J.D., Bowring S.A. (2017) Coupled zircon Lu-Hf and U-Pb isotopic analyses of the oldest terrestrial crust, the >4.03Ga Acasta Gneiss Complex. *Earth Planet. Sci. Lett.*, **458**, 37-48.
- Bédard J.H. (2006) A catalytic delamination-driven model for coupled genesis of Archaean crust and sub-continental lithospheric mantle. *Geochim. Cosmochim. Acta*, **79**, 1188-1214.
- Cameron A.G.W. (1986) The impact theory for origin of the Moon. *Origin of the Moon* (Eds W.K. Hartmann, R.J. Phillips, G.J. Taylor). Houston, TX: Lunar & Planetary Institute, 609-616.
- Condie K.C. (2011) Earth as an evolving Planetary System. Elsevier, 574 p.
- Garnero E.J., McNamara A.K. (2008) Structure and Dynamics of Earth's Lower Mantle. *Science*, **320**, 626-628
- Gilat A., Vol A. (2012) Degassing of primordial hydrogen and helium as the major energy source for internal terrestrial processes. *Geosci. Front.*, **1**, 911-921. doi:10.1016/j.gsf.2012.03.009
- Glukhovskii M.Z., Moralev V.M., Kuzmin M.I. (1977) Tectonics and petrogenesis of the Katarchean complex of the Aldan Shield in connection with the problem of protophylites. *Geotektonika*, (6), 103-117. (In Russian)
- Goldblatt C., Zahnle K.J., Sleep N.H., Nisbet E.G. (2010) The eons of chaos and hades. *Solid Earth*, **1**, 1-3. <http://dx.doi.org/10.5194/se-1-1-2010>
- Grange M.L., Pidgeon R.T., Nemchin A.A., Timms N.E., Meyer C. (2013) Interpreting the U-Pb data from primary and secondary features in lunar zircon. *Geochim. Cosmochim. Acta*, **101**, 112-132. <http://dx.doi.org/10.1016/j.gca.2012.10.013>
- Hain V.E. (2003) *Osnovnye problemy sovremennoi geologii* [The main problems of modern geology]. Moscow, Nauch. mir Publ., 348 p. (In Russian)
- Halla J., Whitehouse M.J., Ahmad T., Bagai Z. (2017) Archaean granitoids: an overview and significance from a tectonic perspective. <http://sp.lyellcollection.org/doi/10.1016/j.epsl.2008.02.011>
- Harrison T.M., Schmitt A.K., McCulloch M.T., Lovera O.M. (2008) Early (N = 4.5 Ga) formation of terrestrial crust: Lu-Hf, $\delta^{18}\text{O}$ and Ti thermometry results for Hadean zircons. *Earth Planet. Sci. Lett.*, **268**(3-4), 476-486.
- Hartmann W.K. (1986) Moon origin: the impact-trigger hypothesis. *Origin of the Moon* (Eds W.K. Hartmann, R.J. Phillips, G.J. Taylor). Houston, TX: Lunar & Planetary Institute, 579-608. <http://dx.doi.org/10.1016/j.epsl.2008.02.011>
- Iizuka T., Horie K., Komiya T., Maruyama S., Hirata T., Hidakaka H., Windley B.F. (2006) 4.2 Ga zircon xenocryst in an Acasta gneiss from northwestern Canada: Evidence for early continental crust. *Geology*, **34**(4), 245-248.
- Jackson M.G., Carlson R.W., Kurz M.D., Kempton P.D., Don Francis, Blusztajn J. (2010) Evidence for the survival of the oldest terrestrial mantle reservoir. *Nature*, **466**, 853-856.
- Jackson M.G., Konter J.G., Becker T.W. (2017) Primordial helium entrained by the hottest mantle plumes. *Nature*, **542**, 340-343.
- Kostitsyn Yu.A. (2012) Age of the Earth's core by isotopic data: matching of Hf-W and U-Pb systems. *Geokhimiya*, (6), 531-554. (In Russian)
- Kuzmin M.I. (2014) Precambrian history of the origin and evolution of the solar system and the Earth. Article I. *Geodynam. Tectonophys.*, 5(3), 625-640. (In Russian)
- Kuzmin M.I., Yarmolyuk V.V. (2017) Biography of the Earth: the main stages of geological history. *Priroda*, (6), 12-25. (In Russian)
- Kuzmin M.I., Yarmolyuk V.V. (2016) Change in the style of tectonic movements in the evolution of the Earth. *Dokl. Akad. Nauk*, **469**(6), 706-710. (In Russian)
- Lauretta D. (2011) A cosmochemical view of the Solar System. *Elements*, **7**(1), 11-16. <http://dx.doi.org/10.2113/gselements.7.1.11>
- Lin D. (2008) Origin of the planets. *V mire nauki*, (8), 22-31. (In Russian)
- Maas R., Kinny P.D., Williams I.S., Froude D.O., Compston W. (1992) The Earth's oldest known crust – a geochronological and geochemical study of 3900–4200 Ma old detrital zircons from Mt. Narryer and Jack Hills, Western Australia. *Geochim. Cosmochim. Acta*, **56**(3), 1281-1300. [http://dx.doi.org/10.1016/0016-7037\(92\)90062-N](http://dx.doi.org/10.1016/0016-7037(92)90062-N)
- Maruyama S., Ebisuzaki T. (2017) Origin of the Earth: A proposal of new model called ABEL. *Geosci. Front.*, **8**, 253-274.
- Masset F., Snellgrove M. (2001) Reversing type II migration: resonance trapping of a lighter giant protoplanet. *Mon. Not. R. Astron. Soc.*, **320**(4), L55-L59.
- McDonough W.G., Sun S.S. (1995) The composition of the Earth. *Chem. Geol.*, **120**(3-4), 223-253. [http://dx.doi.org/10.1016/0009-2541\(94\)00140-4](http://dx.doi.org/10.1016/0009-2541(94)00140-4)
- Myers J.S. (1988) Early Archean Narryer gneiss complex, Yilgarn Craton, Western-Australia. *Precamb. Res.*, **38**(4), 297-307. [http://dx.doi.org/10.1016/0301-9268\(88\)90029-0](http://dx.doi.org/10.1016/0301-9268(88)90029-0)
- Nebel O., Rapp R.P., Yaxley G.M. (2014) The role of detrital zircons in Hadean crustal research. *Lithos*, **190-191**, 313-327.
- Newsom H.E., Taylor S.R. (1989) Geochemical implications of the formation of the Moon by a single giant impact. *Nature*, **338**, 29-34.
- O'Neil J., Carlsons R.W., Paquette J.L., Francisc D. (2012) Formation age and metamorphic history of the Nuvvuagittuq Greenstone Belt. *Precamb. Res.*, **220-221**, 23-44.
- Pease V., Percival J., Smitbies J., Stevens G., Kranendank M. (2008) When did plate tectonics begin? Evidence from the orogenic record. *Geol. Soc. Amer., Spec. Paper*, **440**, 199-228.
- Reimink J.R., Chacko T., Stern R.A., Heaman L.M. (2014) Earth's earliest evolved crust generated in an Iceland-like setting. *Nat. Geosci.*, **7**, 529-533.
- Roth A.S.G., Bourdon B., Mojzsis S.J., Touboul M., Sprung P., Guitreau M., Blichert-Toft J. (2013) Inherited ^{142}Nd anomalies in Eoarchean protoliths. *Earth Planet. Sci. Lett.*, **361**, 50-57.
- Stern R.J. (2008) Modern-style plate tectonics began in Neoproterozoic time: An alternative interpretation of Earth's tectonic history. *Geol. Soc. Amer., Spec. Paper*, **440**, 265-280.
- Taylor D.J., McKeegan K.D., Harrison T.M. (2009) Lu-Hf zircon evidence for rapid lunar differentiation. *Earth Planet. Sci. Lett.*, **279**(3-4), 157-164. <http://dx.doi.org/10.1016/j.epsl.2008.12.030>
- Wood B. (2011) The formation and differentiation of Earth. *Physics Today*, **64**(12), 40-45. <http://dx.doi.org/10.1063/PT.3.1362>
- Wood B.J., Halliday A.N. (2010) The lead isotopic age of the Earth can be explained by core formation alone. *Nature*, **465**(7299), 767-771. <http://dx.doi.org/10.1038/nature09072>

MURZINKA MASSIF IN THE MIDDLE URALS AS AN EXAMPLE OF AN INTERFORMATIONAL GRANITE PLUTON: MAGMATIC SOURCES, GEOCHEMICAL ZONATION, PECULIARITIES OF FORMATION

German B. Fershtater, Nadezhda S. Borodina

Zavaritsky Institute of Geology and Geochemistry, UB RAS, 15 Akad. Vonsovsky St., Ekaterinburg, 620016 Russia,
e-mail: gerfer@online.ural.ru

Received 08.11.2017, accepted 07.05.2018

Murzinka massif constitutes an interformational sheet-like body reaching up 6 km in length steeply dipping to the east. Proterozoic metamorphic rocks of predominantly granulite facies ($P = 5\text{--}6$ kbar, $T = 750\text{--}800^\circ\text{C}$) occur at the base of the massif, with Silurian-Devonian volcanic-sedimentary rocks metamorphosed in the epidote-amphibolite facies occurring in its roof. The petrogenic elements were determined at the Laboratory for Physicochemical Research Methods of the Zavaritsky Institute of Geology and Geochemistry, UB RAS. The content of trace elements was determined at the laboratories of the University of Granada in Spain and at the Institute of Geology and Geochemistry using the ICP-MS method. In the eastern direction, the rocks change their composition from predominantly basic to granitoid as they approach the massif. The gneisses of the granitoid composition experienced a high degree of melting; the anatectic melt formed the western part of the Murzinka massif. The granites form three complexes: 1) Yuzhakovo – veins of biotite orthoclase antiperthite granites varying in K_2O content in the metamorphic rocks of the base of the massif; 2) Vatikha – biotite orthoclase antiperthite granites making up the western part of the Murzinka massif; 3) Murzinka – two-mica predominantly microcline granites occurring in the eastern part of the massif. Vatikha and Murzinka granites have the same isotopic age (about 255 Ma). A clear geochemical zonation is revealed in the massif: from west to east (from the base to the roof), the contents of Rb, Li, Nb, Ta increase in the granites of the Vatikha and Murzinka complexes. In the same direction, the ratios K/Rb, Zr/Hf, Nb/Ta decrease, as well as the contents of Ba and Sr. Naturally, the compositions of such rock-forming minerals as plagioclase and biotite also change. The isotopic characteristics of the granites of the Vatikha ($Sr_1 = 0.70868\text{--}0.70923$ and ϵNd_{255} from -8.9 to -11.9) and Murzinka ($Sr_1 = 0.70419\text{--}0.70549$, ϵNd_{255} from -2.6 to $+2.3$) complexes suggest that the substratum of the former was represented by Proterozoic granite-gneisses, whereas the rocks of the newly formed crust, possibly similar to the Silurian-Devonian volcanogenic-sedimentary rocks, which are at contact with the Murzinka granites, served as the substrate for the latter.

Keywords: granites, geochemical zonation, isotopic characteristics of granites, P - T parameters of granite magmatism

Acknowledgments

The work was carried out within project No. 0393-2016-0020 of the state task of the IGG UB RAS, state registration number AAAA-A18-118052590029-6.

INTRODUCTION

The issue associated with the formation of granite massifs has always been at the forefront of attention of petrologists and geochemists. The use of modern analysis methods (including in-situ methods) combined with detailed geological observations allows us to approach the solution of such fundamental issues of granite formation as the duration and stages of the process, its physicochemical parameters, laws and conditions of granite formation and magmatic evolution, sources of granite magmas and fluids.

This article is aimed at considering these issues using the well-studied Murzinka massif (Middle Urals) as an example. The massif in question was described earlier in [Orogenic granitoid magmatism..., 1994]; however, new more accurate analytical data allow us to return to this unique subject matter.

The massif constitutes an interformational sheet-like body reaching up to 10 km in thickness dipping steeply to the east. It is overlain by presumably Devonian volcanic-sedimentary rocks and underlain by Pro-

terozoic para- and orthorocks of the Murzinka-Aduy metamorphic complex (MMC) [Keil'man, 1974; Koroovko, Dvoeglazov, 1986], intruded by numerous granite veins, which we identified in the Yuzhakovo complex (Fig. 1). The massif includes two isotopically coeval granite complexes. Its western part is composed of orthoclase, magnetite and biotite granites from the Vatikha complex, whereas the eastern part comprises microcline-orthoclase and microcline binary granites from the Murzinka complex [Orogenic granitoid magmatism..., 1994]. The veins of chamber pegmatites making up the famous Ural gemstone belt were formed in the bottom part of the massif [Fersman, 1940; Talantsev, 1988], with common pegmatites characterised by rare-metal mineralisation and various metasomatites being formed over its top.

METHODS

The petrogenic elements were determined at the Laboratory for Physicochemical Research Methods of the Zavaritsky Institute of Geology and Geochemistry,

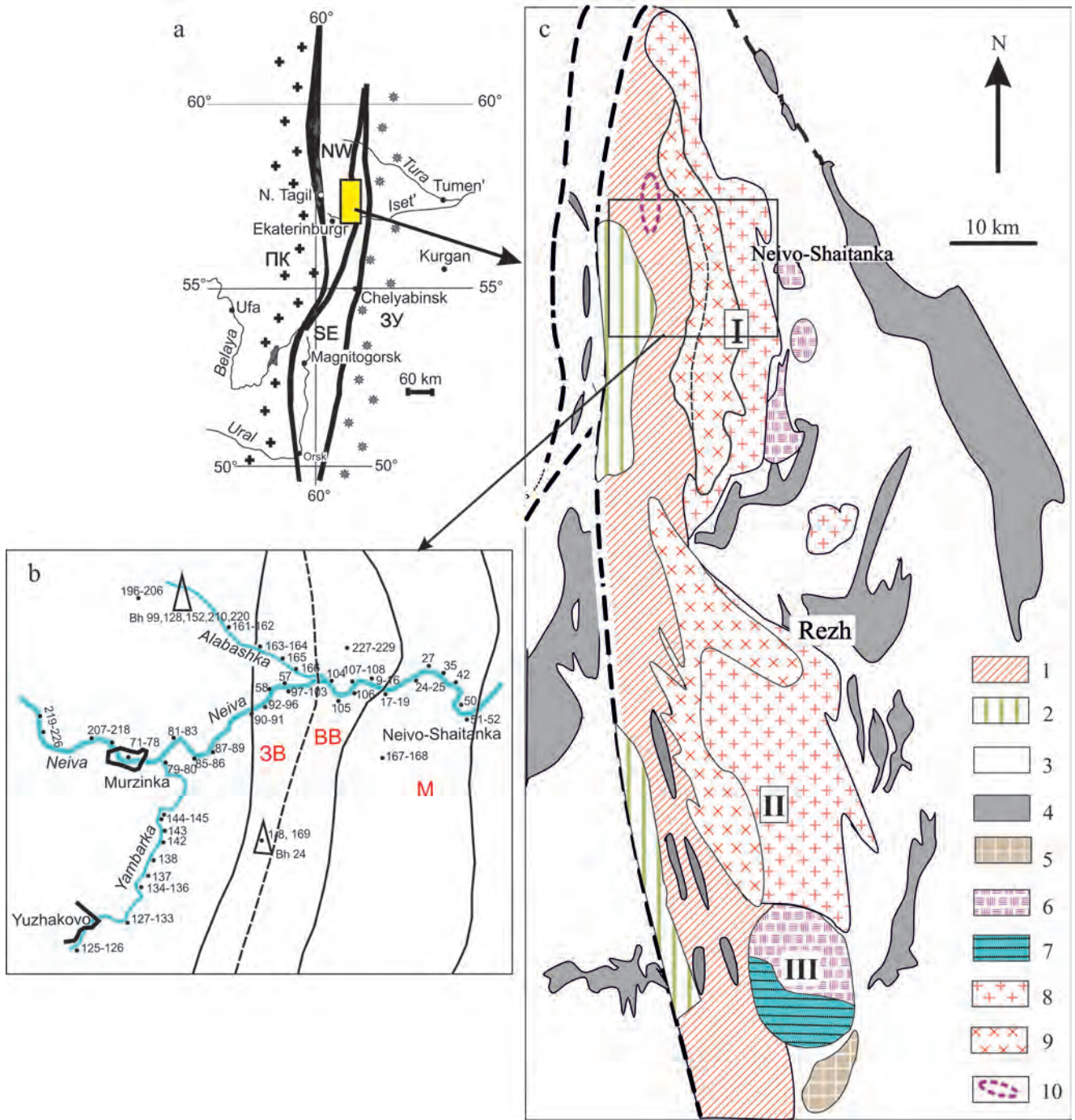


Fig. 1. Location of area under study.

a – the main geological structures of the Urals: ПК – paleocontinental sector, 3У – Trans-Urals, C3 and IOB – island arc-continental megablocks [Fershtater, 2013]. b – a scheme of the placement of Murzinka rock samples mentioned in the text, the contours of the Murzinka massif and approximate areas of the granites of the West Vatikha (WV), East Vatikha (EV) subcomplexes and the Murzinka (M) complex. c – a schematic geological map of Murzinka (I), Aduy (II) and Kamensk (III) massifs, compiled on the basis of the geological map of the Urals, ed. by I.D. Sobolev with authors' changes.

1, 2 – rocks of the Murzinka-Aduy metamorphic complex: 1 – biotite ortho- and paragneisses with interbedded marbles, 2 – high-aluminum ortho- and paragneisses of alkaline-mafic composition; 3 – Silurian-Devonian volcanic-sedimentary rocks; 4 – serpentinites; 5 – Early Devonian migmatized gabbros, trondhjemites and granodiorites; 6, 7 – Carboniferous tonalites, granodiorites and granites (6) and migmatites (7) in Kamensk massif; 8 – two-mica microcline-orthoclase granites, which presumably crystallised from magma formed by the migmatisation of Carboniferous tonalites and granodiorites (Murzinka complex); 9 – biotite antiperthite, essentially orthoclase granites with magnetite, presumably formed through the partial melting of ancient metamorphic strata (Vatikha complex – the dashed line roughly separates the granites of the West and East Vatikha subcomplexes); 10 – Alabashka chamber pegmatite field.

UB RAS (analysts N.P. Gorbunova, L.A. Tatarinova and G.S. Neupokoeva). The content of trace elements was determined at the laboratories of the University of Granada in Spain (analysts F. Bea, P. Montero) using the ICP-MS method and at the Institute of Geology and Geochemistry (analysts D.V. Kiseleva, N.V. Cherednichenko and L.K. Deryugina) using an emission spectral analysis. The accuracy of the analyses comes to 2 and 5 rel % for the concentrations of 50 ppm and 5 ppm, respectively.

Murzinka-Aduy metamorphic complex

At the latitude of the Murzinka granite massif, the rocks of the complex are represented by para- and orthogneisses, whose bulk composition varies from basic to granitoid. The western and central parts of the complex comprise gneisses of mainly basic composition, interstratified with more silicic rocks (Table 1, an. 1–8). In terms of mineral composition, high-alumina (see Table 1, an. 2, 3, 7, 8) and high-alkaline rocks (an. 1, 4–6) are distinguished. The former are represented by the alternation of biotite, biotite-garnet, biotite-cordierite-sillimanite and biotite-corundum gneisses with tourmaline. Corundum gneisses (an. 2) which are similar in terms of mineralogy to corundum syenites from the Ilmeny mountains described in [Levin et al., 1975; Popov, Popova, 1975]: well-formed corundum crystals (0.5–5 cm in size), whose arrangement does not correspond to the gneissic structure, are surrounded by antiperthite plagioclase and immersed in a biotite-plagioclase-quartz-corundum matrix, in which corundum grains are strictly oriented. High-alkaline gneisses are represented by biotite and clinopyroxene-hornblende-biotite varieties with antiperthite plagioclase An_{30-40} characteristic of all metamorphic rocks from the Murzinka complex, as well as a rich complex of accessory minerals: magnetite, sphene, apatite and allanite (see Table 1, an. 4, 5). In terms of mineral and chemical composition, these rocks are close to the so-called vaugnerites – potassium-rich basic and diorite rocks in the Western European variscites (Massif Central, France), which accompany the main phase of granite crust formation and reflect the contribution of the mantle to this process [Sabatier, 1980, 1991; Scarrow et al., 2009]. Researchers attribute the formation of vaugnerites to the most intense, ‘catastrophic’ melting of the crust [Couzinie et al., 2014].

In the area of the Alabashka pegmatite field (see Fig. 1), where many holes were drilled during exploration, the section of metamorphic rocks hosting pegmatite veins is represented by carbonate rocks (calciphyres) interstratified with biotite gneisses of predominantly diorite composition and intruded by the granite and adamellite veins of the Yuzhakovo complex. The metamorphic paragenesis of calciphyres is as follows: calcite, dolomite, phlogopite, diopside and graphite; with the mineral composition of gneisses comprising

biotite, hornblende, sometimes diopside and orthopyroxene, orthoclase, antiperthite plagioclase An_{40-60} , apatite, magnetite. Orthogneisses of diorite and more silicic composition predominate. Paragneisses are characterised by a thin-banded texture and low-strontium content. Granites intrude already metamorphosed rocks. They transect gneissic structures and contain the xenoliths of gneisses and calciphyres metamorphosed in the context of a granulite facies. Rocks that are in contact with the granite veins are skarnified. The following minerals are formed in them: forsterite, diopside porphyroblasts, bytownite An_{70-90} , scapolite, prehnite; phlogopite chloritises; apatite, sphene and sulphides (pyrite, chalcocopyrite) occur in large quantities in them. The skarnification is of the bimetasomatic type, which is manifested in granites by the development of prehnite, scapolite and less commonly diopside. The thickness of endoskarn zones reaches 0.5 m. Unlike granites, chamber pegmatites (Mokrusha and other veins) do not affect the host rocks significantly and have well-defined boundaries with them, without there being any noticeable changes on both sides.

The mineral composition of MMC gneisses – a high titanium content (up to 5.5 wt % in biotite and up to 2 wt % in amphibole), as well as antiperthite plagioclase and poorly structured potassium feldspar – indicates high temperatures of mineral formation corresponding to the granulite facies [Orogenic granitoid magmatism..., 1994].

The easternmost part of the MMC was preserved only in the form of the xenoliths of granite gneisses in Vatikha granites (see Table 1, an. 9–11). The rocks experienced partial melting, whose products formed the western part of the Murzinka massif. The fact that the composition of restite is close to that of adamellite suggests that the composition of protolith was only slightly different from granite and experienced a high degree of partial melting.

The structure of the MMC exhibits latitudinal lateral zonation, which is characterised by an increase in the content of silica in metamorphic rocks from west to east (Fig. 2). This increase reflects the initial change in the composition of the rocks rather than granitisation, which is very weak. The use of some well-known discriminatory diagrams (Fig. 3) confirms the conclusion that rocks that served as the protolith of metamorphic rocks belong to a high-alkaline basalt-andesite series. In this connection, we should recall that G.A. Keil'man [1974] suggested that rocks of the Ilmeny complex constitute the southern continuation of the MMC. The presented data on the rock composition, as well as the presence of such specific gneisses in the MMC as corundum ones, which are not known anywhere in the Urals, except for the Ilmeny Mountains [Levin et al., 1975], confirm this assumption.

The U-Pb age of zircon from a typical biotite diorite gneiss, determined using both the classical method and the LA-ICP-MS, is more than 1600 Ma [Krasnobaev

Table 1. Content of petrogenic (wt %) and trace (ppm) elements in the metamorphic rocks of the Murzinka-Aduy complex

Element	1	2	3	4	5	6	7	8	9	10	11
SiO ₂	49.30	51.64	54.00	55.34	57.17	62.50	66.49	67.66	67.61	69.00	70.15
TiO ₂	2.31	1.12	0.92	1.47	0.90	0.98	0.63	0.85	0.47	0.36	0.26
Al ₂ O ₃	17.91	26.83	16.47	18.19	18.53	16.09	14.35	13.25	16.20	15.55	14.66
Fe ₂ O ₃	2.10	1.21	0.61	2.15	0.46	2.17	2.56	0.70	0.43	0.50	0.46
FeO	8.34	4.33	7.38	5.23	5.00	3.00	2.80	5.60	2.55	2.77	2.90
MnO	0.12	0.03	0.13	0.07	0.10	0.10	0.05	0.05	0.05	0.04	0.05
MgO	3.52	2.45	5	3.16	3.92	2.64	2.72	2.37	0.73	1.26	0.59
CaO	5.44	1.52	6.87	4.52	5.29	4.77	3.11	0.48	1.87	2.34	1.32
Na ₂ O	2.80	5.78	3.44	4.55	4.40	4.36	3.38	2.39	4.89	5.00	3.67
K ₂ O	3.95	3.67	3.2	2.75	2.39	2.00	2.41	5.30	3.26	2.18	4.65
P ₂ O ₅	1.21	0.22	0.25	0.87	0.10	ND	ND	ND	0.17	0.14	0.13
Impurities	2.04	1.17	1.53	1.21	1.33	0.80	0.80	1.00	0.62	0.31	0.59
Σ	99.04	99.97	99.8	99.86	99.59	99.40	99.29	99.65	98.85	99.76	99.43
Li	18.88	73.86	ND	30.00	34.00	25.42	10.59	125.7	14.70	28.00	11.26
Rb	160.8	88.82	73.00	149.0	76.00	66.74	75.76	73.80	31.28	23.00	85.54
Cs	1.83	1.05	ND	2.00	3.00	2.05	1.49	2.32	0.81	1.00	0.62
Be	1.75	6.66	1.00	3.00	3.00	2.21	1.34	1.78	0.68	2.00	1.67
Sr	1370	43.82	460.0	0.00	398.0	345.1	406.1	70.81	745.95	368.0	224.2
Ba	2527	88.74	ND	0.00	431.00	358.8	413.1	185.6	2004.4	468.0	646.7
Sc	13.88	22.22	35.00	16.00	25.00	14.59	14.37	45.24	2.30	9.00	3.53
V	250.2	605.1	170.0	150.0	143.0	102.4	115.7	435.0	25.53	47.00	13.95
Cr	7.58	258.7	49.00	3.00	103.0	94.03	37.19	191.9	0.93	4.00	2.97
Co	17.46	39.74	24.00	15.00	21.00	16.83	13.82	24.80	2.97	5.00	2.16
Ni	18.18	56.31	24.00	18.00	55.00	124.9	22.11	57.32	1.89	2.00	2.44
Cu	28.87	35.19	ND	36.00	8.00	27.81	126.9	18.47	14.99	28.00	7.37
Zn	140.72	29.76	ND	143.0	76.00	64.35	57.18	83.68	60.49	54.00	46.34
Ga	23.39	46.22	ND	16.00	20.00	18.58	14.10	33.45	15.67	16.00	20.26
Y	23.17	1.37	21.00	17.90	19.20	16.94	18.79	7.95	2.78	4.20	6.19
Nb	45.20	7.47	8.00	62.90	18.20	14.22	4.21	2.99	1.55	8.50	5.98
Ta	2.12	0.31	ND	5.10	2.00	1.00	0.23	0.11	0.11	0.80	0.23
Zr	28.83	227.0	123.0	121.0	26.00	21.20	46.12	26.06	62.90	146.0	64.69
Hf	0.96	4.13	ND	1.90	0.80	0.75	1.32	0.52	1.39	2.60	1.90
Mo	3.56	0.17	ND	0.00	0.00	13.18	0.60	0.10	0.07	0.00	0.08
Sn	3.18	1.95	ND	3.30	2.90	2.48	0.54	2.37	0.66	1.80	1.42
Tl	0.75	0.21	ND	0.80	0.40	0.40	0.42	2.61	9.21	9.60	1.18
Pb	13.71	3.45	ND	11.60	11.10	12.41	9.17	9.00	21.62	19.50	28.38
U	2.21	1.74	ND	1.80	0.90	2.03	1.73	0.83	0.78	2.00	1.52
Th	11.35	0.42	ND	15.20	3.00	6.59	4.75	1.12	6.80	9.00	25.50
La	108.5	0.68	21.00	59.40	16.50	18.98	19.54	5.23	9.84	27.70	52.36
Ce	231.7	1.65	ND	140.90	34.30	39.09	41.16	13.36	22.22	48.80	88.00
Pr	21.65	0.29	ND	17.20	4.10	4.56	5.23	1.90	2.50	4.90	11.70
Nd	83.39	1.30	ND	67.70	16.30	17.05	22.06	8.75	9.34	16.40	40.32
Sm	13.45	0.35	ND	11.86	3.65	3.52	4.91	2.09	1.61	2.45	6.19
Eu	3.15	0.07	ND	2.91	1.10	1.05	0.96	0.38	0.40	0.64	0.77
Gd	8.17	0.31	ND	8.78	3.46	3.28	4.35	1.79	0.95	2.08	3.57
Tb	1.00	0.05	ND	1.04	0.59	0.53	0.62	0.24	0.11	0.22	0.41
Dy	5.25	0.31	ND	4.21	3.38	3.19	3.77	1.30	0.60	0.92	1.98
Ho	0.90	0.07	ND	0.70	0.73	0.66	0.75	0.25	0.12	0.16	0.33
Er	2.29	0.21	ND	1.72	2.07	1.98	2.14	0.73	0.40	0.48	0.79
Tm	0.28	0.04	ND	0.20	0.33	0.27	0.28	0.11	0.06	0.06	0.09
Yb	1.60	0.28	3.00	1.13	1.94	1.83	1.72	0.71	0.45	0.32	0.48
Lu	0.20	0.04	ND	0.13	0.28	0.27	0.25	0.10	0.07	0.04	0.06
W	0.55	7.81	ND	ND	ND	1.86	0.74	0.30	0.06	ND	0.09
Ge	1.15	3.24	ND	ND	ND	1.02	0.90	2.35	0.50	ND	0.89
Ag	1.30	0.26	ND	ND	ND	0.44	0.20	0.12	0.14	ND	0.20
As	1.06	0.46	ND	ND	ND	2.5	0.50	0.91	0.03	ND	0.41

Note. 1 – gneiss 73 *Hbl-Bt*, 2 – gneiss 217 *Bt* with corundum, 3 – gneiss 175/42 *Bt-Cpx*, 4 – gneiss 71 *Bt*, 5 – gneiss 127 *Bt*, 6 – gneiss 134 *Cpx-Hbl-Bt*, 7 – gneiss 128/22 *Bt*, 8 – gneiss 220 *Bt-Grt*, 9 – gneiss 85a *Bt* near the contact with the Murzinka massif, 10 – 24/110 a – inclusion in the West Vatikha granite, 11 – 61 inclusion in the West Vatikha granite. 2, 8, 9 – presumably paragneisses, the remaining analyses represent orthogneisses. The number of the borehole given in the numerator, with its depth being stated in the denominator. Trace elements were determined in sample 3 at the laboratory of the Institute of Geology and Geochemistry using the emission spectral method; ND – not detectable.

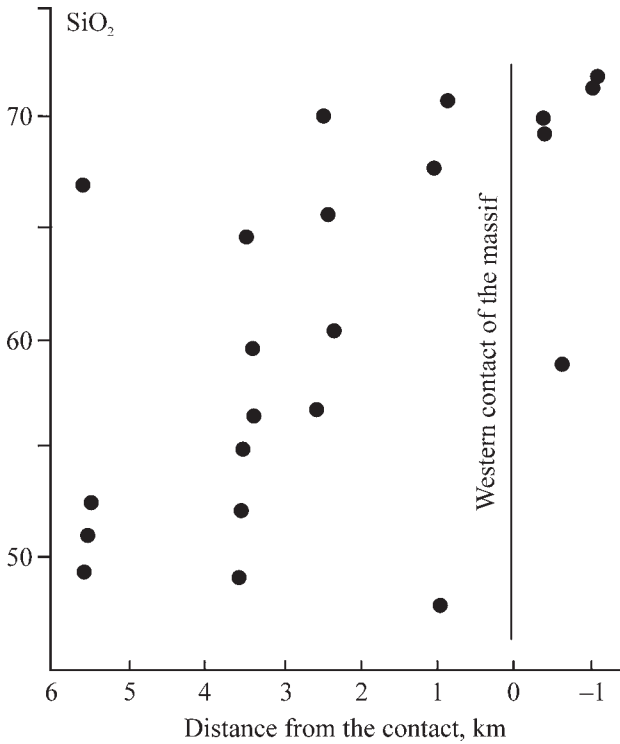


Fig. 2. Dependence of SiO₂ content in gneisses on their distance from the granite massif.

et al., 2005]. The morphological features of zircons indicate their primary crystallisation in the context of a granulite facies and subsequent diaphthorite transformations, which are about 380 million years old.

Chamber pegmatites of the gemstone belt at the base of the granite massif

Among the above-described Mesoproterozoic gneisses at the base of large granite massifs – Murzinska and Aduy – there is a Ural gemstone belt, world-famous for its chamber pegmatites characterised by rich mineralisation [Fersman, 1940]. The main features of pegmatites we will consider using the example of the Mokrusha vein, which is the most famous in the Alabashka pegmatite field (see Fig. 1) and typical of the pegmatites of the entire belt.

The vein occurs among diorite gneisses and carbonate rocks transformed into calciphyres. The host rocks have a submeridional strike and dip east at an angle of 15–20°. The vein occurs along the strike of the host rocks and transects them down the dip. The thickness of the vein ranges from 1.5–2.0 to 9–12 m. As noted above, no noticeable exocontact changes in host gneisses and carbonate rocks are observed. The veins of chamber pegmatites exhibit this feature, which distinguishes them from all other pegmatites associated with the granites of the Murzinka massif and is apparently explained by the fact that most of

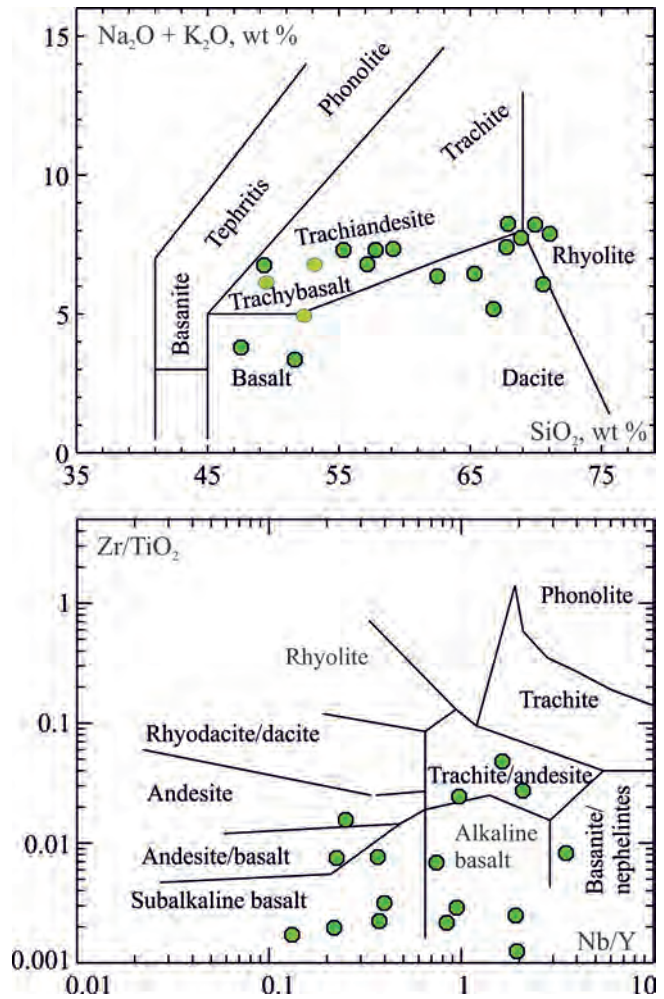


Fig. 3. Position of gneisses in classification diagrams (with authors' simplifications) [Le Maitre, 1989 (Fig. B.14); Winchester, Floyd, 1977 (Fig. 6)].

the fluid in such pegmatites is stored in vugs (cavities) inside the vein and does not interact with host rocks.

A typical cross section of a vein is given using the data of borehole 99 and is as follows. While the biotite granite of the Yuzhakovo complex (Table 2, an. 1) occurs in the hanging wall, the footwall comprises biotite diorite gneiss, which is close in composition to gneiss 128/22 (see Table 1, an. 7). The vein has cross-cutting contacts with both rock varieties. The cross section of the vein section is as follows: 23.7–24.0 m – coarse-graphic pegmatite, 24.0–25.1 m – micro-graphic pegmatite, 25.1–25.8 m – fine-graphic pegmatite, 25.8–27.0 m – block pegmatite, 27.0–29.7 m – spherulitic pegmatite, 29.7–33.2 m – fine-grained pegmatite. The compositions are given in Table 2. Fine-graphic zones (1–2 cm thick) are observed in the upper and lower endocontacts. In these zones, quartz ichthyoglipts are oriented perpendicular to the contact, which is possibly a consequence of quenching.

Table 2. Content of petrogenic (wt %) and trace (ppm) elements in granite from the hanging wall of the Mokrusha pegmatite vein (1) and from graphic pegmatites of this vein (2–5). Borehole 99

Element	1	2	3	4	5	6	Element	1	2	3	4	5	6
SiO ₂	72.11	74.84	75.2	77.02	76.19	74.92	Zr	54.58	11.95	11.03	13.44	40.00	46.29
TiO ₂	0.18	0.05	0.02	0.01	0.01	0.03	Hf	1.13	0.65	1.02	0.92	5.08	2.75
Al ₂ O ₃	14.64	12.99	12.71	12.63	13.18	12.74	Mo	0.57	0.04	0.22	0.16	0.39	0.15
Fe ₂ O ₃	0.38	0.33	0.19	0.11	0.96	0.35	Sn	0.54	0.69	8.92	9.24	15.46	2.20
FeO	1.49	1.87	1.74	1.95	1.92	1.72	Tl	0.41	0.65	1.99	1.70	1.36	1.68
MnO	0.06	0.02	0.03	0.05	0.55	0.04	Pb	15.77	34.79	29.87	26.78	7.34	24.81
MgO	0.28	0.1	0.1	0.1	0.1	0.1	U	59.73	1.56	2.33	1.99	18.12	11.23
CaO	1.21	1.17	0.91	0.58	0.44	0.61	Th	4.99	11.60	2.66	0.96	8.08	22.63
Na ₂ O	3.35	4.11	3.89	5	4.77	4.02	La	33.18	3.93	2.31	1.84	6.50	4.47
K ₂ O	5.78	4	5.05	2.18	1.14	4.88	Ce	54.13	9.06	5.02	3.94	18.13	11.94
P ₂ O ₅	0.08	0.01	0.01	0.01	0.01	0.01	Pr	5.53	1.21	0.54	0.39	2.39	1.67
Impurities	0.39	0.05	0.1	0.21	0.69	0.3	Nd	18.25	4.81	1.80	1.27	9.01	6.84
Σ	99.95	99.57	99.95	99.85	99.96	99.72	Sm	2.34	1.15	0.65	0.40	5.70	2.17
Li	57.31	50.35	405.50	496.86	352.86	12.91	Eu	1.20	0.06	0.01	0.00	0.02	0.06
Rb	60.98	81.23	253.63	348.64	290.42	174.60	Gd	1.31	0.85	0.65	0.45	11.88	1.98
Cs	6.54	5.44	74.95	69.29	52.29	7.85	Tb	0.14	0.11	0.13	0.09	3.47	0.32
Be	2.28	1.57	4.16	4.87	15.70	4.86	Dy	0.72	0.51	0.85	0.55	24.59	1.93
Sr	353.73	10.96	1.11	0.90	2.83	7.56	Ho	0.12	0.08	0.15	0.10	4.24	0.43
Ba	970.37	19.97	8.05	6.82	14.73	8.87	Er	0.30	0.19	0.43	0.28	10.32	1.43
Sc	3.13	1.53	5.63	7.58	17.15	3.74	Tm	0.04	0.02	0.06	0.04	1.34	0.23
V	20.19	1.32	0.33	0.48	0.45	0.44	Yb	0.22	0.15	0.41	0.26	7.48	1.68
Cr	1.01	0.66	1.71	2.28	0.63	1.45	Lu	0.03	0.02	0.05	0.03	0.76	0.27
Co	3.03	0.25	0.07	0.11	0.10	0.15	W	8.70	0.66	2.42	2.24	12.20	0.85
Ni	1.64	0.72	0.31	0.48	0.39	1.45	Bi	0.03	0.04	4.88	3.47	6.35	0.47
Cu	9.95	2.67	2.58	6.47	3.04	3.24	Cd	0.04	0.03	0.08	0.08	0.32	0.06
Zn	49.43	11.15	47.56	63.29	63.00	12.01	Ge	0.71	1.25	2.38	3.08	3.59	1.71
Ga	21.05	16.23	21.31	27.79	30.20	16.07	Ag	0.54	0.24	0.85	0.71	1.18	0.42
Y	3.68	1.57	3.79	3.65	157.88	7.32	Sb	0.36	0.41	0.72	0.71	2.20	0.20
Nb	18.23	7.41	29.51	34.01	40.42	13.04	As	1.27	1.40	5.34	6.05	8.22	0.47
Ta	0.30	0.42	2.74	2.39	4.93	1.70							

Note. 1 – a depth of 23.4 m (granite in contact with the vein); 2–5 – graphic texture: 2 – 23.7 m, 3 – 24.3 m, 4 – 25.1 m, 5 – 43.0 m – fine graphic texture in the upper endocontact of the vein.

The widespread development of graphic intergrowths of quartz with plagioclase and potassium feldspar provided the possibility to study the conditions for the formation of pegmatites of the Mokrusha vein in detail. These structures always arise as a result of eutectic crystallisation under conditions close to the system $P_{H_2O} = P_{total}$. The content of quartz in such intergrowths is strictly correlated with the composition of feldspar and is determined by the pressure during crystallisation [Fershtater, 1987]. The results of studying the cross section of the vein (borehole 99) in terms of the composition of quartz-feldspar intergrowths are given in Table 3.

The obtained data indicate meso-abyssal conditions for the formation of the Mokrusha vein. An increase in the quartz content in quartz-feldspar intergrowths in the granite of the hanging wall, which is in direct contact with the vein, and in the zone of fine-grained pegmatite at the base of the vein (and, accordingly, lower pressure values) is apparently due to a decrease in P_{H_2O} . All other pressure values correspond to $P_{H_2O} = P_{total}$.

Table 3. Quartz content in graphic intergrowths with K-field-spar and plagioclase in the croce section of the Mokrusha vein, borehole 99 (according to the results of counting in thin sections)

Zone	Depth, m	Quartz content, vol %		P_{H_2O} , kb
		$Fsp + Q$	$Pl + Q$	
Host adamellite	23.3–23.7	39	44	2
Coarse-graphic	23.7–24.0	33	40	3
Micro-graphic	24.0–25.1	34	38	3–4
Micro-graphic	25.1–25.8	33	38	3–4
Block	25.8–27.0	–	–	–
Spherulitic	27.0–29.7	33	37	3–4
Fine-grained pegmatite	29.7–33.2	38	41	2

It is important to note that chamber pegmatites of the Mokrusha type exhibit a particular geochemical feature, which reliably distinguishes them from all other pegmatites associated with various granites of the Mur-

zinska massif. Mokrusha pegmatites (see Table 2) are characterised by an extremely low (less than 10 ppm) content of Sr and Ba with low K/Rb (<100) and Zr/Hf (<20) ratios, whereas in all other pegmatites the above-mentioned parameters are similar to those of granites. These features indicate that Mokrusha pegmatite bodies did not participate in the formation of granite massifs. At the same time, such pegmatites in many cases complete the evolutionary trends of granites of the Murzinska massif, which allows us to consider them as the latest manifestations of granite magmatism, which is consistent with the K-Ar age of pegmatite mica coming to 220–250 Ma [Borshchov, Fershtater, 2017]. The presented data suggest that most of chamber pegmatites of the gemstone belt formed after the completion of granite magmatism, which formed the Murzinka massif. It can be assumed that the granite component of chamber pegmatites is not manifested. An example would be the pegmatite fields in Norway and Sweden consisting of many thousands of pegmatite veins that show no connection with granites [Muller et al., 2017].

Yuzhakovo complex of veined granitoids

The granitoids of this complex are localised west of the Murzinska massif, within the metamorphic complex. They do not form large bodies; however, the numerous veins of these rocks often predominate in volume over the host metamorphic rocks.

Early veins (first generation) are represented by biotite gneiss-like plagiogranites, usually in the form of pygmic folds (Table 4, an. 1–3, 5). The rocks comprise antiperthite plagioclase An_{30-40} , quartz and red-brown high-titanium biotite. Rare potassium feldspar is represented by orthoclase, with the accessory minerals including apatite and sphene. The plagiogranite formation is completed by thin plagiopegmatite veins and plagiogranite areas, followed by gneiss-like or massive granites and adamellites characterised by a higher potassium content, which varies widely, reaching 4.78 wt % (see Table 4, an. 4, 6). It should be noted that the gneissic structure of such veins always coincides with their strike, i.e. it is, clearly, syngenetic and, naturally, has a different direction as compared to earlier plagiogranites.

Second-generation veins represented by granites and adamellites are most widespread (see Table 4, an. 7–11). These rocks often exhibit gneissic structures, whose direction does not coincide with that of the gneissic structures in the first-generation veins. Similar associations are repeated in all outcrops and indicate that the granites of the Yuzhakovo complex formed under orogenic conditions: each completed episode of granite formation, whose completion is indicated by the presence of pegmatites, corresponded to its own stress direction. The episodes of tectonic and magmatic activity coincided. It should be noted that all the veins of the Yuzhakovo complex constitute intru-

sive bodies, which are not associated with any noticeable migmatization (partial melting). The development of insignificant quartz-feldspar areas in gneisses, possibly associated with partial melting, precedes the introduction of the earliest veins of the Yuzhakovo granites.

Murzinka Massif

Western part – Vatikha complex. The identification of granites making up the western part of the Murzinka massif as a separate complex was determined by the distinctive petrographic character of rocks including antiperthite plagioclase An_{20-25} and poorly structured feldspath (orthoclase) [Orogenic granitoid magmatism..., 1994]. These mineralogical features bring Vatikha granites closer to the Yuzhakovo ones; however, unlike the latter, the Vatikha granites form a large body, constituting at least half of the total volume of the Murzinka Massif, rather than separate veins. The rocks are characterised by a prismatic-granular structure and contain porphyritic segregations of orthoclase and magnetite. The presence of the latter is due to the increased magnetic field in the western part of the massif, which clearly marks the distribution of Vatikha rocks. The plagioclase present in them is noticeably enriched with the albite component as compared to plagioclase in the Yuzhakovo granites of the same silica content (60–70 and 75–80 mol %, respectively). Accessory minerals are diverse – orthite, apatite, zircon, xenotime and monazite.

In the western part of the complex, the predominating adamellites and granites contain the xenoliths of more melanocratic rocks of granodiorite and adamellite composition, which we interpret as protolith restites preserved under a high degree of the partial melting of rocks having a composition close to that of adamellite (see Table 1, an. 9–11). The granites and adamellites that formed have a specific composition (Table 5, an. 1–4) and are identified as the West Vatikha subcomplex. It is these granites that exhibit the strongest similarities with the Yuzhakovo granites. Granites occurring to the east of the East Vatikha subcomplex are much more uniform in composition (see Table 5, an. 5–7) than the West Vatikha granites; they do not contain antiperthite plagioclase and are slightly enriched with rubidium, as compared to the latter, in accordance with the general geochemical zonation of the massif (see below).

Eastern part of the Murzinka massif – Murzinka complex. These granites intrude the Vatikha granites in the west, as well as volcanic-sedimentary and sedimentary rocks metamorphosed in the context of greenschist and epidote-amphibolite facies in the east. Near the top, granites become leucocratic; the number of aplite and pegmatite veins in them increases, reaching 50–60% of the volume. The contact itself is typically of the injection type: numerous granite apophyses, aplite and pegmatite veins penetrate the host rocks, which un-

Table 4. Content of petrogenic (wt %) and trace (ppm) elements in the granites of the Yuzhakovo complex

No.	1	2	3	4	5	6	7	8	9	10	11
Sample	112a	128	114	112b	129	115_2	130	131	123	128/52	84b
SiO ₂	73.99	72.5	69.81	72.28	72.1	70.21	71.68	70.76	68.9	70.02	71.22
TiO ₂	0.08	0.10	0.19	0.06	0.14	0.26	0.13	0.25	0.39	0.670	0.17
Al ₂ O ₃	15.45	15.9	15.65	14.09	15.8	15.09	15.47	15.29	15.9	13.39	15.38
Fe ₂ O ₃	0.45	ND	1.12	0.53	ND	0.3	0.1	0.39	0.24	2.05	0.26
FeO	0.8	1.37	2.55	3.98	1.69	2.01	1.48	1.61	2.24	2.1	2.61
MnO	0.05	ND	0.05	0.05	0.01	0.05	0.05	0.05	0.05	0.020	0.05
MgO	0.26	0.31	0.61	0.24	0.43	0.59	0.27	0.43	0.56	1.39	0.35
CaO	2.67	2.95	4.19	1.87	3	1.46	2.11	1.31	1.33	1.68	1.66
Na ₂ O	4.56	4.82	3.69	4.03	4.61	3.79	4.25	3.94	3.4	3.17	3.12
K ₂ O	0.67	0.81	0.69	2.2	0.86	4.78	3.15	4.61	5.68	4.99	4.6
P ₂ O ₅	0.05	0.05	0.12	0.05	0.05	0.09	0.11	0.08	0.11	0.131	0.05
Impurities	0.16	0.32	0.65	0.43	0.44	0.33	0.11	0.12	0.24	0.3	0.44
Σ	99.19	99.12	99.37	99.81	98.14	96.7	100.28	100.16	99.04	99.89	99.91
Li	43.45	9	13	31.63	15	38.57	11	15	32.34	9.87	10.07
Rb	2.62	7	14	26.27	25	56.75	40	95	57.76	83.41	48.55
Cs	0.42	0.5	0	0.25	0.8	0.91	1	1	1.71	0.55	0.47
Be	9.59	1.9	1	5.24	1.5	3.53	3	1	2.88	1.35	0.88
Sr	177.9	286	533	283.7	441	298.5	365	521	231.7	413.1	803.2
Ba	104.4	135	78	349.8	238	1143	960	0	1612	1303	1877
Sc	15.89	1.3	10	6.5	21.1	8.97	4	8	5.42	5.03	1.14
V	18.48	12	20	18.38	18	35.31	9	17	46.33	47.90	9
Cr	22.3	0	0	27.44	0	14.72	0	2	15.38	4.95	3.83
Co	3.44	1.3	2	4.09	2.2	4.47	1	3	4.99	4.90	1.4
Ni	32.74	0	0	24.39	0	10.64	0	4	5.25	2.89	3.19
Cu	12.6	0	1	50.38	0	11.5	3	11	11.07	9.70	10.13
Zn	33.85	11	27	42.14	19	95.55	0	33	106.1	66.58	49.59
Ga	39.89	17	16	28.51	15	27.5	12	9	33.46	20.16	15.06
Y	1.61	1	8	0.72	3.7	1.44	5.2	3.2	1.52	3.61	2.17
Nb	4.65	1.3	4.3	1.38	2.3	6.07	4.3	3.3	9.62	7.89	0.87
Ta	0.18	0.1	1.9	0.07	0.2	0.17	0.7	0.3	0.32	0.28	0.07
Zr	47.21	54	14	24.03	121	230.5	143	213	359.5	55.28	83.77
Hf	1.41	1.7	0.3	0.6	3.2	3.51	3	3.9	5.87	1.35	2.15
Mo	2.94	ND	0	1.69	ND	0.65	0	0	0.42	1.41	0.05
Sn	1.61	ND	0.2	1.98	ND	3.31	1.6	1.4	2.2	1.18	0.53
Tl	0.15	ND	0.2	0.2	ND	0.5	0.4	0.5	0.58	0.40	0.66
Pb	15.47	13	6.6	19.14	14	30.61	24.1	33.8	28.63	16.35	22.09
U	0.39	0.5	0.2	0.44	1.9	1.91	0.6	1.7	2.46	1.02	1.23
Th	1.98	3.5	0.5	1.95	11	5.91	6	14.6	10.1	24.74	7.53
La	0.58	3.5	5.4	1.25	15	5.54	12.5	41.7	15.2	101.6	7.61
Ce	1.69	12	16.7	2.48	39	11.94	45.2	70.9	29.79	184.7	16.36
Pr	0.22	0.78	1.5	0.37	3.1	1.36	3.2	7.5	3.05	14.71	1.93
Nd	0.95	2.5	6.1	1.4	11	4.9	11.9	24.7	9.95	46.62	7.4
Sm	0.32	0.6	1.35	0.34	1.8	0.84	2.65	3.36	1.33	5.23	1.38
Eu	0.19	0.53	0.68	0.23	0.85	0.2	1.17	1.11	0.25	1.32	0.48
Gd	0.34	0.4	1.37	0.23	1.3	0.55	2.26	2.44	0.57	2.29	0.86
Tb	0.05	0.05	0.22	0.03	0.15	0.07	0.27	0.22	0.06	0.22	0.1
Dy	0.29	0.26	1.31	0.17	0.72	0.32	1.19	0.79	0.29	0.94	0.52
Ho	0.05	0.03	0.29	0.03	0.15	0.06	0.2	0.12	0.05	0.14	0.09
Er	0.15	0.07	0.86	0.08	0.37	0.14	0.54	0.35	0.14	0.35	0.26
Tm	0.02	0.01	0.14	0.01	0.06	0.02	0.07	0.04	0.02	0.04	0.04
Yb	0.14	0.03	0.89	0.08	0.35	0.12	0.44	0.21	0.15	0.24	0.22
Lu	0.02		0.14	0.01	0.06	0.02	0.06	0.03	0.02	0.03	0.04

Note. 1-6 – the first generation of veins, 7-11 – the second generation of veins, ND – not detectable.

Table 5. Content of petrogenic (wt %) and trace (ppm) elements in the granites of the Vatikha (1–7) and Murzinka (8–12) complexes

No.	1	2	3	4	5	6	7	8	9	10	11	12
Sample	91	92	66	57	106	15	10	17	23	26	42	51
SiO ₂	72.56	71.12	72.48	71.03	73.16	72.88	71.19	74.66	73.87	74.15	72.48	72.65
TiO ₂	0.15	0.13	0.14	0.17	0.17	0.12	0.24	0.47	0.09	0.10	0.14	0.11
Al ₂ O ₃	14.80	14.25	14.88	14.59	14.30	12.99	14.69	13.83	13.65	14.23	15.27	14.74
Fe ₂ O ₃	0.10	0.31	0.49	0.55	0.31	0.45	0.42	0.10	0.34	0.23	0.10	0.45
FeO	1.67	2.51	1.22	2.12	2.04	1.74	2.60	1.61	2.06	2.14	1.58	1.35
MnO	0.05	0.05	0.05	0.05	0.05	0.05	0.05	0.05	0.05	0.05	0.05	0.05
MgO	0.37	0.31	1.40	0.36	0.93	0.98	0.35	0.11	0.29	0.14	0.29	0.24
CaO	1.18	1.35	1.40	1.07	0.93	0.98	1.19	0.96	0.64	0.80	1.48	1.18
Na ₂ O	3.64	3.85	3.88	3.45	3.62	3.79	3.39	3.70	3.51	3.64	4.82	4.50
K ₂ O	5.34	4.68	4.33	5.05	5.15	4.23	4.31	4.50	4.50	4.54	3.19	3.34
P ₂ O ₅	0.08	0.09	0.05	0.08	0.05	0.05	0.07	0.05	0.05	0.05	0.05	0.05
Σ	99.96	98.65	98.24	99.03	98.63	99.33	98.80	99.14	99.05	98.66	99.45	98.66
Li	10.12	11.35	7.00	10.70	9.00	13.00	16.00	17.00	24.00	36.00	100.00	135.00
Rb	61.89	66.71	71.00	86.19	137.0	124.0	131.0	176.0	257.0	266.0	105.0	129.0
Cs	0.37	0.51	0.00	0.63	1.00	1.00	1.00	1.00	1.00	2.00	5.00	8.00
Be	1.71	1.95	2.00	1.22	1.00	2.00	1.00	2.00	2.00	3.00	3.00	6.00
Sr	216.3	212.8	313.0	212.2	142.0	89.0	259.0	107.0	96.0	106.0	200.0	336.0
Ba	1048	895.5	779.0	982.8	482.0	282.0	0.0	318.0	355.0	343.0	721.0	0.0
Sc	1.51	2.89	6.00	3.11	6.00	7.00	8.00	8.00	10.00	8.00	6.00	5.00
V	8.60	14.86	10.00	19.22	4.00	6.00	15.00	4.00	2.00	5.00	14.00	13.00
Cr	1.76	5.95	0.00	37.89	0.00	0.00	0.00	0.00	0.00	0.00	0.00	0.00
Co	1.02	1.90	1.00	2.61	1.00	1.00	2.00	1.00	1.00	1.00	1.00	1.00
Ni	1.20	5.43	0.00	57.45	0.00	0.00	0.00	0.00	0.00	0.00	0.00	0.00
Cu	3.73	11.73	9.00	13.82	1.00	1.00	5.00	1.00	1.00	1.00	7.00	1.00
Zn	33.59	38.17	0.00	47.01	0.00	13.00	28.00	31.00	38.00	26.00	24.00	24.00
Ga	16.68	18.18	14.00	19.59	15.00	18.00	12.00	19.00	21.00	20.00	17.00	10.00
Y	1.69	2.01	2.60	2.39	9.40	6.80	6.90	6.50	12.10	6.90	1.90	2.10
Nb	2.61	4.00	2.80	5.69	11.50	11.10	15.40	14.60	23.30	19.40	14.40	10.20
Ta	0.14	0.27	0.20	0.25	2.20	1.30	1.60	1.20	23.40	2.20	1.50	2.20
Zr	83.13	40.95	149.00	84.88	145.0	93.00	204.0	93.00	103.0	106.0	125.0	106.0
Hf	2.74	1.44	3.10	2.38	3.50	2.60	4.40	2.70	2.90	2.80	3.10	2.50
Mo	0.06	0.39	0.30	8.33	0.00	0.00	0.00	0.00	0.00	0.00	0.00	0.00
Sn	0.78	1.34	0.30	1.73	0.70	1.50	0.70	2.10	5.10	3.00	3.40	4.40
Tl	0.87	0.58	1.90	0.70	1.00	6.80	0.80	1.20	1.30	2.80	4.00	1.10
Pb	30.99	26.54	18.00	31.44	25.50	25.20	28.10	33.40	33.90	27.60	19.90	19.90
U	0.77	0.79	0.70	1.47	2.60	2.20	3.10	2.70	5.50	2.90	1.50	1.30
Th	17.26	26.21	31.40	16.97	37.40	22.00	22.90	22.10	29.20	25.30	3.70	2.20
La	14.48	27.25	14.30	30.68	76.50	38.20	63.50	41.30	44.50	45.10	7.60	5.50
Ce	36.68	42.10	39.80	63.18	140.20	73.20	117.70	77.30	83.60	84.50	14.00	10.70
Pr	3.66	4.72	3.00	7.21	14.70	7.90	11.80	8.30	8.90	9.00	1.60	1.20
Nd	12.54	16.22	10.60	24.15	48.50	25.90	37.40	27.10	29.00	29.40	5.40	4.20
Sm	2.11	2.61	1.98	3.68	8.35	5.02	5.22	5.47	5.93	5.14	0.96	0.80
Eu	0.49	0.52	0.68	0.58	0.67	0.47	0.97	0.57	0.57	0.53	0.29	0.33
Gd	1.09	1.57	1.57	2.01	6.51	3.91	4.06	4.23	4.85	3.98	0.77	0.63
Tb	0.13	0.15	0.17	0.19	0.75	0.48	0.43	0.48	0.65	0.46	0.09	0.09
Dy	0.67	0.73	0.68	0.84	2.63	1.89	1.67	1.79	2.69	1.81	0.37	0.43
Ho	0.11	0.12	0.11	0.13	0.39	0.28	0.29	0.26	0.47	0.28	0.06	0.06
Er	0.30	0.28	0.24	0.33	0.91	0.61	0.81	0.60	1.11	0.67	0.16	0.16
Tm	0.04	0.03	0.03	0.04	0.08	0.07	0.11	0.06	0.16	0.08	0.02	0.03
Yb	0.22	0.20	0.17	0.22	0.44	0.41	0.72	0.37	0.87	0.52	0.14	0.14
Lu	0.03	0.03	0.01	0.03	0.05	0.05	0.11	0.05	0.12	0.07	0.02	0.02

Note. The Vatikha complex: west (1–4) and east (5–7) subcomplexes, the Murzinka complex (8–12): numbers of samples increase from west to east.

dergo strong hydrothermal transformations – micasation, silicification, albitisation, and K-feldsparisation.

The compositions of granites are given in Table 5 (an. 8–12). These are predominantly two-mica varieties. Biotite predominates in the western part, with the role of muscovite growing in the eastern part. Spessartine-almandine garnet, which is more common for aplites and pegmatites, often occurs in paragenesis with muscovite. Plagioclase is characterised by an even higher content of the albite component than in Vatikha granites – An_{12-18} . Antiperthites are absent. Potassium feldspar is represented by both orthoclase and microcline. The role of the latter is growing from west to east. Myrmekite is widespread.

ISOTOPIC STUDIES

Isotopic studies reveal that the granitoids of the Vatikha and Murzinka complexes exhibit approximate uniformity in terms of ages. The ^{207}Pb - ^{206}Pb age of zircon and the Rb-Sr age of the rock are generally the same – 254 ± 5 Ma [Montero et al., 2000; Gerdes et al., 2002], whereas the values of $^{87}\text{Sr}/^{86}\text{Sr}$ and ϵNd_{255} (Table 6) indicate a different substrate.

Yuzhakovo plagiogranites are characterised by a low initial $^{87}\text{Sr}/^{86}\text{Sr}$ ratio and a positive or near-zero ϵNd value, while the eastern granites of the Yuzhakovo complex located near the Murzinka massif (sample 115) and Vatikha granites have high $^{87}\text{Sr}/^{86}\text{Sr}$ ratios and negative ϵNd_{255} values ($\text{Sr}_i = 0.70868$ – 0.70923 and ϵNd_{255} from -8.9 to -11.9), indicating their origin from an ancient sialic substrate. Murzinka granites are markedly different in their geochemical parameters. They are characterised by the low contents of radiogenic Sr ($\text{Sr}_i = 0.70419$ – 0.70549) and the near-zero values of ϵNd_{255} (from -2.6 to $+2.3$), which fall to -8.9 only in the westernmost part of the complex (see Table 6, sample 22). There is practically no doubt that the rocks of the newly formed crust – possibly similar to the Silurian-Devonian volcanic-sedimentary strata that are in contact with Murzinka granites – constituted the substrate of these granites.

Geochemical zonation

The identified granite complexes are markedly different in their geochemical parameters. In terms of most petrogenic elements, the granitoids of different complexes exhibit uniformity, except for the early granites of the Yuzhakovo complex characterised by high calcium and low potassium contents (Fig. 4). The most striking differences are detected in the concentrations of rubidium, according to which granites form a clear evolutionary series (in increasing order of element concentrations): 1) first-generation veins of the Yuzhakovo complex; 2) second generation veins of the Yuzhakovo complex, West Vatikha subcomplex; 3) East Vatikha subcomplex; 4) Murzinka complex. A similar trend is observed for niobium and tantalum. The K/Rb, Zr/Hf and Nb/Ta ratios, as well as barium and strontium contents, decrease in the same direction (Fig. 5). Importantly, the same trend is clearly observed for lithium, whose contents increase sharply in the granites of the Murzinka complex (Fig. 6).

The spatial distribution of the described trends is demonstrated by the geochemical profile of the Murzinka massif (Fig. 7). It is easy to see that within the massif, i.e. in the rocks of the Vatikha and Murzinka complexes, Rb and Li contents gradually increase from west to east and the K/Rb ratio decreases. In terms of potassium content and the K/Rb ratio, the rocks of the Yuzhakovo complex do not exhibit this trend. However, in terms of the K/Rb ratio, the rocks of second-generation veins follow the general trend.

The geochemical zonation of the rocks is naturally reflected in the composition of such rock-forming minerals as plagioclase and biotite. As previously noted, the content of the anorthite component in plagioclase naturally decreases from the Yuzhakovo complex to the Murzinka complex, with the titanium content decreasing and the contents of rubidium and lithium increasing in biotite in the same direction (Fig. 8). Recent data indicate that the described geochemical zonation emerged at the magmatic stage, given that the above-mentioned minerals characterise

Table 6. Sr and Nd isotopic parameters of the rock as a whole for the granites of Yuzhakovo (1–3), Vatikha (4–6) and Murzinka (7–10) complexes according to [Gerdes et al., 2002]

No.	Sample	Rb	Sr	$^{87}\text{Rb}/^{86}\text{Sr}$	$^{87}\text{Sr}/^{86}\text{Sr}$	$^{87}\text{Sr}/^{86}\text{Sr}_i$	Sm	Nd	$^{147}\text{Sm}/^{144}\text{Nd}$	$^{143}\text{Nd}/^{144}\text{Nd}$	ϵNd_{255}	D, km
1	129	26.5	519	0.1476	0.7047	0.70416	1.8	10.63	0.1026	0.512692	4.1	ND
2	128	77.8	393	0.572	0.70629	0.70418	ND	ND	ND	ND	ND	ND
3	115	124	409	0.8803	0.71241	0.70922	2.8	17.69	0.0956	0.512467	-0.05	ND
4	61	60.6	181	0.9711	0.71275	0.70923	3.02	19.45	0.0938	0.51196	-9.9	1.5
5	9	139	130	2.687	0.71886	0.70912	3.34	21.39	0.0945	0.511942	-10.3	4.7
6	17	164	96	4.948	0.72663	0.70868	3.38	16.11	0.1269	0.511911	-11.9	4.8
7	22	214	73	8.523	0.7354	0.70447	3.07	15.89	0.1169	0.512048	-8.9	6.0
8	42	168	250	1.949	0.71166	0.70459	0.92	4.89	0.1142	0.512659	2.3	8.0
9	50	210	106	5.725	0.72496	0.70419	2.87	15.92	0.1088	0.512359	-2.6	9.1
10	51	123	288	1.234	0.70997	0.70549	0.54	2.65	0.1277	0.512634	2.3	9.1

Note. D – distance from the western contact of the massif. See rocks compositions in Tables 4 and 5. ND – not detectable.

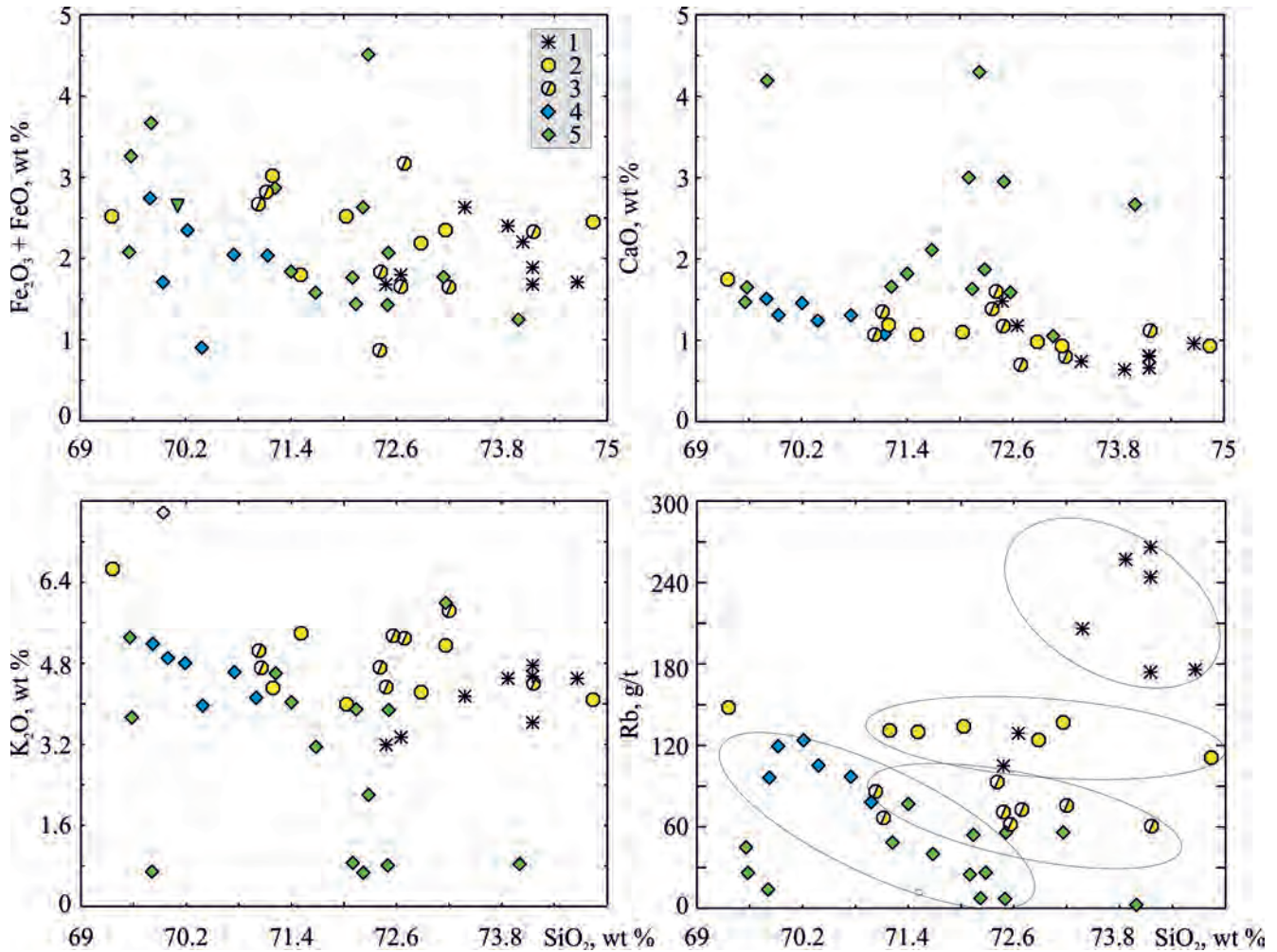


Fig. 4. ($\text{Fe}_2\text{O}_3 + \text{FeO}$), CaO, K_2O , Rb versus SiO_2 for granites.

Complexes: 1 – Murzinka; 2 – West Vatikha; 3 – East Vatikha; 4, 5 – Yuzhakovo: 4 – first generation of veins, 5 – second generation of veins.

precisely this stage of rock formation. As for the intense hydrothermal activity at the top of the massif, it is caused by a fluid released from the crystallising granite melt and is enriched with such elements as rubidium, lithium, niobium and tantalum, which granites are also rich in.

The clearly expressed geochemical zonation of the Murzinka Massif is accompanied by the increasing number of pegmatoid granites in the eastward direction (towards the top of the massif). They are noted throughout the entire cross section of the massif and uniformly share common geochemical features with host granites, thus being part of in the general zonation of the massif. This feature indicates that pegmatoid granites are the products of magmatic evolution that occurred there and confirms the conclusion made earlier about the magmatic nature of zonation drawing on a regular change in the composition of the main rock-forming minerals – plagioclase and biotite. It can be

assumed that during the crystallisation of granite magma saturated with water, even at the magmatic stage, fluid enriched with elements (rubidium, lithium, niobium, tantalum, hafnium and beryllium) is separated and gradually concentrated in the upper part of the massif. Naturally, granites are enriched with the specified elements as well. It can be assumed that the proposed mechanism underlying the fluid-magma differentiation ensures the geochemical zonation of the massif, as well as creates a metasomatic halo and rich mineralisation (niobium, tantalum, molybdenum, beryllium, emeralds) in the zone overlying intrusions, which is most vividly manifested in association with the Aduy massif – the southern continuation of Murzinka.

A clear one-sided geochemical zonation, common for the entire massif, is consistent with its interformational position and stratiform shape, indicating the existence of a single magma chamber where the differentiation of the crystallising melt took place. This is also

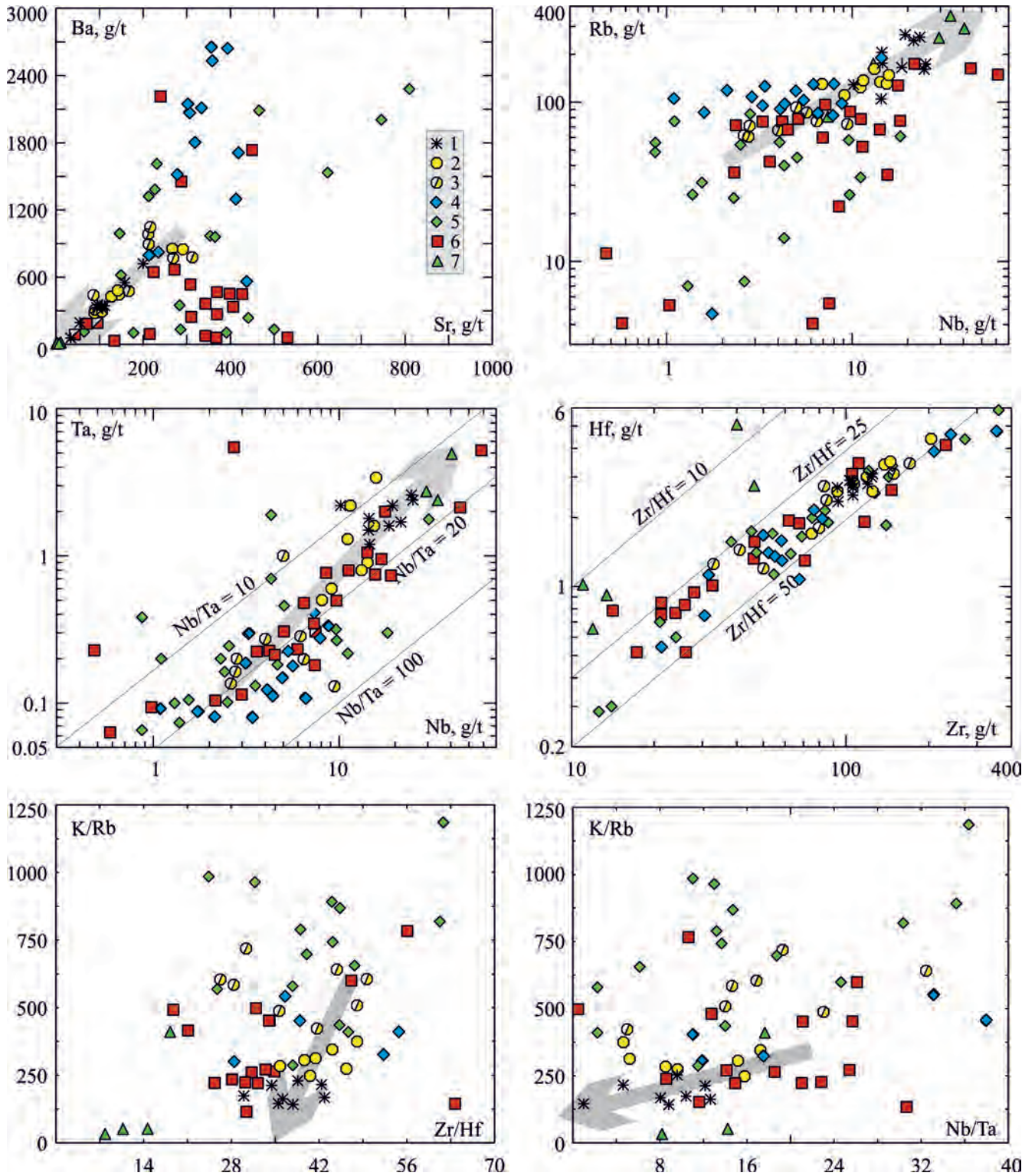


Fig. 5. Diagrams showing the distribution of trace elements in granites, pegmatites and gneisses.

1–5 – the same as in Fig. 4; 6 – gneisses, 7 – chamber pegmatites of the gemstone belt. The thick grey lines with arrows show West-East trends for the granites of the Murzinka massif.

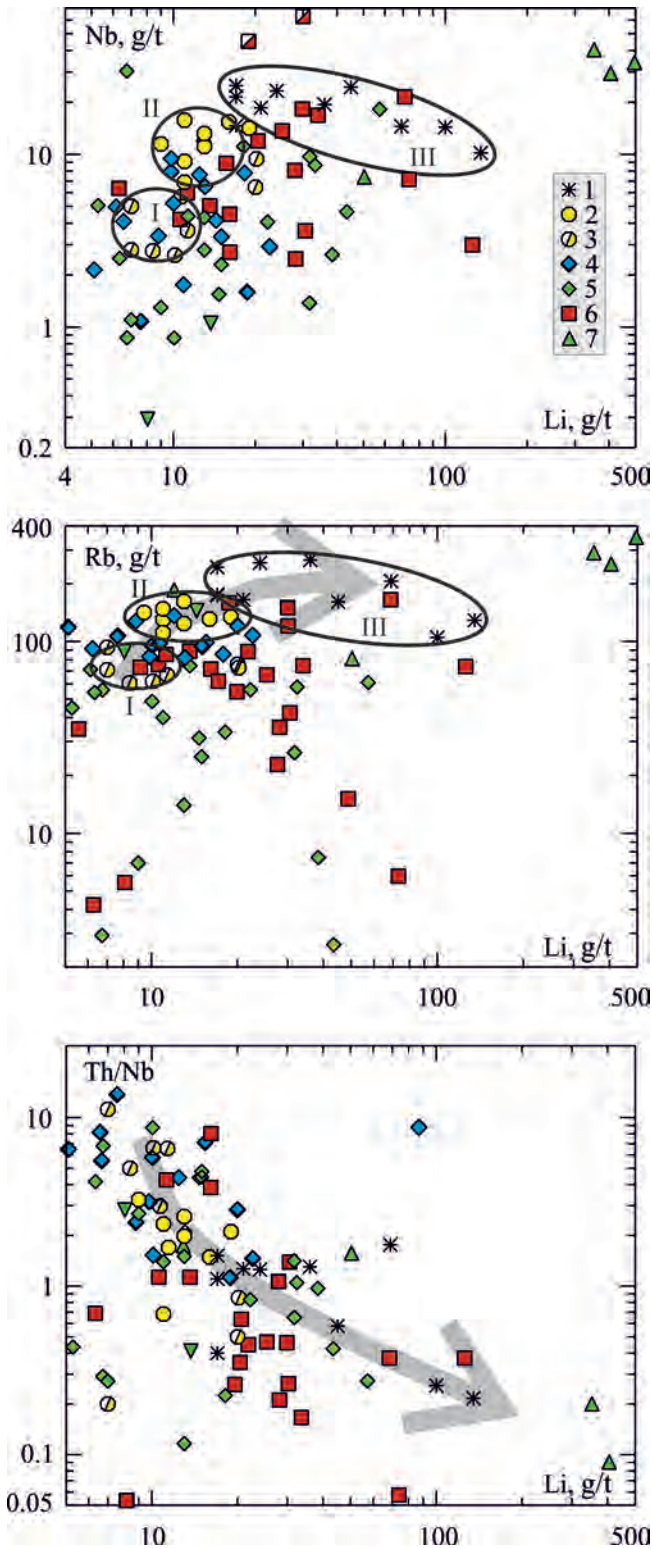


Fig. 6. Nb, Rb and Th/Nb versus Li for granites, pegmatites and gneisses.

Symbols are the same as for Fig. 5. The ovals mark the areas of the West Vatikha (I) and East Vatikha (II) subcomplexes and the Murzinka complex (III) where granites are concentrated.

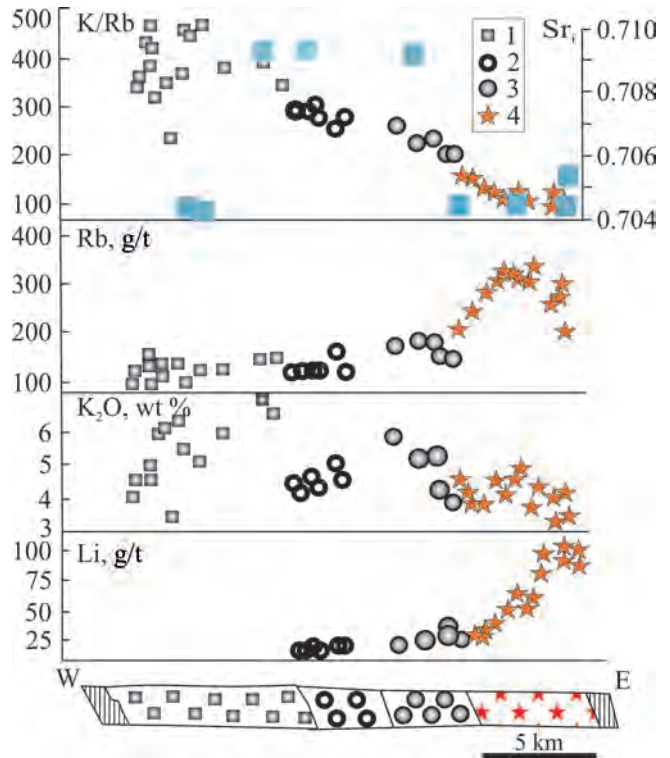


Fig. 7. Distribution of K, Rb, Li in the latitudinal section of granites.

1 – Yuzhakovo, 2 – West Vatikha, 3 – East Vatikha, 4 – Murzinka complexes. In the top diagram, blue bars indicate the values of $^{87}\text{Sr}/^{86}\text{Sr}$.

evidenced by the same isotopic age (Rb-Sr whole-rock and U-Pb zircon ages) of all granitoids being estimated at approximately 255 Ma. However, clear isotopic differences between the Vatikha granites of the western part of the massif and the granites of the Murzinka complex, which make up its eastern half (see Fig. 7), indicate different magmatic sources for both granites. This is also evidenced by the behaviour of potassium, which follows the usual homodromous trends within different complexes, first revealing an increase in the contents in the east for the Yuzhakovo, Vatikha and Murzinka complexes, and then a decrease in the concentration in the latter two (see Fig. 7). Unlike such elements as Rb, Li, Be, Nb and Ta, whose geochemistry is largely determined by fluid transport, the behaviour of potassium follows the laws of crystallisation differentiation. Thus, the modern appearance of the massif results from the evolution of the magmatic melt and the fluid that is in equilibrium with it.

RESULTS AND DISCUSSION

Mesoproterozoic para- and orthogneisses of various compositions, metamorphosed in the context of a granulite facies of regional metamorphism, occur in the bottom of the Murzinka massif. The coexisting horn-

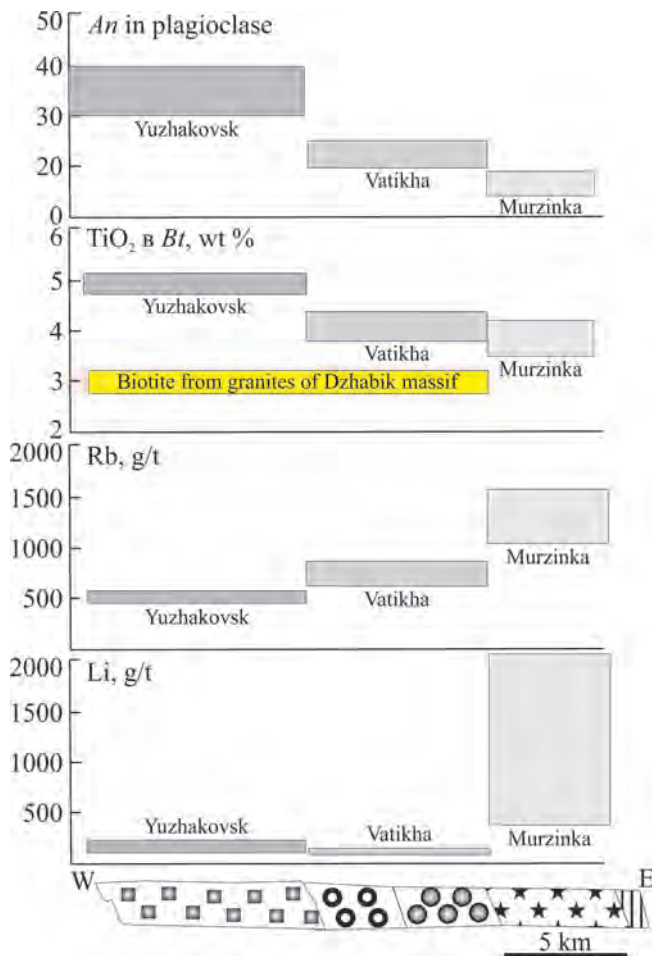


Fig. 8. Content of An minal in plagioclase and TiO₂, Rb, Li in the biotite of Yuzhakovo, Vatikha and Murzinka granites.

blendes and plagioclases of gneisses (for the composition of minerals see the monograph [Orogenic granitoid magmatism..., 1994]) are in equilibrium at a pressure of 5–6 kbar [Fershtater, 1990; Molina et al., 2015] and a temperature of 750–800°C. In the eastern direction, the rocks change their composition from predominantly basic to granitoid as they approach the massif. The gneisses of the granitoid composition experienced a high degree of melting; the anatectic melt formed the western part of the Murzinka massif; the gneisses remained mainly in the form of restites in Vatikha granites.

The rocks of the Yuzhakovo complex form a system comprising two generations of veins and small intrusive bodies occurring among gneisses. The granitoids of the first generation are gneissic, whereas the second-generation granitoids are mostly massive; however, gneissic varieties are also noted. All granitoids form intruded bodies, with the contacts with host gneisses being either well-defined or bearing traces of weak granitisation. Different veins have their own orientation of gneissic structures, which indicates the syntectonic nature of the complex.

The rocks of the complex are characterised by a variety of compositions. The rocks of first-generation veins are enriched with calcium and, for the most part, are depleted of potassium and trace elements associated with it; whereas in the second-generation granitoids, the content of potassium and especially rubidium increases. In terms of the content of niobium, lithium, rubidium and the K/Rb ratio, they exhibit the same trends as the granites of the Vatikha and Murzinka complexes that make up the Murzinska massif and are at the beginning of the evolutionary series (see Figures 4–6).

The absence of noticeable migmatisation and the intrusive contacts of the Yuzhakovo granite veins indicate that the zone of magma generation is located below the modern erosional truncation. Considerable variations in the composition of the granitoids of the Yuzhakovo complex, much more significant than in the rocks of the Vatikha and Murzinka complexes, are evidently caused by fluctuations in the degree of partial melting and the composition of the gneiss protolith.

The granites of the Vatikha and Murzinka complexes make up the western and eastern parts of the Murzinska massif, respectively. In the endocontact zone reaching up to 1–1.5 km in width, Vatikha granites contain the inclusions of granodiorite and adamellite composition, which constitute variously transformed restites of a granite-gneiss substrate. These granites, identified as the West Vatikha subcomplex, are close in terms of their chemical composition and mineralogy to Yuzhakovo granites. To the east, they gradually become enriched with rubidium, lithium and niobium (East Vatikha subcomplex) and, by all indications, exhibit similarities with the granites of the Murzinska complex. The granites of the Vatikha complex possess distinctive ‘crustal’ isotopic characteristics, while the Murzinska granites are very different in their low content of radiogenic strontium and near-zero ϵNd_{255} values. Considering that granites are of the same isotopic age, these data clearly indicate different substrates for Vatikha and Murzinka granites. The presence in the former of numerous granite gneiss inclusions explains the isotopic parameters of granites by the fact that Proterozoic granite-gneisses constituted their substrate, whereas the isotopic parameters of Murzinka granites and their spatial proximity to Paleozoic sedimentary-volcanic strata indicate that the rocks of the newly formed crust of the orogen – common for most Ural granites – served as the granite protolith [Fershtater, 2013].

All granites constitute crystallised cotectic melt and exhibit corresponding trends in the coordinates K₂O–CaO–Na₂O (Fig. 9a), which is an important petrochemical confirmation of their magmatic origin [Shteinberg, 1985; Fershtater, 1987]. The cotectic range of granites of the Yuzhakovo complex is characterised by the highest CaO content, with that of the Murzinka complex showing the smallest content. Based on the po-

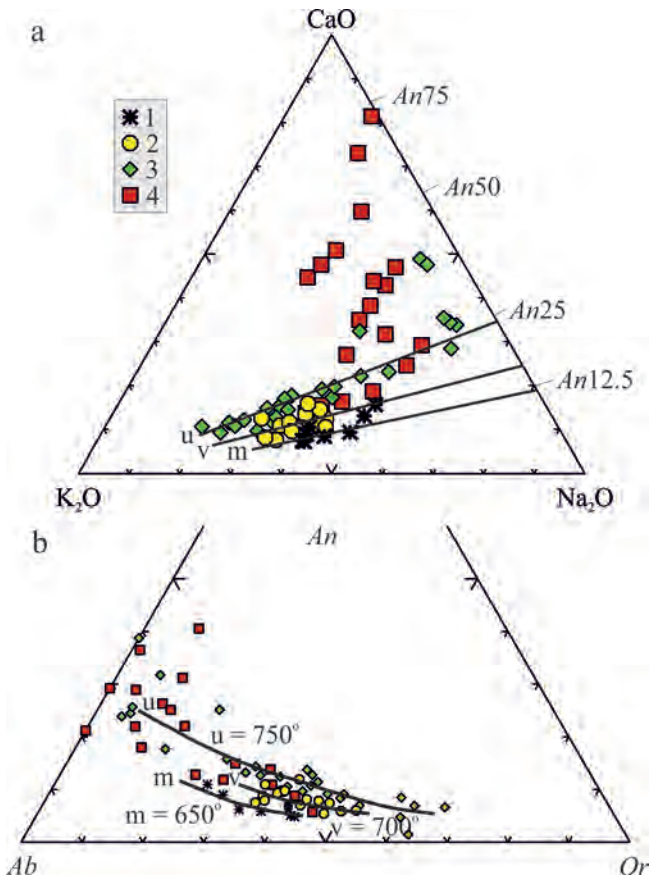


Fig. 9. K₂O–CaO–Na₂O (a) and Ab–An–Or (b) diagrams for granitoids and metamorphic rocks.

1–3 – granitoid complexes: 1 – Murzinka, 2 – Vatikha, 3 – Yuzhakovo; 4 – gneisses.

Letters m, v, u denote trends of the corresponding complexes. In diagram b, these trends correspond to the isotherms of ternary feldspars [Ribbe, 1975, and references in this work]. Note a clear decrease in An content of normative plagioclase from the Yuzhakovo to Murzinka complexes, which was mentioned previously and is evidenced by the direct measurements of plagioclase composition (see Fig. 8). The normative amount of Ab, An, Or is compliant with the mesonorms (normative compositions with biotite and amphibole instead of anhydrous iron-magnesium silicates).

sition of the imaging points of granites from different complexes in the Ab – An – Or diagram (Fig. 9b), considering the known data on the temperature dependences of feldspar compositions [Ribbe, 1975, and references in this work], we can approximately estimate their crystallisation temperature, which drops from 750°C for granites of the Yuzhakovo complex to 650°C for granites of the Murzinka complex. The presence of antiperthite plagioclases in Yuzhakovo and Vatikha granites serves as the mineralogical verification of the given numbers. The use of such an indicator of the order of crystallisation as the fluorine content in apatite inclusions in rock-forming minerals [Fershtater, 1987] provides additional confirmation of granite composition

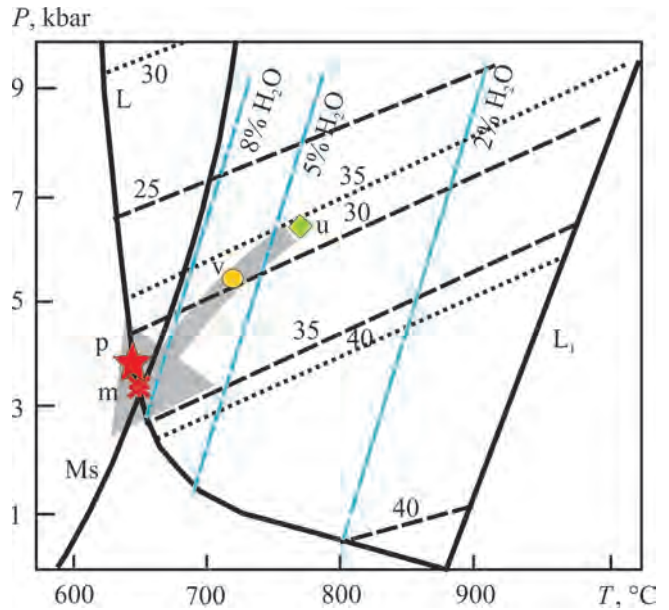


Fig. 10. *T* versus *P* for granitoids. For the principle of plotting and data sources see [Fershtater, 1987, Fig. 33].

The position of the water-saturated (L) and dry (L₁) liquiduses of the system Ab–Q–Or–H₂O and also liquidus lines (blue dashes) for water contents of 2, 5 and 8 wt % is specified according to [Johannes, Holtz, 1996; Holtz et al., 2001]. The dashed lines having indices 40, 35, 30, 25 denote the quartz content in the ternary minimum of the system Ab–Q–Or; the dashed line represents the same in the system Ab–Q–Or–An at An/(An + Ab + Or) = 0.05. Their position is also specified according to the above-mentioned authors. The average contents of quartz in granites of the Yuzhakovo (u), Vatikha (v) and Murzinka (m) complexes are calculated using mesonorms according to the data from Tables 4 and 5; whereas the average contents of quartz in the graphic pegmatite from Mokrusha vein (p) were determined on the basis of calculations carried out in thin sections; the temperatures are taken from Fig. 9b. Ms – stability curve of muscovite in granite [Huang, Willie, 1973]. Other explanations are given in the text.

conforming with granite eutectics. The data presented below indicate a constant fluorine content (2.35–2.95%) in apatite inclusions from all the main minerals of typical granite (samples 44) of the Murzinka complex, which is a consequence of their simultaneous (eutectic) crystallisation from the melt. The fluorine content exceeds 3% only in the late intergranular apatite and the apatite inclusions in the late muscovite replacing biotite. *The fluorine content (wt %) in apatite included in:* plagioclase – 2.35, biotite – 2.48, orthoclase – 2.66, quartz – 2.95, muscovite 1 – 2.57, muscovite 2 – 3.43, intergranular – 3.77.

The *P–T–H₂O* parameters characterising the evolution of granite magmatism are shown in Figure 10. The evolutionary trend indicates a regular change in the *P–T* parameters in the granitoid complexes of the latitudinal cross section of the massif, i.e. from its bottom to the top, from the granitoids of the Yuzhakovo complex to

Murzinka granites. The pressure during the separation of the eutectic granite melt, in this case, varies from 6–7 to 3 kbar, with the water content in the melt increasing from 4–5 to 8 wt %. Murzinka granites are on the aqueous liquidus of granite near the stability curve of muscovite in a granite melt, which is consistent with the two-mica composition of granites.

The melt filled the fault zone at the border of the pre-Paleozoic basement in the west and the newly formed crust composed of Silurian and Devonian volcanic-sedimentary rocks in the east, mainly via the dyke filling mechanism [Petford et al., 1993], as evidenced by the subvertical form of Vatikha and Murzinka granites differing in structure and composition [Orogenic granitoid magmatism..., 1994]. The specified features of the Murzinka massif are to some extent characteristic of the majority of Permian granite massifs of the paleocontinental zone (northwestern megablock) and distinguish them from the granites of the Kochkar anticlinorium, where the uniformly aged granites of the paleocontinental zone (southeast megablock) are most clearly represented [Fershtater, 2013]. Massifs of the latter are confined to dome structures and are formed as a result of diapirism combined with the mechanism of fracture development [Clemens, Mawer, 1992].

In such massifs, separate granite bodies differing in structure and composition form mostly flat deposits [Fershtater, Borodina, 1975].

There is also an issue concerning the nature of the pegmatites of the Ural gemstone belt, which developed within the MMC. The performed studies indicate clear geochemical differences between the chamber pegmatites of the gemstone belt and various pegmatites associated with the granites of the Yuzhakovo, Vatikha and Murzinka complexes. Chamber pegmatites of the gemstone belt occurring in the Proterozoic gneisses constitute a separate episode of magmatism, which according to preliminary data (K-Ar age) completed granite formation in the region and was not directly related to the formation of the Murzinka massif.

The work was carried out within project No. 0393-2016-0020 of the state task of the IGG UB RAS, state registration number AAAA-A18-118052590029-6.

REFERENCES

- Borshchov S.K., Fershtater G.B. (2017) The self-colored belt of the Urals: Alabash ore field, vein Mokrusha. *Putevoditel' Sredneural'skoi polevoi ekskursii. "Granity i evolyutsiya Zemli"*. III Mezhdunar. geol. konf. [Guide of Sredneural'skaya field trip. III Intern. Geol. Conf. "Granites and the evolution of the Earth"]. Ekaterinburg, IGG UrO RAN Publ., 27-37. (In Russian)
- Clemens J.D., Mawer C.K. (1992) Granite magma transport by fracture propagation. *Tectonophysics*, **204**(3-4). 331-360.
- Couzinie S., Moyen J.-F., Villaros A., Paquette J.-L., Scarrow J.H., Marignac C. (2014) Temporal relationships between Mg-K mafic magmatism and catastrophic melting of the Variscan crust in the southern part of Velay Complex (Massif Central, France). *J. Geosci.*, **59**, 69-86.
- Fershtater G.B. (1987) *Petrologiya glavnykh intruzivnykh assotsiatsii* [Petrology of the main intrusive associations]. Moscow, Nauka Publ., 232 p. (In Russian)
- Fershtater G.B. (1990) Empirical plagioclase-hornblende barometer. *Geokhimiya*, (3), 328-335.
- Fershtater G.B. (2013) *Paleozoiskii intruzivnyi magmatizm Srednego i Yuzhnogo Urala* [Paleozoic intrusive magmatism of the Middle and Southern Urals]. Ekaterinburg, UrO RAN Publ., 365 p. (In Russian)
- Fershtater G.B., Borodina N.S. (1975) *Petrologiya magmaticheskikh granitoidov* [Petrology of magmatic granitoids]. Moscow, Nauka Publ., 287 p. (In Russian)
- Fersman A.E. (1940) *Pegmatity* [Pegmatites]. Moscow, AN SSSR Publ., 712 p. (In Russian)
- Gerdes A., Montero P., Bea F., Fershtater G., Borodina N., Osipova T., Shardakova G. (2002) Peraluminous granites frequently with mantle-like isotope compositions: the continental-type Murzinka and Dzhabyk batholith of the eastern Urals. *Intern. J. Earth Sci. (Geol. Rundsch.)*, **91**, 3-19.
- Holtz F., Becker A., Freise M., Johannes W. (2001) The water-saturated and dry Qz-Ab-Or system revised. Experimental results of very low water activities and geological implications. *Contrib. Mineral. Petrol.*, **141**, 347-357.
- Huang W.L., Willie R.J. (1973) Melting relations of muscovite granite to 35 kbar as a model for fusion of metamorphosed subducted oceanic sediments. *Contrib. Mineral. Petrol.*, **42**, 1-14.
- Johannes W., Holtz F. (1996) *Petrogenesis and experimental petrology of granitic rocks*. Springer, Berlin, Heidelberg, New York., 336 p.
- Keil'man G.A. (1974) *Migmatitovye komplekсы podvizhnykh poyasov* [Migmatitic complexes of mobile belts]. Moscow, Nedra Publ., 200 p. (In Russian)
- Korovko A.V., Dvoeglazov D.A. (1986) Geological position and internal structure of the Murzinka metamorphic complex. *Korrelyatsiya i kartirovanie magmaticheskikh i metamorficheskikh kompleksov Urala* [Correlation and mapping of magmatic and metamorphic complexes of the Urals]. Sverdlovsk, IGG UrO RAN Publ., 73-75. (In Russian)
- Krasnobaev A.A., Bea F., Fershtater G.B., Montero P. (2005) Zircon geochronology of the murzinka metamorphic complex (Middle Urals). *Dokl. Akad. Nauk.*, **404**(3), 407-410. (In Russian)
- Le Maitre R.W. (ed.). (1989) *A Classification of Igneous Rocks and Glossary of Terms*. Blackwell, Oxford, 193 pp.
- Levin V.Ya., Koroteev V.A., Zvonareva G.K. (1975) Corundum syenites from Yubileynaya mine. *Materialy k mineralogii Urala* [Materials to the mineralogy of the Urals]. Tr. Il'mensk. gos. zapovednik, 44-49. (In Russian)
- Molina J. F., Moreno J.A., Castro A., Rodriguez, Fershtater G.B. (2015) Calcic amphibole thermobarometry in metamorphic and igneous rocks: New calibrations based on plagioclase/amphibole Al-Si partitioning and amphibole/liquid Mg partitioning. *Lithos.*, **232**, 286-305.
- Montero P., Bea F., Gerdes A., Fershtater G.B., Osipova T.A., Borodina N.S., Zinkova E.A. (2000) Single-zircon evaporation ages and Rb-Sr dating of four major Variscan batholiths of the Urals. A perspective on the timing of deformation and granite generation *Tectonophysics*, **317**, 93-108.

- Muller A., Romer R.L., Pedersen R.-B. (2017) The sveconorwegian pegmatite province – thousands of pegmatites without parental granites. *Canad. Mineral.*, **55**, 283-315.
- Orogennyi granitoidnyi magmatizm Urala* [Orogenic granitoid magmatism of the Urals]. (Ed. G.B. Fershtater). (1994) Miass, IGG UrO RAN Publ., 250 p. (In Russian)
- Petford N., Kerr C.R., Lister R.G. (1993) Dike transport of granitoid magmas. *Geology*, **21**, 845-848.
- Popov V.A., Popova V.I. (1975) To the mechanism for the formation of feldspar glasses around corundum crystals, “Yubileynaya” mine in the Ilmeny mountains *Materialy k mineralogii Urala* [Materials to the mineralogy of the Urals]. Tr. Ilmensk. gos. zapovednik, 50-57. (In Russian)
- Ribbe P.H. (1975) Feldspar mineralogy: short course notes. (Ed. P.H. Ribbe). Blacksburg, Amer. Miner. Soc. Southern print. Co., **2**, 1-52.
- Sabatier H. (1980) Vaugnerites and granites, a peculiar association of basic and acid rocks. *Bull. Mineral.*, **103**, 507-522.
- Sabatier H. (1991) Vaugnerites: special lamprophyre-derived mafic enclaves in some Hercynian granites from Western and Central Europe. *Enclaves and granite petrology*. (Eds J. Didier, B. Barbarin). Elsevier, Amsterdam, 63-81.
- Scarrow J.H., Molina J., Bea F., Montero P. (2009) Within-plate calc-alkaline rocks: insights from alkaline mafic magmas – peraluminous crustal melt hybrid appinites of the Central Iberian Variscan continental collision. *Lithos.*, **110**, 50-64.
- Shteinberg D.S. (1985) *O klassifikatsii magmatitov* [On the classification of magmatites]. Moscow, Nauka Publ., 159 p. (In Russian).
- Talantsev A.S. (1988) *Kamernye pegmatity Urala* [Chamber pegmatites of the Urals]. Moscow, Nauka Publ., 144 p. (In Russian)
- Winchester J.A., Floyd P.A. (1977) Geochemical discrimination of different magma series and their differentiation products using immobile elements. *Chem. Geol.*, **20**, 325-343.

PLUME-RELATED GRANITE-RHYOLITE MAGMATISM

Viktor N. Puchkov^{1,2}

¹*Institute of Geology, Ufa Federal Research Centre, RAS, 16/2 K. Marx St., Ufa 450077, Russia*

²*Zavaritsky Institute of Geology and Geochemistry, UB RAS, 15 Akad. Vonsovsky St., Ekaterinburg 620016, Russia, e-mail: puchkv@ufaras.ru*

Received 27.06.2018, accepted 24.08.2018

Plume-related magmatism is widespread and its existence is well-founded. Mostly, plume-related magmatism is represented by trap rocks, oceanic island basalts (OIB) and oceanic plateau basalts (OPB), although the composition of plume-related igneous products is very diverse. Among others, silicic igneous rocks – rhyolites and granites – play a prominent role. Two main types of plume magmatism are recognised. The former comprises Large Igneous Provinces (LIP) and is thought to be born at the core-mantle boundary within structures called superswells, which produce giant, short-lived mantle upwellings resulting in abundant magmatism on the earth's surface. The latter is represented by time-progressive linear volcanic chains formed by single plumes – thin upward mantle flows being continuously active during longer periods of time. It is shown that the relative volume of silicic magmatism strongly depends on the type of the earth's crust. Among continental trap basalts, silicic magmatism is usually present, being subordinate to the basalts in volume, and belongs to the bimodal type. However, in some cases, continental LIPs are formed predominantly by silicic rocks (silicic LIPS, or SLIPS). Oceanic LIPs are mainly basaltic comprising an insignificant or no amount of silicic rocks. Time-progressive volcanic chains are rarely found on the continents and, as a rule, include a significant silicic component. Oceanic chains are comprised mostly of basalts (OIB), although at the top of volcanoes there are more acid and alkaline differentiates, which, however, usually lack rhyolites and granites, except for the cases when the relics of the continental crust or anomalously thick mafic crust are present. The analysis suggests that the melting of continental crust plays an important role in the formation of plume-related rhyolite-granite magmatism. As for the Urals, the presence of plume-related magmatism in its history has been proven relatively recently. Plume events characterised by the presence of (rhyolite)-granite components include Mashak (1380–1385 Ma), Igonino (707–732 Ma), Mankhambo (mainly Cambrian), Ordovician Kidryasovo, Stepninsky (Permian) and Urals-Siberian (Triassic).

Keywords: *rhyolites, granites, plumes, underplating, LIP, time-progressive volcanic chains*

Acknowledgments

This work is supported by the Russian Science Foundation, Project No. 16-17-10192.

INTRODUCTION

Plume-related magmatism is well-studied. Most of its manifestations are represented by basic volcanites (trap rocks and swarms of dolerite dykes considered as feeders; basalts of oceanic islands and plateaus). However, the spectrum of magmatic manifestations associated with plumes is extremely wide: formation of kimberlites, carbonatites, picrites, alkaline basaltoids, as well as layered basic intrusions. A significant role is also played by acid igneous rocks – granites and rhyolites, with the outcrops of either granites or acid effusive rocks, which depends on the depth of the erosional truncation [Ernst, 2014].

Plumes constitute a part of the global thermochemical convection system: ascending subvertical currents of mantle convection which are deep-seated and therefore manifested on the Earth's surface as intraplate activity zones that do not depend directly on linear interplate structures – subduction and MOR (mid-ocean ridge) zones – although they can interact with them, as well as cause the formation of linear structures (active rifts) by themselves [Puchkov, 2016].

It is reasonable to distinguish between two types of plume manifestations. The first type includes large

igneous provinces (LIP) having a volcanic-product volume of 1–10 million km³ or more and an area of 1–10 million km² [Ernst, 2014]. They are characterised by short activity pulses, usually from 0.5 to several million years, whereas in the case of repeated pulses, their total activity can last up to 20 Ma, rarely longer. The LIPs are commonly attributed to the activity of superplumes – giant upwellings of mantle material from the core-mantle boundary within two vast areas characterised by slow propagation of bipolar S-waves. These two areas are referred to as superswells: South Pacific (Tuzo) and African (Jason). Superswells also constitute the birthplace of smaller single plumes, which, unlike superplumes, trigger much more constant volcanic activity (lasting up to 80 Ma in some cases). Smaller single plumes are less prone to fluctuations and occupy a relatively constant position; therefore, when interacting with moving lithospheric plates they cause the formation of volcanic chains (sometimes discontinuous or with swells) that exhibit linear consistent time progression (time-progressive volcanic chains, TPVC). Such volcanoes were originally called hot spots; this term is still used today; however, it is not a substitute for the term 'plume'. While LIPs and hot spots are only 'symptoms' of the proc-

ess, superplumes and single plumes are equivalent to a ‘diagnosis’.

PLUME-RELATED GRANITE-RHYOLITE MAGMATISM (GLOBAL PERSPECTIVE)

The role of plumes in the generation of granite and rhyolite magmatism is largely determined by how powerful their pulses were and what type of crust they affected. Continental LIPs (Columbia River, Afro-Arabian, Karoo, Kalkarindji, Keweenaw, Ural-Siberian, etc.) are mostly characterised by trap magmatism; however, as a rule, rhyolites and acid pyroclastic rocks are present in a subordinate amount in their cross-sections. In general, the magmatism is of a contrasting nature. In addition, the dating of intrusive rocks from the LIP periphery in some cases reveals that granites (mainly A-type) also belong to trap provinces [Vernikovski et al., 2003]. The analysis of acid volcanic products usually indicates a significant role of contamination associated with the assimilation of rocks from the anhydrous lower layer of the continental crust (granulites, amphibolites) induced by the powerful thermal effect of high-temperature basic magma in the course of underplating. Nevertheless, alternative mechanisms for the formation of acid magma are not excluded [Ernst, 2014 and references in this monograph].

Magmatic areas dominated by acid rocks ($\text{SiO}_2 > 65$ wt %) are distinguished as a separate type of LIPs, parallel to substantially basitic LIPs *sensu stricto*. These provinces are called silicic LIPs [Bryan, Ernst, 2008; Bryan, Ferrari, 2013; Ernst, 2014]. As the Russian version of the term, we propose *kremne-kislye KMP (KKMP)*. Terminologically, the above-described mafic LIPs (MLIPs) and silicic LIPs (SLIPs) can be contrasted. The examples of SLIPs include Whitsunday (Western Australia – Oceania), Kennedy – Connors – Auburn (Northeast Australia), Gawler (Southeast Australia), Sierra Madre Occidental (Mexico), Chon Aike (South America – Antarctica), Malani (India – Seychelles – Madagascar), as well as Guibey and Xiongier (China). Late Paleozoic – early Mesozoic giant granite batholiths of the Central Asian Orogenic Belt (Angara-Vitim, or Barguzin; Khangai; Khentey) probably belong to this type as well [Yarmolyuk et al., 2014]. According to [Ernst, 2014], SLIPs exhibit the following features. 1. SLIPs are characterised by large area extents and volumes of extrusive magmatism, which are equal to or only several times smaller than those of MLIPs. 2. In terms of composition, dacite-rhyolite volcanites and granites, transitional between calc-alkaline I-type and A-type, constitute $> 80\%$ of the volume; with S granites being present in rarer cases. 3. The lithology of volcanites is dominated by rhyolite ignimbrites. 4. The duration of magmatic activity is up to 40 Ma, with individual pulses lasting 3–10 Ma. 5. SLIPs are formed only on the continental crust and are often located on paleo-

and modern continental borders. They result from the anatexis of easily melted hydrous lower crust under the influence of high temperatures caused by non-subduction and non-orogenic conditions (most likely, plume-related underplating).

On the oceanic crust, superplumes form vast volcanic plateaus. As compared to the continental provinces, they are not older than the Mesozoic as evidenced by the fact that the older subducted oceanic crust can only be identified from ophiolites found in folded belts. The largest plateaus in the Pacific Ocean include Ontong Java, Hikurangi, Manihiki, as well as Shatsky and Hess rises. As a rule, granite-rhyolite inclusions are not characteristic of in their cross-sections. Volcanic plateaus formed in the Atlantic-type oceans are different in nature: North Atlantic Igneous Province, Sierra Leone, Rio Grande, Maud Rise, Kerguelen Plateau, etc. These plateaus can include both epioceanic and epicontinental (microcontinents, volcanic passive continental margins) parts. The initial stage of their development is epicontinental rifting which, to one degree or another, is usually accompanied by the formation of acid rocks as in the case of MLIPs described above (LIPs *s.str.*). However, as the process evolved, rift magmatism was replaced by mantle-related basitic magmatism; with rift complexes most often being found deeply buried. Nevertheless, acid igneous rocks sometimes outcrop: granites from the Isle of Skye in Scotland; granites and rhyolites from the Kerguelen Plateau, etc. [North Atlantic Igneous Province..., 2002; Ariskin, 2017].

The ability of single plumes forming time-progressive volcanic chains to produce granite-rhyolite igneous complexes also largely depends on the presence of continental crust, its relics or a simatic crust of anomalous thickness. Epiocenic volcanoes having a granite-rhyolite component are extremely rare; with the acid component being usually represented by trachytes, as well as highly alkaline rocks similar to them [Mazarovich, 2000; Rohde et al., 2013; see also GeoMan.ru: geography library www.geoman.ru/books/item/f00/s00/z0000077/st222.shtml]. Ascension Island could be cited as an exception; however, the volcano located on the island is very young and not connected to any volcanic chains. Of all the islands of the Canary Archipelago, only Gran Canaria, the largest of the Canary Islands, is distinguished by the presence of rhyolites. Rhyolites are also found on Jan Mayen Island, with very few peralkaline rhyolites being noted on Easter Island. The Icelandic plume occupies a special place among single plumes. In this case, the presence of acid volcanites, being estimated at 7%, is noticeable [Ariskin, 2017]. Granites are present as well. The volcanic structure formed by the Icelandic plume together with the Mid-Atlantic Ridge (MAR) is distinguished by an unusually large size, with the crust reaching up to 40 km in thickness, which could be a favourable condition for the anatexis of the lower

crust, where both temperature and pressure are elevated. Nevertheless, the possibility of crystallization-differentiation in basaltic magma, as a rule, is not excluded.

Regular magmatic chains on the continental crust are quite rare. Some of the volcanic chains do not display a clear time sequence, which may be related to the complex dynamic interaction of the plume with the thick lithosphere (its jamming, shearing, strong deflection by mantle wind, etc.). Nevertheless, there are several examples of epicontinental magmatic chains that contain granites and / or rhyolites exhibiting time progression. In particular, they include well-known rhyolite calderas of the Yellowstone Plume [Smith et al., 2009], with the age gradually increasing to the west (from <1.0 Ma to 16.4 Ma). Nigerian anorogenic ring complexes of alkaline granites, granosyenites and volcanites, dated to be between 141 Ma in the south and 213 Ma in the north, constitute another example. The volcanic rocks preserved in the calderas demonstrate the evolution of melts from olivine basalts through hawaiites and mugearites to trachytes and rhyolite ignimbrites [Bowden, Kinnaird, 1984; Kinnaird et al., 2016]. One more example is related to the bimodal Gawler SLIP (Southeast Australia), from which a chain of granite massifs is traced across the entire continent [Ernst, 2014]. The age of magmatism consistently varies from 1.595 Ma in the south to 1.500 Ma in the north.

Summing up the review of international literature sources, it should be noted that granite-rhyolite occupies a prominent place among the products of plume-related intraplate magmatism; with plumes being an independent geodynamic factor of granite-rhyolite magmatism along with orogeny, subduction and the spreading of oceanic crust. Moreover, the volume of granite-rhyolite magmatism depends on the type of crust substratum – oceanic or continental. In the latter case, the volume is significantly higher. This alone suggests that the melting of the continental or transitional crust plays an important role in the origin of magmatism, as confirmed by numerous analytical data. However, the possibility of granites and rhyolites forming due to the remelting of rocks from the oceanic crust (basaltoids and amphibolites) is undeniable. According to experimental data [Khodorevskaya, 2017], this depends on the fluid composition and the features of the fluid regime (in particular, during amphibolite dehydration) or on the interaction of metabasites with aqueous-saline (Na, K)Cl fluid, which is related to seawater. Moreover, there is a possibility that other alternative mechanisms were involved.

PLUME-RELATED GRANITE-RHYOLITE MAGMATISM OF THE URALS

Lately, increased attention has been paid to the magmatic complexes of the Urals (mainly the west-

ern slope), which, judging by many indications, are plume-related [Puchkov et al., 2013, Puchkov, 2018a, б; Kholodnov et al., 2017; etc.]. Only some of them have a distinctive granite-rhyolite component. A brief description of the complexes is given below.

Mashak complex (1380–1385 Ma)

This complex, developed within the Bashkirian Mega-Anticlinorium (BMA), mainly corresponds to the Mashak suite of the Middle Riphean basement (RF2), in the lower parts represented by basalts and subordinate rhyolites, as well as by terrigenous strata (from conglomerates to shales). The suite is developed in the axial and eastern regions of the Bashkirian Anticlinorium, disappearing abruptly to the west in a washout (at a distance of 20 km). This fact, together with the intraplate rift nature of the chemism exhibited by volcanites [Ernst et al., 2006], suggests outcropping of the western flank of the graben, having a distinct Ural strike. The volcanites of the Mashak suite, developed in its lower part, are represented by a typical contrasting rhyolite-basalt series. Rhyolites can be found in the Mashak cross-section throughout most of the Bashkirian Mega-Anticlinorium (Fig. 1). When discussing the genesis of acidic volcanites, it is necessary to consider that among zircons (syngenetic to the eruption process), the presence of more ancient xenogenic varieties (in particular, minerals aged 1597 ± 27 Ma) was established [Krasnobaev et al., 2013a; Puchkov et al., 2013], which may indicate that the melting of more ancient crust components than the Mashak ones was involved in the formation of silicic magma.

In more detail, the importance of assimilation in the formation of the Mashak suite, consisting of picrites, basalts and rhyolites, has been considered recently [Kovalev et al., 2018a, б]. In some cases, U-Pb age determination for zircons from the basalts of the Mashak suite yielded significantly older ages for most or all of the zircons than the true age of volcanites. Thus, two discordant ages were obtained for five zircon grains sampled from the basaltoids of the Kuzelga subsuite – 1985.0 ± 16.0 ($n = 2$) and 1892.4 ± 9.7 ($n = 3$) Ma. In general, the dispersion of $^{206}\text{Pb} / ^{238}\text{U}$ ages determined for single crystals ranges from 1496 Ma to 3152 Ma. The authors proposed a mechanism describing the evolution of the primary mantle plume melt in line with the AFC model (Assimilation \pm Fractional Crystallization). According to this mechanism, picrite (olivine \pm clinopyroxene) originates through fractional crystallization in the primary melt at a temperature of 1100°C and a pressure of 10–11 kbar; the fluid phase accumulates in the uppermost part, whereas ancient host rocks are actively assimilated by basalts, which leads to the formation of rhyolites. In this case, $\epsilon\text{Nd}(T)$ of all rocks in the complex exhibit negative values (from ≈ -1.0 for picrites and basalts to -7.5 for rhyolites), whereas the extrapolated value of the primary melt is positive (mantle).

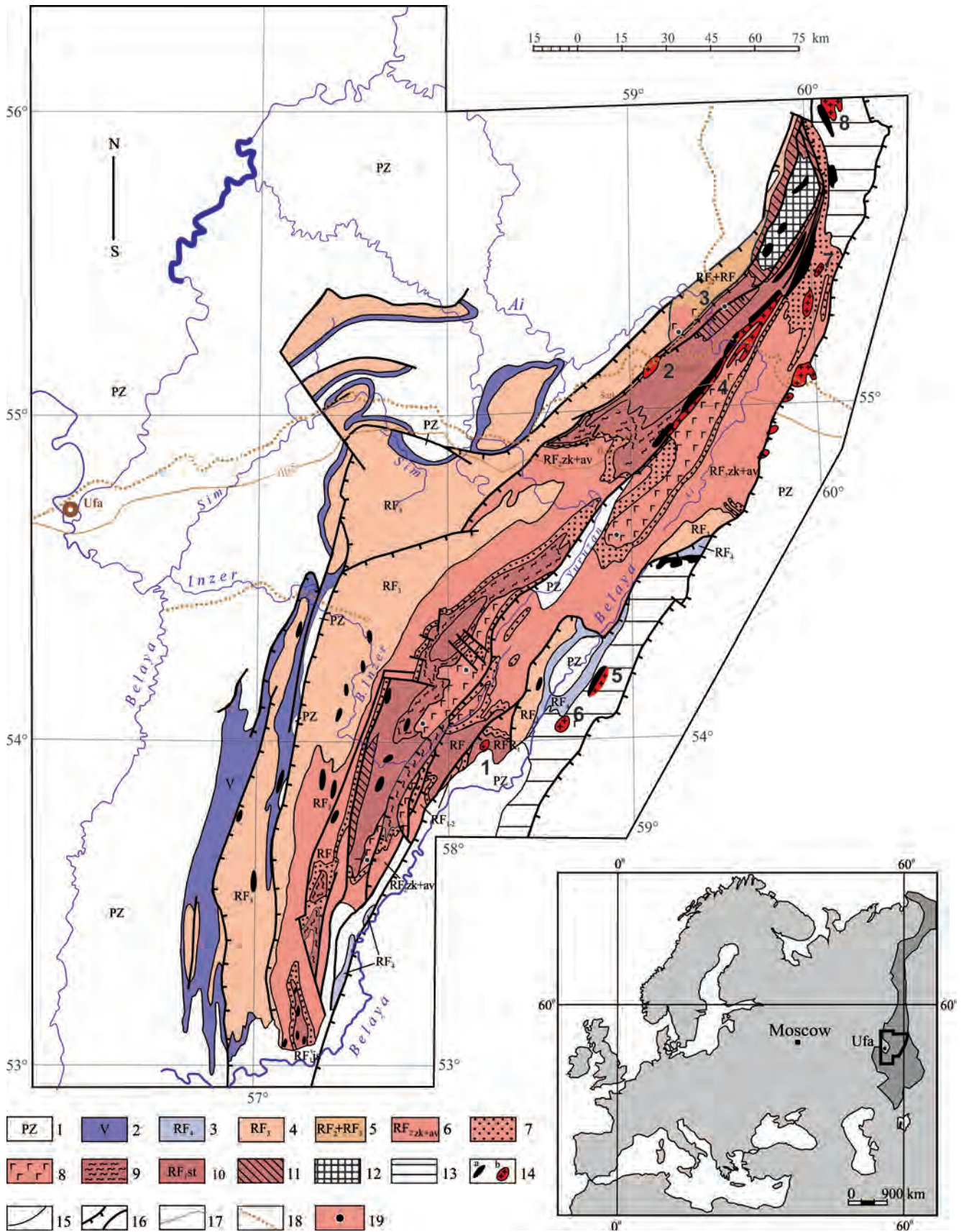


Fig. 1. Map showing the location of the silicic igneous rocks of Mashak, Igonino, Mankhambo and Kidryasovo (?) plume events in the Baskirian mega-anticlinorium and Ufaley anticlinorium (Southern Urals).

1–5 – undivided deposits: 1 – Paleozoic (PZ), 2 – Vendian (V), 3 – Terminal Riphean (RF₄), 4 – Upper Riphean (RF₃), 5 – Middle-Upper Riphean (RF₂ + RF₃); 6–11 – suites: 6 – undivided Zigazino-Komarov and Avzyan (RF₂ zk-av), 7 – Zigalga (Middle Riphean), 8 – Mashak (Middle Riphean), 9 – Bakal (Yusha), 10 – Lower Riphean Satka (Suran), 11 – Lower Riphean Ai (Bolsheizer); 12 – Taratash complex; 13 – Uraltau and Ufaley metamorphic complexes; 14 – igneous rocks: gabbro (a) and granites (b); 15 – geological boundaries; 16 – main tectonic dislocations (thrusts and faults); 17 – highways; 18 – railroads; 19 – sampling points for zircons in the rhyolites of the Mashak suite and in the dikes of the Mashak age.

Numbers in the scheme denote silicic intrusions: 1–4 – Mashak complex: 1 – Akhmerovo, 2 – Berdyaush pluton, 3 – Bagrusha rhyolite dykes, 4 – Ryabinovo and Gubensk massifs; 5, 6 – Igonino complex: 5 – Barangulovo massif, 6 – Mazara massif; 7 – Yurma massif (Cambrian); 8 – Kozlinogorsk gabbro-syenite-granite association (Ordovician).

In addition to volcanites, intrusive silicic complexes occur in the BMA at the Mashak age level (see Fig. 1), which, among others, include Berdyaush rapakivi granites in association with syenites and gabbro xenoliths. To the north of the Berdyaush massif, the Bagrusha complex of rhyolite dykes is developed on the strike of folded structures. Further to the northeast, there are Ryabin and Guba granites, which are closely associated with the gabbroid Kusa-Kopan complex, forming with it a contrasting association. A spatially isolated, more eastern location is occupied by the Akhmerovo granite massif. The results of absolute dating indicate that all these objects belong to the Mashak event [Krasnobaev et al., 2007a; Puchkov et al., 2013 and references given in this work; etc.].

The geochemistry of the Berdyaush pluton (BP) has been most fully studied. Its belonging to A-granites and geochemical closeness to Mashak rhyolites are well-founded [Larin, 2011]. Some researchers suggested granites having a mantle source. However, according to the latest data on the Hf isotope composition of zircons [Ronkin, 2017], rapakivi granites, quartz syenodiorites and nepheline syenites from the BP cannot originate from predominantly mantle melts, given that the range of extrapolated values ϵ_{Hf} (1383)–(3.7–9.4) lies within the area well below the CHUR line. The observed regularity is in good agreement with the data of the Sm-Nd isotopic systematics of BP rapakivi granites, determining $\epsilon_{\text{Nd}}(t)$ (–5.0 ± 0.4)–(–7.3 ± 0.3). Another argument in favour of the above is the difference in the spectra of REE distribution in gabbro zircons and other BP rocks. Similar data is presented in the article by V. Kholodnova et al. [2017]. The presence of gabbro xenoliths in BP, as well as their being derivatives of a substantially depleted mantle, where $\epsilon_{\text{Nd}} = +4.0 \dots +4.9$, can confirm the popular idea that the crust melting during the formation of rapakivi granites is attributed to magmatic underplating caused by the subcontinental mantle rising up [Ernst, 2014].

Igonino complex (706–735 Ma)

It is our understanding that the complex belongs to the lower reaches of the Arshinian (uppermost, or terminal, Riphean, RF₄) approximately covering an interval of 750–600 Ma and named after the Igonino suite, developed within the Arshinian stratotype in the Tirlyan trough [Kozlov et al., 2011]. Accord-

ing to the U-Pb analysis of zircons, the Igonino suite, which is mainly represented by basaltoids and is devoid of rocks more acidic than dacites, was formed during two main stages (pulses) of evolution dated at 707.0 ± 2.3 and 732.1 ± 1.7 Ma [Krasnobaev et al., 2012]. In terms of chemism, the Igonino volcanic complex reveals similarities with the basalts of the East African Rift System and probably could be classified as an intraplate-riftogenic / plume-induced formation of active rifts [Maslov et al., 2018]. The Barangulovo and Mazara granite massifs, which, together with the associating gabbros, belong to the contrasting gabbro-granite Barangulovo complex, are of close age. Gabbro zircons and granite zircons of the Barangulovo massif were earlier dated at $(728 \pm 8 \text{ Ma})$ and $(723 \pm 10 \text{ Ma})$, respectively, using the SHRIMP method [Krasnobaev et al., 20076]. The early and final (slightly younger) stages of granite formation in the Mazara massif were dated at $746.6 \pm 24.3 \text{ Ma}$ and $709.1 \pm 5.2 \text{ Ma}$, respectively [Krasnobaev et al., 2017]. Therefore, the gabbro-granite Barangulovo complex could belong to the same stage of plume activity as Igonino volcanites. A detailed study of zircons from the Mazara massif reveals its primary source (substratum). According to SHRIMP dating, the granite substratum of the massif is estimated to be between 1527 Ma and 1548 Ma, with its final evolutionary stage being concordantly dated at $1388 \pm 16 \text{ Ma}$, which is close to the Mesoproterozoic Mashak stage of magmatism. This could indicate the involvement of rocks from the Mesoproterozoic crust in the melting. At the same time, the granites of the Akhmerovo massif are closest to those of the Mazara massif and could serve as its substratum [Krasnobaev et al., 2017]. The melting could result from the above-mentioned underplating associated with a new plume event.

Kiryabino complex (670–680 Ma)

The complex in question was named after the Kiryabino layered massif (peridotite-pyroxenite-gabbro) dated to $680.0 \pm 3.4 \text{ Ma}$ [Krasnobaev et al., 20136]. The igneous rocks of close age have a relatively limited distribution in the Bashkirian and Kvarqush megantichloria, as well as in the Onega Graben; thus their belonging to the LIP is at issue. The complex includes the Zhuravlik wehrlite-gabbro-granodiorite massif ($671.0 \pm 7.5 \text{ Ma}$), as well as the Troitsk granosyenite massif ($671.0 \pm 24.0 \text{ Ma}$) [Petrov et al., 2005].

Mankhambo complex (564–485 Ma)

The complex in question is named after the largest A-granite massif in the north of the Urals. We believe it is transgressively overlapped by the quartzites and arkoses of the Ordovician Telpos suite and is of Cambrian age (Fig. 2). The complex is represented by A-granites, associating gabbros, as well as a contrasting basalt-rhyolite complex of volcanites. A-granites (anorogenic, alkaline, anhydrous) constitute a special genetic group, as evidenced by the multiple meanings attached to the letter. Firstly, the name reflects the geodynamic situation associated with the predominant development of granites, which gravitate towards the stable (cratonised) areas of the earth's crust, most frequently occurring in rift zones and within the interior of continental plates. Secondly, the granites are characterised by the increased alkalinity indicating their belonging to the differentiates of alkaline basaltic magmas. Thirdly, they exhibit low water saturation, which is typical of the melting products of lower crust granulites. A-granites from the north of the Urals are associated with gabbros and are comagmatic with the volcanites of a contrasting association; with their formation being presumably related to underplating.

The difficulty of defining the boundaries of this complex, as well as interpreting its geodynamic situation in the Urals lies in the fact that in some areas it is closely connected to and sometimes intertwined with subduction-orogenic I-granites and comagmatic volcanic series; in terms of absolute age, A-granites follow I-granites, with the age of the former sometimes overlapping with that of the latter, thus creating an impression of a peculiar geodynamic chaos. Both types of granites are particularly widespread in the Subpolar Urals [Makhlaev, 1998; Kuznetsov et al., 2007]. I-granitoids are represented by a wide range of rocks from quartz diorites to leucogranites, in petrochemical diagrams corresponding to the areas of convergent geodynamic settings and active continental margins. These include the Maldy, partially Naroda, Vangyr, Lapchavozh and Ilyaiz massifs associated with the volcanites of successively differentiated basalt-andesite-dacite series. These massifs form gabbro-diorite-granodiorite-granite series of the specified geodynamic settings. The absolute ages of zircons determined using the methods of thermionic lead emission and the U-Pb dating (including the SHRIMP) range from the Terminal Riphean to the Cambrian (from 695 ± 19 to 515 ± 8 Ma, with the overwhelming predominance of Vendian ages). A-granites represented by Lemva, Tynagota, Naroda (partially), Khartes, Keftalyk, Tynagot, Kozhim, Mankhambo and other massifs exhibit a narrow spectrum of compositions, with leucocratic varieties prevailing. In terms of petrochemistry, they are related to magmatic formations of divergent geodynamic settings. Age datings (Pb-Pb, U-Pb, SHRIMP) range from 564 Ma to 487 Ma (the end

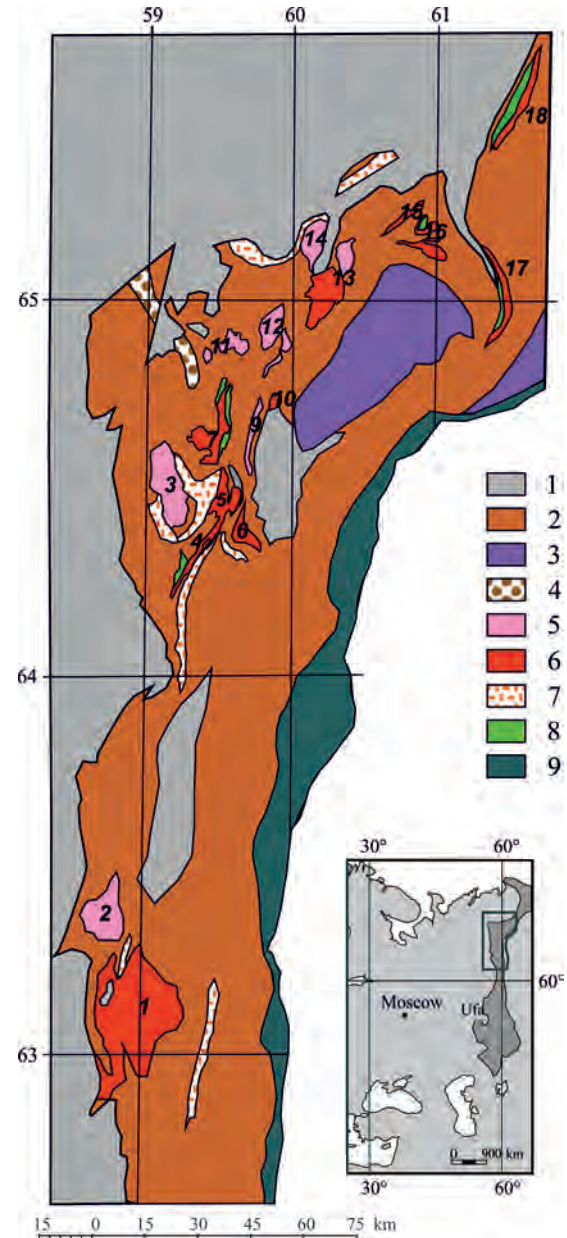


Fig. 2. Map of the Late Proterozoic–Cambrian granite massifs in the Nether-Polar Urals [Puchkov, 1975; Makhlaev, 1998; Kuznetsov et al., 2007].

1 – Paleozoic (Ordovician and younger) sedimentary formations; 2 – Riphean (Meso- and Neoproterozoic) deposits; 3 – Paleoproterozoic metamorphic complex; 4 – Vendian (Ediacaran) polymictic deposits (molasse of Timanides), 5 – I-granites (gabbro-diorite-granodiorite-granite series) predominantly of Vendian ages; 6 – predominantly leucocratic A-granites (mainly Cambrian); 7 – rhyolites of the Neoproterozoic–Cambrian age, undivided; 8 – gabbro of the contrasting gabbro-granite series; 9 – crystalline rocks of the Main Ural Fault.

The numbers in the scheme denote intrusive massifs: 1 – Mankhambo; 2 – Ilyaiz; 3 – Maly Patok; 4 – Torgovaya; 5 – Keftalyk; 6 – Khartes; 7 – Neroyka-Patok; 8 – Vangyr; 9 – Salner; 10 – Nyarta; 11 – Vodorazdel; 12 – Parnuk, Gorodkov and Mankhobeyu; 13 – Naroda; 14 – Maldy; 15 – Khatalamba-Lapcha; 16 – Kozhim; 17 – Tynagota; 18 – Lemva.

of the Vendian period and practically entire Cambrian period), which practically overlap with those of the Ordovician magmatites of the Kidryasovo plume event (see below).

The overlapping of I- and A-granite ages demonstrated using the example of the neighbouring Ilyaiz (519.7 ± 6.3 – 491.0 ± 5.0 Ma) and Mankhambo (522.0 ± 6.0 – 507.2 ± 5.5 Ma) massifs is paradoxical [Udoratina et al., 2017] and may indicate either a partial coexistence of contrasting collision and plume geodynamic mechanisms, originating from different depths; or different substrates, whose melting leads to the formation of different granites (in this case, the Ilyaiz massif is also plume-related). It is known that, in some cases, SLIPs are characterised by the presence of I-granites [Ernst, 2014]. An abnormally high volume of granitoids in plume products could result from high temperatures that remained in the lithosphere following the Timan orogeny, which caused large-scale melting in the crust.

The development of Cambrian A-granites along with I-type granites is characteristic not only of the Subpolar Urals. It was noted in the Polar and Subpolar Urals, Northern Urals (Isherim block), Middle Urals (Ufaley block) and even in the north of the Bashkirian anticlinorium (Yurma massif) [Petrov et al., 2005; Shardakova, 2016; Shardakova, 2017; Shuyskiy et al., 2017; and etc.]. These complexes represented by an uneven broken line to the west of the Main Ural Fault preceded the opening of the Paleoural Ocean in the Early Ordovician, accompanied by the emergence of the Kidryasovo rift complex with the eruption of mainly basic rocks, which reflects the formation of a crust-free oceanic opening, where the continental crust could no longer be melted due to its absence.

Mankhambo A-granites were formed in the presence of slight upward movements of the earth's surface: other than in olistoliths, Cambrian deposits are practically unknown in the Urals and Ural area – only at the very end of the Cambrian, terrigenous deposits began to accumulate locally, which turned into a large-scale accumulation of graben facies in the early Ordovician period.

Kidryasovo complex (475–460 Ma)

The formation of graben facies – coarse clastic strata, whose thickness varies greatly from place to place and whose formation is accompanied mainly by subalkaline basic volcanism – constitutes a direct harbinger of the East European continent splitting against the backdrop of intensified plume-related processes, which ultimately led to the emergence of the Paleoural Ocean and its eastern bound – passive continental margin of the volcanic type [Puchkov, 2002; Puchkov, 2010]. Graben facies, untouched by erosion and not buried by sediments, are dotted along the entire western slope of the Urals, from the Sakmara zone to Baidarat. At the

same time, rhyolites and granites are rather poorly developed. In the Middle Urals near the MUF (Main Ural Fault) zone, there is the Kozinsk suite which supposedly belongs to Ordovician rift formations. It constitutes a thick (up to 3000 m) stratum of quartzitic sandstones and conglomerates containing interbeds of marbles, tufas, basalts, trachybasalts, as well as occasional rhyolites. The subalkaline volcanites of the Polar Urals include faunistically dated acid effusives (Molyudshor Suite) and rhyolite dykes [Puchkov, 1979; Soboleva et al., 2010]. Further north, in the Baidarat zone, the Cambrian(?)–Tremadocian sediments are represented by sandstones, aleurolites and shists; being overlain by the Lower-Middle Ordovician stratum of mottled structure, represented by limestones, schists and aleurolites with basalts, trachybasalts, as well as rhyolites [Puchkov, 2002 and references in this article].

Of particular note is the Kozlinogorsk gabbro-syenite-granite association developed in the Ufaley block of the Middle Urals [Tevelev et al., 2015], which was considered to be Permian and then dated by the cited authors at 476–470 Ma (Floian). The granitoids are moderately alkaline; the whole series is intraplate in terms of its geochemical parameters. Issues concerning the age of the association, as well as its belonging to one or another complex, are debatable. An alternative point of view regarding the age of the association is held by G. Shardakova et al. [2015]. The age determined from the biotites contained in the gabbro using the Ar-Ar method was estimated at 457.8 ± 5.8 Ma. In addition, according to the preliminary results, the vast majority of U-Pb datings of granite zircons yielded ages between 449 Ma and 480 Ma. On the basis of new datings, the authors classified the Kozlinogorsk group of intrusions as Late Ordovician. It is assumed that formations which are spatially combined, similar in composition, but somewhat heterogeneous in ages could be combined into this group, therefore even younger ages can be obtained for alkaline rocks from different intrusions. A similar point of view is held by A. Krasnobayev, who worked with zircon fractions from the alkaline rocks of this association. We believe that it is justifiable to compare it with other known alkaline complexes of the Urals, where, in some cases, carbonatites are known to occur. Most of them are concentrated east of the MUF zone. Among them, the Ilmeny-Vishnevogorsky complex (IVC) is most fully studied. The initial age of its heterogeneous rocks is dated at 440–420 Ma, with isotopic data indicating a significant role of mantle material in the substrate. Such interpretation suggests that the Kozlinogorsk gabbro-granite association might belong to the Ushat complex which is the next one in terms of age.

Ushat complex (440–450 Ma)

This complex was named after a section on the western side of the Taratash Rise (Ushat River). A number of

outcropping subalkaline basaltoids of the BMA, which belong to the Ai and Mashak suites, were the sources of zircons falling in a narrow age range of 435–455 Ma [Krasnobaev et al., 2018]. On the western slope of the Middle Urals, this magmatic stage manifested itself in the syenite-porphyrries of the Verkhnyaya-Serebryanka complex (447 ± 8 Ma [Petrov et al., 2005]). Similar events previously identified in the Southern Urals include the emergence of the most part of the Ilmeny-Vishnevogorsky alkaline carbonatite complex (410–446 Ma), which then underwent transformations at the Late Devonian and Permian collision boundaries with the formation of several types of pegmatites. The issue of the Kozlinogorsk gabbros, syenites and granites belonging to this complex remains unsolved. The analogues of the Ushat complex include the Monteregian group of alkaline intrusions on the Canadian Atlantic coast [Puchkov, 2010].

Timaiz dyke-sill complex belonging to the western slope of the Urals (400–360 Ma, mainly 380–360 Ma)

In an earlier work [Puchkov et al., 2016] we demonstrated that Devonian dyke swarms and associated effusive rocks – whose origin is closely related to the formation of the Devonian Kola-Dneprovsky LIP – were present in this complex from the western slope of the Urals, as well as in Pay-Khoy and Novaya Zemlya. Granitoids and rhyolites are practically absent in this complex. There is only data [Simakov, 1972] on the presence of a microgabbro-syenogranite-alaskite association in the upper the Pechora River intruding the Middle Devonian rocks and dated at 276 ± 13 and 296 ± 12 Ma (Lower Permian) using the K-Ar method; however, most likely, these ages are underestimated (otherwise there is nothing to tie them to). Their Devonian age is not ruled out. In addition, we can name only a single dyolite dyke in the Devonian Aptechnogorsk complex (Nizhniye Sergi, Middle Urals).

Stepninsky monzonite-granite complex (280–285 Ma)

The geological unit in question was named after the Permian Stepninsky monzodiorite-granite complex represented by a chain of intrusions extending from the northwest to the southeast (Uysky, Vandyshevsky, Biryukovsky, Stepninsky). The intrusions intersect three structural zones of the Southern Urals and the overlying fold structure. The complex in question was described in detail in [Fershtater, 2013]. Preliminary data on the age of massifs (281 ± 2 , 281 ± 2 , 280 ± 2 and 286 ± 2 Ma, respectively), which were obtained using SHRIMP-2 (VSEGEI), indicate their Early Permian age. The plume nature of the complex has been suggested for a long time, which is based on the overlying

character of intrusions [Puchkov et al., 1986]. In terms of its geochemical features [Snachev et al., 2018], the range of rocks from the Stepninsky complex clearly fits into two main reference trends: monzonite (monzogabbros, monzodiorites, syenites) and calc-alkaline; which indicates that different mechanisms were involved in the formation of intermediate-basic and acid rocks. At the same time, gabbros are found within the OIB (ocean-island basalt) fields, which makes them similar to rift/plume complexes of mantle origin. The formation of acid rocks exhibiting the calc-alkaline trend can be explained by the melting of the crust rather than by subduction which ended there long ago. Initially, we assumed that granites exhibited a regular time progression; however, it was not confirmed, which is very rare for a fold area.

Triassic Ural-Siberian (250–230 Ma)

A Triassic LIP, partially including the territory of the Ural-Novaya Zemlya fold zone, covers a vast territory of Siberia; thus, this province should be called Ural-Siberian. Magmatic events which occurred at the Permian-Triassic boundary are considered to be the manifestations of a giant superplume. In the Urals and the Ural region, these include the outwellings of Triassic trappean basalts, occurring from Turgay to Pay-Khoy. In the Polar Urals and Siberia, the outwellings of trappean rocks began simultaneously at the Permian-Triassic boundary (250 Ma ago). Acid effusives, which give a contrasting character to basalt eruptions, are characterised by a highly subordinate distribution and are found in the Middle Urals, east of Kamensk-Uralsky (in the Borisovo and Pershino quarries, dated as the Early Triassic using the U-Pb method) [Puchkov, 2010 and references in this work]. It is known, that Triassic traps occur in the grabens of the West Siberian basin overlying the following Ural structures: North Sosva, Danilovo and Polovinkino [Ivanov et al., 2016]. Moreover, only the Danilovo graben is characterised by the presence of a contrasting basalt-rhyolite formation, which could be due to a more sialic composition of the basement.

In [Puchkov, 2010] we examined the data presented in the works on the Triassic datings derived from small acid intrusions, spatially isolated from Triassic volcanites (Malaya-Cheka and Kisinet complexes), as well as from the Murzin-Aduy collision granites [Popov, 2003; Tevelev et al., 2009]. These datings are quite contradictory; thus, they do not give a clear indication that the formation of these granitoids coincided with the onset of trap magmatism. Nevertheless, our attempt to confirm the Triassic age of the alkaline granitoids from the Malaya Cheka complex led to the conclusion about its Carboniferous age [Salikhov et al., 2013].

CONCLUSION

A general review of the conditions under which plume processes can lead to the formation of silicic melts, as well as the consideration of rhyolite-granite magmatism as a component of plume magmatism using a number of volcanic and intrusive complexes of the Urals as an example, suggest that, along with the spreading, subduction and collision, plume tectonics is a powerful independent factor regulating silicic magmatism on the continental and transitional crust. In some cases, it can be associated with active-type rifting, which is the consequence of deeply originating plume-related processes – not their cause. However, in many cases, no signs of grabens or their relics are observed. As for the reasons behind the formation of acid melts, it is impossible to deny the possibility of basaltic magma differentiation or its segregation; however, it seems that the main reason, remains to be the melting of the crust and, in particular, its more ancient silicic components under the influence of the initial plume-related basic magma.

This study is supported by the Russian Science Foundation (project No. 16-17-10192).

REFERENCES

- Ariskin A.A. (2017) *Magmaticeskije formatsii geodinamicheskikh obstanovok. Kurs lektsii* [The Course of lectures: Magmatic formations of geodynamic situations]. Lectures 15, 16a, 16b. URL: <http://www.planetology.ru/lectures/ariskin/?language=russian>. (In Russian)
- Bowden P., Kinnaird J.A. (1984) The petrology and geochemistry of alkaline granites from Nigeria. *Phys. Earth Planet. Interiors*, **35**, 199-211.
- Bryan S.E., Ernst R.E. (2008) Revised definition of Large Igneous provinces (LIPs) *Earth Sci. Rev.*, **86**, 175-200.
- Bryan S., Ferrari L. (2013) Large igneous provinces and silicic large igneous provinces: Progress in our understanding over the last 25 years. *Geol. Soc. Amer. Bull.*, **125**, 1053-1058.
- Ernst R. (2014) *Large Igneous Provinces*. L.: Cambridge University Press, 653 p.
- Ernst R.E., Pease V., Puchkov V.N., Kozlov V.I., Sergeeva N.D., Hamilton M. (2006) Geochemical Characterization of Precambrian magmatic suites of the southeastern margin of the East European Craton, Southern Urals, Russia. *Geological Digest. Geol. Institute of the Ufimian scientific centre of RAS*, (5).
- Fershtater G.B. (2013) *Paleozoiskii intruzivnyi magmatizm Srednego i Yuzhnogo Urala* [Paleozoic intrusive magmatism of the Middle and Southern Urals]. Ekaterinburg, UrO RAS Publ., 365 p. (In Russian)
- Ivanov K.S., Fedorov Yu.N., Erokhin Yu.V., Ponomarev V.S. (2016) *Geologicheskoe stroenie fundamenta Priural'skoi chasti Zapadno-Sibirskogo neftegazononogo megabasseina* [Geological structure of the basement of Cis-Uralian part of the West-Siberian oil and gas megabasin]. Ekaterinburg, IGG UrO RAS Publ., 302 p. (In Russian)
- Khodorevskaya L.I. (2017) Influence of fluid regime on the melting of rocks of oceanic crust (experimental data) at 900–1000°C, 5–10 kbar. *Granity i evolutsia Zemli mantiya I kora v granitobrazovanii* [Granites and the Earth's Evolution: the Mantle and the Crust in Granite Origin]. *Proc. 3rd Int. geol. conf.* Ekaterinburg, 341-343. (In Russian)
- Kholodnov V.V., Fershtater G.B., Shagalov E.S., Sharda-kova G.Yu. (2017) The Riphean magmatism and ore formation, before the opening of the Uralian Paleoocean (the western slope of the Southern Urals). *Litosfera*, **17**(2), 5-26. (In Russian)
- Kinnaird J.A., Nex P.A.M., Milani L. (2016) Tin in Africa. *Episodes*, **39**(2), 361-380.
- Kovalev S.G., Vysotsky S.I., Kovalev S.S. (2018a) *Model formirovaniya magmaticeskikh porod Shatakского kompleksa* [Model of the origin of magmatic rocks of the Shatak complex]. *Geol. Vestn.*, **1**(2). In print. (In Russian)
- Kovalev S.G., Puchkov V.N., Vysotsky S.I., Kovalev S.S. (2018b) Finds of "ancient" zircons in igneous rocks of the Shatak complex (Southern Urals) and their petrogenetic consequences. *Dokl. AN*. In print. (In Russian)
- Kozlov V.I., Puchkov V.N., Krasnobaev A.A., Nekhorosheva A.G., Busharina S.V. (2011) Arshinian – a new straton of the Riphean in the stratotypical sections of the Southern Urals. *Geol. Sbornik IG USC RAS*, **9**, 3-8. (In Russian)
- Krasnobaev A.A., Kozlov V.I., Puchkov V.N., Busharina S.V., Sergeeva N.D., Paderin I.P. (2013a). Zircon geochronology of the Mashak volcanics and the problem of an age of the boundary between the Lower and Middle Riphean (Southern Urals). *Stratigr. Geol. Korrel.*, **21**(5), 3-20. (In Russian)
- Krasnobaev A.A., Kozlov V.I., Puchkov V.N., Larionov A.N., Nekhorosheva A.G., Berezhnaya N.G. (2007b). On the age of Barangulovo gabbro-granite complex, Southern Urals. *Geol. Sbornik IG USC RAS*, **6**, 7-16. (In Russian)
- Krasnobaev A.A., Kozlov V.I., Puchkov V.N., Rodionov N.V., Nekhorosheva A.G., Kiseeva K.N. (2007a). Akhmerovo massif – a representative of Mesoproterozoic intrusive magmatism in the Southern Urals. *Dokl. Akad. Nauk*, **418**(2), 241-246. (In Russian)
- Krasnobaev A.A., Puchkov V.N., Sergeeva N.D. (2013b) Zirconology of the Kiryabinsky pyroxenite-gabbro complex (Southern Urals). *Dokl. Akad. Nauk*, **450**(2), 204-208. (In Russian)
- Krasnobaev A.A., Puchkov V.N., Sergeeva N.D. (2018) Polychronous zirconology of the Navysh volcanics of the Ai Formation. *Dokl. Akad. Nauk*, **478**(1), 74-80. (In Russian)
- Krasnobaev A.A., Kozlov V.I., Puchkov V.N., Sergeeva B.D., Busharina S.V. (2012) New data on the zircon geochronology of the Arshinian volcanics (Southern Urals). *Litosfera*, **4**, 127-140. (In Russian)
- Krasnobaev A.A., Puchkov V.N., Sergeeva N.D., Busharina S.V. (2017) Mineralogy, U-Pb (TIMS, SHRIMP) age and REE in zircons of granites of the Mazara massif (Southern Urals). *Geokhimiya*, **6**, 497-512. (In Russian)
- Kuznetsov N.B., Soboleva A.A., Udoratina O.V., Gertseva M.V., Andreichev V.L., Dorokhov N.S. (2007) Pre-uralian tectonic evolution of the north-eastern and east-

- tern frame of the East European platform. P. 2. *Litosfera*, (4), 32-45. (In Russian)
- Larin A.M. (2011) *Granity rapakivi i assotsiiruyushchie porody* [Rapakiwi-granites and associated rocks]. St.Petersburg, Nauka Publ., 402 p. (In Russian)
- Makhlav L.V. (1998) On what depends the mineral composition of granites. *Soros educational J.*, **11**, 120-125. (In Russian)
- Maslov A.V., Kovalev S.G., Puchkov V.N., Sergeeva N.D. (2018) Arshinian series of the Riphean of the Southern Urals: on the question of geodynamic nature of the rock associations. *Dokl. Akad. Nauk*, **480**(1), 1-5. (In Russian)
- Mazarovich A.O. (2000) *Geologicheskoe stroenie Tsentralnoi Atlantiki: razlomy, vulkanicheskie sooruzheniya i deformatsii okeanskogo dna* [Geological structure of the Central Atlantica: faults, volcanic edifices and deformations of oceanic floor]. Moscow, Nauchnyi Mir Publ., 176 p. (In Russian)
- North Atlantic Igneous Province: Stratigraphy, Tectonic, Volcanic and Magmatic Processes. (2002) (Eds D.W. Jolley, B.R. Bell). *Geol. Society, London, Special Publ.*, **197**, 1-13.
- Petrov G.A., Maslov A.V., Ronkin Yu.L. (2005) Pre-Paleozoic magmatic complexes of the Kvarqush-Kamenogorsk anticlinorium (Middle Urals): new data on geochemistry and geodynamics. *Litosfera*, (4), 42-69. (In Russian)
- Popov V.S., Bogatov V.I., Petrova A.Yu., Belyatski B.V. (2003) Age and probable sources of granites of the Murzinsk-Aduj block, Srednij Urals. *Litosfera*, **4**, 3-18. (In Russian)
- Puchkov V.N. (1975) *Strukturnye svyazi Pripolyarnogo Urala i Russkoi platformy* [Structural connections of Pre-Polar Urals and Russian Platform]. Leningrad, Nauka Publ., 202 p. (In Russian)
- Puchkov V. (1979) *Batialnye komplekсы passivnykh okrain geosynklinalnykh oblastei* [Bathyal complexes of passive margins of geosynclines]. Moscow, Nauka Publ., 260 p. (In Russian)
- Puchkov V. (2002) Paleozoic evolution of the East European continental margin involved into the Urals. *Mountain Building in the Uralides: Pangea to the Present* (Eds D. Brown, C. Juhlin, V. Puchkov). *AGU Geophysical Monograph Series*, **132**, 9-32.
- Puchkov V.N. (2010) *Geologiya Urala i Priuralya (aktualnye voprosy stratigrafii, tektoniki, geodinamiki i metallogenii)* [Geology of the Urals and Cis-Urals (actual topics of stratigraphy, tectonics, geodynamics and metallogeny)]. Ufa, DizainPoligrafServis Publ., 280 p. (In Russian)
- Puchkov V.N. (2016) Relationships of plate-tectonic and plume processes. *Geotektonika*, **4**, 88-104. (In Russian)
- Puchkov V.N. (2018a) Relationships of plate-tectonic and plume processes in the Urals. *Materialy L Tektonicheskogo soveshaniya. T. 2* [Materials of the L-th Tectonic Meeting. V. 2]. Moscow, GEOS Publ., 124-127. (In Russian)
- Puchkov V.N. (2018b) Plumes – a new word in the geology of the Urals. *Litosfera*, **18**(4), 483-499. (In Russian)
- Puchkov V.N., Bogdanova S.V., Ernst R., Kozlov V.I., Krasnobaev A.A., Söderlund U., Wingate M.T.D., Postnikov F.V., Sergeeva N.D. (2013) The ca. 1380 Ma Mashak igneous event of the Southern Urals. *Lithos*, **174**, 109-124.
- Puchkov V.N., Ernst R.E., Hamilton M.A., Söderlund U., Sergeeva N. (2016) A Devonian >2000 km long dolerite swarm belt and associated basalts along the Urals-Novozemelian fold-belt: part of an East-European (Baltica) LIP tracing the Tuzo Superswell. *GFF J.*, **138**(1), 6-16.
- Puchkov V.N., Krasnobaev A.A., Sergeeva N.D., Busharina S.V., Shokalsky S.P. (2017) Zircons, Age, and Geological Setting of Rhyodacite-Porphry from the Bagrussha Complex (South Urals). *Earth Sci.*, **477**(1), 1295-1300.
- Puchkov V.N., Rapoport M.S., Fershtater G.B., Ananyeva E.M. (1986) Tectonic control of the Paleozoic granitoid magmatism on the eastern slope of the Urals. *Issledovaniya po petrologii i metallogenii Urala* [Studies on petrology and metallogeny of the Urals]. Sverdlovsk, IGG UNTz AN SSSR Publ., 85-95. (In Russian)
- Rohde J.K., Bogaard P. van den, Hoernle K., Hauff F., Werner R. (2013) Evidence for an age progression along the Tristan-Gough volcanic track from new ⁴⁰Ar/³⁹Ar ages on phenocryst phases. *Tectonophysics*, **604**, 60-71.
- Ronkin Yu.L. (2017) Isotope geology of rapakiwi granites and related rocks of the Southern Urals: Rb-Sr, Sm-Nd, Lu-Hf AND U-Pb constraints. *Granites and the Earth's Evolution: the Mantle and the Crust in Granite Origin*. Proc. 3rd Int. geol. conf. Ekaterinburg, IGG UB RAS Publ., 239-241.
- Salikhov D.N., Moseychuk V.M., Puchkov V.N. (2013) On the age of alkaline granitoids of the Magnitogorsk gabbro-granite series. *Litosfera*, (5), 165-171.
- Shardakova G.Yu. (2016) Geochemical features and isotopic age of the granitoids of the Bashkirian meganticlinorium – the evidence of pulses of endogenic activity in the junction zone of the Uralian orogeny and the East European platform. *Geokhimiya*, (7), 607-622. (In Russian)
- Shardakova G.Yu. (2017) Vendian-Cambrian granitoids of the western slope of the Urals: features of the composition, geodynamic settings, sources, problems. *Granites and the Earth's Evolution: the Mantle and the Crust in Granite Origin*. Proc. 3rd Int. geol. conf. Ekaterinburg, IGG UB RAS Publ., 341-343.
- Shardakova G.Yu., Saveliev V.P., Puzhakov B.A., Petrov V.I. (2015) New data on the chemical composition and age of the rocks of Kozlinogorsk complex. *Ezhegodnik-2014, Proc. IGG UrO RAS*, **162**, 148-154. (In Russian)
- Shuyskiy A.S., Udoratina O.V., Meng Fancong, Geng Jianzhen (2017) Riftogenic A-type granites of the Polar Urals: new data problems. *Granites and the Earth's Evolution: the Mantle and the Crust in Granite Origin*. Proc. 3rd Int. geol. conf. Ekaterinburg, 361-363.
- Simakov G.V. (1972) Intrusive rocks at the headwater of the Pechora River, the North Urals. *Trudy VII Geologicheskoi konferentsii Komi ASSR* [Proc. VII geol. conf. Komi ASSR]. Syktyvkar, Komi Branch, Academy of Sciences USSR, 121-123. (In Russian)
- Smith R.B., Jordan M., Steinberger B., Puskas C.M., Farrel J., Waite G.P., Husen S., Wulung Chang, O'Conner R. (2009) Geodynamics of the Yellowstone hotspot and mantle plume: seismic and GPS imaging, kinematics, and mantle flow. *J. Volcanol. Geotherm. Res.*, **188**, 26-56.
- Snachev A.V., Puchkov V.N., Snachev V.I., Romanovskaya M.A. (2018) Petrogeochemical features and con-

- ditions of crystallization of monzodiorite-granite massifs of the Plast area. *Vestn. MGU, Ser. Geol.* In print. (In Russian)
- Soboleva A.A., Yudovich Ya.E., Ketris M.P., Vasiliev A.V. (2010) The green schists of the Lemva zone. *Vestn. IG KNC RAS*, **1**, 14-20. (In Russian)
- Tevelev A.I.V., Kosheleva I.A., Khotylev A.O., Prudnikov I.A., Tevelev Ark.V. (2015) The Data on the Composition and Age of the Kozlinogorsk Gabbro-Alkaline Granite Complex on the Western Slope of the Southern Urals. *Moscow University Geol. Bull.*, **70**(4), 338-349.
- Tevelev A.I.V., Kosheleva I.A., Furina M.A., Belyatskij B.V. (2009) Triassic magmatism of the Middle and Southern Urals: geochemistry, isotopic geology, geodynamics. *Vestn. MGU, Ser. Geol.*, **2**, 29-38. (In Russian)
- Udoratina O.V., Andreichev V.L., Kapitanova V.A., Cobble M.A., Geng J.Z. (2017) Granites of Mankhambo and Ilyaiz massifs and rare metal rocks of Mankhambo massif (Northern Urals). *Granites and the Earth's Evolution: the Mantle and the Crust in Granite Origin*. Proc. 3rd Int. geol. conf. Ekaterinburg, 300-303.
- Vernikovskiy V.A., Pease V.I., Vernikovskaya A.E., Romanov A.P., Travin A.V. (2003) First report of Early Triassic A-type granite and syenite intrusions from Taymyr: product of the northern Eurasian superplume. *Lithos*, **66**, 23-36.
- Yarmolyuk V.V., Kuzmin M.I., Ernst R.E. (2014) Intraplate geodynamics and magmatism in the evolution of the Central Asian Orogenic Belt. *J. Asian Earth Sci.*, **93**, 158-179.

ANCIENT AGE OF ZIRCONS AND ISSUES ASSOCIATED WITH THE GENESIS OF DUNITES FROM GABBRO-ULTRABASITE COMPLEXES OF OROGENIC AREAS AND CENTRAL-TYPE PLATFORM MASSIFS

Vsevolod N. Anfilogov¹, Artur A. Krasnobaev², Vyacheslav M. Ryzhkov¹

¹*Institute of Mineralogy, Ural Branch of RAS, Ilmeny Reserve, Miass, 456317 Russia,
e-mail: anfilogov@mineralogy.ru*

²*Zavaritsky Institute of Geology and Geochemistry, UB RAS, 15 Akad. Vonsovsky St., Ekaterinburg, 620016 Russia,
e-mail: krasnobaev@jgg.uran.ru*

Received 17.01.2018, accepted 15.06.2018

The determination of ancient ages of zircons in dunites from the orogenic regions and central-type platform massifs raised a number of issues: 1) the equilibrium of zircon with dunite material and, as a result, the possibility of determining the age of dunite using zircon; 2) polychronic zircons in dunites and the mechanism for the formation of zoned zircon crystals; 3) the origin of the oldest dunite material dated at more than 2500 Ma; 4) mechanism for the formation of zoned zircon crystals in dunite. The article presents results of studying phase equilibrium in the system MgO–SiO₂–ZrO₂, which confirmed the possibility of zircon crystallisation in equilibrium with olivine and pyroxene. It was found that zircon is stable in dunite up to 1450°C, whereas at higher temperatures zircon is replaced by baddeleyite. It is shown that zoned zircon crystals can be formed in dunite as a result of the gradual transformation of zircon into baddeleyite and vice versa. Drawing on the experimental data, the authors proposed a mechanism for the accumulation of dunite material in the form of restite, which forms during the partial melting of mantle peridotite, as well as the possible way for dunite restite to raise to the surface in the form of diapir. The difference between the Ural alpine-type ultrabasites and the ultrabasites of the Platiniferous Belt is discussed. It is proposed that the alpine-type ultrabasite occur closer to the surface where they actively interact with water.

Keywords: *dunite, zircon, age, phase equilibrium, baddeleyite, restite, origin*

Acknowledgments

The work was supported by the UB RAS program No. 15-18-5-12.

INTRODUCTION

Ultrabasite formations are the main components of Earth's orogenic systems. In addition, they constitute the earliest intrusive formations showing the initial stage in the development of linear tectonic-magmatic systems [Kuznetsov, 1964; Pinus et al., 1973; Velinskii, 1979]. However, despite a long history of studying ultrabasite massifs, their genesis is still debatable [Kuznetsov, 1964; Pinus et al., 1973; Pushkarev, Ferstater, 1995; Ivanov, 1997; Efimov, 2010; Malitch et al., 2012]. The most problematic issues associated with ultrabasite formations are as follows: how and where ultrabasic material accumulated, its state of matter upon introduction into the upper levels of the Earth's crust, as well as the mechanism of its introduction. The following views on the genesis of ultrabasites are expressed in the literature [Velinskii, 1979].

1. According to the first view, ultrabasites were formed through the introduction and crystallisation of ultrabasic melt or the crystallisation differentiation of basaltic magma in magmatic chambers. It is believed that the ultrabasic melt was formed during the melting of the upper mantle substance. A high (more than 1500°C) temperature of the ultrabasite melt [Hiroshi, Kushiro, 1993] is not consistent with the chill margins of ultrabasite massifs, as well as with the absence of evidence of the effect of this temperature on the host

rocks [Kuznetsov, 1964; Pinus et al., 1973]. In addition, ultrabasite melt heated to this temperature cannot reach the surface without assimilating the material of the surrounding rocks and thus changing its composition. Despite these contradictions, this view continues to be discussed in the literature [Ivanov, 1997; Saltykov et al., 2008; Simonov et al., 2011].

2. According to the second view, the variety of rocks in the ultrabasite formation is explained by metasomatic processes in the rocks of the upper mantle [Moskaleva, 1959]. The research work of V. Velinskii [1979] and A. Efimova [1995] showed that metasomatism is widespread in ultrabasite massifs; however, being superimposed, it cannot be involved in the formation of primary rocks of ultrabasite massifs.

3. The third view, which considers refractory residue formed from the upper mantle material during the production of basalt melt to be the source of ultrabasites, in our opinion, is the most justified [Pinus et al., 1973; Velinskii, 1979].

GEOLOGICAL STRUCTURE OF ULTRABASITE MASSIFS

One of the most comprehensive works on the study of ultrabasites is the monograph by V. Velinskii [1979], which describes in detail the geological structure and petrography of alpine-type ultrabasite massifs of the

Cenozoic Kamchatka-Koryak orogenic region. Due to young age, these massifs have preserved many structural features that cannot be observed in more ancient orogenic zones where they were erased or deformed by superimposed processes. Studies conducted by V. Velinskii allow us to draw the following conclusions.

1. Ultrabasite massifs are commonly associated with the formations of orogenic systems in their early stage of development, represented by siliceous-volcanogenic deposits.

2. Ultrabasites are predominantly shaped as plates or lenses of various thickness, occurring concordantly within the host rocks. Most often they are introduced into the central parts of anticlinal structures. The position of bodies is determined by the dip angle of the fault, which they are associated with.

3. Well exposed contacts of ultrabasites with host rocks possess a pronounced tectonic character.

4. Eclogite-like garnet-containing rocks were found in the axial part of a number of elongated lentoid ultrabasites.

5. Gabbroid outcrops are associated with all large ultrabasite massifs. Plagiogranite intrusions are also associated with ultrabasites and gabbroids. Gabbro intrusions break through and metamorphose ultrabasic rocks.

A number of important conclusions made drawing on the study of the geological structure of the ultrabasite massifs of the Ural Platiniferous Belt are given in a review paper by A. Efimova [2010].

1. The internal structure of large ultrabasite massifs was formed in the course of high-temperature plastic flow and dynamic metamorphism, which led to the formation of huge volumes of hot tectonites around ultrabasites.

2. The clearly manifested metamorphism of the granulite and amphibolite facies is confined to the contours of the massifs, being absent outside of them.

3. Tectonic-metamorphic evolution (not generation) of the initial ultrabasite material from the Platiniferous Belt could take place in a zone whose depth did not exceed 25 km (about 10–15 km).

4. Dunites are always surrounded by a pyroxenite shell and never come into contact with gabbro.

AGE OF ULTRABASITE MATERIAL

The age of the material composing ultrabasite massifs constitutes one of the most important characteristics exhibited by ultrabasites, the issue of whose genesis is impossible to solve without its determination. In recent years, absolute age has been determined for a number of dunites through U-Pb dating of zircon crystals. This was made possible by using SHRIMP-II – a secondary ion mass spectrometer [Ireland, Williams, 2003]. The results of these studies were quite unexpected. Firstly, it was found that zircons in dunites are polychronic and their age in the same massif can vary from

140 to 2400–2850 Ma. Secondly, ancient zircons dated at 2850–2400 Ma were discovered in the five studied massifs: the Kytlym and Nizhny Tagil massifs in the Urals, the Kondyor and Inagli massifs in the Aldan Province), as well as the Galmoenansky Massif (South Koryakia), [Bea et al., 2001; Knaupf, 2009; Malitch et al., 2009; Krasnobaev et al., 2011; Anikina et al., 2012; Malitch et al., 2012; Ibragimova et al., 2015] (Fig. 1).

Ancient zircons dated up to 3000 Ma are also found in the gabbro-ultrabasite complex of the Mid-Atlantic Ridge [Bortnikov et al., 2008; Shulyatin et al., 2012; Simonov et al., 2013]. This indicates that 3.0–2.5 Ga ago dunites accumulated in the upper mantle or at the base of the lithosphere, which served as material for the formation of ultrabasite massifs of the orogenic system during subsequent activation. The obtained results also indicate that before being introduced into the upper layers of the Earth's crust ultrabasite material underwent a long evolution, which was accompanied by the resetting of the U-Pb zircon chronometer. These results can be considered as a fundamental contribution to studying the history of Earth's geological development, if we prove that zircons in dunites are not xenogenic, engulfed by dunites from other, more acidic rocks, and the ages of zircons correspond to real events that took place during the formation and evolution of dunite materials.

It is traditionally believed that zircon is a mineral present in acidic rocks and that it is unstable if surrounded by dunite material. For this reason, a number of researchers consider zircons in dunites as foreign material engulfed by dunite from host rocks or hypothetical acidic magmas in the process of its formation and introduction [Bea et al., 2001; Bortnikov et al., 2008; Malitch et al., 2012]. Thus, the xenogenicity of zircons in dunite requires a more detailed discussion. Clearly, xenogenic zircon crystals must be present in

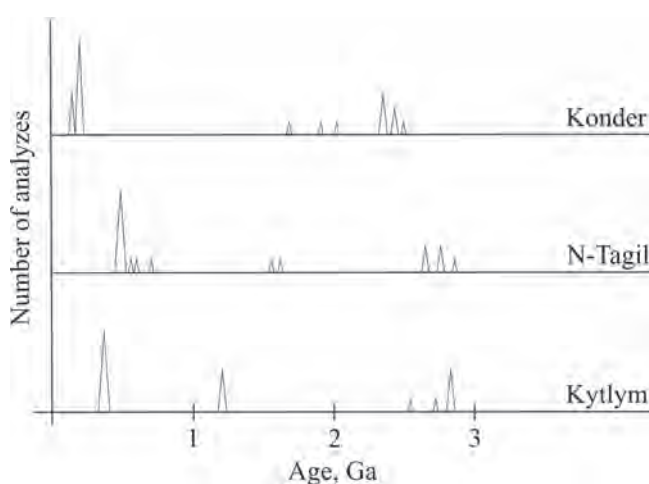


Fig. 1. Absolute ages of zircons from the Nizhny Tagil and Kytlym massifs (Urals) and the Kondyor Massif (Aldan Shield).

dunite as part of rock fragments enveloped by dunite, whose composition is different from that of dunite. The sampling of dunite material from Ural ultrabasite massifs to determine the absolute age revealed no material other than dunite in all the massifs. Figures 2 and 3 show the photographs of zircon crystals from the dunite of the Kytlym Massif. Obviously, if these crystals originate from more acidic rocks and are not in equilibrium with dunite, then they must undergo intense corrosion. However, the beautiful faceting of crystals and the brilliant lustre of facets are not consistent with the assumption about their xenogenic nature.

The host rocks of the Kondyor ultrabasite massif in the Aldan Province are composed by Middle Riphean sedimentary rocks and Early Archean metamorphic rocks, whereas the youngest zircons in dunites are dated at 140–180 Ma old [Malitch et al., 2012].

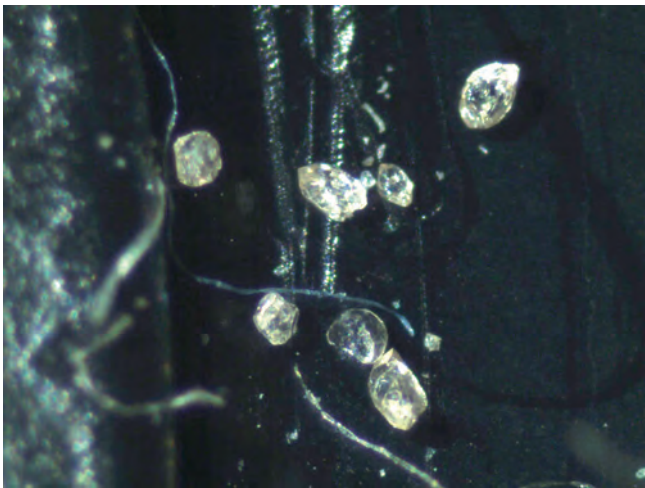


Fig. 2. Zircon crystals from dunites of the Kytlym Massif (Northern Urals).

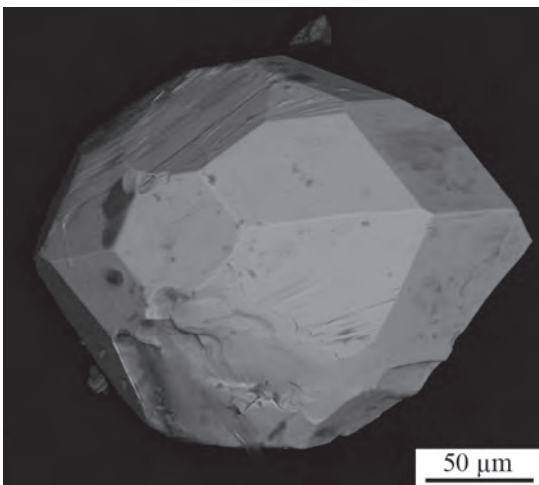


Fig. 3. A zircon crystal from the dunite of the Kytlym Massif, a backscattered electron image.

This brings up the question, where and from which rocks dunite could engulf zircons of this age. There is a point of view that ancient zircons were engulfed by the mantle melt from the rocks of the continental crust, which descended into the mantle during paleosubduction [Bea et al., 2001]; however, according to O. Shulyatin et al. [2012], it is completely incomprehensible how isotopic geochronological data could be stored in zircon crystals at temperatures of 1500–1600°C. In addition, it is difficult to explain why xenogenic zircons dated at more than 2.5 Ga are present in all the studied massifs located in different tectonomagmatic provinces.

PHASE EQUILIBRIA IN THE SYSTEM MgO–ZrO₂–SiO₂

The issue associated with the equilibrium between zircon and dunite, which largely determines the correctness of ages yielded by zircons, can only be solved experimentally drawing on the study of phase equilibria in the system MgO–SiO₂–ZrO₂, which is the basis for determining the stability field of zircon in equilibrium with olivine and pyroxene.

The reference literature [Toropov et al., 1969] gives a diagram showing phase equilibria in the system MgO–SiO₂–ZrO₂ (Fig. 4); however, its correctness raises serious doubts. The area of zircon crystallisation forms a closed field inside the diagram. The position of this area suggests the presence of the ternary compound $m\text{MgO}-n\text{ZrO}_2-q\text{SiO}_2$ – which is absent in this system – rather than zircon. The SiO₂–ZrO₂ side of the diagram is adjacent to the area of two liquids, which

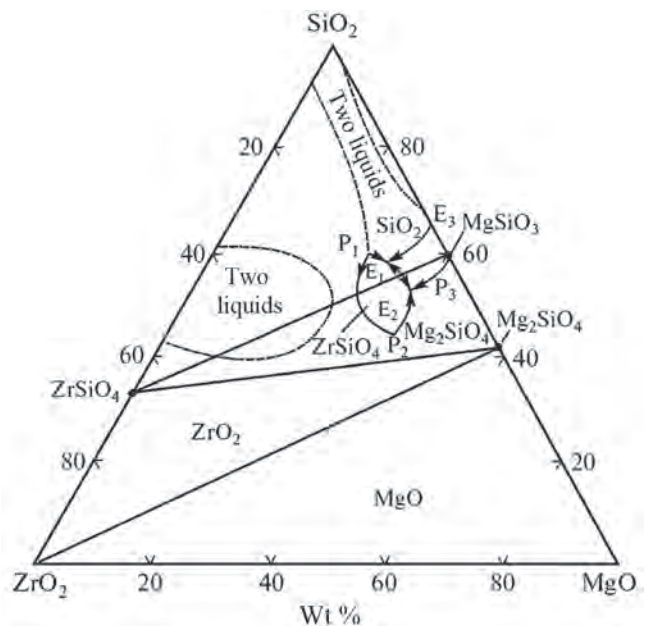


Fig. 4. Diagram of phase equilibria in the system MgO–ZrO₂–SiO₂ [Toropov et al., 1969].

is absent in the binary diagram of $\text{SiO}_2\text{-ZrO}_2$ [Toropov et al., 1969]. This was the basis for the experimental verification of the diagram of the system $\text{MgO-SiO}_2\text{-ZrO}_2$ and for the determination of the real area of zircon crystallisation in equilibrium with Mg_2SiO_4 , MgSiO_3 , and SiO_2 . The experiment results were published in [Ryzhkov et al., 2016].

The diagram showing the phase equilibria that we obtained is shown in Figure 5. This diagram contains 6 fields: I – $\text{MgSiO}_3 + \text{SiO}_2$; II – $\text{MgSiO}_3 + \text{ZrO}_2$; III – $\text{ZrSiO}_4 + \text{SiO}_2$; IV – $\text{MgSiO}_3 + \text{Mg}_2\text{SiO}_4$; V – $\text{ZrO}_2 + \text{MgO}$; VI – $\text{ZrSiO}_4 + \text{ZrO}_2$. The four upper fields, especially fields II and IV, are of interest for solving the issue associated with the stability of zircon in dunite. In field II, zircon is in equilibrium with pyroxene. Along the line separating fields II and IV, zircon is stable in the presence of pyroxene and olivine. With an increase

in the MgO content and a compositional transition of the system into field IV, olivine interacts with zircon forming baddeleyite:



Reaction (1) exhibits two important features: 1) the change in free energy in the reaction at a temperature of $1400\text{--}1500^\circ\text{C}$, calculated according to the data given in [Robie et al., 1978], is close to zero; 2) total molar volumes of phases in the left and right sides of the equation are equal. Given these features, the equilibrium (1) will depend only on the composition of the system. At point P, baddeleyite appears on the liquidus curve (see Fig. 5). The presence of field II in the diagram solves one of the most important issues – the possibility of zircon crystallisation in dunite at a very low concentration of ZrO_2 .

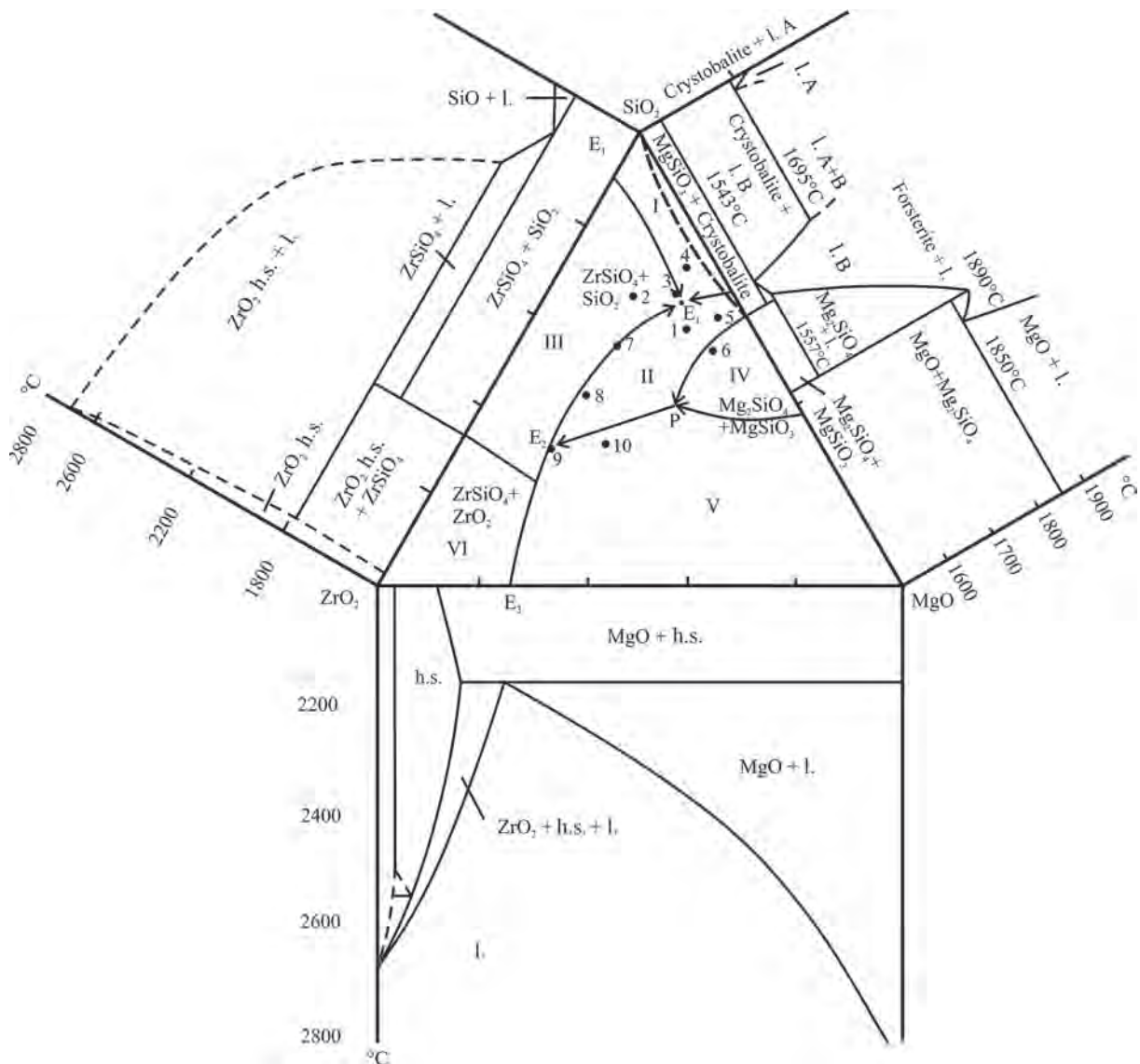


Fig. 5. Diagram of phase equilibria in the system $\text{MgO-ZrO}_2\text{-SiO}_2$ (experimental data).

The formation of baddeleyite in zircon should be considered as acid-base interaction. In this process, a strong base (MgO) takes silica from a weak base (ZrO_2). In accordance with the principle of acid-base interaction, baddeleyite rims around zircon grains appear during the interaction of zircon with olivine, as well as upon introduction of any strong base into the system (for example, CaO in the form of $CaCO_3$). Such processes are observed in rodingites and kimberlites [Corfu et al., 2003; Mitsyuk et al., 2005; Kuznetsov, Mukatova, 2013]. Conversely, in komatiite rock series zircon replaces baddeleyite [Kulikova et al., 2010].

In addition to studying phase equilibria in the system $MgO-SiO_2-ZrO_2$, a series of experiments was carried out to test the stability of zircon in natural dunite. Olivine powder selected from dunite was used as model dunite material [Anfilogov et al., 2015]. It was found that at temperatures above 1450°C a rim (an aggregate of baddeleyite and pyroxene) is formed around the zircon grain (Fig. 6). Note that the model composition of the mixture in the experiments was in field IV (see Fig. 5). Therefore, the interaction of olivine with zircon led to the formation of baddeleyite and pyroxene according to reaction (1). Thus, experiments have shown that zircon remains unchanged in dunite when heated to 1400°C. The results of above-mentioned experimental studies suggest that the absolute age determinations made using zircon reflect the time of real events occurring during the formation and transformation of dunite material.

The second issue associated with determining the age of ultrabasites consists in the need to explain the

mechanism for the formation of zircon generations and zoned zircon crystal in dunite yielding different ages. At the initial stage, when dunite material is generated in the mantle as refractory restite, zoned zircon crystals can form during their growth in the melt; however ultrabasite massifs show several ages, each corresponding to its own generation of zircon crystals or a new zone in a zoned crystal. The problem is that these generations, zones, are formed in solid dunite material, where the introduction of ZrO_2 from the outside is impossible.

New zircon generations are most likely to form in solid dunite if zircon transforms into baddeleyite and vice versa, which occurs according to reaction (1) [Anfilogov et al., 2017]. Given that the concentration of ZrO_2 in solid dunite is constant, the composition of the equilibrium association, which is formed in the course this reaction, will depend only on the concentrations of MgO and SiO_2 in the system.

Baddeleyite rims in zircon grains were found in the zircons of the Kondyor Massif [Ronkin et al., 2013]. The replacement of baddeleyite with zircon was established by A. Davidson and O. van Breemen [1998] in the Greville metagabbro province (Ontario). The zircon, which replaced baddeleyite, was found to be 75 million years younger than baddeleyite.

POSSIBLE MECHANISM UNDERLYING THE FORMATION AND EVOLUTION OF DUNITE MATERIAL

The distribution of zircon ages in ultrabasite massifs (see Fig. 1) allows us to distinguish three stages of their evolution:

- 1) 3000–2400 Ma – formation and accumulation of dunite in the area of basalt melt production;
- 2) 2000–1250 Ma – metamorphism of dunite in deep intermediate foci;
- 3) 500–150 Ma – the introduction of dunite as part of ultrabasites into the upper layers of the Earth's crust. For Ural ultrabasites, the last stage dated at 430–450 Ma corresponds to the early stages in the formation of the Ural orogenic system.

The first stage is of greatest interest. If we proceed from the model according to which ultrabasite material constitutes restite accumulated during the production of basalt melt from the mantle peridotite, then the interval 3000–2400 Ma should correspond to the time when powerful outflows of basalts took place. This period of Earth's geological history was marked by the formation of granite-greenstone belts, which indeed contain large volumes of volcanites of the basic and ultrabasic composition [Glikson, 1980]. The age interval during which these belts were formed is shown in Fig. 7.

Using the restite model to describe the formation and accumulation of dunite, it is necessary to consider at what depth and under what P - T conditions dunite restite is formed. Given that the geothermal gradient

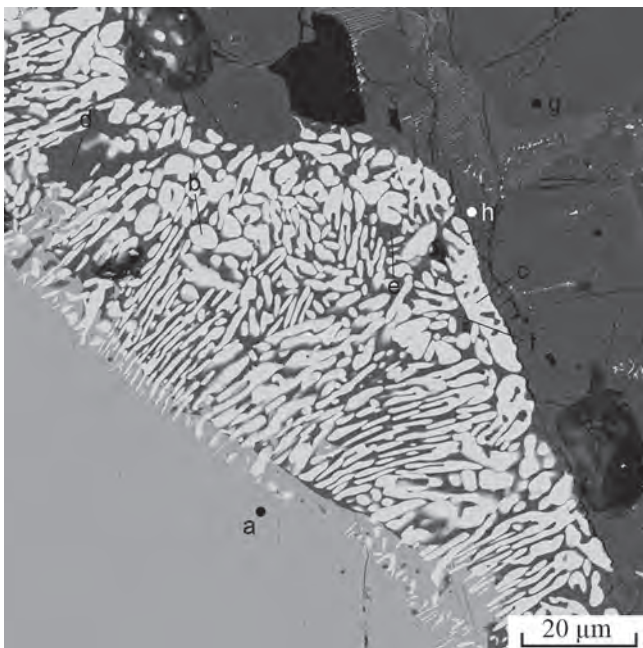


Fig. 6. Rim of baddeleyite lamellae (white) in zircon grain (grey). $T = 1550^\circ\text{C}$.

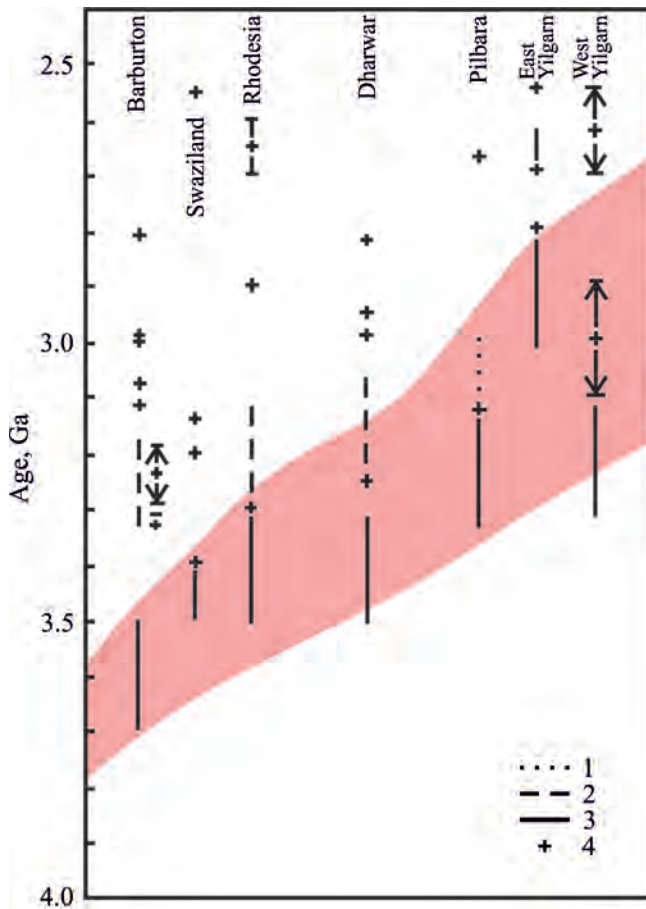


Fig. 7. Formation time of granite-greenstone belts [Glikson, 1980].

1 – sedimentary rocks, 2 – basic-acidic volcanites, 3 – ultra-basic-basic volcanites, 4 – formation of granites.

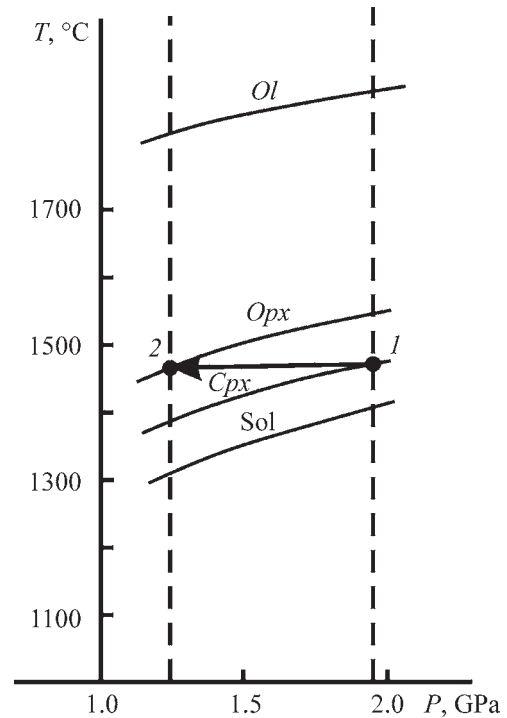


Fig. 8. Fragment of the diagram showing the melting of peridotite at a pressure of up to 2 GPa [Takahashi, 1986].

Sol – solidus line, Cpx – melting of clinopyroxene, Opx – melting of orthopyroxene, Ol – transition to olivine melt; point 1 – *P-T* conditions for the melting of peridotite at a depth of 60 km, point 2 – *P-T* conditions at a depth of 40 km. The arrow indicates the change in the restite composition associated with the isothermal rise of diapir from a depth of 60 km to a depth of 40 km.

was significantly higher during the formation of granite-greenstone belts than the modern one [Savel'eva et al., 2013], it can be assumed that the basalt melt was produced from the mantle peridotite at a depth of not more than 60 km and at a pressure of $P \leq 2$ GPa. A fragment of the diagram showing the melting of spinel lherzolite KLB-1 can be seen in Figure 8 [Takahashi, 1986]. The solidus temperature of lherzolite at a depth of 60 km and at a pressure of 1.9 GPa is 1400°C. At a temperature of 1460°C, clinopyroxene passes into the melt; olivine and orthopyroxene accumulate in restite. Further changes in the composition of the melt and restite occur according to the following scheme. At temperatures above 1300°C, spinel lherzolite becomes ductile. The shear stress in it decreases from 5 kbar at 1000°C and to 0.5 kbar at a temperature of more than 1300°C [Carter, Ave'Lallement 1970; Anfilogov, Khachai, 2007]. The emergence of melt in lherzolite reduces shear stress by an order of magnitude. This creates conditions for the rise of partially molten lherzolite in the form of diapir. When the diapir is rising, the degree of its melting increa-

ses and the melting temperature of pyroxene decreases due to a decrease in pressure. At a depth of 40 km pyroxene melts at a temperature of 1450°C. Only olivine remains in restite, with restite acquiring dunite composition (see Fig. 8). Moreover, the melt fraction in diapir reaches 40% [Takahashi, 1986]. During the movement of diapir, the basalt melt is separated from restite, with the latter, due to its high density, accumulating in the form of a dunite layer at the base of the lithosphere at a depth of 30–40 km. The question arises about the source of ancient zircons in dunite. The most likely source of zircon crystals is mantle peridotite, whose partial melting results in the formation of dunite restite. The possible existence of zircon in mantle peridotite, which was generated during the Earth's formation, is confirmed by the presence of zircon in meteorite material [Lizuka et al., 2015], finds of zircon crystals in kimberlites [Mitsyuk et al., 2005] and xenoliths of mantle peridotites [Salop, 1982]. In the course of partial melting of peridotite, zircon crystals remain in ultrabasite restite and thus get into dunite.

With the subsequent activation of the magmatic process, dunite in the form of diapir can be pushed to the surface. Clearly, there are two ways to bring dunite to the surface. One of them is realised during the formation of small concentrically zoned massifs such as the Kondyor and Inagli massifs. The rise and introduction of dunite material in these massifs occurred simultaneously with the manifestations of alkaline magmatism represented by alkaline gabbroids, syenites and carbonatites [Karetnikov, 2006; Malitch et al., 2012; Ibragimova et al., 2015]. The formation of these rocks involves the active participation of volatile components, including water. The introduction of dunite could be preceded by its partial serpentinisation, which led to a sharp decrease in shear stress and contributed to the formation of a small ductile diapir. A similar mechanism for the formation of the Kondyor Massif was proposed in [Burg et al., 2009].

A different mechanism was active upon the introduction of large alpine-type massifs and massifs of the Ural Platiniferous Belt. These massifs were formed under the conditions of the Earth's crust stretching caused by the emergence of foci of the partial melting of mantle peridotite at a depth of about 100 km. The melting was accompanied by a pressure increase, which led to the formation of a stretch region and a dome-shaped elevation on the surface above the melting zone [Anfilogov, Khachai, 2007]. If there was a layer of dunite restite directly above the melting zone, accumulated during the previous magmatic activation, then as a result of heating and increasing plasticity, the dunite material will be extruded to the surface in the form of a large diapir. When the diapir is raising, a situation may arise when the excess pressure acting on the diapir is balanced by the lithostatic pressure. In this situation, a dunite diapir can change the direction of movement from vertical to horizontal. As a result, a horizontally occurring ultrabasite body will be formed. Such a transition from the vertical to the horizontal direction of movement has been established for the Kimpersay Massif (South Ural) [Savel'ev et al., 2008].

The rise of dunite diapir to the surface will precede the rise of basalt melt forming in the melting zone. Eventually, an age-related relationship between dunite and gabbro develops, which is characteristic of ultrabasite massifs: the age of gabbro associated with ultrabasites is several million years younger than that of ultrabasite.

In conclusion, it is necessary to consider the fundamental differences between alpine-type ultrabasites and ultrabasites from the Platiniferous Belt and central-type massifs. Research conducted by G. Pinus, E. Velinskii and et al. [Pinus et al., 1973] showed that for them, as well as for other ultrabasites, the 'restite' mechanism underlying the accumulation of ultrabasic material is the most justified one. The distribution of U-Pb zircon age turned out to be essentially the same.

All types of ultrabasites contain ancient zircons yielding an age of more than 2500 Ma. The comparison of U-Pb ages, petrography, petrochemistry and geochemistry of rare elements born by alpine-type Ural ultrabasites with the ultrabasites of the Platiniferous Belt revealed no fundamental differences between them as well [Chashchukhin et al., 2007; Savel'ev et al., 2008]. The only significant characteristics of alpine-type ultrabasites from the Urals that distinguish them from the ultrabasites of the Platiniferous Belt are a high degree of serpentinisation and chromite content [Chashchukhin et al., 2007; Savel'ev et al., 2008].

These differences can be explained if we assume that upon introduction, the material of alpine-type ultrabasites rises closer to the surface than the ultrabasites of the Platiniferous Belt. As a result, it finds itself in the area of active pore fluid flow, which occurs in thermal fields around magmatic bodies [Lykov, 1954; Kadik, Stupakov, 1970; Anfilogov, Purtov, 1976; Anfilogov, 2010]. The interaction of intruded hot ultrabasites with the pore fluid will lead to their intense serpentinisation, redistribution of chromium and its concentration in the form of ore bodies.

Important results were obtained when determining the U-Pb age of zircons taken from the chromite-enriched dunite of the Voykar-Synya Massif in the Polar Urals [Savel'eva et al., 2013]. Five age groups of zircons have been established: 1) 2565 Ma, 2) 2304–2363 Ma, 3) 1873–2038 Ma, 4) 480–552 Ma, 5) zircons younger than 350 Ma. This indicates that the dunite material of chromite-bearing alpine-type ultrabasites underwent the same evolutionary stages as the massifs of the Platiniferous Belt and central-type platform massifs, with the differences between them arising after their introduction into the host rocks rather than in the mantle.

CONCLUSIONS

1. The studying of phase equilibria in the system MgO–SiO₂–ZrO₂ revealed that zircon can crystallise in equilibrium with pyroxene and olivine. This suggests that the U-Pb age of zircon in dunite determines the time when dunite material was formed and its subsequent evolution.

2. The distribution of zircon ages in ultrabasite massifs helps to distinguish three stages of their evolution: 1) 3000–2400 Ma – formation and accumulation of dunite material; 2) 2000–1250 Ma – metamorphism of dunite material in intermediate foci; 3) 500–150 Ma – the time of dunite introduction (established for different massifs) into the upper levels of the Earth's crust.

3. Drawing on the experimental data about the melting of garnet lherzolite, a mechanism is proposed for the formation of dunite material during the partial melting of mantle peridotite, its accumulation in the melting zone and subsequent displacement into the upper layers of the crust in the form of diapirs.

4. We examined the conditions leading to the formation of alpine-type ultrabasites, which explain their differences from the ultrabasites of the Ural Platiniferous Belt.

The work was supported by the UB RAS program No. 15-18-5-12.

REFERENCES

- Anfilogov V.N. (2010) Origin of andesite and rhyolite of complementary magma series. *Litosfera*, (1), 37-46. (In Russian)
- Anfilogov V.N., Khachai Yu.V. (2000) Hydroextrusion is a possible mechanism for the movement of diapirs, domes and mantle plumes. *Geokhimiya*, (8), 873-878. (In Russian)
- Anfilogov V.N., Khachai Yu.V. (2007) Superplumes: tectonics, magmatism, metamorphism. "Geodinamika formirovaniya podvizhnykh pojasov zemli". Materialy Mezhdunar. konferentsii ["Geodynamics of the formation of mobile belts of the earth". Materials of the Intern. conf.]. Ekaterinburg, IGG, UB of RAS, 6-9. (In Russian)
- Anfilogov V.N., Krasnobaev A.A., Ryzhkov V.M., Valizer P.M. (2017) Replacement of zircon with baddeleyite as a likely mechanism of the formation of zoned zircon crystals in ultrabasic rocks. *Dokl. Earth Sci.*, **475**(2), 946-948.
- Anfilogov V.N., Purtov V.K. (1976) Mechanism of interaction of pore solutions with magmatic bodies. *Geokhimiya*, (9), 1400-1403. (In Russian)
- Anfilogov V.N., Ryzhkov V.M., Blinov I.A., Krasnobaev A.A., Kabanova L.Y., Valizer P.M. (2015) Stability of zircon in dunite at 1400–1550°C. *Dokl. Earth Sci.*, **464**(1), 963-966.
- Anikina E.V., Krasnobaev A.A., Rusin A.I., Busharina S.V., Kapitonov I.N., Lokhov K.I. (2012) Isotope-geochemical characteristics of zircon from dunites, clinopyroxenites and gabbro Platinum belt of the Urals. *Dokl. Akad. Nauk*, **443**(6), 711-715. (In Russian)
- Bea F., Fershtater G.B., Montero P., Whitehouse M., Levin V.Ya., Scarrow J.H., Austrheim H., Pushkariev E.V. (2001) Recycling of continental crust into mantle as revealed by Kytlym dunite zircons, Ural. *Terra Nova*, **13**(6), 407-412.
- Bortnikov N.S., Sharkov E.V., Bogatkov O.A., Zinger T.F., Lepekhina E.N., Antonov A.V., Sergeev S.A. (2008) Finds of young and ancient zircons in gabbroids of the Markov deep, mid-atlantic ridge, 5°54'-5°02.2' N (results of SHRIMP-II U-PB dating): implication for deep geodynamics of modern oceans. *Dokl. Earth Sci.*, **421**(1), 859-866.
- Burg J.P., Bodiner J.L., Gerya T., Bedini R.M., Boudier F., Daurtria J.M., Prikhodko V., Efimov A., Pupier E., Balanec J.L. (2009) Translithospheric mantle diapirism. Geological evidence and numerical modeling of the Kondyor ultramafic complex (Russian Far-East). *J. Petrol.*, **50**(2), 289-321.
- Carter N.L., Ave'Llallement H.G. (1970) High temperature flow of dunite and peridotite. *Geol. Soc. Amer. Bull.*, **81**, 2181-2202.
- Chashchukhin I.S., Votyakov S.L., Shchapova Yu.V. (2007) *Kristalloghimiya khromshpineli i oksitermobarometriya ul'tramafitov skladchatykh oblastei* [Crystallochemistry of chrome spinels and oximeterometry of ultramafites of folded regions]. Ekaterinburg, 310 p. (In Russian)
- Corfu F., Hanchar J.M., Hoskin P.W.O., Kinny P. (2003) *Atlas of zircon texture*. *Rev. Mineral. Geochim.*, **53**, 469-500.
- Davidson A., van Breemen O. (1998) Baddeleyite-zircon relationship in coronic metagabbro, greville province, Ontario: implication for geochronology. *Contrib. Mineral. Petrol.*, **100**, 291-299.
- Efimov A.A. (1995) High-temperature aqueous metamorphism in the Platiniferous Belt of the Urals: Tectonic regime and metamorphic reactions. *Aktual'nye problemy magmaticheskoi geologii, petrologii i rudoobrazovaniya* [Actual problems of magmatic geology, petrology and ore formation]. Ekaterinburg, Uralgeolkom, IGG UB RAS, 150-156. (In Russian)
- Efimov A.A. (2010) Results of a 100-year study of the Platinum Belt of the Urals. *Litosfera*, (5), 134-153. (In Russian)
- Glikson A. (1980) Stratigraphy and evolution of primary and secondary greenstone complexes; data on the shields of the southern hemisphere. *Rannaya istoriya Zemli* [Early history of the Earth]. Moscow, Mir Publ., 264-285. (In Russian)
- Heuman L.M., LeCheminant A.N. (1993) Paragenesis and U-Pb systematics of baddeleyite (ZrO₂). *Chem. Geol.*, **110**, 95-126.
- Hiroshi K., Kushiro I. (1993) Partial melting of dry peridotite at high pressure: Determination of composition of melts segregated from peridotite using aggregates of diamonds. *Earth Planet. Sci. Lett.*, **114**, 477-489.
- Ibragimova E.K., Rad'kov A.V., Molchanov A.V., Shatova N.V., Shatov V.V., Lepekhina E.N., Antonov A.V., Tolmacheva E.V., Solov'ev O.L., Terekhov A.V., Khorokhorina E.I. (2015) The results of U-Pb (SHRIMP II) dating of zircons from dunites of Inagli massif (Aldan Shield) and the problem of the genesis of concentrically zoned complexes. *Regional. Geol. Metallogeny*, (62), 64-78. (In Russian)
- Ireland T.R., Williams I.S. (2003) *Rev. Mineral. Geochim.*, **53**, 215-241.
- Ivanov O.K. (1997) *Kontsentricheski-zonal'nye piroksenit-dunitovye massivy Urala: mineralogiya, petrologiya, genesis* [Concentrically zoned pyroxenite-dunite massifs of the Urals: mineralogy, petrology, genesis]. Ekaterinburg, URGU Publ., 488 p. (In Russian)
- Kadik A.A., Stupakov E.P. (1970) Modeling of temperature fields near magmatic bodies with considerable radial extent. *Geokhimiya*, (1), 43-53. (In Russian)
- Karetnikov A.S. (2006) Age and genesis of platinum mineralization of the Konder massif: paleomagnetic and radioisotope data. *Litosfera*, (3), 96-107. (In Russian)
- Knaupf O.V. (2009) U-PB age of zircons from dunite-clinopyroxenite nuclei of Kytlymsky (Middle Urals) and Galmoenensky (South Koryakia) zonal massifs of the Ural type. *Vestn. SPbGU*, (4), 64-71. (In Russian)
- Krasnobaev A.A., Anikina E.V., Rusin A.I. (2011) Zirconology of dunite of the Nizhny Tagil massif (Middle Urals). *Dokl. Earth Sci.*, **436**(2), 290-294.
- Kulikova V.V., Bychkova Ya.V., Kulikov V.S. (2010) Baddeleyite is the main mineral for isotopic dating of mafic-ultramafic komatiite series of the southeastern Fennoscandian shield. "Sovremennaya mineralogiya: ot teo-

- rii k praktike*". Tezisy XI s"ezda Rossiiskogo mineralogicheskogo obshchestva ["Modern mineralogy: from theory to practice". Abstracts of the XI Congress of the Russian Mineralogical Society], 212-214. (In Russian)
- Kuznetsov D.V., Mukatova A. (2013) The formation of baddeleyite during the disilication of zircon in the rodingitized highly granular granitites of the Mindyak massif in the Southern Urals. *Ezhgodnik-2012. Tr. IGG UrO RAN* [Yearbook-2012. Proc. IGG UB RAS], **160**, 224-228. (In Russian)
- Kuznetsov Yu.A. (1964) *Glavnye tipy magmaticheskikh formatsii* [The main types of magmatic formations]. Moscow, Nedra Publ., 387 p. (In Russian)
- Lizuka T., Yamaguchi T., Hibiya Y., Amelin Y. (2015) Meteorite zircon constrains on the bulk Lu-Hf isotope composition and early differentiation of the Earth. *Proc. Nat. Acad. USA*, **112**(17), 5331-5336.
- Lykov A.V. (1954) *Yavleniya perenosa v kapillyarnoporistykh telakh* [Transport phenomena in capillary-porous bodies]. Moscow, Gos. Izd. technical and theoretical literature Publ., 296 p. (In Russian)
- Malitch K.N., Efimov A.A., Ronkin Yu.L. (2009) Archean U-Pb isotope age of zircon from dunite of the Nizhny Tagil massif (the Uralian Platinum belt). *Dokl. Earth Sci.*, **427**(1), 851-855.
- Malitch K.N., Efimov A.A., Badanina I.Yu. (2012) The age of Kondyor massif dunites (Aldan province, Russia): first U-Pb isotopic data. *Dokl. Earth Sci.*, **446**(1), 1054-1058.
- Mitsyuk S.S., Zinchuk N.N., Koptil' V.N., Kutuzova E.Ya., Lashkevich I.V. (2005) New indicators of zircons of kimberlite origin. *Geologiya almazov – nastoyashchee i budushchee* [Geology of diamonds – present and future]. Voronezh, St.Univ. Publ., 674-720. (In Russian)
- Moskaleva S.V. (1959) On the age and structure of the Kraka massifs in the Southern Urals. *Dokl. Akad. Nauk SSSR*, **127**(1), 170-173. (In Russian)
- Pinus G.V., Velinskii V.V., Lesnov F.P., Bannikov O.L., Agafonov L.V. (1973) *Al'pinotipnye giperbazity Anadyro-Koryakskoi skladchatoi sistemy* [Alpinotype hyperbasites of the Anadyr-Koryak fold system]. Novosibirsk, Nauka Publ., 320 p. (In Russian)
- Pushkarev E.V., Fershtater G.B. (1995) Mineralogical and petrochemical discreteness of rocks and the problem of the origin of primary melts of dunite-clinopyroxenite-syenite-gabbro complexes. *Aktual'nye problemy magmaticheskoi geologii, petrologii i rudoobrazovaniya* [Actual problems of magmatic geology, petrology and ore formation]. Ekaterinburg, Uralgeolkom, IGG, UB RAS, 100-110. (In Russian)
- Robie R.A., Hemingway B.S., Fisher J.R. (1978) Thermodynamic properties of minerals and related substances at 298.15K and 1 bar Pressure and at higher temperatures. *Geol. Surv. Bull.*, **1452**, 456.
- Ronkin Yu.L., Efimov A.A., Lepikhina G.A., Maslov A.V., Rodionov N.V. (2013) U-Pb dating of the baddeleyite-zircon system from Pt-bearing dunite of the Konder massif, Aldan shield: new data. *Dokl. Earth Sci.*, **450**(2), 607-612.
- Ryzhkov V.M., Anfilogov V.N., Blinov I.A., Krasnobayev A.A., Valizer P.M. (2016) Phase equilibria in the MgO-SiO₂-ZrO₂ system. *Dokl. Earth Sci.*, **469**(2), 824-827.
- Salop L.I. (1982) *Geologicheskoe razvitiye Zemli v dokembrii* [Geological development of the Earth in the Precambrian]. Leningrad, Nedra Publ., 343 p. (In Russian)
- Saltykov A.K., Nikitina L.P., Matukov D.I. (2008) U-Pb age of zircon from xenoliths of mantle peridotites in Cenozoic alkaline basalts of the Vitim plateau (Eastern Baikal region). *Zapiski RMO*, (3), 1-22. (In Russian)
- Savel'ev D.E., Snachev V.I., Savel'eva E.N., Bazhin E.A. (2008) *Geologiya, petrologiya i khromitonosnost' gabbro-giperbasitovykh massivov Uzhnogo Urala* [Geology, petrology and chromite content of gabbro-hyperbasite massifs in the Southern Urals]. Ufa, 319 p. (In Russian)
- Savel'eva G.N., Batanova V.G., Berezhnaya N.A., Presnyakov S.L., Sobolev A.V., Skublov S.G., Belousov I.A. (2013) Polychronous formation of mantle complexes of ophiolites (Polar Urals). *Geotektonika*, (3), 43-57. (In Russian)
- Shulyatin O.G., Andreev S.I., Belyatskii B.V., Trukhalev A.I. (2012) Age and stage of formation of igneous rocks of the Mid-Atlantic Ridge by geological and radiological data. *Region. Geol. Metallogeny*, **50**, 28-36. (In Russian)
- Simonov V.A., Kovyazin S.V., Prikhod'ko V.S. (2011) Genesis of platiniferous massifs in the Southeastern Siberian platform. *Petrology*, **19**(6), 549-567.
- Simonov V.A., Puchkov V.N., Prikhod'ko V.S., Stupakov S.I., Kotlyarov A.V. (2013) Conditions of crystallization of dunites of the Nizhny Tagil platinum-bearing ultrabasic massif (the Urals). *Dokl. Akad. Nauk*, **449**(6), 692-695. (In Russian)
- Skolotnev S.G., Ipat'eva I.S., Beltenev V.E., Lepekhina E.N. (2010) Younger and older zircons from rocks of the oceanic lithosphere in the central atlantic and their geotectonic implications. *Geotectonics*, **44**(6), 462-492.
- Takahashi E. (1986) Melting of dry peridotite KLB-1 up to 14 GPa: Implication on the origin of peridotitic upper mantle. *J. Geophys. Res.*, **91**, 9367-9382.
- Toropov N.A., Barzakovski V.P., Lapin V.V., Kurzeva N.N. (1969) Diagrammy sostoyaniya silikatnykh system. Spravochnik. T. 1 [Diagrams of the state of silicate systems. Reference book. V. 1]. Leningrad, Nauka Publ., 822 p. (In Russian)
- Velinskii V.V. (1979) *Al'pinotipnye giperbazity perekhodnykh zon ocean-kontinent* [Alpin-type hyperbasites of ocean-continent transition zones]. Novosibirsk, Nauka Publ., 264 p. (In Russian)

XENOCRYSTS AND MEGACRYSTS OF ALKALINE OLIVINE-BASALT-BASANITE-NEPHELINITE ASSOCIATION MAKHTESH RAMON (ISRAEL): INTERACTION WITH CARRIER MAGMAS AND CRYSTALLOGRAPHIC TRANSFORMATIONS

Zinovi Yudalevich, Yevgeny Vapnik

Department of Geological and Environmental Sciences, Ben-Gurion University of the Negev, P.O.B. 653, Beer-Sheva, 84105 Israel, e-mails: zinovi@bgu.ac.il, vapnik@bgu.ac.il

Received 19.01.2018, accepted 15.02.2018

The article considers xenocrysts and megacrysts hosted in the rocks of Early Cretaceous olivine-basalt-basanite-nephelinite association that outcropped in the erosion crater of Makhtesh Ramon (Natural Reserve of Mishmar ha-Nagev, Israel). This magmatic rock association contains a wide spectrum of xenoliths trapped at different crustal levels. These are upper mantle, lower and upper crustal xenoliths. Mantle xenoliths are represented by peridotites, olivine clinopyroxenites, clinopyroxenites, olivine websterites, websterites and their amphibole-bearing analogues. Lower crustal xenoliths are mafic granulites, such as metagabbros and plagioclases, whereas upper crustal xenoliths are the fragments of Neoproterozoic tuffs. Xenocrysts and megacrysts are the fragments of xenoliths that chipped from them on their way to the surface. Alterations in xenoliths, xenocrysts and megacrysts caused by the host melt constitute a common petrographic feature. Xenocrysts and megacrysts are mainly represented by minerals that are compatible with the magmatic rock association. These are olivine, clinopyroxene, amphibole, nepheline, plagioclase, anorthoclase, apatite, magnetite and spinel. The xenocrysts of quartz and orthopyroxene are incompatible with the SiO_2 -undersaturated host rock of this magmatic association. Main reasons determining the interaction between magma and xenoliths include rapid decompression, metamorphism and metasomatism. Xenocrysts are subjected to metamorphism that corresponds to high-temperature facies of contact metamorphism, up to the partial melting of xenocrysts. Metasomatism is directed at equalising the compositions of xenocrysts and eponymous minerals that crystallised from the host melt. There are several important criteria adopted to identify xenocrysts and distinguish them from phenocrysts. These are partial melting, solid-phase decomposition, decrystallisation of primary (before-trapping) textures, recrystallisation and self-faceting of initially xenomorphic grains into the crystals with perfect habits. The chemical composition of xenocrysts has mineral and geochemical indications of xenogenic origin, as well as the signs of a newly-formed substance.

Keywords: *melting, solid-phase decomposition, decrystallisation, self-faceting, xenocrysts, megacrysts, xenoliths, magmatic rocks, Makhtesh Ramon, Israel*

Acknowledgments

The authors express their gratitude to Prof. M. Eyal (Ben-Gurion University, Beer-Sheva, Israel), who was responsible for the overall management of works on studying the magmatism of Makhtesh Ramon. The authors are thankful to O. Dvir (Hebrew University of Jerusalem), V.V. Hiller (IGG UB RAS, Russia), Prof. Ya. Kazir and Ph. students B. Elisha, Ts. Golan, I. Gendelman (Ben-Gurion University, Israel) for the assistance in studying chemical compositions of minerals; Dr. R. Granot (Ben-Gurion University) for providing new data on the Ar-Ar-ages of the studied rocks. The authors are grateful to Prof. G.B. Fershtater (IGG UB RAS, Russia) for comprehensive consultations on petrological issues associated with the study of deep-seated xenoliths and xenocrysts.

INTRODUCTION

During their rise to the earth's surface and under decompression, xenoliths disintegrate, decompose into monomineral fragments (xenocrysts and megacrysts) and enter into a geochemical interaction with the carrier melt, get partially or completely absorbed by it, thus becoming a part of a single magmatic system. In terms of shape and size, xenocrysts and megacrysts, as a rule, externally resemble phenocrysts and their identification constitutes an urgent petrological task.

The present article examines the petrographic and geochemical features of xenocrysts and megacrysts widely developed in the igneous rocks of Makhtesh Ramon, as well as demonstrates the similarities between changes occurring in them and transformations in xenoliths. Special attention is paid to the morphologi-

cal tendency of initially xenomorphic xenocrysts and megacrysts to take crystallographically regular forms, which complicates their identification as minerals alien to the host rocks.

GENERAL GEOLOGICAL DATA ON THE AREA

Tectonically, the area belongs to the territory of the Levant – the continental margin of the Eastern Mediterranean, in the east limited by the transform fault of the Dead Sea, within which the rocks of the Proterozoic crystalline basement are overlain by a thick cover of Meso-Cenozoic deposits.

Makhtesh Ramon constitutes a sublatitudinal mountain depression (45 km long and 10 km wide), whose formation is explained by the erosion of a large

anticline having gently sloping northern and steeply falling southern wings during the formation of the Syrian Arc echoing the collision of the African and Arabian plates with the Alpine-Himalayan orogenic belt in the Late Cretaceous. The stratigraphic cross section of the area up to a depth of more than 1 km is represented by Middle and Upper Triassic deposits (Gevanim, Saharonim and Mohilla FMS: limestones, marls, sandstones, gypsums), Lower and Middle Jurassic deposits (Mishor, Ardon, Inmar и Mahmal FMS: laterites, limestones, dolomites, marls, sandstones, clays), as well as Lower and Upper Cretaceous deposits (Arodagl + Lower Hatira Fm + Upper Hatira Fm, Hazera, Sayarim и Mishash FMS): conglomerates, sandstones, marls, clays, silicas) (Fig. 1). Two long intervals between sedimentation were established: 1. the Upper Triassic – beginning of the Jurassic; 2. the Upper Jurassic – the Lower Cretaceous (up through and including the Barremian Stage). Clearly, the Late Triassic and Early Cretaceous magmatic activities in the area resulted in the tectonic activity, which coincided in time with these breaks.

GEOLOGICAL, PETROGRAPHIC AND GEOCHEMICAL FEATURES EXHIBITED BY IGNEOUS ROCKS IN THE AREA

Basic data on the age, composition, as well as the geodynamic regime for the formation of magmatites in the area were considered in [Garfunkel, Katz, 1967; Bonen et al., 1980; Lang, Steinitz, 1989; Baer et al., 1995; Eyal et al., 1996; Samoilov, Vapnik, 2005; Vapnik et al., 2007; Yudalevich et al., 2014]. As a result, one Triassic and two Early Cretaceous associations manifested in the form of lava flows and small intrusions (sills, laccoliths and dykes) were identified. The Triassic Saharonim Association is represented by alkaline olivine basalts (K-Ar age of 213.6 Ma, Upper Triassic, Norian Stage) and is chronologically associated with the pre-Jurassic stage of laterite formation Mishor Fm. Early Cretaceous magmatites are divided into two rock groups: 1) an early bimodal group composed mainly of alkaline basalts, gabbro and syenites (K-Ar age of 129–140 Ma, Early Cretaceous, Valanginian – Barremian stages); 2) a later group made up of olivine, basalt, basanite and nephelinite (Ar-Ar age of 112.9–119.0 Ma, Early Cretaceous, Aptian stage).

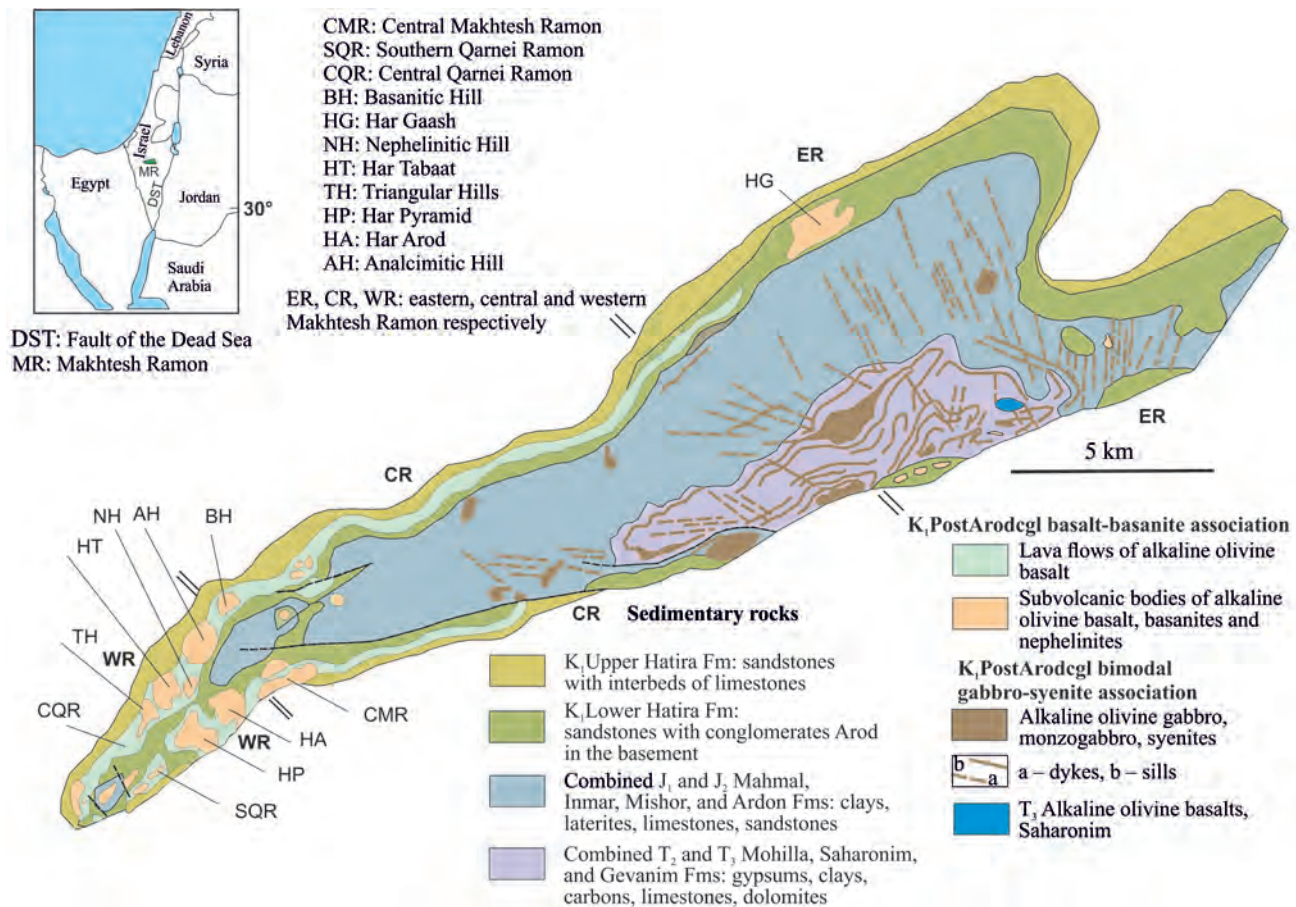


Fig. 1. Location and a schematic geological map of Makhtesh Ramon.

Cretaceous associations identified using radiological data reveal geological evidence of their different ages: the earlier one is overlain by Arod conglomerates lying at the base of Lower Hatira Fm, i.e. it is pre-conglomerate – PreArodagl. However, the rocks of the later association overlie and intrude these conglomerates, as well as Lower Hatira Fm sandstones occurring above, i.e. they are post-conglomerate – PostArodagl. In turn, the sandstones of Upper Hatira Fm rest erosively on magmatites, thus fixing their geological age between Lower and Upper Hatira Fms.

All magmatic manifestations in the area belong to one OIB-like alkaline geochemical type.

Xenoliths and xenocrysts have not been found in the Triassic and Early Cretaceous associations yet; however, they are widely developed in the PostArodagl group, which is the most complex in terms of internal structure and composition. It comprises lava flows, tuffaceous and tuffaceous-sedimentary deposits, pyroclastic diatremes, subvolcanic stocks, dykes and sills. The association is represented by olivine basalts and microgabbros, basanites, nephelinites, as well as their melilite and analcime variations, often containing volcanic glass. All the rocks are of black, dark green or green-grey colour, porphyritic texture and are practically indistinguishable in composition under field conditions. The inclusions of olivine and clinopyroxene are of cross-cutting nature; in addition, plagioclase phenocrysts are found in basalts, and melilite phenocrysts are observed in nephelinites. Their number ranges from 5–8 to 34%, with their size varying from 0.6 mm to 2.0 cm. The bulk of basalts and basanites are composed of olivine, clinopyroxene and plagioclase, calcite, micromicaceous or pelitomorphous minerals such as chlorophaeite and saponite, nepheline and analcime (in basanites), as well as melilite (in the foidite group), excluding plagioclase.

There are deep-seated (mantle and lower crustal) and upper crustal xenoliths (tuffs of the Proterozoic base, sedimentary cover rocks). Deep-seated xenoliths are characterised in [Bonen et al., 1980; Stein, Katz, 1989; Vapnik, 2005], while a more complete list of them, including lower crustal ones, is given in [Fershtater et al., 2016; Fershtater, Yudalevich, 2017]. These studies examined primarily the interaction between xenoliths and host melts at a deep-seated mantle-lower crustal level.

The present study is aimed at studying phenomena occurring in xeno- and megacrysts during uplift and decompression, which takes them to the magma surface, as well as associated mineralogical, petrochemical and morphological transformations.

The deep-seated xenoliths of the PostArodagl association are represented by mantle dunites, harzburgites, lherzolites, wehrlites, olivine clinopyroxenites and clinopyroxenites, olivine websterites, websterites and their amphibolite varieties, lower-crustal metagabbros (granulites), apatite-magnetite and clinopy-

roxene-apatite-magnetite rocks. In addition to the deep-seated xenoliths, there are xenoliths of Late Proterozoic tuffs.

Along with xenoliths, xeno- and megacrysts are widespread in rocks. A common petrographic feature of xenoliths, xeno- and megacrysts are alterations caused by the host melts and minerals in the late stage of their crystallisation, represented by oligoclase-andesine, potassium feldspar, clinopyroxene, titanomagnetite, apatite, biotite, rhonite, calcites, zeolites and saponite-chlorophaeites.

Xeno- and megacrysts are genetically similar formations and differ only in size. They constitute fragments of xenoliths, which appear in the course of transporting xenoliths to the magma stabilisation sites. Xenocrysts are close to phenocrysts in size and usually do not exceed 1.2 mm, whereas megacrysts are much larger and reach 15.0 cm across.

ANALYTICAL STUDIES

The compositions of minerals given in the tables were determined using a CAMECA SX-100 microanalyser at the Institute of Geology and Geochemistry UB RAS (Ekaterinburg, operator V.V. Hiller), Institute of Geology SB RAS (Novosibirsk, V.V. Sharygin), as well as using a JEOL microanalyser (ISP-MS and ER-MA) at the Hebrew University of Jerusalem (analyst O. Dvir).

CHARACTERISTICS OF XENOCRYSTS

Xeno- and megacrysts differ from phenocrysts in the following characteristics: 1 – xenomorphic (porphyroclastic) outlines and the development of near-contact corrosion; 2 – rock jointing, optical defects and decrystallisation; 3 – the diffuse effect of host magma; 4 – melting and formation of decomposition structures; 5 – non-conformity with the paragenesis of host rocks ('prohibited' minerals). The bulk of xeno- and megacrysts are represented by compatible minerals, with only the xenocrysts of quartz and orthopyroxene being incompatible with the host rocks undersaturated with SiO₂.

Quartz. The size of the xenocrysts varies from 0.2 mm to 1.2 mm, with their shape being round or oval. It is usually surrounded by a clinopyroxene rim made up of the smallest adjacent and optically differently oriented microlites having a tendency to form a regular pyroxene form, common to the entire rim. The intergranular gaps in the rim are filled with dark brown glass of orthoclase composition. At the border with the pyroxene rim, quartz is often melted into yellow or greenish-brown glass (Fig. 2a) enriched with MgO (35.56–36.37 wt %). The difference in the composition of the glasses is given in Table 1. Sometimes quartz undergoes decrystallisation with a polymorphic transition to tridymite and cristobalite. On

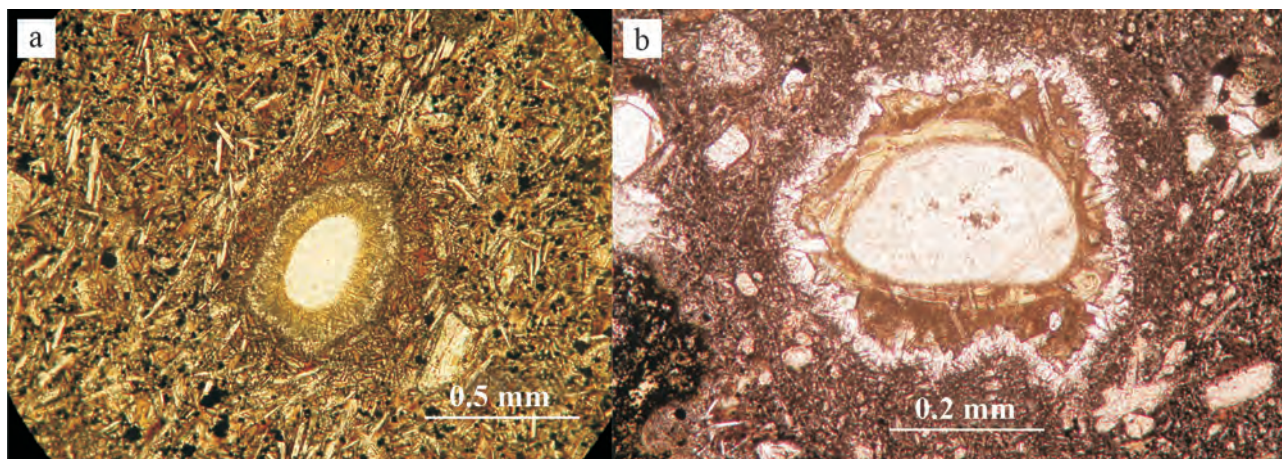


Fig. 2. Quartz xenocrysts and products of their alteration.

a – BH-16 (olivine basalt) and b – CMR-178 (nephelinite). Quartz xenocryst transitioned into fine-grained tridymite-cristobalite aggregate with the melting zone being composed of greenish-brown glass and light green saponite. The outer zone is composed of microlitic clinopyroxene. PPL.

Table 1. Chemical composition of xenocrysts and products of their alteration, wt %

		SiO ₂	TiO ₂	Al ₂ O ₃	Cr ₂ O ₃	FeO	MnO	MgO	CaO	Na ₂ O	K ₂ O	Total	Mg*	An	
Products of quartz alteration	1(3)	61.86	–	1.96	–	–	–	35.98	0.2	–	–	100	–		
	2(3)	54.2	–	–	–	6.59	–	16.35	22.59	0.77	–	100	0.85		
	3(1)	65.34	–	14.26	–	4.83	–	0.73	–	2.01	12.81	99.98	–		
	4(1)	43.87	4.28	9.72	–	7.55	–	11.97	21.62	0.98	–	99.99	0.78		
Orthopyroxene and products of its alteration	1(2)	54.41	–	4.2	–	5.93	–	34.57	–	–	–	99.11	0.93		
	2(1)	47.91	–	5.39	–	8.49	–	32.07	5.41	–	–	92.27	0.73		
	3(1)	38.95	–	2.41	–	24.16	–	33.38	0.66	–	0.44	100	0.76		
	4(2)	51.92	–	2.76	–	9.51	–	13.76	19.62	1.94	–	99.51	0.76		
	5(1)	51.96	0.14	1.98	–	21.62	0.52	21.45	1.1	0.04	–	98.81	0.7		
	6(4)	36.55	–	–	–	30.72	–	30.77	0.26	–	–	98.3	0.7		
	7(1)	34.98	–	–	–	40.1	–	23.41	0.2	–	–	98.69	0.57		
	8(4)	52.98	0.5	0.59	0.07	10.63	–	14.72	18.29	0.93	–	–	98.71	0.76	
	9(1)	50.93	0.29	2.94	–	13.33	–	11.54	19.7	0.68	–	–	99.41	0.66	
	10(43)	54.59	–	3.43	0.26	6.77	–	33.73	0.89	–	–	–	99.67	0.92	
	11(7)	51.43	0.15	1.83	0.04	24.91	0.59	19.27	1.12	0.07	0.01	–	99.45	0.64	
Olivine	1(3)	40.93	0.03	–	–	10.8	0.18	47.35	0.13	–	–	99.42	0.91		
	2(2)	39.07	0.05	0.06	–	20.47	0.54	39.59	0.32	–	–	100.1	0.82		
	3(1)	40.12	–	–	–	14.8	–	44.33	0.18	–	–	99.43	0.87		
	4(1)	39.2	–	–	–	19.76	–	41.04	–	–	–	100	0.83		
	5(2)	38.15	–	–	–	24.84	–	36.57	0.45	–	–	100.01	0.77		
	6(1)	38.11	–	–	–	24.32	–	37.62	–	–	–	100.05	0.78		
	7(10)	37.33	0.02	0.04	–	26.19	0.44	35.11	0.42	–	–	–	99.55	0.75	
	8(19)	39.18	–	–	–	19.06	0.37	40.99	0.34	–	–	–	99.94	0.83	
Clinopyroxene	1(1)	50.36	1.19	4.45	0.74	3.74	–	14.56	24.22	0.51	–	99.77	0.9		
	2(2)	44.77	3.56	8.11	0.51	6.84	–	12.3	23.08	0.83	–	100	0.8		
	3(2)	50.7	0.68	5.52	0.93	4.14	–	16.37	20.95	1.09	–	100.38	0.9		
	4(1)	47.51	2.07	6.37	–	7.17	0.14	13.36	22.96	0.42	–	100	0.81		
	5(49)	44.27	3.86	8.13	–	8.13	0.12	11.08	23.16	0.47	0.11	99.33	0.76		
	6(15)	44.44	3.88	9.64	–	6.22	0.21	12.33	21.61	0.79	–	99.12	0.82		

Table 1. Ending

		SiO ₂	TiO ₂	Al ₂ O ₃	Cr ₂ O ₃	FeO	MnO	MgO	CaO	Na ₂ O	K ₂ O	Total	Mg*	An
Amphibole and products of its alteration	1(1)	39.35	7.93	11.98	–	12.27	–	12.86	13.98	2.06	0.57	101	0.71	–
	2(9)	25.41	11.88	16.46	–	20.24	–	12.73	11.71	1.57	–	100	0.59	–
	3(3)	38.49	–	–	–	24.08	–	36.85	0.61	–	–	100.03	0.78	–
	4(3)	44.82	4.09	8.23	–	6.01	–	12.84	23.26	0.75	–	100	0.83	–
	5(3)	52.81	–	29.86	–	–	–	–	–	12.29	5.04	–	–	57
	6(9)	40.15	5.81	13.31	–	9.88	0.19	12.29	11.91	2.49	1.05	97.08	0.74	–
	7(5)	25.79	10.62	16.92	–	18.93	–	13.75	11.78	1.72	–	99.51	0.62	–
	8(6)	41.42	1.57	13.19	0.39	9.05	0.08	16.16	10.84	2.91	0.86	96.47	0.8	–
	9(11)	40.12	4.83	13.54	–	10.11	0.11	12.18	11.97	2.18	2.04	97.08	0.75	–
	10(5)	24.96	11.96	18.18	–	13.22	0.7	15.86	10.04	1.6	–	96.52	0.73	–
	11(4)	25.11	11.05	13.64	–	26.21	0.24	10.61	11.07	1.47	–	–	0.48	–
Plagioclase	1(4)	53.67	0.32	27.98	–	0.81	0.04	0.21	10.45	4.97	0.58	99.03	–	54
	2(2)	51.85	–	30.25	–	–	–	–	12.93	4.38	0.59	100	–	61
	3(2)	54.35	0.25	27.14	–	0.84	0.05	0.67	9.95	7.01	0.73	100.99	–	44
	4(1)	50.79	–	30.34	–	–	–	–	14.77	3.61	0.49	100	–	68
	5(2)	54.87	–	28.19	–	0.56	–	0.01	11.16	5.3	0.22	100.31	–	54
	6(7)	51.55	–	30.38	–	–	–	–	12.95	4.51	0.61	100	–	67
		SiO ₂	TiO ₂	Al ₂ O ₃	Cr ₂ O ₃	FeO	MnO	MgO	CaO	Na ₂ O	P ₂ O ₅	F	Cl	Total
Magnetite and spinel	1(3)	–	14.94	4.8	–	77.84	–	2.43	–	–	–	–	–	100.01
	2(1)	–	20.83	5.76	–	70.9	–	2.51	–	–	–	–	–	100
	3(63)	0.04	21.46	6.43	0.51	63.89	0.85	4.77	0.12	–	–	–	–	98.07
	4(1)	0.03	10.27	13.54	7.81	57.85	0.37	6.95	0.06	–	–	–	–	96.88
	5(1)	–	0.83	38.01	25.14	19.26	0.13	15.47	–	–	–	–	–	98.84
	6(1)	0.02	17.22	7.58	3.66	63.26	0.6	4.86	0.08	–	–	–	–	97.28
	7(1)	–	–	63.34	–	13.27	–	23.39	–	–	–	–	–	100
	8(1)	–	15.38	10.42	–	67.06	0.8	6.08	0.02	0.24	–	–	–	100
Apatite	1(3)	–	–	–	–	0.59	–	–	53.49	0.36	41.18	3.77	0.61	100
	2(6)	–	–	–	–	–	0.13	–	52.33	–	40.93	6.17	0.44	100

Note. The number of analyses involved in the calculation of average contents is given in parentheses after the sequence number.

Alteration products of quartz xenocrysts: HP-6G: 1 – moderate yellow green glass at the periphery of quartz, 2 – fine-grained clinopyroxene at the outer border of glass, 3 – dusky red glass filling the interstices between the fine grains of clinopyroxene, 4 – clinopyroxene from host basanite matrix.

Chemical composition of orthopyroxene xenocrysts and products of their alteration: BP-14G: 1 – xenocryst of lherzolite type, core; 2 – rim adjacent to the zone of decomposition, products of orthopyroxene decomposition: 3 – olivine, 4 – clinopyroxene. TH-16: 5 – xenocryst of gabbro type; products of xenocryst decomposition: 6–7 – olivine, 8–9 – clinopyroxene. Orthopyroxene from xenoliths: 10 – lherzolite type, 11 – gabbro type.

Chemical composition of olivine: NH-596: 1 – megacryst, core, 2 – rim. BP-1G: 3 – megacryst, core, 4 – intermediate zone, 5 – rim, 6 – zone of megacryst decrystallisation. 7–8 – olivine from host magmatic rocks: 7 – prismatic microphenocrysts in rock matrix, 8 – melt inclusions hosted in the olivine and clinopyroxene of peridotites.

Chemical composition of clinopyroxene xenocrysts: BH-11: 1 – xenocrysts, core. BH-1G: 2 – rim. HP-10G: 3 – megacryst, core, 4 – rim. 5 – prismatic microphenocrysts in rock matrix, 6 – melt inclusions hosted in the olivine and clinopyroxene of peridotites.

Chemical composition of amphibole and products of its alteration: BH-1G: 1 – kaersutite megacryst, 2–5 – products of kaersutite decomposition: 2 – rhonite, 3 – olivine, 4 – clinopyroxene, 5 – plagioclase. HP-205: 6 – kaersutite hosted in wehrlite. BH-19G: 7 – rhonite from clinopyroxenite. BH-20: 8 – pargasite xenocryst hosted in lherzolite. 9 – 11 – kaersutite and rhonite from host magmatites: 9 – kaersutite phenocrysts from basanites and nephelinites. HT: 10 – rhonite hosted in melt inclusions in olivine and clinopyroxene from lherzolites. 11 – rhonite from remnant glasses in nephelinites.

Chemical composition of plagioclase: HP-6: 1 – megacryst, core, 2 – megacryst, rim. SQR-012a: 3 – xenocryst, core, 4 – xenocryst, rim. 5 – plagioclase hosted in gabbro xenoliths. 6 – microlitic plagioclase in basanites.

Chemical composition of magnetite and spinel: A-6: 1 – magnetite megacryst, core, 2 – magnetite megacryst, rim; 3 – titanomagnetite phenocrysts hosted in magmatic rocks. BH-20: 4 – chrome spinel xenocryst. NH-536: 5 and 6 – chrome spinel xenocryst: 5 – core, 6 – rim. HA-21: 7 and 8 – hercynite megacryst: 7 – core, 8 – rim.

Chemical composition of apatite: HA-6: 1 – megacryst of fluorapatite. 2 – ultra-fluorine apatite hosted in basaltoids.

the outside, this aggregate is surrounded by a greenish-brown glass having isolated areas of saponite (Fig. 2b) and often zeolite. Judging by the composition of glass surrounding relict quartz, this was facilitated by the diffusion of magnesium and volatiles into the melting zone. Unlike the matrix pyroxene of the host rocks, fine-grained clinopyroxene formed on quartz is richer in SiO_2 and has a higher magnesium number ($\text{Mg}^* = 0.83\text{--}0.88$); does not contain TiO_2 and Al_2O_3 (see Table 1). Quartz with a clinopyroxene rim is also found without glass formation, veined with calcite and buffered by it from the accreting microclinopyroxene aggregate.

Orthopyroxene. In the studied rocks, orthopyroxene is very unstable and is easily identifiable by the development of reaction kelyphite rims around it, represented by symplectic intergrowths of olivine and clinopyroxene (Fig. 3a) – products of the solid-phase decomposition of orthopyroxene peridotites, websterite and granulites. The width of rims comes up to 0.6 mm, with the structure being predominantly microequigranular, linearly elongated and with the long axes of decomposed minerals often arranged transversely to the boundary of the preserved orthopyroxene. In places, the olivine-clinopyroxene aggregate retains only small relicts of orthopyroxene (Fig. 3b), sometimes completely replacing it; in such cases, the aggregate acquires hypidiomorphic outlines (Fig. 3c). Some xenocrysts directly accrete newly formed augite or titanium augite from the host rocks (Fig. 3d). Complex bipyroxene inclusions (Fig. 3e), consisting of xenogenic ortho- and clinopyroxene (fragments of lherzolites or websterites) constitute noteworthy examples. In them, the orthopyroxene component has a symplectic olivine-clinopyroxene rim, with no changes occurring in the clinopyroxene part of the inclusions and both of these minerals accreting a newly-formed clinopyroxene. It is characteristic that bipyroxene xenocrysts also tend to develop a crystallographic form, which is typical of this group of minerals. The interstices of symplectic intergrowths are filled with feldspar, oligoclase, zeolite, saponite and calcite. Similar decomposition products of orthopyroxene are observed in the marginal zones of deep-seated xenoliths, including gabbros, where in places it is completely replaced by symplectite (Fig. 3f).

The petrochemical data (see Table 1) reveal two specific types of orthopyroxene xenocrysts: 1 – lherzolite having a high magnesium number ($\text{Mg}^* = 0.93\text{--}0.87$), 2 – gabbro having a low magnesium number ($\text{Mg}^* = 0.70$). According to this indicator, the composition of symplectic olivine and clinopyroxene is unstable and varies from 0.60 to 0.78 in peridotites, ranging from 0.57 to 0.76 in orthopyroxene gabbro, i.e. to up to values close to similar matrix minerals and the microphenocrysts of the host rocks. In the zone of orthopyroxene directly bordering the decomposition rim, its magnesium number decreases significantly, where-

as the contents of Al_2O_3 , CaO and sometimes K_2O increase (see Table 1).

Minerals compatible with host basic and ultrabasic alkaline rocks include olivine, clinopyroxene, amphibole, plagioclase, magnetite, spinel, apatite, nepheline and anorthoclase.

Olivine. The usual grain size comes to 0.3–0.8 mm, reaching 2–3 cm in megacrysts. The form varies from xenomorphic to idiomorphic. Corroded grains are often found with traces of pressure experienced before they were engulfed by ascending magma, fixed in the form of undulose extinction, which is unusual for the olivine (Fig. 4a). Some xenocrysts are decrystallised to one degree or another into a fine-grained mass having a microgranoblastic texture, with the size of individual grains ranging from 0.01 to 0.1 mm. Decrystallisation is mainly localised in grain margins, in places being developed in the form of spots or stripes (Fig. 4b), with smaller grains sometimes being decrystallised completely.

The chemical analysis of olivines (see Table 1) reveals that its central and marginal zones differ significantly in MgO and FeO contents, as well as in the magnesium number, 0.91–0.87 (depleted peridotites) and 0.82–0.83 (close to the magnesium number of olivine in the host rocks), respectively.

Clinopyroxene. The size of clinopyroxene is close to that of phenocrysts (0.6–0.8 mm); sometimes it forms megacrysts reaching up to 15 cm across. Its colour varies from colourless and slightly yellowish and brownish to brown-green, brownish-green and dirty green. As compared to orthopyroxene and olivine, it is more resistant to the influence of host rocks and is not accompanied by any noticeable phenomena of decomposition and decrystallisation. Nevertheless, a disturbance of its initial structure still occurs and is manifested by the formation of fractures and grains having a deconsolidated porous structure, which creates the effect of a non-specific shagreen surface. In the clinopyroxenes of large xenoliths, such structures are observed only in the areas where they are in contact with the host rocks and disappear in the inner parts, which indicates their occurrence under the influence of the host melt (Fig. 5a). Two types of mega- and xenocrysts of clinopyroxene are distinguished: 1 – ordinary; 2 – polygranular, i.e. intergrowths of several optically differently oriented grains combined into a pyroxene habit (see Figures 5c–f). Complex grains most often have a porous structure and accrete pure clinopyroxene from the host rocks. Grains having a green-grey (chromium diopside) porous central zone, as well as augite and titanium-augite non-porous marginal zones (see Fig. 5b) are also widespread, indicating the duality of the genesis of such formations. The pores are filled with minerals of most host rocks: feldspar, nepheline, titanite, zeolite, saponite, less often biotite, apatite and amphibole. In places, two-mineral olivine-clinopyroxene intergrowths occur, which are linked by a com-

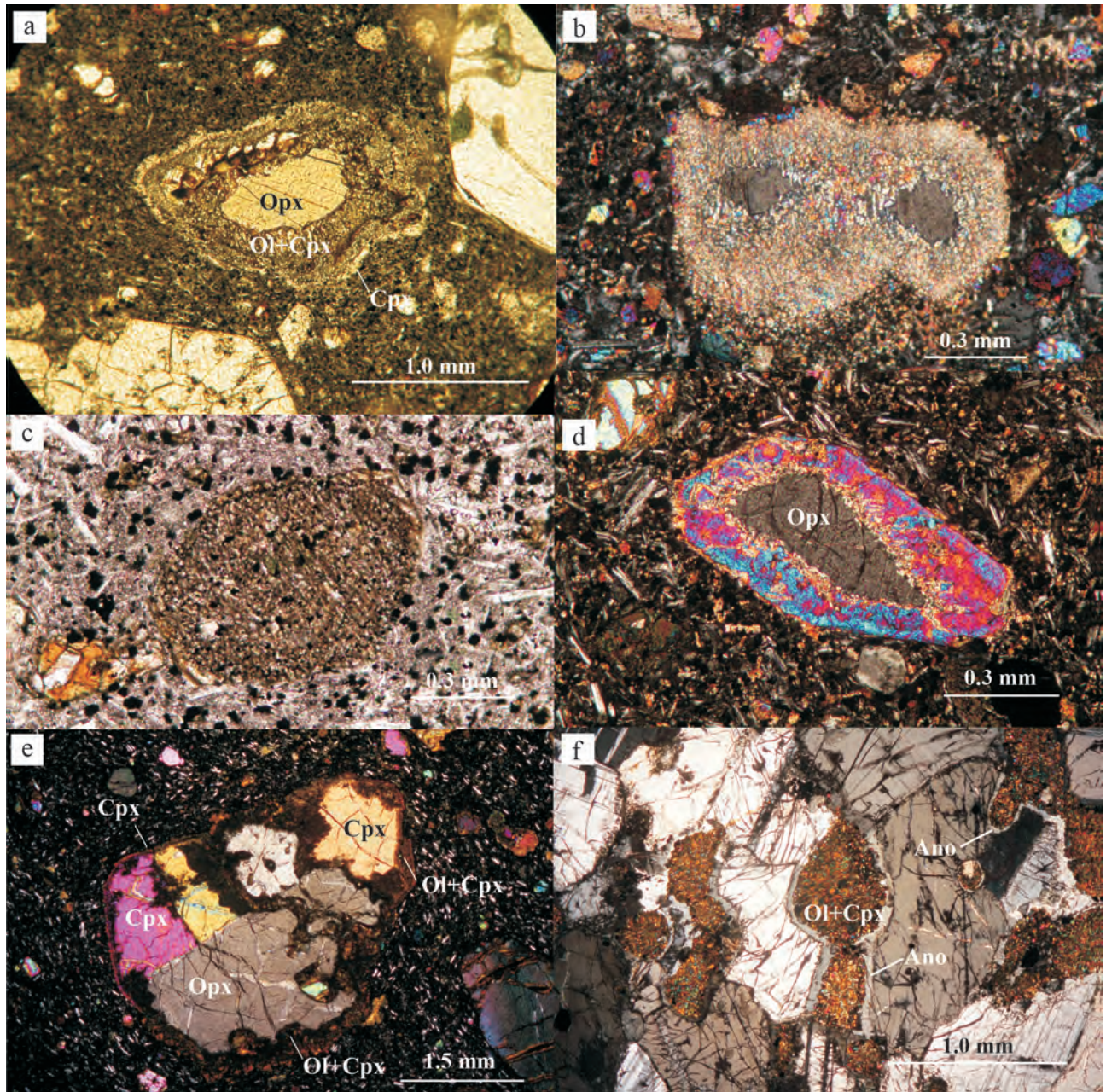


Fig. 3. Orthopyroxene xenocrysts and products of their alteration.

a – BH-107 (basanite): relic of *Opx* (greyish orange one in the centre) surrounded by the products of its decomposition: keliphitic rim composed of *Ol-Cpx* aggregate. The outer rim is composed of newly formed *Cpx* which growth was related to basanite crystallisation. PPL; b – HA-141 (basanite): almost complete pseudomorph of *Ol-Cpx* symplectite after *Opx* (two brownish grey relicts in the centre). XPL; c – SQR-45 (olivine basalt): *Opx* is completely replaced by *Ol-Cpx* symplectite and acquired subhedral pyroxene habit. PPL; d – CMR-622 (olivine basalt): bimodal xenocryst of pyroxene composed of *Opx*, brownish grey in the centre, overgrown by *Cpx* during the crystallisation of host melt. XPL; e – CMR-826 (olivine basalt): complex multigrain *Opx-Cpx* xenocryst (result of self-faceting) having a subhedral habit, in which *Opx* is recognised by *Ol-Cpx* symplectite with iddingsite after olivine. *Cpx* is recognised by a thin rim of *Cpx* overgrowth related to the crystallisation of host basalt. PPL and XPL, respectively; f – TH-53 (olivine basalt): xenolith of norite showing complete pseudomorphs of *Ol-Cpx* symplectite after orthopyroxene; symplectite is surrounded by thin anorthoclase (light grey) rims of metasomatic origin. XPL.

mon form characteristic of clinopyroxene, suggesting their kinship with peridotite xenoliths.

The chemical composition of clinopyroxenes (see Table 1) shows an increase in the concentrations of

TiO₂, Al₂O₃ and FeO from the central to marginal zones of xenocrysts, with a decrease in SiO₂ and MgO in the opposite direction, including Mg*, which ranges from 0.90 to 0.87 (clinopyroxene peridotite) to 0.80

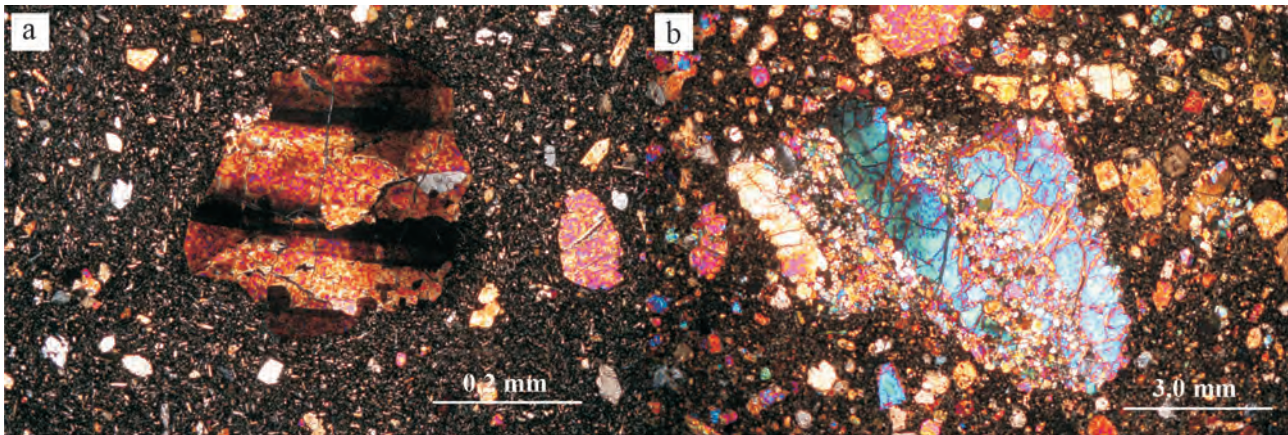


Fig. 4. Olivine xenocrysts.

a – HT-586 (basanite): remnant zebra-like texture of olivine xenocryst, that was acquired before the trapping of the grain by the host melt. XPL; b – NH-602 (nephelinite): Partly decrystallised megacryst of olivine; decrystallisation occurred according to pressurised textures. XPL.

(marginal zones of xenocrysts and phenocrysts of the host rocks). The internal parts of the xenocrysts are enriched with Cr_2O_3 (up to 0.95 wt %).

Amphibole is represented by kaersutite, whose size varies from that commensurate with phenocrysts to that of megacrysts (4.8×2.8 cm across). Its form is idiomorphic and hypidiomorphic. It is extremely unstable and is always characterised by a peculiar decomposition structure – polycrystalline symplectite, which forms partial or complete pseudomorphs after it with a large proportion of rhonite (Fig. 6a – c). In cases of incomplete pseudomorphs, kaersutite is usually located in their inner part. The same decomposition structures, both complete and incomplete, are developed in the xenoliths of peridotites and pyroxenites; however, they are xenomorphic and occupy intergranular spaces between olivine and pyroxene in them (Fig. 6d). In addition to rhonite, symplectite also includes titanium augite, olivine, plagioclase, titanomagnetite, zeolites and saponite. Individual xenocrysts are surrounded by a titanium augite rim. Along with titanomagnetite participating in the decomposition of amphibole, the marginal zone of symplectitic pseudomorphs is enriched with the metasomatic titanomagnetite of the host basanites (Fig. 7). The structure of decomposition zones is eutectoid graphic.

The chemical composition of kaersutite and its decomposition products is shown in Table 1. Kaersutite differs from the primary pargasite of xenoliths in a lower magnesium number (0.71 and 0.80, respectively) and a higher content of TiO_2 (6.15 and 1.57 wt %, respectively), which is close to that of phenocrysts hosting magmatites. The magnesium number of rhonite (0.59–0.62) is lower than that of the rhonite from melt inclusions (0.73) and phenocrysts (0.75), with the magnesium number of rhonite from residual glasses and of late magmatic rhonite is even lower (0.48). All types

of rhonite are characterised by a high content of TiO_2 (10.62–11.96 wt %). The olivine and clinopyroxene of symplectites are unequal in terms of the magnesium number (0.78 and 0.83, respectively). The composition of plagioclase in them varies from An_{53} to An_{62} (average An_{57}).

Plagioclase. The grain size comes up to 3.6×2.0 cm, with the form varying from xenomorphic to hypidiomorphic. The central zones are represented by An_{44-54} , whereas plagioclase An_{65-69} corresponding to the plagioclase of the host rocks is always developed along the margins. It is characterised by the development of crape structures and reactive interaction with the carrier magma, whose thermal effect is manifested by melting, less often decrystallisation. The initial stage of melting is manifested by the formation of a weakly birefringent porous zone (0.06–0.1 mm wide) having point inclusions of light brown, green or yellowish glass in the marginal zones of plagioclase or along the cracks in it (Fig. 8a). In the areas of more intense development of glass and simultaneously with it in plagioclase fingerprint-like structures are formed (Fig. 8b).

In the presence of calcite, the zones associated with the melting and development of such structures increase up to 0.2 mm. Xenocrysts, in which solid-phase decomposition of plagioclase into An_{18-21} and An_{60-62} takes place (Fig. 8c), are found more rarely. The most common type of changes is represented by the eutectoid symplectitic intergrowths of plagioclase with titanium augite developing along its margins, along cracks and sometimes throughout the xenocryst area (Fig. 8d). In some places, the self-faceting of xenocrysts into prismatic forms that are characteristic of plagioclase is observed, which is also typical of the xenoliths of anorthosites (see Fig. 8b) recrystallised into megacrysts. Similar changes occur in the plagioclase of megababbros.

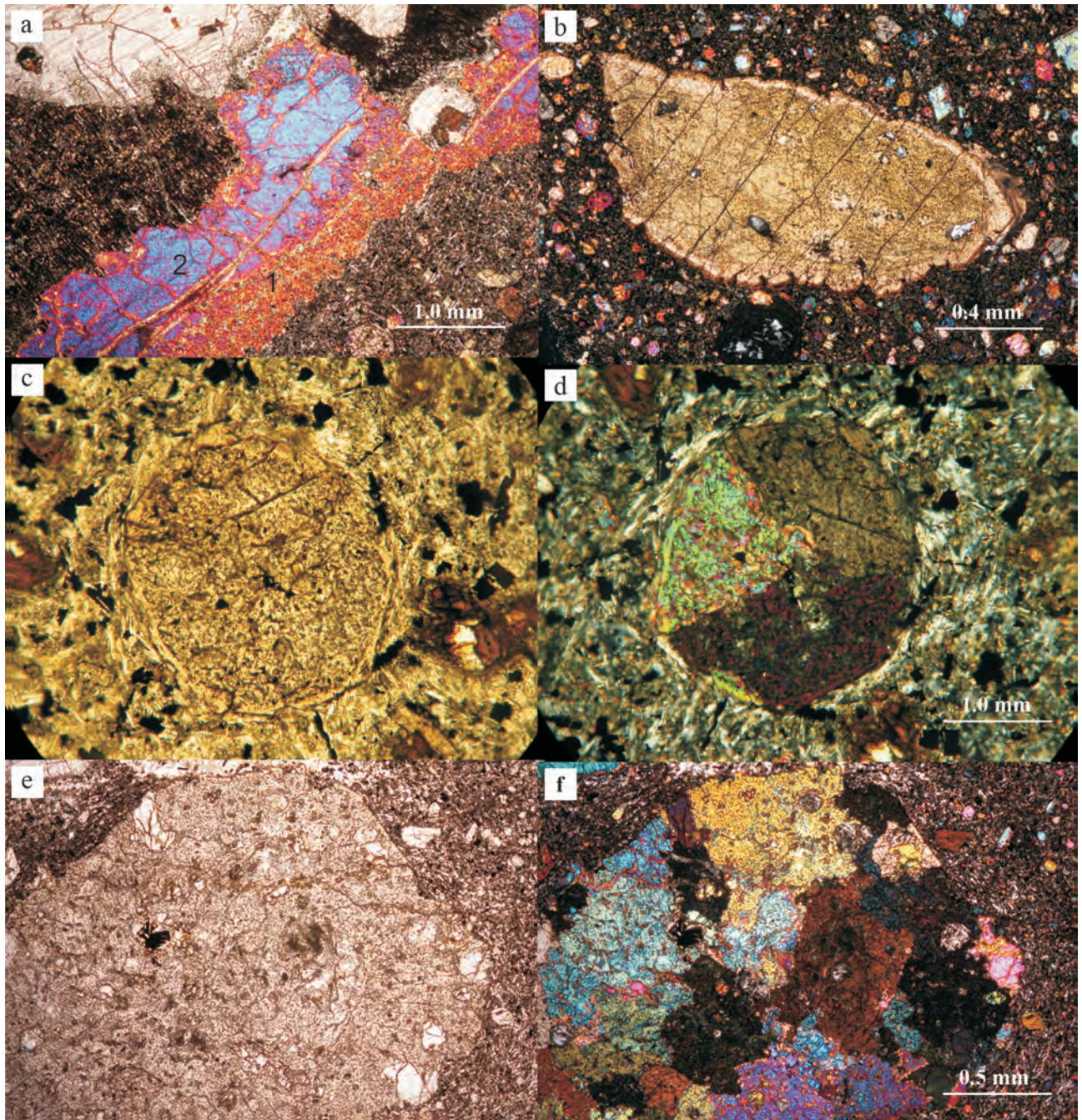


Fig. 5. Xenocrysts of clinopyroxene.

a – HP-385 (basanite): 1 – non-porous part of wehrlite xenolith remote from the contact with basanite; 2 – porous spongy zone of clinopyroxene at the contact with basanite is replaced by anhedral multi-mineral symplectite; the symplectite is of moderate brown colour and shows oriented texture with voluminous rhonite, XPL; b – (nephelinite): spongy xenocryst of fractured light brown chromian diopside overgrown by rims of newly-formed augite and titanium augite. XPL; c and d – BH-11 (basanite): the xenocryst of spongy clinopyroxene composed of three differently oriented grains with a thin rim of newly-formed augite; the augite rim shows sectorial extinction that is partly subordinated to the optical orientation of xenocryst segments. PPL and XPL, respectively; e and f – BH-815-17 (basanite): spongy multi-grained xenocryst of clinopyroxene from the xenolith of pyroxenite recrystallised into a subhedral habit. PPL and XPL, respectively.

The chemical composition (see Table 1) emphasizes the similarity of xenocrysts with the plagioclase of metagabbros, as well as their more basic peripheral rim with the plagioclase of the host basalts.

Anorthoclase. It is developed primarily in the form of megacrysts up to 3.5×2.8 cm in size. Sometimes anorthoclase preserves secondary muscovite (Fig. 9b), which clearly forms even before the xenocryst is en-

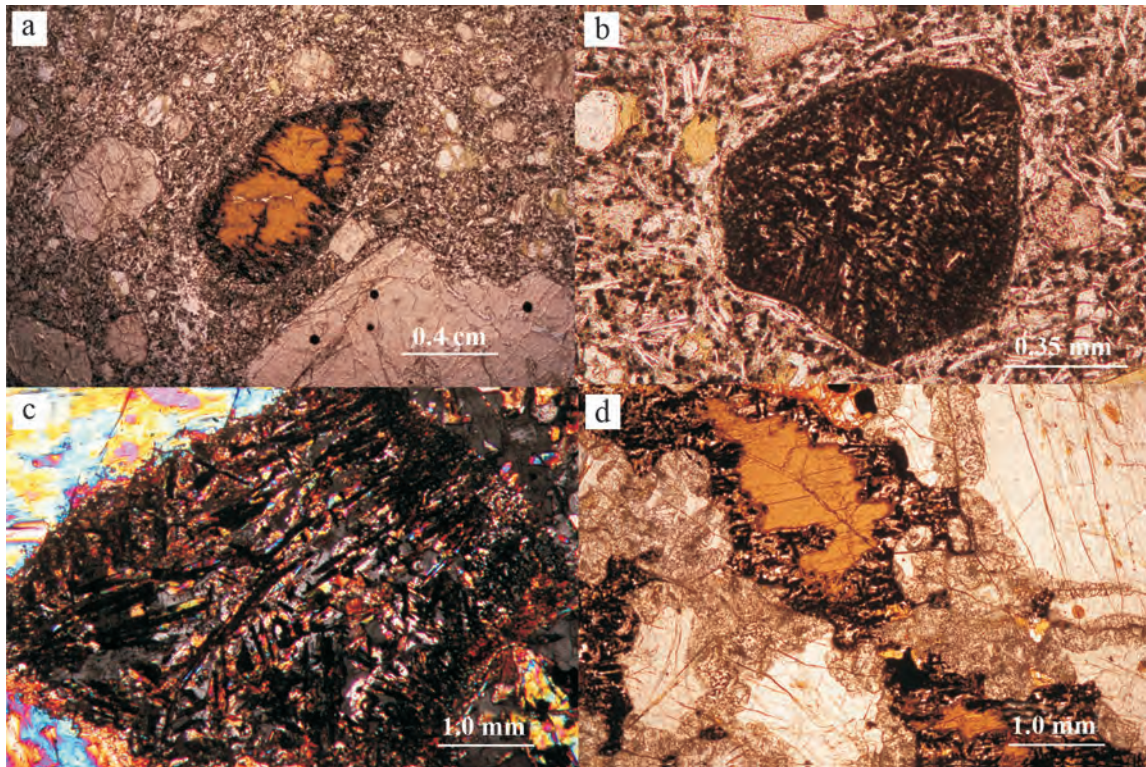


Fig. 6. Amphibole xenocrysts and products of their alteration.

a – CMR-734 (olivine basalt): a xenocryst of kaersutite with decomposition products composed of multi-mineral symplectite, which forms a keliphitic rim and fills the fractures; the xenocryst acquires a subhedral habit. PPL; b – HP-171 (olivine basalt): euhedral pseudomorphs of multi-mineral symplectite after amphibole; the symplectite is composed of voluminous rhonite (dark grey to greyish-black prismatic phase), titanium augite, olivine and plagioclase. PPL; c – BH-36 (basanite): complete pseudomorph of amphibole by multi-mineral symplectite, composed of rhonite (elongated brownish-grey to greyish-black prisms), plagioclase, clinopyroxene and olivine. XPL; d – CMR-749 (olivine basalt): anhedral kaersutite in the xenolith of clinopyroxenite is rimmed by a multi-mineral symplectite aggregate. PPL.

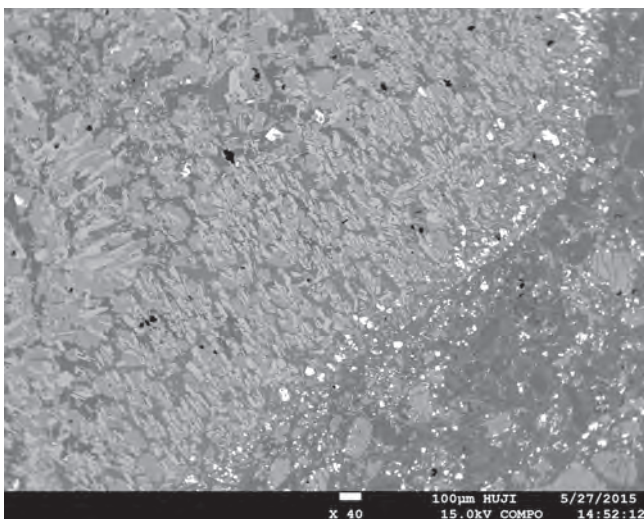


Fig. 7. BH-1G (basanite); BSE.

Complete pseudomorph of polycrystalline symplectite with voluminous rhonite after amphibole. Fine-grained inclusions of titanomagnetite, which formation was related to basanite crystallisation, are clearly seen in the endocontact zone of symplectite.

gulfed by the host rocks. In its marginal part, a melting zone (0.15 to 1.2 mm wide) is developed in places in the form of colourless and light brown or brownish glass, which at the border with relict anorthoclase is replaced by a zone of fingerprint-like structures (Fig. 9b). Sometimes changes are limited by the formation of such structures along the margins of a xenocryst (see Figures 9a and c), sometimes affecting the whole xenocryst. Xenocrysts are often veined with zeolite, calcite and, less commonly, saponite, as well as rimmed by them (1.2 mm wide zones). Similar changes with the formation of superimposed spherulitic and fingerprint-like structures occur to sodium-potassium feldspar also in the xenoliths of crystalloclastic tuffs of the Proterozoic crust (Fig. 9d).

The petrochemical characteristic of anorthoclase consists in the presence of quartz and hypersthene in the normative composition, which determines its formation from parent magma saturated with SiO_2 , whereas normative nepheline is characteristic of anorthoclase from the host rocks (as an indicator of crystallisation from SiO_2 -undersaturated melt). The composition of the glass resulting from the melting of anorthoclase

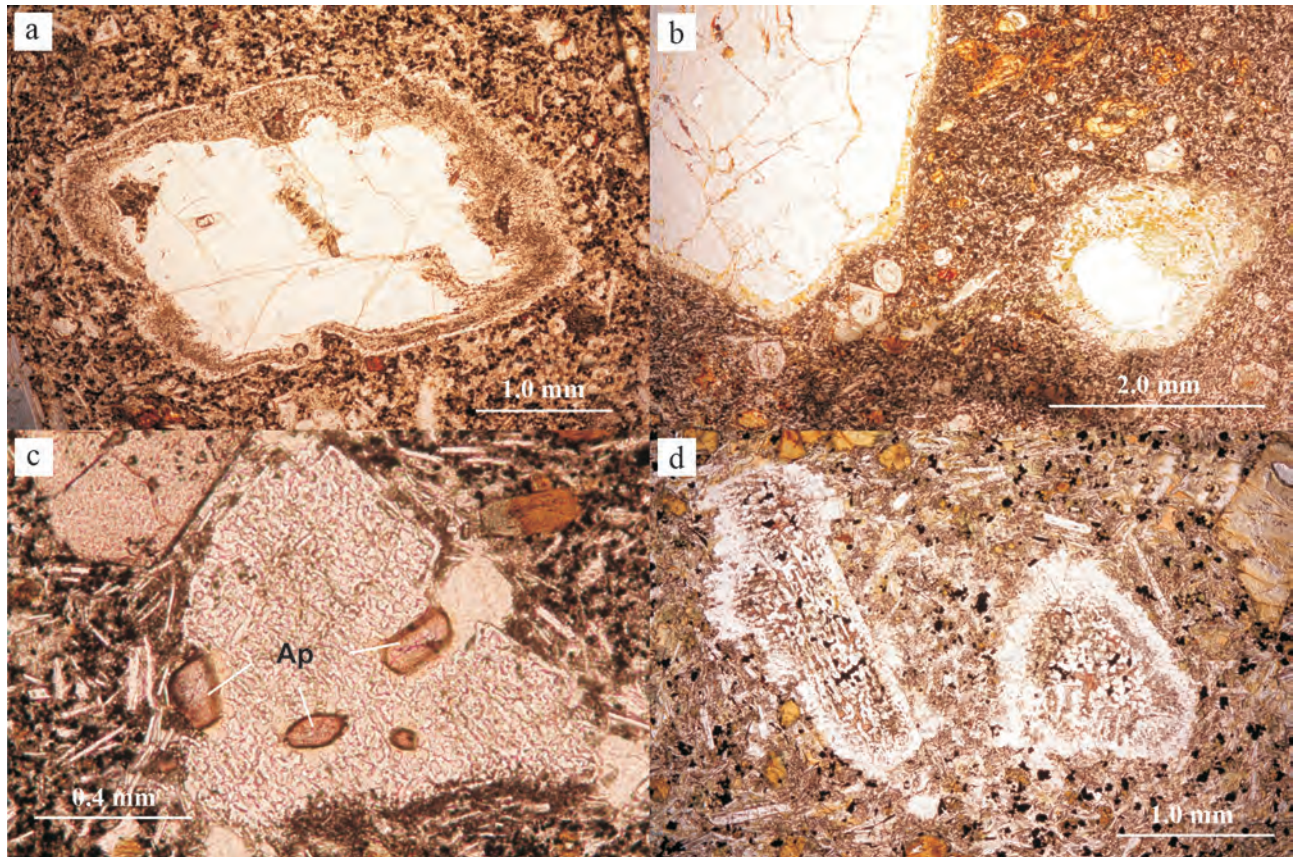


Fig. 8. Plagioclase xenocrysts.

a – SQR-30-1 (olivine basalt): a plagioclase xenocryst rimmed by a porous zone composed of newly-formed plagioclase; this is the initial stage of plagioclase alteration by the host melt. PPL; b – TH-43b (basanite): a fragment of anorthosite xenolith showing multi-grain xenocryst of plagioclase with the traces of partial melting in the border zone; the melting is revealed by the formation of pale yellowish-orange glass; the adjacent smaller xenocryst shows more extended rate of melting, with both pale yellowish-orange and dusky yellow spots of glass being observed. PPL; c – CMR-1096 (olivine basalt): a plagioclase xenocryst having a ‘per-esterite’ texture of decomposition into albite-oligoclase and labradorite; the light brown inclusions in plagioclase are composed of fluorapatite of the host basanite. PPL; d – HP-197 (basanite): xenocrysts of plagioclase completely recrystallised into titanium augeite-plagioclase symplectite displaying finger-print texture; the xenocrysts are rimmed by newly-formed plagioclase, whose content corresponds to host basanite. PPL.

reveals the addition of TiO_2 , FeO , MgO , and volatiles, as well as the removal of Na_2O (Table 2).

Magnetite and spinel. Magnetite is found in the form of fragmented grains, with their size ranging from 0.3 mm to 2.0 cm. Reactive interaction with the host rocks is manifested by the development of a myrmekitic rim (0.03–0.22 mm wide) consisting of small inclusions of clinopyroxene, oligoclase and zeolite in its marginal zone (Fig. 10a). Myrmekitic rims clearly constitute deconsolidated near-contact zones, which the products of late crystallisation of basanites and nephelinites could permeate relatively easily.

Spinel is represented by two types: 1 – red-brown chromium spinel, 2 – grey-green and greenish-black hercynite spinel. The grains are clastic, with their size coming up to 1.0–1.3 mm. Usually, they have a titanomagnetite rim ranging from 0.04 to 0.2 mm in width (Fig. 10b, c). The formation of this rim is asso-

ciated with the crystallisation of the bulk of the host rocks, including its late fluid phase represented by zeolite and saponite. Similar near-contact changes in spinel are also observed in peridotite xenoliths (Fig. 10d).

Geochemical data (see Table 1) show a significant increase in the content of TiO_2 in the marginal zones of magnetite and spinel up to the values close to those of titanomagnetite of the host rocks.

Apatite. It is found in the form of turbid grey fragmented grains up to 2.9 mm in size, in places with a well-developed plane-parallel texture, shear fractures and traces of decrystallisation, often covering their entire area (Figures 11a–c). It is veined with zeolite or saponite. The size of decrystallised apatite domains is from a micron to 0.13 mm. The same changes are observed in the xenoliths of apatite-magnetite and apatite-clinopyroxene-magnetite rocks (Fig. 11d). Decrystallisation constitutes an im-

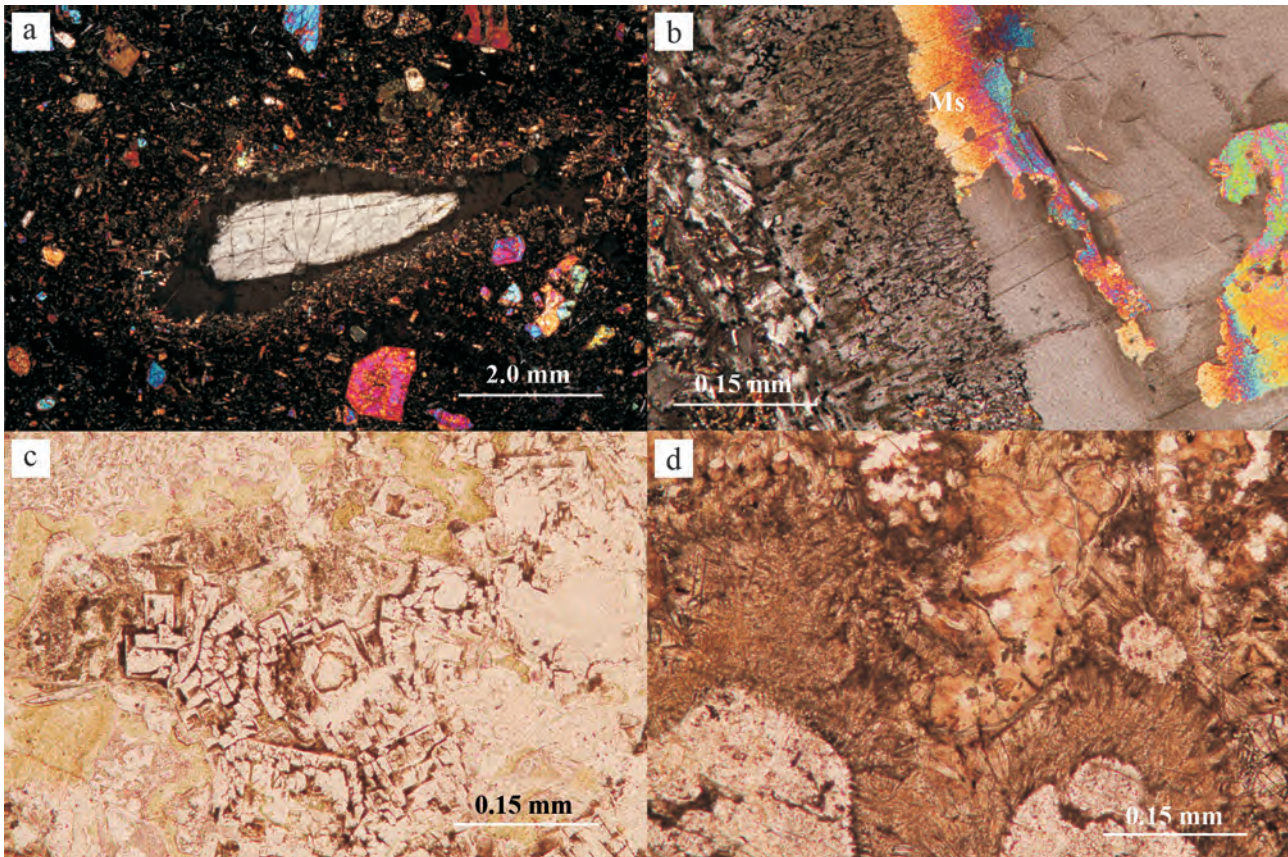


Fig. 9. Anorthoclase xenocrysts.

a – HG-2 (basanite). A xenocryst of anorthoclase rimmed by a melting zone. The glass phase is uncolored or of moderate brown colour. XPL; b – SQG-30-2 (olivine basalt). The rim of multi-grained anorthoclase xenocryst recrystallised into tiny domains with the formation of fingerprint-like texture and partial replacement of plagioclase by muscovite. XPL; c – HG-1907-3 (basanite). Completely recrystallised anorthoclase xenocryst with the fragment of fingerprint-like texture and moderate brown and pale olive glass. XPL; d – MG-2-2 (basanite). A xenolith of the upper crustal tuffs of the Zenifim Fm. Spherulitic texture develops around feldspars due to contact metamorphism induced by host basanite. PPL.

Table 2. Chemical composition of anorthoclase xenocrysts and products of their alteration, wt %

Element	1	2	3	4	5	Component	1	2	3	4	5
SiO ₂	65.94	66.35	60.23	60.42	63.51	qu	3.51	4.80	16.58	29.13	–
TiO ₂	0.15	0.01	0.33	0.41	0.38	or	23.22	20.45	24.76	21.69	25.23
Al ₂ O ₃	20.79	20.40	18.93	18.97	21.17	ab	64.99	60.42	28.77	16.84	50.58
FeO	0.29	0.10	3.76	3.27	0.50	an	6.20	13.84	8.28	7.39	9.78
MnO	–	–	0.01	0.06	0.03	ne	–	–	–	–	4.39
MgO	–	–	0.91	–	0.15	c	1.65	0.05	5.77	9.01	–
CaO	1.24	1.06	1.67	1.49	2.38	hy	0.12	0.54	8.64	5.44	–
Na ₂ O	7.67	7.42	3.40	1.99	7.88	di	–	–	–	–	1.46
K ₂ O	3.92	5.40	4.19	3.67	4.27	wo	–	–	–	–	0.11
Total	100.00	100.74	93.43	91.18	100.27	il	0.30	0.06	0.63	0.78	0.72

Note. HG-3: 1 – megacryst. HG-2: 2 – megacryst, 3–4 – glass at the periphery of megacryst (product of its melting), 5 – anorthoclase from the matrix of host basanites.

portant difference between xenocrysts and the violet-blue microphenocrysts of fluorine-apatite host rocks. The apatite from xenocryst is also enriched with fluorine (see Table 1), most likely, under the influence of host magmatites.

Nepheline is much less common than other types of xeno- and megacrysts. It is found in the form of megacrysts reaching up to 4.0×2.0 cm in size, veined by zeolite, calcite and saponite, and often being surrounded by a continuous or interrupted rim of the same min-

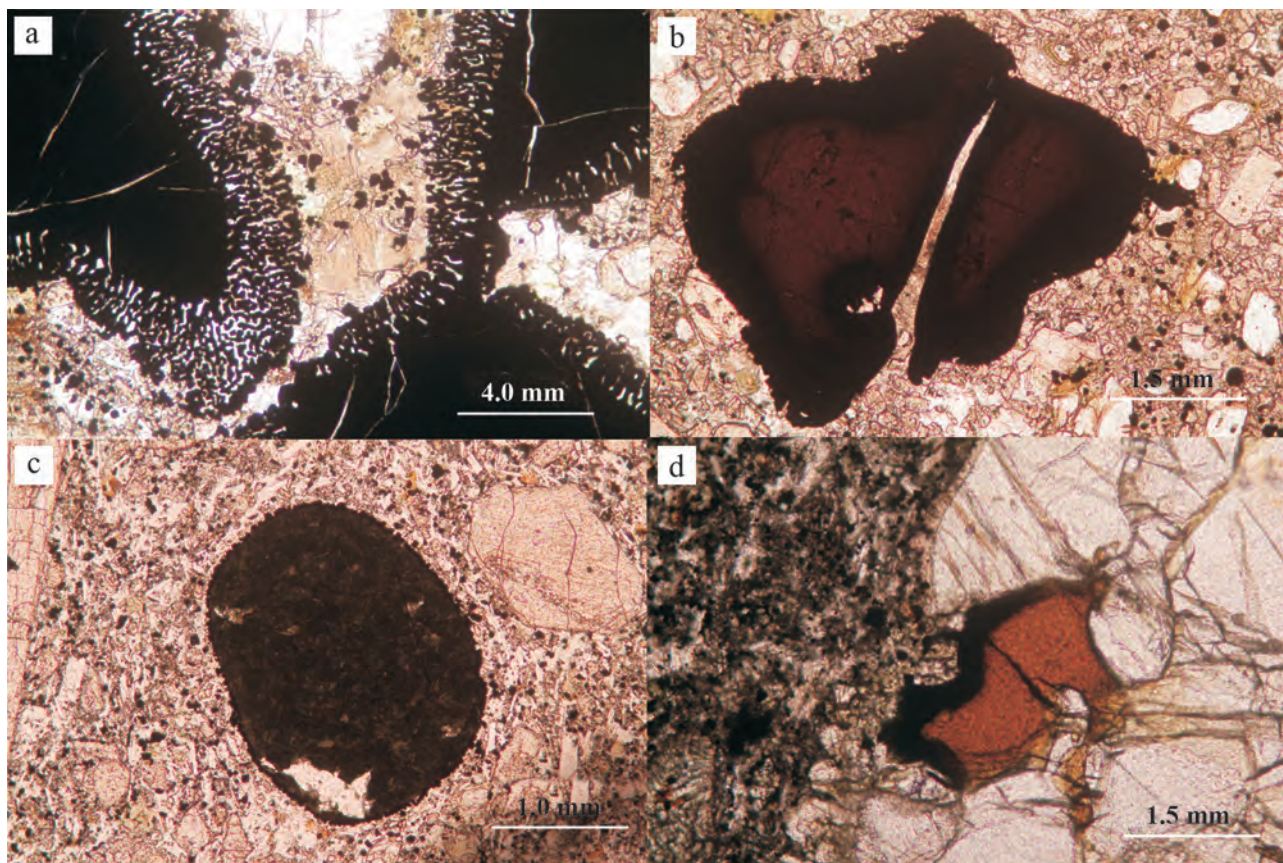


Fig. 10. Xenocryst of magnetite and spinel.

a – NH-254 (nephelinite). Myrmekite texture contouring the fragments of disintegrated magnetite megacryst. PPL; b – NH-369 (nephelinite). The xenocryst of chromian spinel showing a gradual transition into titanium magnetite. The veinlet of host melt contains zeolite at its end part and is completely surrounded by a rim enriched in titanium magnetite. PPL; c – TH-734 (basanite). A xenocryst of hercynite spinel with a thin rim of titanium magnetite, which formation occurred due to the crystallisation of host melt. PPL; d – HP-70 (olivine basalt). Chromian spinel in the xenoliths of lherzolite. The rim of titanium magnetite was formed only at the contact with host rocks. PPL.

erals (Fig. 12). No reactive changes were noted at the boundary of nepheline with the host rocks. For the rocks of PostArodgl association, nepheline phenocrysts, which could be confused with xenocrysts, are generally not characteristic. In them, it is observed only as an interstitial mineral in the bulk of basanites and nephelinites.

RESULTS AND DISCUSSION

The presence of mantle and lower crustal high-density xenoliths along with the products of their disintegration (xeno- and megacrysts) in alkaline basalt and ultrabasic magmas of lower density and viscosity is due to their rapid rise to the earth's surface at a speed of 0.5–10 m/s [Ringwood, 1975; Kuo, Kirpatrick, 1985; Snelling, 2007]. A rapid rise causes decompression of xenoliths engulfed by magma, which were formed at a higher pressure, structural and polymorphic transformations of their constituent minerals, and ultimately leads to their melting. The lower limit determined by

the thermodynamic conditions of these processes completely correlates with the results of studying melt and fluid inclusions in pyroxenes and olivines of the mantle xenoliths from Makhtesh Ramon, engulfed by the melt in the pressure range 5.9–8.1 kbar and temperatures of 1140–1350°C [Vapnik, 2005].

When magma is rising to the surface, xenoliths engulfed by it decompose into smaller fragments and individual minerals (xenocrysts) as a result of decompression. The latter are identified by similarities with xenolith minerals, in particular by deformity, characteristic sponginess ('clogging up'), reaction products, etc. Along with xenocrysts, the host rocks contain megacrysts that look like phenocrysts and often have a regular crystallographic form. There are different points of view on their genesis. Some researchers [Binns et al., 1970; Wilkinson, 1975; Evans, Nash, 1979; Ehrenberg, 1982; Irving, Frey, 1984; Dobosi et al., 2003; Kowabata et al., 2011] believe that the megacrysts of augite, spinel, anorthoclase, kaersutite, as well as other minerals, are formed during the crystallisation of host alka-

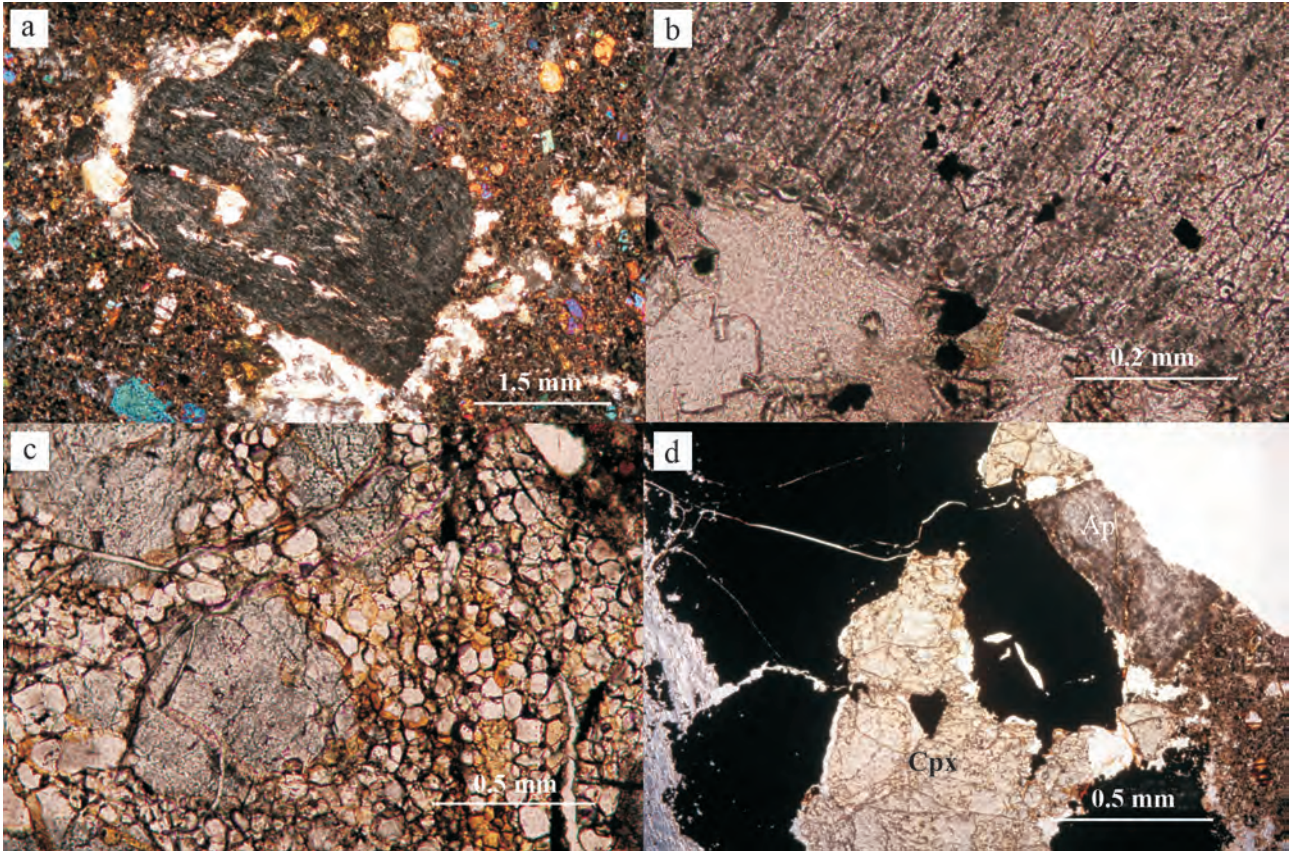


Fig. 11. Apatite xenocrysts.

a and b – HA-2 (basanite). A xenocryst of decrystallised apatite with fractures filled by zeolite. The enlargement shows the decomposition of apatite into numerous tiny domains. PPL; c – HA-6 (basanite) A fragment of partly decrystallised megacryst of apatite. PPL; d – HA-12 (basanite). A xenolith of apatite-clinopyroxene-magnetite rock. The moderate brown grain of decrystallised apatite is on the right side. PPL.

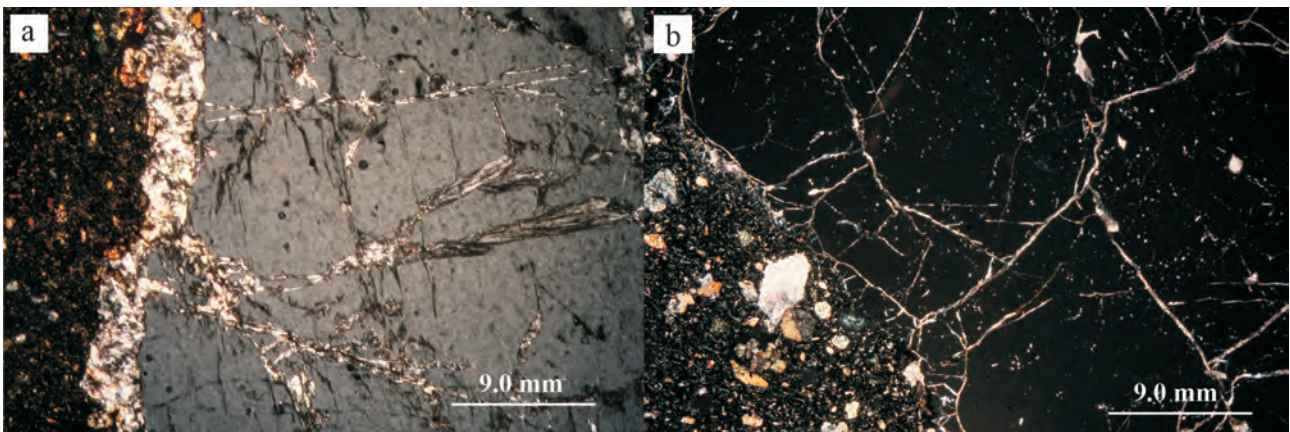


Fig. 12. Nepheline xenocrysts.

a – HG-2035 (nephelinite). A fractured xenocryst of nepheline, with the outer rim and veinlets being composed of zeolite. The genesis of zeolite is related to the crystallisation of host nephelinite. XPL; b – HG-2013 (basanite). Analogous to the previous sample, but the veinlets are composed of calcite. XPL.

line-basaltic magmas and constitute products of deep-seated intermediate foci or fragments of previous meta-

somatites. However, others [Shulze, 1987; Righter, Carmichael, 1993; Barns, Roeder, 2001; Rankenburg

et al., 2004] call them xeno-megacrysts – fragments of peridotites, gabbros, pyroxenites and syenites – due to the inconsistency with the conditions for the formation of host magmas. In [Nielson, Nakata, 1994; Shaw, Eyzaguirre, 2000], the key emphasis is placed on the heterogeneity of megacrysts: some of them are rejected by the metasomatic mantle, others constitute cumulates of the host magmas.

The effect of the host melt on the solid phases engulfed by it is characterised by a wide range of transformations of the latter: changes in petrographic and chemical features, solid-phase decomposition reactions, decrystallisation and recrystallisation. Being separated from xenoliths, individual constituent minerals are surrounded by melt and, as a result, experience an even more significant temperature shock, which generally corresponds to pyrometamorphism, leading to melting.

Melting

Xenocrysts displaying clear signs of melting include quartz and feldspar. Quartz is primarily engulfed by magma from the Mesozoic formations in the area, partially from Proterozoic tuffs and quartz-bearing granulites, which indicates that interaction between quartz and the host melt takes place at a relatively small depth. The melting point of quartz (1723–1728°C) is 350–400°C higher than the temperature at which melt inclusions in the minerals of xenoliths from Makhtesh Ramon are engulfed [Vapnik, 2005]. Nevertheless, its melting is an obvious fact and clearly occurred at a lower temperature. According to [Ostrovskii et al., 1959; Kennedy et al., 1962], the melting of quartz with its preliminary transition to tridymite and cristobalite under the conditions of crustal pressure can occur in the temperature range of 1200–1300°C, i.e. under conditions that are completely consistent with the engulfment of the aforementioned melt inclusions.

The melting of plagioclase begins with the formation of a turbid grey deconsolidated rim along its margins with a small amount of glass and the development of lattice and fingerprint-like structures (with interstitial glass between plagioclase domains). As shown by the experiments of [Tsuchiyama, 1985, 1986; Nelson, Montana, 1992], plagioclase easily undergoes such transformations at low pressure and high temperature (1190–1307°C), i.e. under thermodynamic conditions that are quite applicable to the interaction between xenocrysts and alkaline basaltoids in Makhtesh Ramon.

The megacrysts of anorthoclase are subject to more intense melting than quartz and plagioclase. At the boundary with the host melt, it melts to form glass or spherulite, followed by a zone of lattice and fingerprint-like structures. The emergence of a spherulitic structure, as suggested by [Arzill, Carroll, 2013], indicates the extreme heating of the mineral under crustal pressure, which is confirmed by the corresponding

transformations in the potassium feldspar of xenoliths from Proterozoic tuffs.

Solid-phase decomposition

The processes of solid-phase decomposition, represented by symplectites, are characteristic of the xenocrysts of orthopyroxene, amphibole, sometimes plagioclase; they are manifested in the form of kelyphite rims, linear zones and complete pseudomorphs.

Orthopyroxene decomposes into a microlite aggregate of olivine and clinopyroxene. This phenomenon is extensively covered in the literature [Kutolin et al., 1976; Agafonov et al., 1978; Messiga, Bettini, 1990; Arai, Abe, 1995; Kogarko et al., 2001; Villaseca et al., 2010] and reproduced in experimental studies [Boivin, 1980; Brearley, Scarfe, 1986; Shaw et al., 1998]. A feature distinguishing the described decomposition structure from the one observed by the indicated authors is the absence of glass in it, which in the intergranular spaces is replaced with feldspars, as well as zeolite and saponite rich in the hydroxyl component.

Symplectites after kaersutite are composed of rhonite, titanium-augite, olivine, plagioclase, titanomagnetite and late magmatic minerals. Rhonite is an indicator of the thermodynamic conditions for the solid-phase decomposition of amphibole and, according to [Kyle, Price, 1975; Johnston, Stout, 1984; Vapnik, 2005; Lopez et al., 2006; Grapes, Keller, 2010; Sharygin et al., 2011], is stable in the temperature range 1000–1260°C and pressures of 0.5–4.0 kbar. The experimental studies of orthopyroxene [Brearley, Scarfe, 1986; Shaw, 1999; Kogarko et al., 2001; Miller et al., 2012] and amphibole [Ban et al., 2004] show that their decomposition results in the formation of glass rich in SiO₂. In the studied samples, such glass was not found. The presence of minerals such as zeolite, saponite, and calcite in the interstitial of decomposition products indicates the importance of the fluid component of the magmatic melt in this process. The likelihood of such reactions involving the rapid crystallisation of the melt into a fine crystalline mass (without glass formation) is also experimentally justified [Chepurov et al., 2013].

Another form of solid-phase decomposition is occasionally observed in plagioclase xenocrysts and is manifested by the formation of a peristerite structure in them, which differs from the ordinary peristerites of metamorphic rocks in the higher compositions of coexisting plagioclases – An₁₈₋₂₁ and An₆₀₋₆₂. The probability of such a structure in main plagioclases was experimentally reproduced in [Ribbe, 1960] and was suggested in [Miyashiro, 1976].

Decrystallisation and recrystallisation

Decrystallisation (thermal destruction) as a sign indicating the difference between xenocrysts and phenocrysts is most clearly manifested in olivine and ap-

atite, less often in plagioclase. It develops by forming areas in xenocrysts, which have a micrograin structure and are confined to marginal or weakened (linear) zones. The combination of the newly formed structure with pressurised structures ('zebra-like' in olivine, plane-parallel in apatite, bent in plagioclase) within a single grain suggests that decrystallisation is a reaction to the removal of residual stress in these minerals under new decompression conditions. In addition, it exhibits a tendency for the equalization of the composition of restructured xenocrysts and the eponymous minerals of the host rock matrix.

Recrystallisation (thermal reconstruction) constitutes one of the most important processes characterising the structural rearrangement of xenocrysts under the influence of the surrounding high-temperature melt. Almost all minerals of xenocrysts, both mono- and polygranular, underwent structural rearrangement. They share the ability to transform initially xenomorphic grains (before the disintegration of xenoliths) into crystallographically regular forms similar to the phenocrysts of the host rocks. By analogy with the processes considered in biology and biophysics, this phenomenon of morphological rearrangement is called structural homeostasis [Goryainov, Ivanyuk, 2010]. Particularly interesting in this respect are multi-grain intergrowths, which in fact are small xenoliths of clinopyroxenes, olivinites and plagioclases characterised by a granoblast structure, illustrating a clear tendency to reacquire their genetically characteristic form, clearly observed in clinopyroxenes and olivines. Transformation is also characteristic of initially xenomorphic (in xenoliths) kaersutite, of its varieties completely transformed into symplectites, as well as of complete symplectites after orthopyroxene. Other minerals are sometimes used, including minerals similar to them in chemistry, for example, olivine and orthopyroxene in clinopyroxene in order to build a perfect habit. In the course of self-faceting, a certain sequence can be established: the crystallographic rearrangement of the granoblast aggregate within the framework of a common perfect habit – the emergence of the initial signs of twinning and zoning – optical homogenisation, i.e. the transformation of variously oriented grains into a normal crystal. The ability of crystals to restore the forms of natural faceting under the conditions of free growth, along with their self-organisation, has long been known and has been described as the 'method for the crystallisation of balls' by Artemyev [Shubnikov, 1935] and 'the spontaneous crystallisation by Lukirsky' [Geguzin, 1987] and is explained by the tendency of the mineral to provide the least surface energy.

GEOCHEMICAL TRANSFORMATIONS

When interacting with the carrier melt, all ontogenetic changes occurring in xenocrysts are directed at the geochemical equalisation of their compositions

with minerals crystallising from this melt and are manifested by the diffuse and infiltration substitution of xenocrysts with the chemical elements of the surrounding melt. Diffuse substitution is most noticeable in the marginal zones of xenocrysts and is manifested by the emergence of marginal zones in them, which completely correspond to the minerals of the host rocks in terms of composition. Thus, the xenocrysts of clinopyroxene, orthopyroxene and amphibole accrete augite and titanium augite, with plagioclase acquiring a high-anorthite rim, whereas spinel and magnetite get a titanomagnetite rim. Bimodal crystals, in which the xenocryst is a seed component inducing the development of a later phase associated with crystallisation of the host melt, are obtained.

On the whole, the geochemical data reveal a tendency for the xenocrysts of pyroxene and olivine to decrease magnesium contents, increase the concentrations of iron contents, and, accordingly, decrease the magnesium number to those of the host mineral rocks in the direction from the centre to the marginal zone.

Statistical geochemical data on the distribution of SiO₂ (wt %), magnesium number and anorthite number in xenoliths, xenocrysts and eponymous minerals of host magmatites are of interest. The histograms (Figures 13 and 14) and the diagram (Fig. 15) reflect the distribution of SiO₂ values (wt %) and the magnesium number in the olivines and clinopyroxenes of xenoliths, xenocrysts and host magmatites. In constructing them, data from previous studies were used, in which all inclusions in the rocks of the studied association were phenocrysts and, therefore, were identified as a group of phenocrysts without being divided into phenocrysts and xenocrysts. As Figures 14 and 15 show, the magnesium number in the olivines and clinopyroxenes of xenocrysts and xenoliths reveal a tendency towards the equalisation with the eponymous minerals of the host rocks. Mg* = 0.85–0.87 should be considered the boundary value, the limiting value for the olivine and clinopyroxene of melt inclusions in the minerals of xenoliths of peridotites, matrix grains and microphenocrysts of the host rocks. Higher values apply to xenoliths and xenocrysts. The distribution of SiO₂ (see Fig. 13) in clinopyroxenes and olivines also follows this trend and, at the same time, illustrates that the increased primary contents of this element are well correlated with increased magnesium numbers (see Fig. 15) in xenoliths and xenocrysts, which distinguishes them from phenocrysts. In terms of silica content, the dividing line is at 40.0 wt % for olivines and 50.0 wt % for clinopyroxenes: higher contents are characteristic of xenoliths and xenocrysts, with lower contents being typical of host rocks, thus emphasising their belonging to the geochemical type of silica-saturated and undersaturated rocks, respectively. The presence of the undivided inclusions of olivine and clinopyroxene characterised by high SiO₂ and magnesium numbers in the samples of the magmatic rock group that exceed the boundary sta-

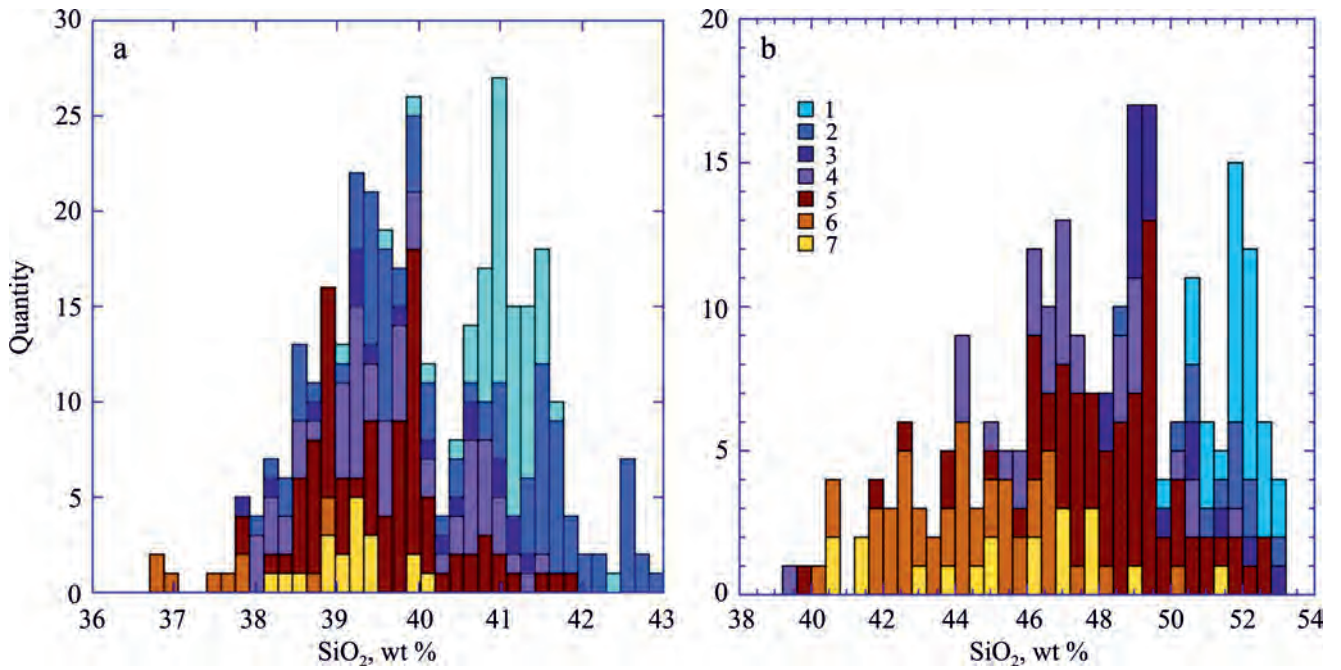


Fig. 13. SiO₂ content in olivine (a) and clinopyroxene (b) hosted in xenoliths (including xenocrysts) and magmatic rocks.

Xenoliths: 1 – harzburgites, 2 – lherzolites, 3 – wehrlites, 4 – clinopyroxenites and websterites; magmatic rocks: 5 – all mineral inclusions without being subdivided into phenocrysts and xenocrysts, 6 – mineral inclusions in matrix and prismatic microphenocrysts from host magmatic rocks, 7 – mineral phases in melt inclusions hosted in the olivine and clinopyroxene of peridotite xenoliths.

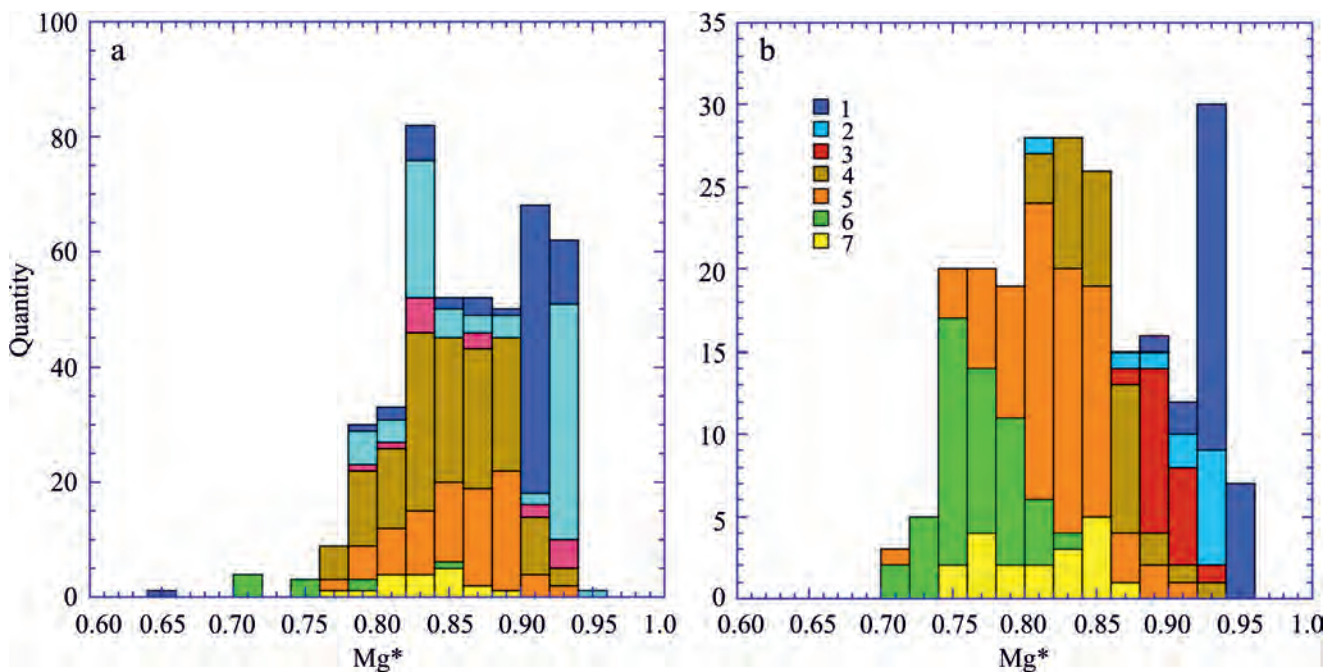


Fig. 14. Mg* distribution in olivine (a) and clinopyroxene (b) hosted in xenoliths (including xenocrysts) and magmatic rocks.

Xenoliths: 1 – harzburgites, 2 – lherzolites, 3 – wehrlites, 4 – clinopyroxenites and websterites; magmatic rocks: 5 – all mineral inclusions without being subdivided into phenocrysts and xenocrysts, 6 – mineral inclusions in matrix and prismatic microphenocrysts from host magmatic rocks, 7 – mineral phases in melt inclusions hosted in the olivine and clinopyroxene of peridotite xenoliths.

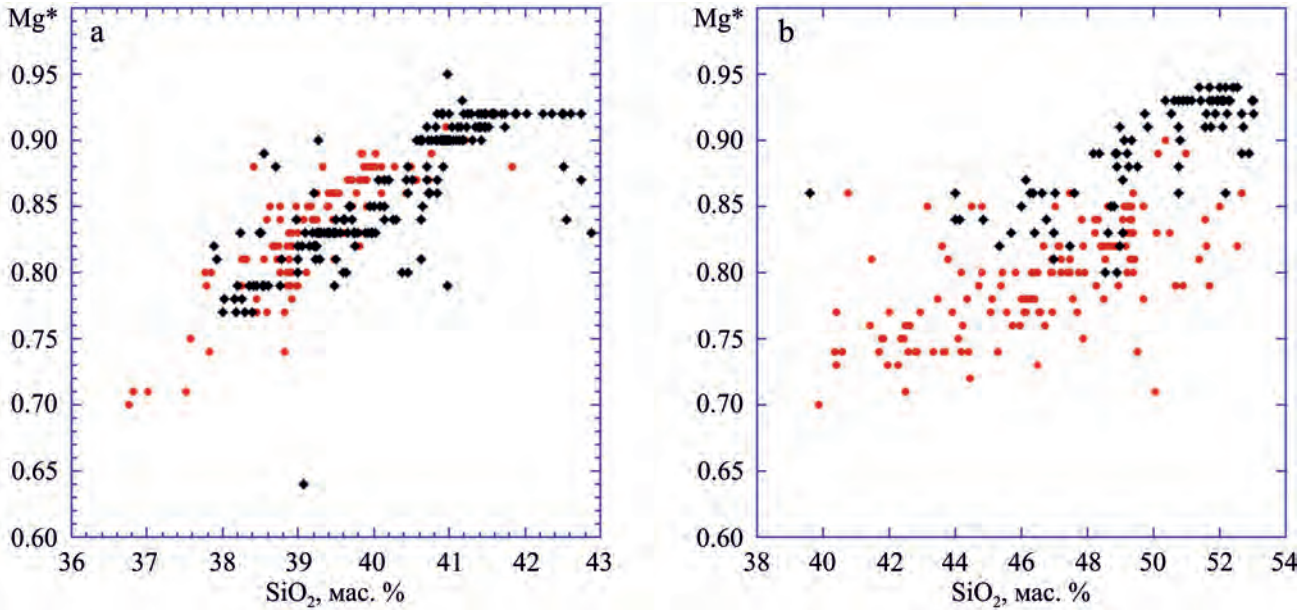


Fig. 15. Correlation between SiO_2 and Mg^* in olivine (a) and clinopyroxene (b) hosted in xenoliths (including xenocrysts) and magmatic rocks.

Black rhombi denote combined sample of harzburgites, lherzolites, wehrlites, clinopyroxenites and websterites; red circles denote combined sample of all magmatic rocks.

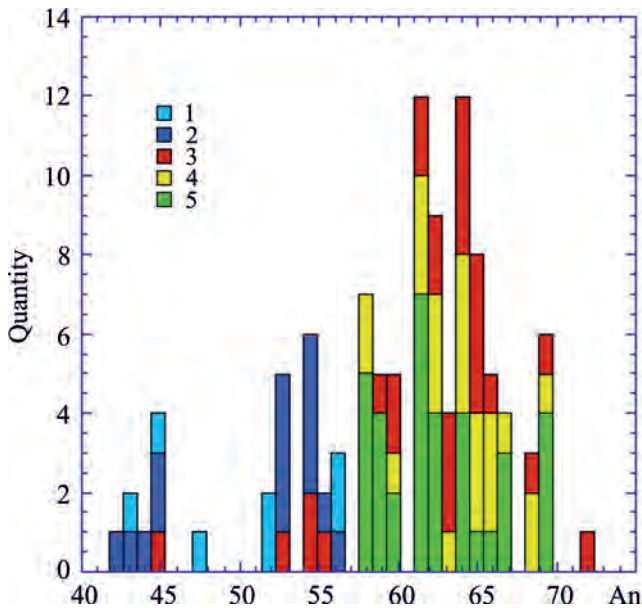


Fig. 16. Anorthite distribution in plagioclase hosted in metagabbro xenoliths (granulites), xenocrysts, and magmatic rocks.

1 – metagabbro, 2 – xenocrysts, 3 – mineral inclusions in host olivine basalts and basanites (all mineral inclusions without being subdivided into phenocrysts and xenocrysts), 4 – prismatic micropheocrysts, 5 – microliths.

tistical values indicates the presence of xenocrysts in these samples. If we consider the distribution of the An-component in the plagioclases of xenocrysts, me-

tagabbros and host rocks (Fig. 16), we can see that the interface between them and the plagioclase of the host rocks runs at An_{57-58} : lower values (from An_{42} to An_{57}) are characteristic of xenocrysts and xenoliths, whereas higher values (from An_{57} to An_{73}) are typical of host basaltoids. At the same time, the group of undivided inclusions reveals values characteristic of plagioclase xenocrysts.

Infiltration metasomatism covers almost all xenocrysts to one degree or another, given that decompression disarranges the structure of crystals, leads to their deconsolidation and the formation of fractures that facilitate the percolation of the host magma and its fluids through them. This is especially noticeable in the xenocrysts of clinopyroxene, in which traces of percolation are marked by the so-called spongy structures, manifested by a non-specific shagreen texture. The formation of such structures constitutes a complex issue and has been considered in a number of works. Some researchers believe that partial melting of the mantle triggers the infiltration of gas-water fluids [Dal Negro et al., 1989; Francis, 1991; Carpenter et al., 2002], whereas others explain it by the interaction of xenoliths with magmatic fluids when rising to the surface under the conditions of rapid pressure reduction [Kutolin et al., 1976; Agafonov et al., 1978; Tsuchiyama, 1986; Wang et al., 2012], which completely consistent with our data.

The peculiar symplectites of plagioclase, represented by its eutectoid intergrowths with titanium augite, also belong to the products of infiltration substitution.

The plagioclase in them has a lattice and fingerprint-like structure, the same as in the zones of initial melting of this mineral. However, due to the diffusion of FeO, MgO, and TiO₂ from the surrounding melt titanium augite is formed in it. A similar situation involving the enrichment of symplectic pseudomorph after kaersutite with titanomagnetite at the boundary with the host basalt is shown in Fig. 7. The same type of metasomatism should include the formation of myrmekite texture in the marginal zone of magnetite xenocrysts, which bears only an external resemblance to the real myrmekite texture of solid-phase decomposition and is caused by the penetration of minerals in the final stage of crystallisation of the host melt into its deconsolidated margins.

CONCLUSION

The study shows the important role of ordinary microscopic observations, which provide the opportunity to detect clear signs of differences between genetically heterogeneous formations – phenocrysts and xenocrysts – coexisting in a single magmatic system. Some xenocrysts, in particular, quartz and orthopyroxene, which are incoherent with respect to the alkaline-basaltoid and nephelinite melts hosting them, are identified easily, whereas the identification of other minerals (in particular olivine, clinopyroxene, amphibole, plagioclase, anorthoclase, nepheline, magnetite and apatite) nominally corresponding to the possible crystalline phases of the melts, is often difficult. Nevertheless, the use of a number of informative petrographic and geochemical features makes it quite possible. The main factors that trigger mechanisms underlying the interaction between the melt and xenoliths are decompression, high-temperature metamorphism and metasomatism. Decompression leads to the disintegration of xenoliths into smaller fragments and individual minerals, the destruction, as well as deconsolidation, of these minerals, the formation of pores, caverns and channels, activating the percolation of fluids dissolved in the melts. Metamorphism corresponds to the highest temperature facies of contact metamorphism; for a number of minerals, it results in partial melting, while metasomatism developing in this context is directed at equalising the compositions of xenocrysts and crystallisation products of the melt hosting them.

The most important criteria contributing to the identification of xenocrysts include partial melting, solid-phase decomposition, decrystallisation of initial structures (before-trapping), recrystallisation (self-faceting) of initially xenomorphic grains into crystallographically more perfect forms, as well as a change in composition due to the metasomatic effect of the host magma.

REFERENCES

- Agafonov L.V., Kutolin V.A., Lesnov F.P. (1978) Influence of basaltic magma on xenoliths of ultramafic and mafic rocks, and relative stability of minerals in basaltic melt. *Materialy po petrologii i mineralogii ultraosnovnykh i osnovnykh porod* [Materials on petrology and mineralogy of ultramafic and mafic rocks]. Novosibirsk, Nauka Publ., 67-84. (In Russian)
- Arai S., Abe N. (1995) Reaction of orthopyroxene in peridotite xenoliths with alkali basalt melt and its implication for genesis of alpine-type chromitite. *Amer. Mineral.*, **80**, 1041-1047.
- Arzilli F., Carroll M.R. (2013) Crystallization kinetic of alkali feldspars in cooling and decompression induced crystallization experiments in trachytic melt. *Contrib. Mineral. Petrol.*, **166**, 1011-1027.
- Baer G., Heimann A., Eshet Y., Weinberger R., Musset A., Sherwood G. (1995) The Saharonim Basalt: A Late Triassic – Early Jurassic intrusion in south-eastern Makhtesh Ramon. *Isr. J. Earth Sci.*, **44**, 1-10.
- Ban M., Witt-Eickschen G., Klein M., Seck H. (2004) The origin of glasses in hydrous mantle xenoliths from the West Eifel, Germany: incongruent break down of amphibole. *Contrib. Mineral. Petrol.*, **148**, 511-523.
- Barns S., Roeder P. (2001) The range of spinel composition in Terrestrial mafic and ultramafic rocks. *J. Petrol.*, **42**, 2279-2302.
- Bédard J.H. (1988) Comparative amphibole chemistry of the Monteregean and White Mountain alkaline suits, and the origin of amphibole megacrysts in alkali basalts and lamprophyres. *Miner. Mag.*, **52**, 91-103.
- Bentor Y. (1952) Magmatic intrusion and lava sheets in the Raman area of the Negev (southern Israel). *Geol. Mag.*, **89**, 129-140.
- Binns R., Duggan M., Wilkinson J. (1970) High pressure-megacryst in alkaline lavas from northeastern South Wales with chemical analyses. *Amer. J. Sci.*, **269**, 132-168.
- Boivin P. (1980) Données expérimentales préliminaires sur la stabilité de la rhönite à 1 atmosphère. Application aux gisements naturels. *Bull. Minéral.*, **103**, 491-502.
- Bonen D., Perlman I., Yelin J. (1980) The evolution of trace element concentrations in basic rocks from Israel and their petrogenesis. *Contrib. Mineral. Petrol.*, **72**, 397-414.
- Brearely M., Scarfe C.M. (1986) Dissolution rates of upper mantle minerals in alkali basalt melt at high pressure: an experimental study and implications for ultramafic xenoliths survival. *J. Petrol.*, **27**, 1157-1182.
- Carpenter R., Edgar A., Thibault Y. (2002) Origin of spongy textures in clinopyroxenes and spinel from mantle xenoliths, Hessian Depression, Germany. *Mineral. Petrol.*, **74**, 149-162.
- Chepurov A.I., Zhimulev E.I., Agafonov L.V., Sonin V.M., Chepurov A.A., Tomilenko A.A. (2013) The stability of ortho- and clinopyroxenes, olivine, and garnet in kimberlitic magma. *Geol. Geofiz.*, **54**(4), 533-544. (In Russian)
- Dal Negro A., Manoli S., Secco L., Piccirillo E.M. (1989) Megacrystic clinopyroxenes from Victoria (Australia): crystal chemical comparisons of pyroxenes from high and low pressure regimes. *Eur. J. Mineral.*, **1**, 105-121.

- Dobosi G., Downes H., Emdey-Istin A., Jenner J. (2003) Origin of megacrysts and pyroxenite xenoliths from the Pliocene alkali basalts of the Pannonian basin (Hungary). *J. Mineral. Geochem.*, **178**, 217-237.
- Ehrenberg S. (1982) Petrogenesis of garnet lherzolite and megacrystalline nodules from the Thumb, Navajo volcanic field. *J. Petrol.*, **23**, 507-547.
- Evans S., Nash W. (1979) Petrogenesis of xenoliths-bearing basalts from southeastern Arizona. *Amer. Mineral.*, **64**, 249-267.
- Eyal M., Becker A., Samoilov V. (1996) Mt. Arod – an Early Cretaceous basanitic volcano with a fossil lava lake. *Israel J. Earth Sci.*, **45**, 31-38.
- Fershtater G., Yudalevich Z. (2017) Mantle metasomatism and magma formation in continental lithosphere: data on xenoliths in alkali basalts from Makhtesh Ramon, Negev desert, Israel. *Petrology*, **25**, 181-205.
- Fershtater G.B., Yudalevich Z.A., Khiller V.V. (2016) Xenoliths in alkaline basaltoids of Makhtesh Ramon (Negev, Israel) as indicators of mantle metasomatism and magma genesis. *Litosfera*, (3), 5-26. (In Russian)
- Francis D. (1991) Some implications of xenolith glasses for the mantle sources of alkaline mafic magmas. *Contrib. Mineral. Petrol.*, **108**, 175-180.
- Garfunkel Z., Katz A. (1967) New magmatic features in Makhtesh Ramon, southern Israel. *Geol. Mag.*, **104**, 608-629.
- GeguzinYa.E. (1987) *Zhivoi kristall* [Living crystal]. Moscow, Nauka Publ., 192 p. (In Russian)
- Goryainov P.M., Ivanyuk E.G. (2010) Energetic percolation, as a reason of self-organization of lithospheric complexes. "Problemy geologii poleznykh iskopaemykh i metallogenii". Mezhdunar. konf. ["Problems of geology of ore deposits and metallogeny". International conference]. Moscow, 205. (In Russian)
- Grapes R.H., Keller J. (2010) Fe²⁺-dominant rhönite in undersaturated alkaline basaltic rocks, Kaisersuhl volcanic complex, Upper Rhine Graben, SW Germany. *Eur. J. Mineral.*, **22**, 285-292.
- Irving A.J., Frey F.A. (1984) Trace element abundance in megacrysts and their host basalts: constraints on partition coefficients and megacrysts genesis. *Geochim. Cosmochim. Acta*, **48**, 1201-1221.
- Johnston A.D., Stout J.H. (1984) Compositional variation of naturally occurring rhönite. *Amer. Mineral.*, **70**, 1211-1216.
- Kennedy D., Wasserburg G., Heard H., Newton R. (1962) The upper three-phase region in the system SiO₂-H₂O. *Amer. J. Sci.*, **260**, 501-521.
- Kogarko L., Kurat G., Ntafos T. (2001) Carbonate metasomatism of the oceanic mantle beneath Fernando de Noronha Island, Brazil. *Contrib. Mineral. Petrol.*, **140**, 577-587.
- Kowabata H., Hanui T., Chang Q., Kimura J-I., Nichols A.R.L., Tatsumi Y. (2011) The petrology and geochemistry of Saint Helena alkali basalt: evaluation of the oceanic crust-recycling model of HIMU OIB. *J. Petrol.*, **52**, 791-838.
- Kuo L.C., Kirpatrick R.J. (1985) Dissolution of mafic minerals and its implications for the ascent velocities of peridotite-bearing basaltic magmas. *J. Geol.*, **93**, 691-700.
- Kutolin V.A., Agafonov L.V., Chepurov A.I. (1976) Relative stability of olivine, pyroxenes, and garnet in basaltic magma and composition of the upper crust. *Dokl. Akad. Nauk*, **321**(5), 1218-1221. (In Russian)
- Kyle P., Price R. (1975) Occurrences of rhönite in alkali lavas of the McMurdo volcanic group, Antarctica, and Dunedin volcano, New Zealand. *Amer. Mineral.*, **60**, 722-728.
- Lang B., Hebeda E., Priem H., Steinitz G., Verdumen E. (1988) K-Ar and Rb-Sr Ages of Early Cretaceous Magmatic Rocks from Makhtesh Ramon, Southern Israel. *Israel J. Earth Sci.*, **37**, 65-72.
- Lopez M., Pompilio M., Rotolo S.R. (2006) Petrology of some amphibole-bearing volcanics of pre-Ellitico period (102 – 80 ka), Mt. Etna. *Periodico di Mineralogia*, **75**, 151-166.
- Messiga B., Bettini E. (1990) Reaction behavior during kelyphite and symplectite formation: a case study of mafic granulites and eclogites from the Bohemian Massif. *Eur. J. Mineral.*, **2**, 125-144.
- Miller C., Zanetti A., Thoni M., Konzett J., Klotzli U. (2012) Mafic and silica-rich glasses in mantle xenoliths from Wau-en-Namus, Libya: textural and geochemical evidence for peridotite-melt reactions. *Lithos*, **128-131**, 11-26.
- Miyashiro A. (1976). *Metamorfizm i metamorficheskie poyasa* [Metamorphism and metamorphic belts]. Moscow, Mir Publ., 535 p. (In Russian)
- Nelson S.T., Montana A. (1992) Sieve-textures plagioclase in volcanic rocks produced by rapid decompression. *Amer. Mineral.*, **77**, 1242-1249.
- Nielson J., Nakata J. (1994) Mantle origin and flow sorting of megacryst – xenolith inclusion in mafic dikes of Black Canyon, Arizona. *US Geol. Surv. Prof. Paper*, **1541**, 41 p.
- Ostrovskii N.Yu., Mishina G.P., Povilaitis V.M. (1959) P-T projection of SiO₂-H₂O system. *Dokl. Akad. Nauk SSSR*, **126**(3), 645-646. (In Russian)
- Rankenburg K., Lassiter J., Brey G. (2004) Origin of megacrysts in volcanic rocks of the Cameron vole: chain-constraints on magma genesis and crustal contamination. *Contrib. Mineral. Petrol.*, **147**, 129-144.
- Ribbe P. (1960) An X-ray and optical investigation of the peristerite plagioclases. *Amer. Mineral.*, **45**, 626-644.
- Righter K., Carmichael I.S.E. (1993) Mega-xenocrysts in olivine basalts: fragments of disrupted mantle assemblages. *Amer. Mineral.*, **78**, 1230-1245.
- Ringwood A.E. (1975) Origin and petrology of the Earth's mantle. *McGraw-Hill*, 618 p.
- Samoilov V., Vapnik Ye. (2007) Fractional melting – the determining factor in the origin of thephrite-basanite-nephelinite rock suite: evidence from western Makhtesh Ramon, Israel. *N. Jb. Mineral. Abh.*, **184**(2), 181-195.
- Sharygin V.V., Kotai K., Sabo Ch., Timina T.Ju., Terek K., Vapnik Ye., Kuz'min D.V. (2011) Rhönite in alkaline basalts: silicate melt inclusions in olivine phenocrysts. *Geol. Geofiz.*, **52**(11), 1695-1717. (In Russian)
- Shaw C.S.J. (1999) Dissolution of clinopyroxene in basanite magma between 0.4 and 0.2 GPa: further implications for the origin Si-rich alkaline glass inclusions in mantle xenoliths. *Contrib. Mineral. Petrol.*, **135**, 114-132.
- Shaw S.J.S., Eyzaguirre J. (2000) Origin of megacrysts in the mafic alkaline lavas of the West Eifel volcanic field, Germany. *Lithos*, **50**, 75-95.
- Shaw S.J.S., Thibault Y., Edgar A.D., Lloyd F.E. (1998) Mechanism of orthopyroxene dissolution in silica-undersaturated melts at 1 atmosphere and implications for the

- origin of silica-rich glass in mantle xenoliths. *Contrib. Mineral. Petrol.*, **132**, 354-370.
- Shubnikov A.V. (1935) *Kak rastut kristally* [How crystals grow]. Moscow; Leningrad, Academy of Sciences of the USSR Publ., 174 p. (In Russian)
- Shulze D. (1987) Megacrysts from alkali volcanic rocks. *Mantle xenoliths* (ed. P.H. Nixon), 443-451.
- Snelling A.A. (2007) Rapid ascent of basalts magmas. *Acts and Facts*, **36**, 10.
- Stein M., Katz A. (1989) Composition of the subcontinental lithosphere beneath Israel: Inferences from peridotitic xenoliths. *Israel J. Earth Sci.*, **38**, 75-87.
- Tsuchiyama A. (1985) Dissolution kinetics of plagioclase in the melt of the system diopside–albite–anorthite, and origin of crusty plagioclase in andesites. *Contrib. Mineral. Petrol.*, **89**, 1-19.
- Tsuchiyama A. (1986) Melting and dissolution kinetics: application to partial melting and dissolution of xenoliths. *J. Geophys. Res.*, **91**(B9), 9395-9406.
- Upton B.G.J., Finch A.A., Slaby E. (2009) Megacrysts and salic xenoliths in Scottish alkali basalt derivatives of deep crustal and small-melt fractions from upper mantle. *Miner. Mag.*, **73**, 943-956.
- Vapnik Y. (2005) Melt and fluid inclusions and thermobarometry of mantle xenoliths in Makhtesh Ramon, Israel. *Israel J. Earth Sci.*, **54**, 15-28.
- Vapnik Y., Sharygin V., Samoilov V., Yudalevich Z. (2007) The petrogenesis of basic and ultrabasic alkaline rocks of western Makhtesh Ramon, Israel: melt and fluid inclusion study. *Inter. J. Earth Sci.*, **96**, 663-684.
- Villaseca C., Ancochea E., Orejana D., Jeffries T.E. (2010) Composition and evolution of the lithospheric mantle in Central Spain: inferences from peridotite xenoliths from the Cenozoic Calatrava volcanic field. *Petrological evolution of the European lithospheric mantle* (Eds M. Coltorti, H. Downes, M. Grégoire, S.Y. O'Reilly). Geol. Soc., London, Spec. Publ., **337**, 125-151.
- Wang Y., Han B., Griffin W.L., Zhang L., Shu G. (2012) Post-entrainment mineral – magma interaction in mantle xenoliths from Inner Mongolia, Western North China craton. *J. Earth Sci.*, **23**, 54-76.
- Wilkinson J.F.G. (1975) Ultramafic inclusions and high pressure megacrysts from a nephelinite sill Nandewar Mountains, New Wales, and their bearing on the origin of certain ultramafic inclusions in alkali volcanic rocks. *Contrib. Mineral. Petrol.*, **51**, 235-262.
- Yudalevich Z.A., Fershtater G.B., Eyal M. (2014) Magmatism of Makhtesh Ramon: geology, geochemistry, petrogenesis (natural reserve of Har Ha-Negev, Israel). *Litosfera*, **3**, 70-92. (In Russian)

GEO-PETROLOGICAL MODEL FOR THE FORMATION OF DIAMOND-BEARING FLUID-EXPLOSIVE BRECCIA STRUCTURES (URAL TYPE)

Lyudmila N. Sharpenok, Lyudmila I. Lukianova, Oleg V. Petrov

A.P. Karpinsky Russian Geological Research Institute (VSEGEI), 74 Sredny ave., Vasilyevsky Island, St.Petersburg, 199106 Russia, e-mail: Lyudmila_sharpenok@vsegei.ru

Received 26.12.2017, accepted 06.06.2018

The geo-petrological model of diamond-bearing fluid-explosive breccia formations constitutes a well-structured system of features that are typical of several similar formations in the Cis-Ural and West Ural areas of the Perm Territory. The model reflects a number of basic common factors associated with the morphology of these structures, their rock composition and the conditions for their formation. In this paper, the authors characterise regional and local geological positions featuring diamond-bearing formations, as well as the parameters common for the areas of their development. The necessity of mineralogical and geochemical studies of black sand, while prospecting for diamond-bearing targets is highlighted. This will help identify specific mineral associations and geochemical anomalies typical of these widespread formation areas. The description of a geological structure associated with the best-studied deposit (Efimovsky) is given in detail. The description of this deposit is used as an example to illustrate the shape of breccia bodies and their polyphase structure, as well as show their texture and rock structure specifics. Special attention is paid to the petrographic characteristics of all kinds of fluid-explosive breccias, which to a different extent contain clastic, protomagmatic and newly formed fluidogenic material. The paper gives the characteristics and specifics of mineral grains of various origin, many of which are abundant in gas-liquid inclusions characterised by block extinction, while quartz possess planar elements. The authors examined the differences in the diamond potential of rocks belonging to different successive evolution phases of fluidogenic breccia formations. When studying newly discovered breccia structures that have a limited number of features, the model considered in the paper will help to predict the missing features and assessment criteria for diamond potential.

Keywords: *geo-petrological model, Cis-Ural and West Ural areas of the Perm Territory, diamond-bearing fluid-explosive breccia formations, Efimovsky deposit, petrographic and mineralogical characteristics of breccias, diamond potential*

INTRODUCTION

Diamond-bearing breccias, as well as structures formed by them, developed in the Cis-Ural and West Ural parts of the Perm Territory, constitute the prototype of Ural fluid-explosive formations. To date, 19 such features (2 deposits and 17 occurrences) have been identified here, with their total resource base being estimated at 5270 thousand carats. The model is based on the most studied deposits and occurrences in the Efimovsky, Rybyakov, Vishera and Yayva areas. In the course of work, we obtained documentation of natural outcrops, mine workings, the core samples of boreholes and quarries for these sites. In addition, to build a complete model, we used material on other features of this region (Malaya Porozhnaya, Yuzhnaya Rassolnaya, Ilya-Vozh, Volynka, etc.), as well as on similar features of some other regions in Russia and abroad [Diamond-bearing..., 2011].

GEOLOGICAL STRUCTURE OF THE VISHERA DIAMOND-BEARING AREA

Tectonically, the ore areas under study are located at the junction of large tectonic structures of the Urals, Timan and the eastern border of the East European Platform. Geologically and structurally, they are confined to the diamond-bearing West-Ural megazone located between the Ural foredeep and the Central Ural megazone. The West Ural structure is composed main-

ly of Paleozoic and, to a lesser extent, Precambrian heavily displaced sedimentary formations, thrust over to the west and, in turn, overlain by large allochthons displaced from the Central Ural megazone. It is characterised by the presence of the Archean-Early Proterozoic crystalline basement of the East European platform, which is established using geophysical data and confirmed by deep-hole prospecting. According to geophysical parameters, the crust of the zone belongs to the intracratonic subtype formed in the Archean – Early Proterozoic [Berlyand, 2007]. The basement is composed of deeply metamorphosed and dislocated sedimentary and igneous rocks of the Archean and Lower Proterozoic. It has a block structure characterised by intense fragmentation by deep-seated faults, including by strike-slip and thrust faults, and occurs at a depth of 4–6 km [Grinson, 1971].

Like other diamond-bearing regions of the Perm Cis-Urals, the Vishera area is confined to the marginal zones of the platform having a rigid shallowly occurring Precambrian basement complicated by actively moving zones [Luk'yanova et al., 1997, 2005; Berlyand, 2007; Petrov et al., 2012]. It is characterised by the gradient zones of the gravitational field – negative gravimetric anomalies, including specific zones in the form of ‘chains’ of negative discontinuous anomalies, as well as anomalies in the endogenous heat flux. In addition to gravimetric anomalies, it exhibits a qualitative geomagnetic feature characteristic of the region – the presence of subvertical inhomogeneities in petro-

magnetic and density sections along with local magnetic anomalies of low intensity (3–20 nT). They are detected using the method of spectral-spatial analysis of geomagnetic lateral fields, and, as shown by studies in the Vishera and Yayva areas [Petrova, Mavrichev, 2004; Diamond-bearing..., 2011], are presumably associated with fluid-explosive diamond-bearing rocks. The movement of fluidogenic material containing xenogenic clasts of various compositions along weakened zones from depth to the surface is also reflected in the petromagnetic section in the form of magnetisation inhomogeneities. Detailed geophysical works (gravity survey, scale 1:10,000; electrical prospecting using vertical electrical sounding) showed that in the gravity field fluid-explosive breccia bodies are characterised by negative anomalies often fixing linear zones. In geoelectric sections, ‘mudded’ (argillizite) breccia varieties yield ρ_k values of 200–600 ohm·m, whereas ‘sandy’, essentially quartz varieties, show values of 900–1500 ohm·m.

The characterisation of diamond-bearing areas should be supplemented by the results of the following studies.

– Identification of mineralogical associations indicative of the diamond potential [Zhukov et al., 1978]. They are characterised by the constant presence of limonite, hematite, kyanite, staurolite, tourmaline, rutile, corundum, pyrope, almandine pyrope, chrome spinels, spinel and native metals in various quantitative proportions. The granulometric feature of these associations consists in their heterogeneity, whereas the morphogenetic feature is the constant presence of rounded grains (spherites) having a smooth shiny and finely-rough (corroded) surface (limonite, hematite and carbonates).

– Detection of geochemical anomalies in such elements as Co, Ni, Cr, Ce, Be, Ba, Ti, Pb, Zn, As, Y and Ag using primary and secondary dispersion halos.

According to the regional geological-and-structural position, the following features are characteristic of diamond-bearing regions.

1. Significant thicknesses of the sedimentary cover overlying the basement (4.0–7.0 km) and of the Earth’s crust (from 35–40 to 45–50 km).

2. Gradient zones of the gravitational field (negative gravimetric anomalies, including specific zones in the form of ‘chains’ of negative discontinuous anomalies), as well as anomalies in the endogenous heat flux.

3. The fragmentation of the basement by the zones of deep-seated faults, which are favourable for the penetration of endogenous fluids into the earth’s crust, as well as the presence of so-called structural ‘traps’ on the path of fluid movement to the surface, especially promising in terms of fluid unloading. They include the intersections of deep-seated faults; the junctions of faults with the sides of large subsidence structures (aulacogens) or rises of Precambrian complexes; zones of thrust fault planes at the contacts with heterochronous (Precambrian and Paleozoic) complexes; an-

ticlinal cores and large forms of relief lowering complicated by crushed zones.

4. The manifestation of epeirogenic movements of various directions and amplitudes at certain stages in the development of the mobile system, contributing to the forward movement and introduction of deep fluids.

5. The widespread development of the following sedimentary deposits in the cover: *sandy* – a favourable environment for the localisation of penetrating fluids with the formation of sheet-like bodies, veins, stockwork zones and other breccia structures; *silty-clay*, which constitute a screen that impedes the movement of fluids to the surface and contributes to their concentration in a closed system.

6. The manifestations of basic-ultrabasic magmatism in the area, which is an indirect sign of possible diamond-bearing breccias, given that there is supposed to be some link with these rocks – an inherited paragenetic connection in the absence of a genetic one.

7. The increased diamond potential of the territory along with the discovery in the area of predominantly curved-faced rounded (Ural or Brazilian type) diamonds with specific geochemical and mineralogical anomalies.

The main and largest tectonic structure of the Vishera diamond-bearing area is the Polyudovo-Kolchik anticlinorium, which in the southwest and northeast is confined by deep-seated steeply dipping faults manifested in geophysical fields and overlain by allochthonous plates of large thrust and oblique-slip faults of various ages (Fig. 1). The anticlinal core is represented by Upper Riphean-Vendian carbonate and terrigenous deposits, with the sides being composed of Paleozoic rocks and with Upper Ordovician quartz sandstones and conglomerates or Upper Silurian carbonate rocks occurring at its base. It should be noted that the whole set of faults creates the key-like structure of the region, formed by a network of subparallel oblique-slip fault structures. At the intersection points of the faults complicated by crushed zones, a network of fractures develops – weakened zones that serve as the pathways for the products of endogenous processes, including the transfer and redeposition of ore material, the introduction of magma with the formation of plagioperidotite-essexite and dolerite hypabyssal formations, as well as diamond-bearing fluid-explosive rocks.

The Polyudovo-Kolchik anticlinorium is divided into two large anticlines separated by a synclinal saddle: Kolchik in the northwest and Tulym-Parma in the southeast. Anticlinal cores are formed by carbonate and terrigenous rather contorted Lower Riphean-Ordovician rocks of the platform cover, which descend to the northeast accompanied by the complications of dip-slip and oblique fault nature. Paleozoic (Silurian – Permian), also terrigenous-carbonate, weakly displaced deposits of the upper structural layer of the cover occur in the sides of anticlines. In the southwest and northeast, the anticlinorium is confined by deep-seated

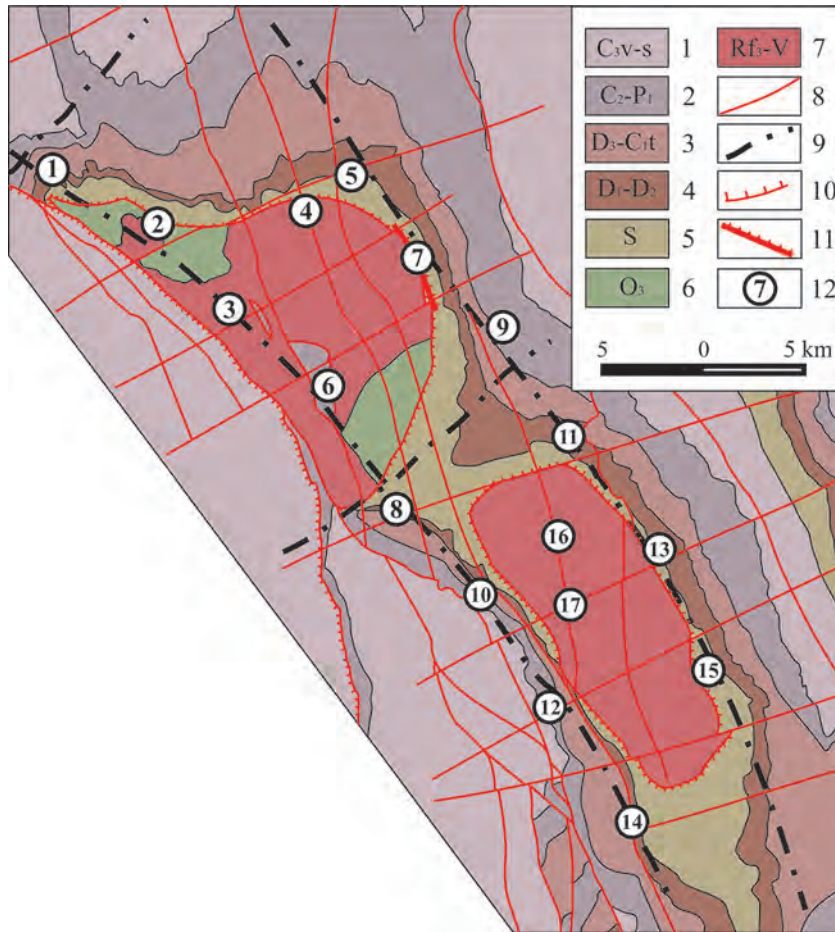


Fig. 1. Geological and structural scheme of the Polyudovo-Kolchim anticlinorium [Diamond-bearing..., 2011].

1–5 – Paleozoic sediments: 1 – Visean-Serpukhovian, 2 – Middle Carboniferous–Lower Permian, 3 – Upper Devonian–Tournaisian, 4 – Lower to Middle Devonian, 5 – Silurian; 6–7 – Riphean–Lower Paleozoic sediments: 6 – Ordovician, 7 – Riphean-Vendian; 8 – tectonic faults; 9 – regional deep faults hidden under overlying sediments; 10 – boundaries of structural tectonic levels; 11 – fragment of the Kolchim thrust; 12 – ore clusters: 1 – Storozhevsky, 2 – Klyuchevskoy, 3 – Dresvyanaya Steppe, 4 – Churochinsky, 5 – Zhalinsky, 6 – Burkochimsky, 7 – Efimovsky, 8 – Svetlinsky, 9 – Volynka, 10 – Ilya-Vozh, 11 – Vodorazdelny, 12 – Poludeno-Kolchim, 13 – Kocheshor, 14 – North Kolchim, 15 – Verkhny-Tulym, 16 – Bystrinsk, 17 – Lower Kocheshor.

faults. They were manifested in physical fields; however, in most cases, they were overlain by Paleozoic deposits, including by thrusts. It is along these deep-seated faults that the manifestations of diamond-bearing fluid-explosive breccia formations are located (or projected onto them). Only a few of them gravitate towards lower-order en echelon faults.

Fluid-explosive formations of the Efimovsky deposit, which is the most studied one, are confined to the northeastern part of the Kolchim anticline. Here, Vendian terrigenous deposits occur under gently dipping Silurian-Carboniferous terrigenous-carbonate deposits with the complications of strike-slip nature (Fig. 2). The boundary between them is tectonic – along the area of the Kolchim thrust of the northwest strike with a moderate northeast dip (17°) of the fault plane, which was established by drilling activities. In addition, to the northeast of the Kolchim thrust the deposit gravitates

to the section of the hidden Ishkov fault having a steep east dip ($75\text{--}80^\circ$) of the fault plane and a vertical amplitude of movement (40–60 m).

GEOLOGIC ASPECTS OF STRUCTURES AND COMPOSITION FLUID-EXPLOSIVE BRECCIA (FEB) FORMATIONS

The position of fluidogenic breccias in the given scheme indicates that the fluid explosions occurred along the zones of these major tectonic displacements, including along the interformational thrusts. Using all possible ways to head to the surface and penetrate into the host rocks, as a result of explosions fluids formed dyke-, sill-, cone-, vein- and sometimes stockwork-like breccia bodies. The most numerous dyke-like bodies are confined to steeply dipping faults of predominantly the northeast strike (see Fig. 2) at a thickness of

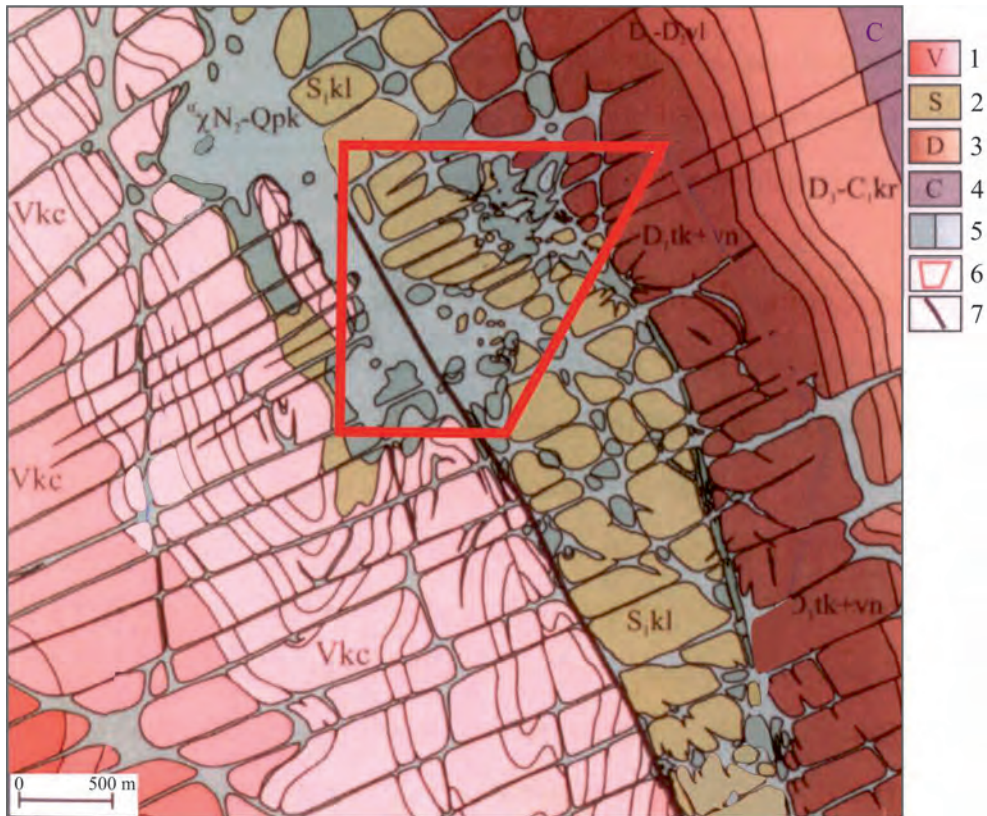


Fig. 2. Geological scheme of the Efimovsky deposit (by I.P. Teterin et al., unpublished report ‘Permgeologodobycha’, 2009).

1 – Vendian system (V kc – Kocheshor Formation, lower and upper strata); 2 – Silurian system (S kl – Kolchim Fm); 3 – Devonian system (D₁tk + vn – Takatin and Vanyashin Fm, D₁-D₂ vl – Volynka stratum, D₃-C₁ kr – siliceous stratum); 4 – Carboniferous system (C – West-Uralian Fm); 5 – fluid-explosive breccias (dark grey – the Polyudovo-Kolchim complex, light grey – the Efimovsky complex); 6 – contours of the Efimovsky deposit; 7 – fragment of the Kolchim thrust.

100–500 m. However, the Efimovsky deposit is formed mainly by two subtabular and sill-like bodies, injecting fault planes of the northwest strike, with a thickness of up to 70 m and a length of up to 7 km. They are predominantly associated with the Kolchim thrust; divided by the stratum of Lower Silurian dolomites; and transected by the dyke-like breccia bodies. The size of breccia bodies, which rarely have a cone-shaped form, varies from fractions of a meter to 400 m and more, and they usually form dyke-, sill- and vein-like apophyses into the basement rocks, creating a complex stockwork form.

The contacts of breccia bodies are usually indistinct, given that central parts of the bodies having a low number of clasts are enriched by them to their periphery and finally replaced by authigenic breccias. In addition, all the variety of fluidogenic breccia bodies are characterised by uneven contours of body walls and tree-like junctions, apophyses and veins, whose thickness, gradually decreasing, often reaches 1–2 mm at a length of tens of centimetres (Fig. 3).

The size of breccia bodies also varies; however the vast majority of them average tens of meters across

reaching up to 2 km in length; they can usually be observed up to 200–300 m, rarely up to 500–600 m. The FEB bodies (all the diversity of which in the Urals and in some other regions is often called tuffisites) are very specific, having a spotted-mottled-yellowish-, greenish-or greyish-brown colouring. Macroscopically, they have the appearance of clay, sandy-clay, sandy, conglomerate-like rocks with unevenly dispersed fragments and sometimes implicitly manifested stratification and fluidisation. They contain a different number of fragments (from 20 to 60–70%), varying in size (from fractions of a millimetre to several metres), composition (usually polymictic) and form.

The nature of clasts undoubtedly constitutes an important indicator of diamond-bearing breccias. As in all breccias, angular clasts are constantly present and sometimes predominate. Due to explosive processes, as a rule, they are to some degree exposed to fragmentation and disintegration. However, the specificity of fluidogenic breccia, in particular, the rocks of the Efimovsky deposit, is that, along with angular clasts, almost constantly there are rounded clasts in them, sometimes with a shell-like cleavage. These clasts got their



Fig. 3. Different forms of fluid-explosive breccias [Diamond-bearing..., 2011].

shape after being in a mobile solid-gas stream, where they underwent abrasive, tumbling processing, rather than as a result of rolling, like in the case of sedimentary rocks. In addition, fluid-explosive breccia contains disintegrated 'shadowy' clasts, as well as the clasts of mineral grains with microexplosive fragmentation, reflecting a sharp drop of pressure with decompression, which constitutes their reliable identification feature. There are also shock-induced transformations of the fragments in the breccias under consideration manifested predominantly in the grains of the fragmented quartz of planar deformation features, sometimes shock-induced twinning, radial jointing, changes in refraction values, etc. Lithoclasts (terrigenous and carbonate rocks) and their mineral components (mostly quartz, rarer feldspar and dolomite) dominate the composition of clasts. There are also constant clasts of metamorphic rocks of the basement, alien to the host rocks, and of the cover engulfed and carried by the fluid flow. The borders of clasts with the binder mass differ in character – they can be both clear and indistinct, corrosion or reaction ones. The marginal zones of clasts are heavily fractured, filled with a cementing mass or gas-liquid inclusions, as they constitute the areas of their most syngenetic transformations. In some cases, the clasts in whole may be replaced by a fluidogenic mineral association or recrystallised.

The appearance of FEBs having a variety of fragments is complemented by the constant presence (in different ratios) of mineral grains of different origin. Some of them are minerals – for example, quartz – formed during the regeneration or granulation of clastic grains, while others are newly formed. The latter (quartz, carbonates, biotite, muscovite, hematite, goethite, etc.) crystallize mainly at the final stage in breccia formation and are not deformed if they have not been exposed to repeated explosions; they are often idiomorphic and do not contain gas-liquid inclusions. In addition, fluid flows are characterised by the discharge

of the ore components of the fluid into the forming breccias (extraction during decompression), which leads to mineralisation, as well as diamond content [Endogenic..., 2018].

A characteristic feature of diamond-bearing breccias is the presence in them of protomagmatic minerals and magmatic mineral inclusions (xenoliths?) – outliers from the fluid-generating medium. These minerals and inclusions are rare, in many cases replaced by a mineral association similar to breccia cement, in which case they are identified by the morphology of grains and inclusions or detected in the heavy rock fraction. In general, phlogopite, olivine (serpentine), pyroxenes, pseudoleucite, leucosene, pyrope (sometimes having a kelyphite rim), picroilmenite, chrome spinel and other minerals are found in diamond-bearing breccias, which suggests a deep-seated, possibly mantle, origin of the fluid. In thin sections, these minerals are rare, they are mainly observed in areas with porphyritic textures, within which breccias, in accordance with the classification, look like magmatogenic-fluidogenic ones.

Protomagmatic mineral grains are replaced to varying degrees by potassium feldspar, hydromica, quartz, carbonate, pyrite or an illite-smectite aggregate, often being predominant in the binder mass of the rock. In addition, in recent years, lenticular-striated inclusions of the magmatic lamproite component are found in them, which are close to orendites and madupites in composition [Luk'yanova, Sharpenok, 2004]. A microprobe study of the binder mass of these breccias carried out in thin sections, as well as using X-ray phase analysis, helped to detect microlites of sanidine (10–300 μm), whose amount sometimes reaches 5% of the mass and composition corresponds to the composition of lamproitic sanidine [Luk'yanova et al., 2005].

The diamond mineral association in Ural FEBs includes diamond, pyrope, chrome spinel, picroilmenite, chromium-bearing diopside, moissanite, native Pt, Hg, Fu, Bi, oxide (Mn-Fe-Ti) and silicate spherules and

slags, kimberlite zircon, florencite and senaite [Chaikovskii, 2004]. The diamonds of this association have specific features uniting them with diamonds from Brazil, South-West Africa and Northeast Yakutia. Among them, curved-faced colourless (less often very light golden, pink or greenish-blue) dodecahedrons having a smooth relief, strong lustre and high transparency predominate; with about 80% of them being gemstones.

In general, the characterised diamond-bearing breccias, as a rule, have a heterogeneous breccia-taxite appearance in the absence, in most cases, of clastic material sorting. At the same time, along with mottled ataxite, mottled banded, banded (pseudo-layered) and fluid textures, which are close to eutaxitic texture, are noted in them. In some cases, they are due to sorting, kinetic redistribution of the material, rather than sedimentation; in other cases, however, matter suspended in the fluid is differentiated according to its size and concentrated during the laminar flow of a solid-gas flow or disintegrated clasts are pulled in the direction of the fluid flow with the formation of elongated layers, gradually merging with cement. Finally, both ataxitic and eutaxitic textures may be due to the coexistence of inclusions or streams of immiscible phases in the fluid. The decrystallisation of these phases during explosive phenomena leads to a mottled or oriented, flow-like arrangement of fluid components. Thus, it is the emulsion nature of the fluid that determines the mottled, lenticular-banded or fluid textures of FEBs, including ignimbrite- or even lava-like ones.

Indistinct borders and transitions are often noted between all structural varieties. So, in the case of a sequential increase in the binder mass of quartz-micaceous, illite-smectite striae, tuff-like breccias gradually acquire an ignimbrite shape. Resorption and reaction relationships of the binder mass with mineral grains (signs of the multi-stage manifestations of the fluid phase), as well as granulation and recrystallisation of minerals, most often quartz, are also characteristic. The high porosity and gas saturation of rocks, as well as clusters and minerals contained in them, also constitutes a very important and almost constant indicator of these breccias.

Like the rocks in general, the binder mass of fluidogenic breccias is also heterogeneous, consisting of fluidogenic cement, which contains this or that amount of a finely fragmented fraction. As a rule, it comprises a wide variety of structures. Tuff-like structure (sometimes called sandy, tuffsite, ashy) is the most common, with streaky-fluid, fluid, ignimbrite, lava-like structures, etc. being observed less frequently.

For fluidogenic breccias, it is natural that within bodies and even within the same thin section, various structural and compositional varieties (generations) of breccias are combined, between which – along with gradual, indistinct transitions – injection relationships are often established. This indicates their polyimpulse formation, whereas the relationships between the gen-

erations reflect close in time, but, most likely, successive pulses of the fluid-explosive process. Explosive manifestations can also be replaced by pneumatolitic, pneumatolite-metasomatic and hydrothermal-metasomatic, including dolomitisation.

Geological mapping and a large amount of mining work carried out in separate areas of diamond-bearing breccia formations revealed that their internal structure is heterogeneous. Thus, if we exclude from consideration authigenic breccias (sandstones, carbonate rocks, etc.), then at least three main generations of rocks (with internal facies and sometimes phase varieties), differing in their material composition, texture and structural features and, finally, diamond potential, exist as part of separate bodies (for example, the northern section of the Efimovsky deposit; Fig. 4).

In the early phase of the fluid-explosive process, polymodal (small-coarse clastic) tuff-like FEBs rich in clasts were formed. The different-sized fragments of Devonian sandstones and Silurian dolomites are immersed in a binder mass consisting of fragments of small and finely clastic fraction cemented by a fibrogranular quartz-micaceous cement. These breccias are associated with a low and very inhomogeneous diamond content.

The binder mass of these breccias can have two generations. The first is characterised by the filling of spaces between quartz crystalloclasts by mica-clay aggregate. The binder mass of the second generation includes both fragments of individual crystals and breccias with the cement of the first generation (Fig. 5). It is also characterised by a mica-clay composition with a high content of fine-grained sericite and a significant amount of ore mineral (iron oxides and hydroxides).

It should be noted that quartz crystalloclasts joined by a binder mass of the first generation have mainly angular facets. A distinctive feature of similar grains – already concentrated in the second-generation binder mass – is the predominance of rounded shapes in faceting (Fig. 6).

The grain borders of quartz are strongly corroded; reaction relationships with the cement are often observed (Fig. 7). Relatively large clasts of quartz are broken by a system of differently oriented fractures, often including gas-liquid chains. Both large and relatively smaller quartz crystalloclasts in most cases are characterised by undulose or block extinction.

The second phase of the explosive process (see Fig. 7) resulted in the formation of breccias moderately and inhomogeneously rich in the clastic basement rocks of breccia and finer dimension, as well as mineral grains cemented by smectite-hydromica fluidogenic mineral association.

Rock clasts are characterised by different morphology. Lithoclastic formations characterised by rounded and sometimes indistinct or transitional borders with respect to the binder mass are widespread. The formation of such borders in lithoclasts is caused by the pene-

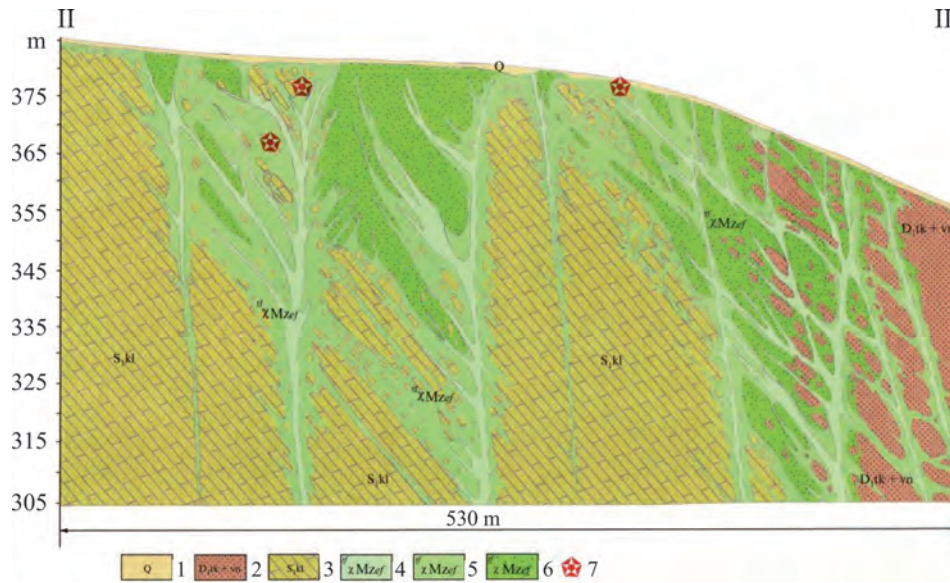


Fig. 4. Geological cross section of the northern area of the Efimovsky deposit [Diamond-bearing..., 2011].

1 – Quaternary deposits (clays, crushed stone and blocks of bedrock); 2 – Takatin and Vanyashin Devonian formations (sandstones); 3 – Silurian Kolchim suite (dolomites); 4–6 – Efimovsky complex: 4 – argillizite fluid-explosive breccias of the third phase, 5 – fluid-explosive breccias of the second phase, 6 – fluid-explosive breccias of the first phase; 7 – diamond finds.

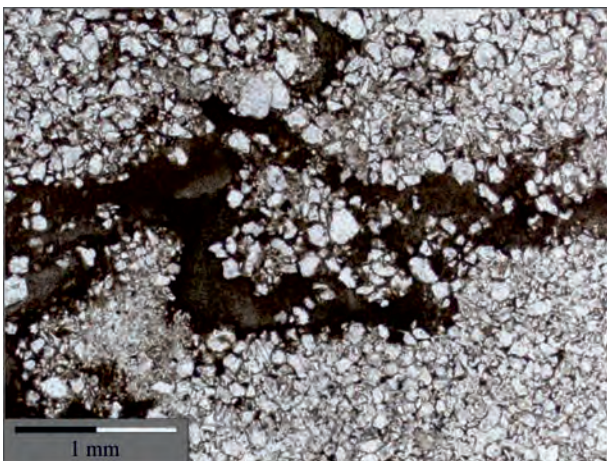


Fig. 5. Clasts of aposandstone breccia, cemented by first-generation binder mass and enclosed in second-generation cement.

tration of cement minerals through the various types of fractures: both those formed during brecciation processes and along the primary fractures of bedding, with the replacement of brecciated sedimentary rocks. The predominant aggregates developing from rock clasts include quartz-sericite-clay (in the case of substitution of quartz sandstones, less often argillites) and clay-ore ones (in the case of the substitution of clasts, presumably, of the main effusive rocks), in which iron oxides and hydroxides predominate (Fig. 8).

Breccias are characterised by a fairly significant distribution of crystalloclasts enclosed in a cementitious

mass. Quartz grains are most often found among the crystal clasts. In most cases, they have rounded, largely corroded borders. A lot of, especially large, grains of the mineral are broken by a differently oriented system of fractures, along which the development of gas-liquid inclusions is observed. Almost all quartz crystalloclasts are characterised by block extinction and a lot of them have planar features (Fig. 9).

Breccias of this generation are characterised by the maximum diamond content for the Efimovsky deposit; however, like for the early breccias, it is inhomogeneous. The shape of productive bodies is diverse. They include simple and complex lenses, pockets, steeply dipping columns consisting of pocket-like and lenticular inclusions, veins and irregularly shaped injections. As a result of studying some of the bodies in detail, up to 5–7 varieties of breccias having both phase and facies relationships have been identified. It is not possible to reliably assess the diamond potential of each of them; however, the maximum diamond contents gravitate toward the lower parts of the sill.

The final stage in the formation of the sill-like breccia body of the Efimovsky deposit is fixed by the formation of very dense argillizites with a small amount of xenogenic material. The diamond content of these rocks is extremely low.

Lithoclasts immersed in a quartz-mica-clay cementitious mass make up no more than 30–35% of the total breccia. Among the rock clasts, argillites and siltstones predominate, with quartz sandstones being relatively rare. Elongated lithoclasts with rounded smooth, often indistinct borders are very widespread (Fig. 10). The smoothest transitions are observed between the bind-

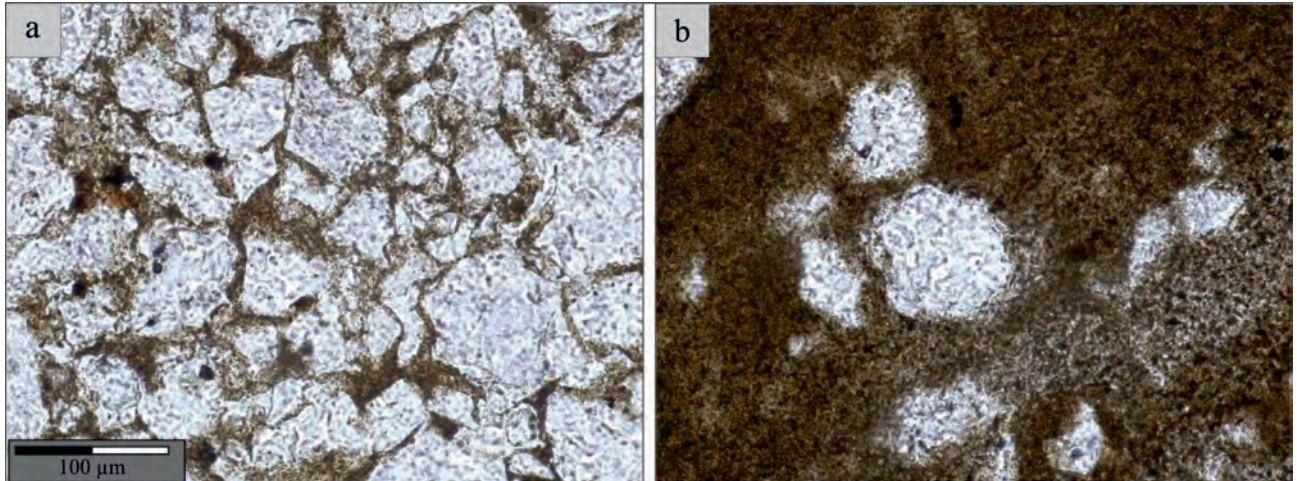


Fig. 6. Grains of quartz characterised by different morphology, enclosed in the cementing mass of the first (a) and second (b) generations.

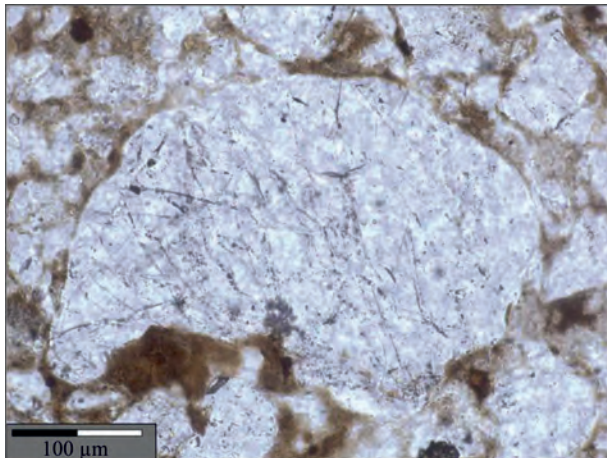


Fig. 7. Quartz grain having rounded corroded borders, broken by a system of differently oriented fractures with gas-liquid inclusions.

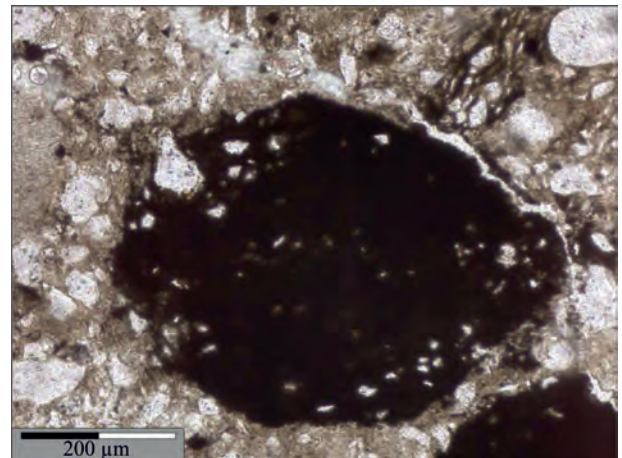


Fig. 8. Crystalloclast (olivine) replaced by an aggregate of ore minerals.

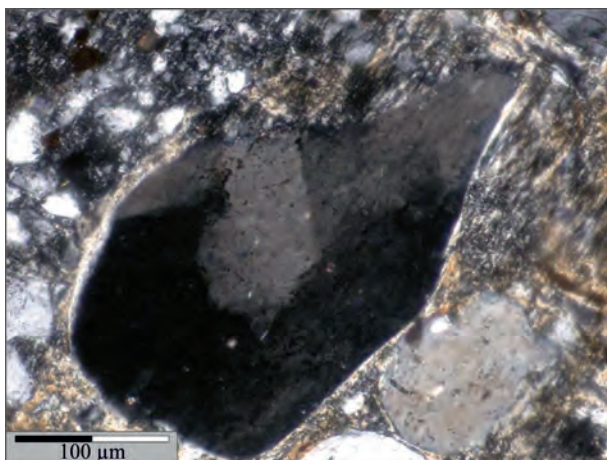


Fig. 9. Quartz grain characterised by distinctive block extinction.

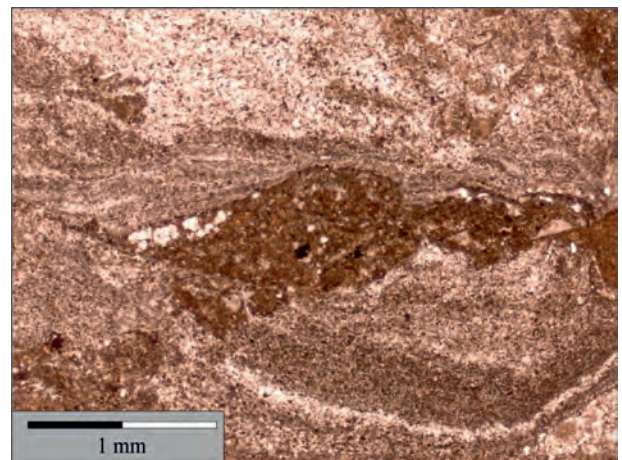


Fig. 10. A clast of rock in the binder mass.

er mass and clasts of argillites, which, apparently, are largely replaced by cement minerals during fluidisation processes.

Crystalloclasts are rarely present in these breccias. Among them, different-sized clasts of quartz grains predominate, which in most cases have rounded corroded borders. Quite often, the chains of quartz grains oriented along the flow structures are observed. Individual quartz grains are often broken by variously oriented fractures along which chains of gas-liquid inclusions develop, and have a pronounced block extinction.

Cementing mass constitutes a fine-grained quartz-sericite-clay aggregate exhibiting quite significant variations in the mineral composition and well-marked traces of the flow. The binder mass minerals include both newly formed minerals (sericite, newly formed quartz and partly clay minerals) and finely crushed grain fragments formed during brecciation. Relatively rarely, the general fine-grained background of cement reveals individual rather large, in many cases strongly curved, newly formed grains of biotite and muscovite. Finely-dispersed aggregates of ore minerals characterised by a predominance of iron oxides and hydroxides have a significant and very uneven development in the binder mass.

In the breccias of predominantly the first and second phases of brecciation, protomagmatic minerals sometimes occur along with newly formed minerals and clastic material in the binder mass in thin sections. Of these, the most common is zircon. In most cases, these are fragments of individual grains, less commonly, individual minerals having prismatic or long-prismatic idiomorphic faceting. According to [Zhukov et al., 1978; Diamond-bearing..., 2011], a fairly wide spectrum of protomagmatic minerals is distinguished in crushed and stream-sediment samples for fluid-explosive formations of the Efimovsky deposit; however, in thin sections these minerals are extremely rare and are significantly susceptible to secondary changes, which greatly complicates their identification.

FEBs have some specific chemical characteristics. Given that these rocks constitute an additive result of the interaction and coexistence of components of various origins, the chemistry of diamond-bearing FEBs can be considered only in a comparative aspect. The studies on the chemical characteristics of these rocks in the Vishera area of the Urals [Landa, Luk'yanova, 2003; Diamond-bearing..., 2011] revealed their dual nature. Being similar to the upper crustal formations in a number of parameters, which is primarily due to the presence of absorbed substance of the host rocks in them, they at the same time possess certain characteristics that reflect their deep-seated origin and similarity with rocks classified, for example, in Central Italy as madupite lamproites. They are similar in terms of their elevated contents of titanium, phosphorus, magnesium, potassium, trace and rare-earth elements, as well as the specific distribution of petrogenic elements, REEs and

refractory lithophiles. The level of ratios of indicative elements (Rb/Sr, U/Th, etc.), as well as the nature of the variability in the contents of elements are shown on a number of charts [Diamond-bearing..., 2011].

In general, FEBs under consideration exhibit a potassium specificity. Their potassium content correlates with the content of titanium, phosphorus, chromium, manganese, iron, sometimes barium, strontium and vanadium. In addition, the rocks are usually abnormally enriched with silicon and ore minerals, which, according to F.A. Letnikov [1992], is the effect of exceptionally high extraction of silica and ore minerals from fluid. Thus, the petrogeochemical features of the breccia rocks in question allow us to consider the composition and depth of the primary fluid source, generating breccia, which is rather relative than definite and depends on the composition of the components of magmatic origin present in them, including protomagmatic minerals (phlogopite, pseudo-leucite, sanidine, olivine, pyroxenes, alkaline amphiboles, chrome spinels, etc.).

CONDITIONS FOR THE FORMATION OF FLUID EXPLOSIVE BRECCIAS

Briefly given diverse compositional characteristics of the diamond-bearing FEBs of the West Urals, as well as the injective nature of the bodies formed by them (in a closed system), allowed their researchers to validate both their endogenous origin and the deep-seated (mantle?) origin of the fluid flow. This flow was formed as a result of fluid explosions, similar in composition to their magmatic (rock and mineral) components – lamproites [Luk'yanova, Sharpenok, 2004].

Clearly, the formation of a diamond-bearing fluid thermodynamic system [Zhukov, 2000] occurred under unstable *PT*-conditions. These conditions existed both during its genesis at the deep-seated (mantle?) level and during its subsequent evolution and formation at the crustal and surface levels. The instability of *P-T* conditions in the thermodynamic system generating these breccias at the mantle level caused, first of all, the discreteness of the crystallisation medium of barophilic minerals, in particular diamonds. In accordance with this, the processes of their predominant growth in the melt alternated with the predominance of dissolution. This led to the formation of crystals with a zoned distribution of table-cut and curved-faced shapes [Shfranovskii, 2001]. The curved habit of a diamond is a more stable form when dissolution processes dominate in the crystallisation medium. It is this fact that predetermined the sharp predominance of relatively large curved-faced diamonds (Ural or Brazilian type) with a small content of table-cut crystals in fluidogenic diamond-bearing breccias. Thus, the discovery of curved-faced diamonds in the area under study constitutes a direct qualitative criterion for the identification of diamond-bearing fluidogenic breccias.

Further development of the fluid thermodynamic system was associated with the pulsed movement of the fluid under periodically repeated stretching conditions at the subcrustal and crustal levels. Under these conditions, a specific flow, which constituted a solid-liquid-gas phase, moved towards the earth's surface along deep-seated faults accompanied by a complex system of oblique-slip faults in active mobile zones. This forward movement, with the processes of stretching and compression alternating, also had a pulsating character, which led to the existence of a multitude, often the thinnest (hairy-like) apophyses into the host rocks with them being crushed (Fig. 11).

The liquid-gas phases of the fluid were transformed by the way of extraction and pneumatolysis during explosions predominantly into mineral masses, as well as into newly formed grains of minerals. Mineral masses cement primary protomagmatic mineral formations,

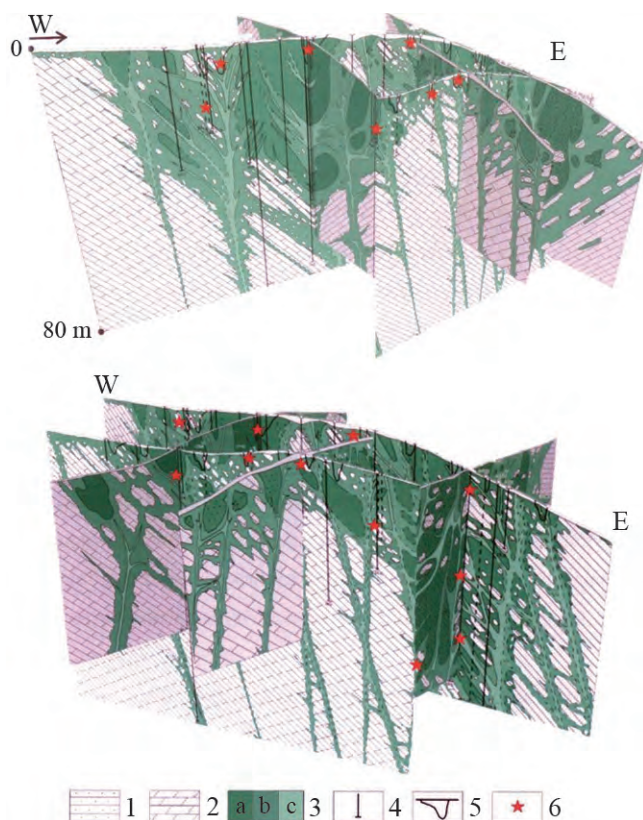


Fig. 11. Three-dimensional model of the northern part of the Efimovsky deposit [Korotchenkova, 2012] built drawing on the materials of [Petukhov, Teterin, 2007].

1 – sandstones of the Takatin suite; 2 – dolomites of the Kolchim suite; 3 – fluid-explosive breccias: a – the first phase, b – the second phase, c – the third phase; 4 – boreholes, 5 – excavation ditches, 6 – diamond finds.

including pseudomorphs after them, various xenoliths and mineral grains trapped during explosions, resulting in the formation of FEBs. Recurring pulses of these phenomena lead to the formation of complex diamond-bearing structures.

The above-listed features of a typical ore-bearing diamondiferous breccia structure allow us to validate a working geological and petrological model, whose main components are presented in Table 1.

CONCLUSIONS

The model for the formation of a fluid-explosive diamond-bearing structure includes the following main elements:

- the position of the diamond-bearing structure in the marginal zone of the ancient platform and its location at the junction of two large structures (Timan and Urals) explains the significant development of heat and mass transfer of matter, as well as of the general high-energy state of the system, resulting in melt-fluid formations at the upper mantle or lower crustal levels;

- the fragmentation of the basement by deep-seated faults, including strike-slip and thrust faults, the development of numerous discontinuous faults in the rocks of the platform cover; they cause a significant flow of deep-seated solid-gas-liquid fluids to the surface, where, due to the existence of structural traps, fluid mixes with low-temperature meteorite waters and interacts with overlying rocks, thus causing explosive processes that lead to the formation of fluid-explosive structures;

- compression and decompression phenomena, leading to the crushing of the clasts of host rocks, the solid components of the fluid flow, the mineral grains of various origin and the breccias of the previous phases with the formation of fluidogenic breccia rocks characterised by specific mineral formation (explosion-extraction-pneumatolysis);

- the polyphase (polyimpulse) development of the breccia complex, the interaction of fluid with the basement rocks, meteorite waters and the substance of highly mineralised brines led to the formation of three types of fluid-explosive breccias having different diamond potential: early – medium-large crystal-lithoclastic breccias having a small amount of cement (apostone breccias); mature – small-medium lithocrystalloclastic polyfacies breccias ('sandy-clay') with a significant amount of binder mass consisting of micaceous-quartz-clay cement and clasts of rocks and minerals of a fine fraction; late – small, finely clastic, predominantly crystalloclastic argillizite breccias; fluid-explosive breccias of the second type are the richest in diamonds, whereas the first type of breccias reveal little diamond potential and diamonds are practically absent in breccias belonging to the third type.

Table 1. Main characteristics of diamond-bearing fluid-explosive breccia formation

Diamond-bearing breccia formations	Characteristics – criteria				Examples of deposits and occurrences	
	Geological and structural		Geophysical			
	Regional	Local	Petrographic	Mineralogical		
FEBs of hidden fluid explosions, spatially separated from the source of fluids	1. Confinement to the marginal parts of ancient platforms complicated by mobile zones 2. Fragmentation of the basement by deep-seated faults, including oblique-slip faults 3. Widespread development of sandy, clay and carbonate deposits in the cover 4. Occurrences of basic and ultrabasic magmatism 5. Increased diamond potential of the territory	1. Widespread development of faults, excessive fracturing 2. Discordant rocks, intervals in sedimentation 3. Presence of erosion depressions 4. Placers of curved-faced diamonds 5. Discovery of fluid-explosive breccia formations	I. Regional homogeneities 1. The gradient zones of gravimetric anomalies, as well as the 'chains' of negative discontinuous anomalies 2. Anomalies in the endogenous heat flux Subvertical inhomogeneities in petromagnetic and density sections along with local magnetic anomalies of low intensity (3–20 nT) II. Local heterogeneities In the gravity field, fluid-explosive breccia bodies are characterised by negative anomalies. In geoelectric sections, argillizite breccia varieties yield ρ_k values of 200–600 ohm·m, whereas essentially quartz varieties show values of 900–1500 ohm·m	Highly heterogeneous appearance of rocks: tuff-like and argillizite breccias (often conglomerate-like, sandy) Ataxitic breccia, structures with micaceous-quartz-clay, argillizite and tuff-like cement A variety of xenoclats, including deep-seated ones exhibiting signs of explosive crushing The combination of mineral grains of various origin: xenogenic and newly formed (quartz, mica and carbonates)	I. Abnormally high levels of correlatable Ni, Mn, Zn, Pb, Cd, Ag, Y and Yb. Of the listed elements, the combination of Ni, Mn, Zn and Pb is the optimal indicator of diamond potential 2. Potassium petrochemical specificity. The correlation of K_2O content with Ti, P, Cr, Mn and Fe	Efimovsky, Malaya Porozhnaya, Rybikov, Ilyavozh, Volynka (Perm Territory); Luzhsky District, Leninograd Region; Minas Gerais, Brazil
Diamond-bearing fluid-explosive breccias (Ural type)			Indicative mineralogical association: limonite, hematite, kyanite, staurolite, tourmaline, rutile, corundum, pyrope-almandine, spinels and native metals The constant presence of spherulites (limonite, hematite and carbonates), pyrite, barite, manganese, occasional diopside and hornblende There are also pyrope, diamonds, picroilmenites chrome-diopside, chrome spinels	Specific non-metallic, diamond: decahedrons, their clasts, crystals having a transitional habit; cluster crystal		

REFERENCES

- Almazonosnye flyuidno-eksplozivnye obrazovaniya Perm'skogo Priural'ya* (2011) [Diamond-bearing fluid-explosive formations of the Permian Cis-Urals]. (Eds O.V. Petrov, N.V. Mezhelovsky, L.I. Luk'yanova). Moscow; St.Petersburg, GEOKART, GEOS, VSEGEI Publ., 240 p. (In Russian)
- Berlyand N.G. (2007) *Glubinnoe stroenie litosfery Urala* [Deep structure of the Ural Lithosphere]. St.Petersburg, VSEGEI Publ., 255 p. (In Russian)
- Chaikovskii I.I. (2004) *Petrologiya i mineralogiya eksplozivno-gryazevogo vulkanizma Volgo-Ural'skoi almazonosnoi subprovintsii*. Dis. ... dokt. geol.-min. nauk [Petrology and Mineralogy of Explosive-mud Volcanism in the Volga-Ural Diamond-bearing Subprovince. Dr. geol and min. sci. diss.]. Syktyvkar, 48 p.
- Endogennye rudonosnye brekchiyevye obrazovaniya. Metodicheskie rekomendatsii po vyyavleniyu endogennykh brekchiyevykh obrazovaniy razlichnykh geneticheskikh tipov i otsenke ikh potentsial'noi rudonosnosti primenitel'no k zadacham Gosgeol'kart* (2018) [Endogenic ore-bearing breccias. Methodological recommendations on the identification of endogenic breccias of different genetic types and their potential ore-bearing evaluating in relation to the tasks of State Geological Mapping]. (Eds L.N. Sharpenok). St.Petersburg, VSEGEI Press, 104 p. (In Russian)
- Grinson A.S. (1971) *Glubinnoe stroenie oblasti sochleneniya struktur Russkoi platformy, Timana i Urala po geologo-geofizicheskim dannym (v svyazi s poiskami skrytykh proyavlenii osnovnogo-ul'traosnovnogo magmatizma)*. Dis. ... kand. geol.-min. nauk [Deep structure of the joint area of the Russian platform, Timanian and Uralian structures from geological and geophysical data (in terms of search for concealed mafic-ultramafic magmatism occurrences). Cand. geol. and min. sci. diss.]. Leningrad, 20 p. (In Russian)
- Korotchenkova O.V. (2012) *Efimovskoe mestorozhdenie almazov: geologiya, tipomorfnye mineraly i lokal'nyi kontrol' almazonosnosti*. Dis. ... kand. geol.-min. nauk [Efimovskoye diamond deposit: geology, typomorphic minerals and local diamond potential control. Cand. geol. and min. sci. diss.]. Syktyvkar, 18 p. (In Russian)
- Landa E.A., Luk'yanova L.I. (2003) On geochemical features of tuffizite in the Krasnovishersky District (Northern Urals). *Geokhimiya*, (2), 162-171. (In Russian)
- Letnikov F.A. (1992) *Sinergetika geologicheskikh system* [Synergetics of Geological Systems]. Novosibirsk, Nauka Publ., 230 p. (In Russian)
- Luk'yanova L.I., Landa E.A., Shafranovskii G.I. (2005) Diamond-bearing rocks of the Urals and the Siberian Platform joint zone. *Region. Geol. Metallogeny*, **26**, 103-114. (In Russian)
- Luk'yanova L.I., Lobkova L.P., Mareichev A.M., Kazak A.P., Zhukov V.V. (1997) Bedrock diamond sources in the Urals. *Region. Geol. Metallogeny*, (7), 88-97. (In Russian)
- Luk'yanova L.I., Sharpenok L.N. (2004) Lamproite diamond-bearing fluidites of the Urals. *Geologiya i mineral'nye resursy Evropeiskogo Severo-Vostoka Rossii*. Mater. XIV geol. s"ezda Respubliki Komi. T. IV [Geology and mineral resources of European North-Eastern of Russia. Proc. XIV Geol. Conference Komi Republic. V. IV]. Syktyvkar, 50-52. (In Russian)
- Luk'yanova L.I., Zhukov V.V., Kirillov V.A., Kuznetsov G.P., Kuznetsov N.S., Landa E.A., Lobkova L.P., Morozov G.G., Ostroumov V.R., Rybal'chenko A.Ya., Teterin I.P., Shadenkov E.M. (2000) Subvolcanic explosive rocks of the Urals as possible bedrock sources of diamond placers. *Region. Geol. Metallogeny*, (12), 134-157. (In Russian)
- Petrov O.V., Luk'yanova L.I., Proskurnin V.F. (2012) The problem of searching for primary diamond sources in junction zones of platforms and fold areas. *Region. Geol. Metallogeny*, **50**, 64-72. (In Russian)
- Petrova A.A., Mavrichev V.G. (2004) Geomagnetic method for forecasting primary diamond deposits: Case study of the Krasnovishersky District. *Effektivnost' prognozirovaniya i poiskov mestorozhdenii almazov: Proshloe, nastoyashchee i budushchee (Almazy-50)*. Mat-ly nauch.-praktich. konf. [Efficiency of diamond deposits forecasting and exploration: past, present and future (Diamonds-50). Scientific and Practical Conference Proceedings]. St.Petersburg, VSEGEI Publ., 261-263. (In Russian)
- Petukhov S.N., Teterin I.P. (2007) *Otchet o geologicheskom izuchenii (poiski i otsenka) rossypanykh i korennykh mestorozhdenii almazov na "Rassol'ninsko-Dresvyanskom" uchastke neдр v Krasnovisherskom raione Permskoi oblasti* [Report on the geological study (exploration and evaluation) of placer and primary deposits of diamonds "Rassolninsko-Dresvyanskom" subsoil in Krasnovishersk district of the Perm region]. Perm, Fond ZAO "Permgeologodobycha".
- Shafranovskii G.I. (2001) New data on the morphology of diamonds from the Krasnovishersky District. *Mat-ly Vseros. soveshch.* [Proc. All-Russian Conf.]. Syktyvkar, 148-149. (In Russian)
- Zhukov V.V. (2000) Classification of diamond deposits from morphogenetic features of crystals. *Geologicheskaya sluzhba i mineral'no-syr'evaya baza Rossii*. Tez. dokl. Vseros. s"ezda geologov i nauch.-praktich. konf. Kn. 2 [Geological Survey and the Mineral Base of Russia. Abstracts All-Russian Congress of Geologists and Scientific and Practical Conference. B. 2]. St.Petersburg, VSEGEI Publ., 253-254. (In Russian)
- Zhukov V.V., Litinskaya I.A., Markova I.B. (1978) Mineralogical associations of terrigenous formations in the North-East of Siberian platform. *Geologiya pribrezhnykh zon morya* [Geology of the coastal zones of the sea]. Leningrad, NIIGA Publ., 70-87. (In Russian)

U-Pb DATING OF NIOBIUM MINERALS FROM THE PYROCHLORE GROUP (ILMENY-VISHNEVOGORSKY CARBONATITE-MIASKITE COMPLEX, SOUTH URALS)

Irina L. Nedosekova¹, Viktor A. Koroteev¹, Boris V. Belyatsky², Viktor V. Sharygin^{3,4},
Elena N. Lepechina², Sergej V. Pribavkin¹

¹Zavaritsky Institute of Geology and Geochemistry, UB RAS, 15 Akad. Vonsovsky St., Ekaterinburg, 620016
Russia, e-mail: vladi49@yandex.ru

²A.P. Karpinsky Russian Geological Research Institute (VSEGEI), 74 Sredny ave., St.Petersburg, 199106 Russia

³V.S. Sobolev Institute of Geology and Mineralogy SB RAS, 3 Akad. Koptuga ave., Novosibirsk, 630090 Russia
⁴Novosibirsk State University, 2 Pirogova St., Novosibirsk, 630090 Russia

Received 26.12.2018, accepted 15.03.2018

The article covers the U-Pb dating of minerals belonging to the pyrochlore group from the rare-metal ore deposits of Ilmeny-Vishnevogorsky carbonatite-miaskite complex (South Urals). Individual pyrochlore crystals were dated through a new technique of in-situ U-Pb dating using SHRIMP-II, which was developed at VSEGEI (St.Petersburg). The U-Pb dating of high-uranium pyrochlore (more than 2.5 wt % UO₂) was carried out employing laser ablation and ICP-MS. The U-Pb systems of studied pyrochlore samples indicate a multi-stage formation of rare-metal niobium mineralisation. The earliest age of ore formation (378 ± 4.9 Ma) is yielded by the U-Pb systems of U-bearing pyrochlores from the carbonatites of the Potanino deposit. This period of ore formation is probably associated with the final stages in the crystallisation of the alkaline-carbonatite magmatic system. The next periods of ore formation (230 ± 1.5 Ma) are widely manifested in the Vishnevogorsky and later in the Potanino deposit (217.2 ± 1.9 Ma), which is probably associated with the remobilisation and redeposition of alkaline-carbonatite and rare-metal substances at the post-collision stage in the evolution of Ural carbonatite complexes.

Keywords: U-Pb dating, pyrochlore-group minerals, Ilmeny-Vishnevogorsky complex, Urals

Acknowledgments

The work was carried out under the RFBR project No. 17-05-00154 and in line with the state task of the IGG UB RAS No. AAAA-A18-118052590028-9.

INTRODUCTION

The dating of ore mineralisation and genesis remains a challenge despite the development of analytical methods of isotope geochronology. It is known that zircon is the best geochronometer; however, the origin of zircon – if it is present in ores – is not always definite; sometimes it is of xenogenic origin. Minerals of the pyrochlore group (Ca, Na, U, Th, REE, Sr, Ba, vacancy)₂(Nb, Ti, Ta)₂O₆(F, OH, O), as minerals bearing rather high concentrations of uranium and thorium, are a geochronological alternative to zircon and can be used for dating ore-formation processes. Pyrochlores were not widely used as geochronometers due to their highly metamict crystal structure [Lumpkin and Ewing, 1995], as well as various secondary changes and the instability of the uranium-thorium-lead system [Pöml et al., 2007]. Nevertheless, thanks to modern methods for the in situ analysis of isotopic systems, it has become possible to solve the problem of dating various generations of pyrochlore and to use pyrochlore as a geochronometer mineral. Thus, in situ isotope analysis of individual phases and domains of mineral grains reveals sections of pyrochlore crystals suitable for performing dating [Wetzel et al., 2010]. In international practice, works on dating py-

rochlore are rare; however, they exist. Dating can be performed through several analytical methods – using a secondary-ion mass spectrometer (SIMS) [Wetzel et al., 2010] or laser ablation combined with ICP [Milonig et al., 2012, 2013; Bracciali et al., 2013; Deng et al., 2013].

Given that, unlike zircon, pyrochlore has divalent cations (including calcium and lead) occupying crystallographic position A, all minerals from the pyrochlore group contain a relatively high proportion of ordinary (non-radiogenic) lead (Pb_c), as compared to radiogenic one (and, accordingly, low ²⁰⁶Pb/²⁰⁴Pb isotope ratios). The proportion of ordinary lead in pyrochlores sometimes constitutes tens of per cent, which is extremely high and not typical of the used intralaboratory and international geochronological standards when employing in situ methods of analysis. Thus, it is easier to find standards having a minimum content of ordinary lead among the most common dating minerals – zircon, baddeleyite, monazite, apatite. In addition, with accurate and careful measurement of Pb isotopic composition, as well as the right correction for the composition of ordinary (non-radiogenic) Pb, the resulting reproducibility of the obtained geochronological data reaches ± 2% and provides a satisfactory agreement between SIMS age estimates and data obtained using

other isotope-geochronological methods (ID-TIMS, LA-ICP-MS).

In order to assess the age and duration of rare-metal mineralisation, we performed U-Pb isotopic dating of niobium ore minerals from the Vishnevogorsk and Potanino niobium deposits associated with the Ilmeny-Vishnevogorsky carbonatite-miaskite complex which is located within the Ural orogen.

The Ilmeny-Vishnevogorsky complex is a prototype of linear carbonatite complexes – an independent type of carbonatite formations associated with the linear zones of alkaline metasomatism and syenite-nephelinesyenite magmatism. Their origin is still debatable [Levin et al., 1997; Mitchell, 2005; Rass et al., 2006; Nedosekova et al., 2009, 2010, 2012, 2016; Ivanov et al., 2010; Ivanov, 2011; Rusin et al., 2012; Nedosekova et al., 2013; Bagdasarov, 2014]. The least studied issues include the age and origin of rare-metal (Zr-Nb-REE) ore mineralisation, as well as its relation to various magmatic phases, post-magmatic evolution and metamorphic processes.

GEOLOGICAL POSITION AND COMPOSITION OF THE ILMENY-VISHNEVOGORSKY MIASKITE-CARBONATITE COMPLEX

The Ilmeny-Vishnevogorsky miaskite-carbonatite complex is located at the junction of the South and Middle Urals, in the East Urals megazone, which, along with the Tagil-Magnitogorsk and Trans-Ural megazones, forms the Eastern (paleo-island arc) sector of the Urals, constituting a complex tectonic collage of oceanic, island-arc and collision complexes having micro-continental blocks [Puchkov, 2010]. The East Urals megazone is characterised by a wide distribution of granitoids and gneisses, as well as the presence of micro-continental blocks of Precambrian (?) crystalline crust (Taldyk, Murzinka-Aduy, Kayraky, partly Sysert-Ilmenogorsky, etc.).

The Ilmeny-Vishnevogorsky complex occurs in the axial part of the Sysert-Ilmenogorsky anticlinorium, in the Lower Proterozoic rocks of the Selyankino, Ilmenogorsky and Vishnevogorsky strata (PR1), in the submeridional (collision) structure, stretching from north to south for over 100 km, with the maximum width of 4–6 km (Fig. 1). The complex includes two relatively large (20–25 × 6 km) intrusive miaskite massifs (Vishnevogorsky and Ilmenogorsky), numerous stratal and dyke-like bodies of miaskites, syenites and miaskite-pegmatites, stratal and vein-shaped bodies of carbonatites, as well as thick zones of fenitisation in the host rocks of Vishnevogorsky and Ilmenogorsky suites. Miaskite massifs are connected by the Central Alkaline Belt composed of fenites, feldspar metasomatites, small miaskite and syenite bodies, as well as melanocratic carbonate-silicate rocks and carbonatites.

Carbonatites characterised by ore niobium mineralisation are widely developed in the northern part of

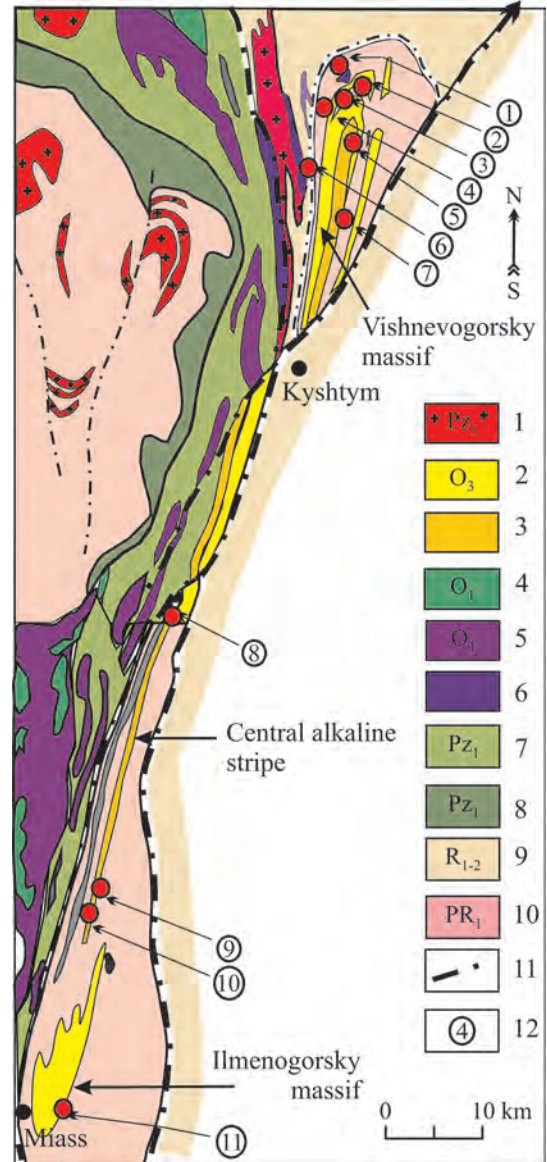


Fig. 1. Geological structure of the Ilmeny-Vishnevogorsky alkaline-carbonatite complex according to [Levin et al., 1997; Zoloev et al., 2004].

1 – granites (Pz₃); 2, 3 – Ilmeny-Vishnevogorsky complex (O₃): 2 – miaskites of the Vishnevogorsky and Ilmenogorsky massifs, 3 – metasomatites, carbonatites, silicate-carbonate rocks of the Central Alkaline Belt; 4 – ophiolite gabbro (O₁); 5 – ophiolite ultrabasites (O₁); 6 – Buldym meta-ultrabasites (PR[?]); 7 – volcanogenic-sedimentary rocks of the Tagil-Magnitogorsk megasynclinorium (Pz₁); 8 – garnet-mica schists and eclogites of the eastern margin of the Ufaley middle massif (Pz₁); 9 – plagioclase schists and quartzites of the Sysert-Ilmenogorsky middle massif (R₁₋₂); 10 – plagiogneisses, granite migmatites, crystalline schists, amphibolites, quartzites of the Sysert-Ilmenogorsky and Ufaley middle massifs (PR₁₋₂); 11 – tectonic faults and non-conformities; 12 – main ore deposits and occurrences of Nb and REE associated with carbonatites (numbers in circles): 1 – Buldym (Nb and REE); 2, 3 – Vishnevogorsky (Nb) (2 – zone 125; 3 – zones 140 and 147); 4 – Spirikhya (REE); 5 – Svetly (Nb); 6 – Kagansky (REE); 7 – Potanino (Nb); 8 – Uvildy (Nb); 9 – Baydashevo (Nb); 10 – Ishkul (Nb); 11 – Ilmeny, pit 97 (Nb and REE).

the complex – in the apical part of the Vishnevogorsky miaskite massif and in the ‘saddle-like’ miaskite deposit (Vishnevogorsky niobium deposit). They also occur in the root part of the massif – Purgino ore occurrence (see Fig. 1). Carbonatites make up stratal, dyke-like and vein-shaped bodies (up to 10 m in thickness and hundreds of meters long), forming an ore zone of 4 km in length and 30 m in width (ore zone 147, Vishnevogorsky niobium deposit). The richest ore zone of this deposit (zone 140) is associated with the northern miaskite satellite (‘saddle-like deposit’), which occurs in the hinge of the Vishnevogorsky anticline, 50 m north of the Vishnevogorsky massif, and comprises a system of subparallel veins (carbonatites, albites and miaskitic pegmatoids). Carbonatites are also found in the fenite halo of the Vishnevogorsky intrusion (in the fenitised rocks of the Vishnevogorsky suite), forming stockworks and veins.

Early carbonatites (sövite I), which occur in the form of schliers and stratal bodies mainly in the root of the Vishnevogorsky intrusion, have a calcite composition and contain nepheline, feldspars, biotite, as well as accessory zircon, black-brown pyrochlore (hatchettolite), ilmenite, apatite, etc. Late carbonatites (sövite II) widely developed in the apical part of the Vishnevogorsky massif (often being confined to fold hinges) form coarse-grained leucocratic zones and veins in miaskites and early carbonatites, which are composed of calcite and large crystals (up to n cm) of fluorapatite, red and yellowish-brown pyrochlore, ilmenite, biotite, pyrrhotite and pyrite. In the exocontact fenite haloes of miaskite intrusions, late carbonatites are also represented by coarse-grained calcite veins and contain pyroxene (aegirine-augite), red-brown pyrochlore, apatite, ilmenite and titanite.

Numerous deposits and ore occurrences of pyrochlore-bearing carbonatites have been identified and explored in the Central Alkaline Belt (see Fig. 1). The largest of the deposits (Potanino niobium deposit) is located in the eastern contact of the Central Alkaline Belt, forming a linear, sometimes stockwork-like zone in miaskites and fenites (about 15 km long and up to 40 m thick). In addition, the following ore occurrences have already been identified in this area: Ishkul, Baydashevo, Uvildy and Svetloe Lake [Levin et al., 1997] (see Fig. 1).

GEOCHRONOLOGY OF THE ILMENY-VISHNEVOGORSKY COMPLEX

The first Rb-Sr and U-Pb isotope-geochronological data for rocks from the Ilmeny-Vishnevogorsky complex were reported in the 1970s–1980s. Miaskites from the Ilmeny-Vishnevogorsky complex yielded Rb-Sr whole-rock isochron ages of 446 ± 12 Ma (O_3) (Ilmenogorsky massif), 436 ± 31 Ma (S_1) and 478 ± 55 Ma (O_1) (Vishnevogorsky massif), which were interpreted as the age of miaskitic magma intrusion and crystalli-

sation at the final stages of rifting in the lower – upper Ordovician (O_1 – O_3) [Kononova et al., 1979; Kramm et al., 1983]. In addition, Rb-Sr mineral isochrons obtained for miaskites show an age of 245 ± 8 Ma, which corresponds to the age of metamorphism.

The U-Pb dating of zircons from the miaskites of the Ilmeny-Vishnevogorsky complex performed using isotopic dilution yielded Lower Silurian ages: 434 ± 15 Ma [Kramm et al., 1993] and 422 ± 10 Ma [Chernyshev et al., 1987]. A range of ages from the Lower Silurian to the Upper Devonian was obtained using in situ methods for dating zircons (SHRIMP and laser ablation). The age of zircons from the miaskite-pegmatites, miaskites and malignites of the Ilmenogorsky massif is estimated at 432 ± 3.7 Ma (S_1), 419 ± 7 Ma (S_2), 417 ± 7 Ma (S_2), 383 ± 14 Ma (D_3), respectively [Krasnobaev et al., 2010a, 2014], with zircons from the carbonatites of the Vishnevogorsky massif yielding 419 ± 20 Ma [Krasnobaev, et al., 2010b] and 417 ± 3 Ma (S_2) [Nedosekova et al., 2010, 2012, 2016].

In addition, the U-Pb isotope systems of zircons from the Ilmeny-Vishnevogorsky complex reveal subsequent metamorphic processes, accompanied by the loss of radiogenic Pb, dated at 261 ± 14 Ma [Chernyshev et al., 1987] and 279 ± 10 Ma (P) [Krasnobaev et al., 2010a]. A significant number of zircon grains from miaskites and miaskite-pegmatites U-Pb dated using in situ methods showed Permian ages: 269 ± 6 and 251 ± 6 Ma, respectively [Krasnobaev et al., 2014]; as well as Rb-Sr mineral isochrons obtained earlier [Kononova et al., 1979; Kramm et al., 1983].

The Sm-Nd mineral isochron for the carbonatites of the Vishnevogorsky massif, constructed using 5 analytical points (mineral fractions of calcite, biotite, apatite, pyrochlore and bulk sample), yielded a Lower Silurian age of 425 ± 44 Ma (S_1), thus showing the carbonatite magmatic stage in the functioning of the alkaline-carbonatite magmatic system [Nedosekova, Belyatskii, 2012]. In addition, a Sm-Nd mineral isochron obtained for the carbonatites from the saddle-like miaskite deposit shows an age of 388 ± 50 Ma (end of D_2) [Ivanov et al., 2010], probably reflecting the final stage in the formation of the Ilmeny-Vishnevogorsky miaskite-carbonatite complex.

Thus, the U-Pb, Rb-Sr and Sm-Nd geochronological data of alkaline rocks and carbonatites from the Ilmeny-Vishnevogorsky complex indicate multistage magma formation at the stage of Palaeozoic activation (≈ 440 – 390 Ma), as well as large-scale processes of alkaline metasomatism and pegmatite formation at the stage of Hercynian orogeny (≈ 350 – 250 Ma) and subsequent post-collision extension (≈ 250 – 240 Ma).

NB-ORE MINERALISATION

More than ten deposits and ore occurrences of niobium, zirconium and rare earths have been identified in the Ilmeny-Vishnevogorsky complex (see Fig. 1). The

Vishnevogorsky deposit – the first deposit in Russia where the industrial mining of Nb raw materials was carried out – is associated with pyrochlore-bearing carbonatites in the apical part of the Vishnevogorsky miaskite intrusion. The Potanino niobium deposit along with the Svetloe Lake, Baydashevo, Ishkul and Uvildy ore occurrences, which are also associated with carbonatites, have been explored in the Central Alkaline Belt [Levin et al., 1997; Zoloev et al., 2004].

The Nb-ore mineralisation of rare-metal deposits at the Ilmeny-Vishnevogorsky miaskite-carbonatite complex is represented by the minerals of the pyrochlore supergroup: pyrochlore proper, Uranpyrochlore (hatchettolite), betafite, as well as Ta-, REE- and Sr-bearing minerals of the pyrochlore group. Such minerals as ilmenorutile, columbite, fersmite, chevkinite-(Ce) are less common [Es'kova, Nazarenko, 1960; Es'kova et al., 1964; Efimov et al., 1985; Levin et al., 1997; Nedosekova, Pribavkin, 2015; Nedosekova et al., 2017]. The main ore minerals of the carbonatite deposits at the Ilmeny-Vishnevogorsky complex are those belonging to the pyrochlore group. Pyrochlore is present in various rocks – in miaskites and syenites, especially in their pegmatoid varieties, in miaskite-pegmatites, syenite-pegmatites, carbonatites and alkaline metasomatites (albitite, fenite, glimmerite, etc.). In the most significant amounts, pyrochlore is found in both early and late carbonatites (sövites I and II, respectively) of the Vishnevogorsky miaskite massif and the Central Alkaline Belt [Levin et al., 1997; Zoloev et al., 2004; Nedosekova, 2007; Nedosekova et al., 2009, 2017].

In miaskites and syenites, pyrochlore is represented by octahedral crystals of dark brown, sometimes orange colour (0.01–0.1 mm in size). In pegmatoid varieties, the size of pyrochlore increases up to 0.5 cm, whereas in pegmatites it comes up to several centimetres. The distribution of pyrochlore is uneven. In pegmatites and albitites, it forms streaky clusters and small disseminated particles, with crystal sizes ranging from 2–3 mm to several centimetres. In silicocar-

bonatites (melanocratic carbonate-silicate rocks) and in early carbonatites (sövite I), pyrochlore forms small grains of black and greenish-black colour (U-pyrochlore) (Fig. 2a). In late carbonatites (sövite II), pyrochlore forms octahedral and cubo-octahedral crystals (0.05–1.5 cm in size) of red-brown and yellow colour (Fig. 2b, c), containing relics of early (black) pyrochlore with traces of dissolution and transformation. The internal structure of pyrochlore crystals of late carbonatites is shown in Fig. 3a–f: relics of black U-(Ta)-bearing pyrochlore, surrounded by an intermediate zone of U-bearing hydrated pyrochlore, are sometimes preserved in the cores of crystals, whereas the peripheral part of the crystal is composed of light brown Sr-bearing pyrochlore (see Fig. 3e).

The Ilmeny-Vishnevogorsky complex has several minerals of the pyrochlore group, whose formation is associated with certain evolutionary stages in the functioning of the alkaline-carbonatite magmatic system, as well as the metamorphic transformations of the complex [Nedosekova et al., 2017]. According to the latest nomenclature of the pyrochlore group (pyrochlore supergroup) drawing on the predominant cation or anion in sites B = Nb, Ti, Ta; A = Ca, Na, REE, Y, Sr, Ba, Mn, Mg, U, Th; and Y = O, OH, F [Atencio et al., 2010], pyrochlores of the Ilmeny-Vishnevogorsky and Buldym complexes can be classified as U-(Ta)-bearing oxycalciopyrochlores (or uranium-pyrochlores, according to [Hogarth, 1977]) and fluorocalciopyrochlores (including Ta-, REE_{Ce}- and Sr-bearing varieties). U- and Sr-bearing varieties include kenopyrochlores having an A-site vacancy of over 50% relative to the A-site cations. The pyrochlore compositions are presented in ternary diagrams characterising the occupancy of sites A, B and Y (Fig. 4).

U-(Ta)-bearing oxycalciopyrochlores (15–24 wt % UO₂, 1–14 wt % Ta₂O₅) are found in early high-temperature carbonatites (sövite I) and silicocarbonatites of the Central Alkaline Belt (Potanino deposit, Uvildy ore occurrence) [Levin et al., 1997; Nedosekova et al.,

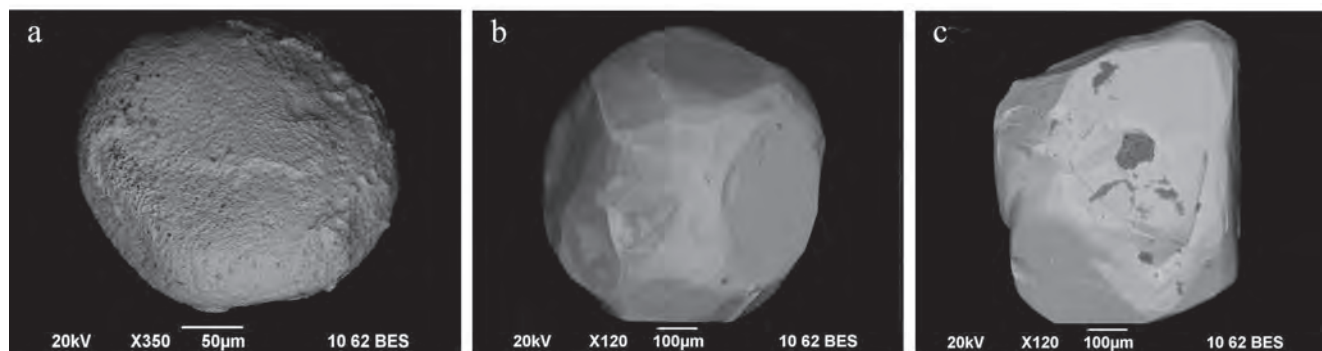


Fig. 2. Morphological features of pyrochlores from the Ilmeny-Vishnevogorsky complex: uranpyrochlore from early carbonatites, Uvildy Nb-occurrence (a); Sr-REE-bearing pyrochlores from late carbonatites, Vishnevogorsky Nb-deposit (b, c).

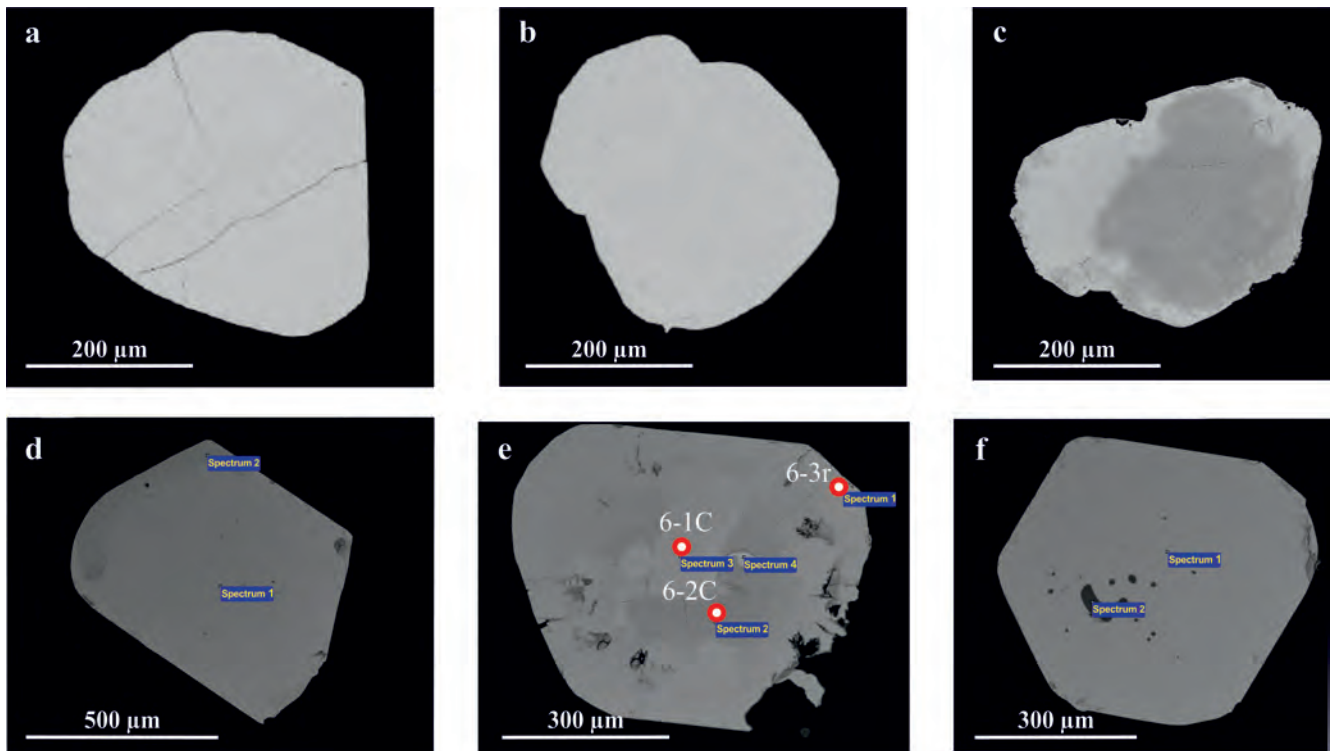


Fig. 3. Morphology and internal structure of pyrochlore crystals from the carbonatites of the Ilmeny-Vishnevogorsky complex (sample 331, sövite II, Vishnevogorsky deposit), BSE-image.

Analysis points correspond to those given in Table 1.

2009]. This type of pyrochlore is probably formed earlier than others (during the late magmatic stage of crystallisation), as evidenced by the relics of U-bearing pyrochlore in the later generations of Sr-bearing pyrochlore from late carbonatites (sövite II) [Levin et al., 1997] (see Fig. 3c, e).

Fluorcalciopyrochlores characterised by the maximal content of Nb_2O_5 (65–69 wt %), the most stoichiometric composition and the lowest content of microimpurities are widely developed in feldspar veins and in the late calcite carbonatites from the saddle-like maskite deposit of the Vishnevogorsky massif. These pyrochlores comprise the main ore zones of the Vishnevogorsky deposit (ore zones 140 and 147). They are also found in the Potanino deposit.

Ta-bearing varieties of fluorcalciopyrochlore (1.5–5.0 wt % Ta_2O_5 ; 0–4.2 wt % UO_2) are found in nepheline pegmatites in the apical part of the Vishnevogorsky massif (ore zone 147), as well as in the carbonatites of the Potanino deposit. This pyrochlore is formed at the stage of pegmatite crystallisation.

Sr- and REE-bearing fluorcalciopyrochlores (3–6 wt % of LREE_2O_3 , 1.5–4.5 wt % of SrO) are widespread in late carbonatites (sövite II) and in exocontact fenites of the Vishnevogorsky and Potanino deposits. These pyrochlore varieties form octahedral and cubo-octahedral crystals (see Figures 2 and 3d, f) exhibiting signs of metasomatic growth, as well as form rims

around U-bearing relict (?) cores of pyrochlore (see Fig. 3c, e). It is likely that the formation of these pyrochlore varieties occurs at the final evolutionary stages (late carbonatite and syenite-pegmatite) of the complex and may also be associated with the metamorphic transformations at the collision stage.

METHODS OF ANALYSIS

The chemical composition of pyrochlores and aeschynites from the Ilmeny-Vishnevogorsky complex was studied at 60 nA and 20 kV using a CAMEBAX microprobe, with a probe beam size of 2 μm (analyst V.V. Sharygin, IGM SB RAS, Novosibirsk), as well as using a Cameca-100 microprobe (analyst D.V. Zamyatin, IGG UB RAS).

The U-Pb dating of high-uranium pyrochlore was carried out using LA-ICP MS (DUV-19). Pyrochlores having a uranium oxide content of less than 2.5% were dated through a method for the in situ U-Pb dating of individual pyrochlore crystals using a SHRIMP-II secondary-ion mass spectrometer, which was developed at the A.P. Karpinsky Russian Geological Research Institute (VSEGEI, St.Petersburg). A detailed description of the procedure is given in [Lepkhina et al., 2016]. The measurements of U-Th-Pb isotope ratios and element concentrations in pyrochlores, along with the standard calibration, were carried out using

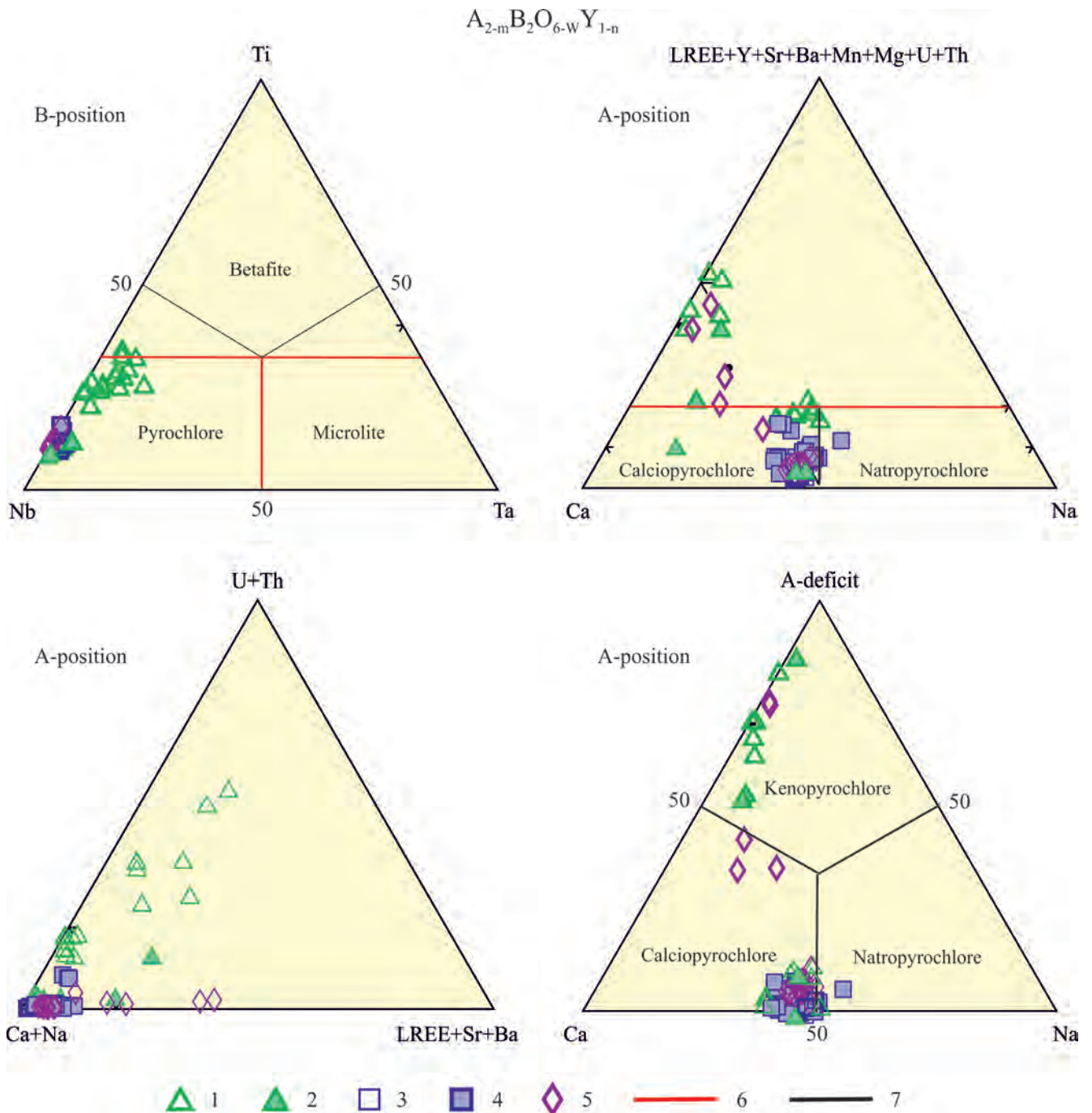


Fig. 4. Ternary composition diagrams showing the occupancy of sites B and A in the pyrochlore structure (p.f.u.).

1 – U-(Ta)-bearing oxycalcipyrochlores, 2 – Ta-bearing fluorcalcipyrochlores, 3 – fluorcalcipyrochlores, 4 – REE-Sr-bearing fluorcalcipyrochlores, 5 – Sr-REE-bearing fluorcalcipyrochlores, 6 – IMA classification for the pyrochlore group by [Hogarth, 1977], 7 – IMA classification for the pyrochlore group by [Atencio, 2010].

the SHRIMP-II ion microprobe at the Centre for Isotope Research (VSEGEI, St.Petersburg). Given that pyrochlore is significantly different from zircon in terms of crystallochemical features, at the stage preceding the analytical measurements of U-Pb ratios in pyrochlores from our collection, we experimentally selected the optimal regime and sequence for record-

ing the ionic currents of elements taking mineral matrix composition and possible isobaric overlaps into account, as well as developed a scheme for measuring and calculating U-Pb ages. In situ dating of pyrochlore was accompanied by a detailed determination of the chemical composition of crystals at the micro-level.

Pyrochlore-331 (sövite II, Vishnevogorsky massif), which is characterised by relative areal geochemical homogeneity with an age of 230 ± 1.3 Ma and a U content of 1.500 ± 365 g/t, was used as an internal laboratory standard. Regular mass spectrometric analysis of pyrochlore-331 (over a period of 10 months) demonstrates acceptable for the standard dispersion of the obtained $^{206}\text{Pb}/^{238}\text{U}$ ratios when performing calibration according to the linear dependence of $\ln(\text{Pb}/\text{U})$ on $\ln(\text{UO}/\text{U})$. The measured $^{206}\text{Pb}/^{238}\text{U}$ ratios of pyrochlore were normalised against a value of 0.0363, which corresponds to 230 Ma (according to the model of [Stacey, Kramers, 1975]). With an average of 10–15 analyses per session, the error in measuring isotope ratios for a standard varies within 1–2% (2σ). The concentration of ^{238}U in the analysed pyrochlore samples was estimated relative to the average uranium content in pyrochlore-331 (≈ 1500 g/t). The correction of the measured Pb isotopic composition for non-radiogenic lead and the corresponding age was based on the Pb_c model composition and on the use of the Stacey–Kramers model [Stacey, Kramers, 1975], respectively. Errors associated with individual analyses (of ratios and ages) were calculated at the 1σ level, whereas the errors of calculated concordant ages are given in Figures 5–7 at the 2σ level. The processing of primary MS data along with the construction of concordia plots for the obtained isotope ratios was performed using the SQUID and ISOPLOT/EX programs [Ludwig, 2003].

U-Pb DATING OF MINERALS BELONGING TO THE PYROCHLORE GROUP (ILMENY-VISHNEVOGORSKY COMPLEX). RESULTS AND DISCUSSION

We studied the U-Th-Pb isotopic system of three chemically characterised pyrochlore samples from the Ilmeny-Vishnevogorsky complex belonging to different stages of ore formation: a) from early carbonatites (U-(Ta)-oxycalcio-pyrochlore, sample K-37-95, sövite I, Potanino deposit); b) from late carbonatites (Ta-bearing fluorcalcio-pyrochlore, sample K-43-62, sövite II, Potanino deposit); c) from late carbonatites (REE-Sr-bearing fluorcalcio-pyrochlore, sample 331, sövite II, Vishnevogorsky deposit). The representative analyses of the studied pyrochlore samples (characterising the core and rim of crystals) and their conversion to a crystal-chemical formula. are given in Table 1. The optical and backscattered-electron (BSE) images of pyrochlore varieties are shown in Figures 2 and 3.

As mentioned earlier, a sample of pyrochlore-331 from the Vishnevogorsky deposit was selected as an isotope-geochemical and geochronological standard. According to [Atencio et al., 2010], this pyrochlore is classified as Sr-REE-bearing (1.5–4.5 wt % SrO and 1.0–2.5 wt % LREE) fluorcalcio-pyrochlore. It occurs in late carbonatites (sövites II) – in biotite-calcite carbonatites with apatite, ilmenite, pyrrhotite, pyrite (api-

cal part of the Vishnevogorsky miaskite massif). Pyrochlore forms large and small octahedral crystals and grains of brown, light brown (almost yellow) and red-brown colour.

The U-Pb isotopic analysis of this pyrochlore using in situ methods (SHRIMP-II, LA-ICP-MS), as well as isotope dilution employing chromatographic separation of elements and ID-TIMS revealed satisfactory repeatability of results. Thus, the dates of pyrochlore-331 grains obtained using two in-situ methods differ by no more than 0.5–1.0 Ma, with the uranium content varying within 30% (SHRIMP-II and LA-ICP-MS). The measured Pb isotopic composition of the internal standard for pyrochlore was corrected for the isotopic composition of the non-radiogenic component according to the lead composition in syngenetic calcite (Pb acceptor mineral characterised by a high Pb/U ratio), as well as the corresponding parameters of the model curve [Stacey, Kramers, 1975] for the evolution of Earth's Pb isotopic composition 230 Ma ago: $^{207}\text{Pb}/^{206}\text{Pb} = 0.851$, $^{208}\text{Pb}/^{206}\text{Pb} = 2.082$ and $^{206}\text{Pb}/^{204}\text{Pb} = 18.35$. Within the obtained error margins, the age and concentration characteristics of the pyrochlore grains in question are reproduced satisfactorily, thus the age and U content of pyrochlore-331 (230 ± 1.3 Ma and 1500 ± 365 g/t, respectively) were used for further U-Pb measurements of pyrochlore samples from the collection.

Using the age and concentration characteristics of pyrochlore-331, we measured the U-Pb ratios of the pyrochlore collection acquired from the rare-metal deposits of Ural carbonatite complexes relative to the U/Pb ratios of pyrochlore-331 grains, which were measured in the same session in the capacity of the calibration standard. Despite significant variations in the content of uranium (from 300 g/t to 1.9%), thorium (from 1400 g/t to 3%) and a high proportion of non-radiogenic lead (from 9 to 65% of ^{206}Pb), the U-Pb isotopic systems of the studied fluorcalcio-pyrochlores were practically closed and the age within the error margins was concordant. Relatively high contents of radiogenic lead ($^{206}\text{Pb}_{\text{rad}} = 14\text{--}300$ g/t) account for the low error associated with individual measurements of isotopic ratios and results reproducibility, which expressed in terms of age leads to an error of concordant estimates at a level of 1–6 Ma. The results of U-Th-Pb isotope analysis for pyrochlores are presented in Table 2 and shown in Figures 5–7.

Uranpyrochlores formed in the early stages of carbonatite genesis in the sövites I of the Central Alkaline Belt (sample K-37-95, U-(Ta)-bearing oxycalcio-pyrochlore, Potanino deposit) are characterised by a slightly open U-Pb system and yield an age of 378.3 ± 4.9 Ma (see Fig. 5). The detected departure from the closed nature of the isotopic system of these pyrochlores reflects an increased degree of metamictisation of the crystal structure of the mineral due to the high content of radioactive U and Th, as well as the impact of late processes associated with the post-

Table 1. Chemical compositions (wt %) and formulae (p.f.u.) of the pyrochlore-group minerals from the Ilmeny-Vishnevogorsky carbonatite-miaskite complex, Urals

Element	1	2	3	4	5	6	7	8	9	10	11	12	13	14	15	16
	Sample K37-95				Sample K43-62				Sample 331							
	Analysis points															
	2c	2r	8c	4r_alt	2	3	5	9	1-1c	1-2r	7-1c	7-2r	6-1c*	6-2c_alt*	6-3r*	8-1c
Nb ₂ O ₅	38.72	39.58	45.60	50.42	63.83	61.66	62.03	63.44	65.58	60.23	66.59	65.64	60.33	52.08	59.26	66.98
Ta ₂ O ₅	4.02	4.20	4.37	4.39	2.12	3.53	2.92	2.30	0.02	0.27	0	0.13	0.31	0.00	0.00	0.00
TiO ₂	12.50	12.06	9.48	7.95	4.32	4.89	4.60	4.47	4.23	5.06	3.33	4.52	4.45	4.42	3.51	3.24
SiO ₂	0.00	0.12	0.00	0.00	0.00	0.00	0.00	0.00	0.01	4.99	0.00	0.00	1.58	0.00	0.00	0.00
UO ₂	22.11	21.00	16.43	12.44	0.08	1.80	0.83	0.00	0.16	0.57	0.19	0.21	3.72	3.72	0.85	0.2
ThO ₂	0.78	0.80	0.59	1.11	2.05	1.59	1.97	2.26	0.56	0.78	0.63	0.61	0.3	0.53	0.59	0.46
Fe ₂ O ₃	0.00	0.02	0.00	0.81	0.06	0.07	0.07	0.07	0.03	1.59	0.04	0	1.52	1.69	1.5	0.02
Y ₂ O ₃	0.12	0.10	0.05	0.07	ND	ND	ND	ND	0.1	0.04	0.13	0.11	0.1	0	0.03	0.15
La ₂ O ₃	0.31	0.41	0.44	0.61	0.32	0.22	0.59	0.14	0.51	1.49	0.22	0.54	0.37	0.7	1.08	0.68
Ce ₂ O ₃	0.72	1.02	1.11	1.82	0.88	0.82	1.33	0.56	1.43	4.52	0.96	1.42	1.52	2.42	2.98	1.96
Nd ₂ O ₃	0.94	0.95	0.95	0.94	0.38	0.26	0.37	0.12	ND	ND	ND	ND	ND	ND	ND	ND
MnO	0.00	0.00	0.00	0.02	ND	ND	ND	ND	0	0.74	0.00	0.00	0.21	0.42	0.5	0.04
MgO	0.03	0.01	0.01	0.02	ND	ND	ND	ND	ND	ND	ND	ND	ND	ND	ND	ND
CaO	11.06	10.65	11.08	6.65	15.48	15.47	15.03	16.07	14.98	6.69	15.04	14.37	11.68	6.04	12.24	13.2
BaO	0.00	0.00	0.00	0.14	ND	ND	ND	ND	0	1.58	0.06	0	0.77	2.39	0.73	0
SrO	0.28	0.31	0.46	0.44	0.56	0.39	0.47	0.47	1.53	4.4	1.02	1.44	1.97	5.01	3.27	1.8
PbO	0.91	0.91	0.53	0.50	ND	ND	ND	ND	0.18	0.46	0.19	0.33	0.48	0.31	0.05	0.46
Na ₂ O	5.11	5.40	5.79	0.16	6.55	6.51	6.53	6.48	6.99	0.35	7.12	6.98	3.64	0.05	2.09	6.71
K ₂ O	0.01	0.01	0.01	0.57	ND	ND	ND	ND	ND	ND	ND	ND	ND	ND	ND	ND
F	1.44	1.51	1.38	1.65	5.25	4.74	4.86	5.21	4.58	0.50	4.29	4.43	2.76	0.24	2.13	4.21
Total	99.04	99.04	98.25	90.71	101.87	101.95	101.59	101.58	100.89	94.26	99.81	100.73	95.71	80.02	90.81	100.11
O = F ₂	0.61	0.64	0.58	0.69	2.21	2.00	2.05	2.19	1.93	0.21	1.81	1.87	1.16	0.10	0.90	1.77
Total	98.44	98.41	97.67	90.02	99.67	99.95	99.55	99.39	99.0	94.0	98.0	98.9	94.55	79.92	89.9	98.3

The formulae are designed for two cations in site B (p.f.u.)

B-position																
Nb	1.250	1.270	1.425	1.491	1.764	1.712	1.734	1.753	1.804	1.460	1.845	1.793	1.632	1.673	1.753	1.850
Ta	0.078	0.081	0.082	0.078	0.035	0.059	0.049	0.038	0.000	0.004	0.000	0.002	0.005	0.000	0.000	0.000
Ti	0.672	0.644	0.493	0.391	0.199	0.226	0.214	0.205	0.194	0.204	0.153	0.205	0.200	0.236	0.173	0.149
Fe ³⁺	0.000	0.004	0.000	0.040	0.003	0.003	0.003	0.003	0.001	0.064	0.002	0.000	0.068	0.090	0.074	0.001
Sum B	2.000	2.000	2.000	2.000	2.000	2.000	2.000	2.000	2.000	2.000	2.000	2.000	2.000	2.000	2.000	2.000

A-position																
Ca	0.847	0.810	0.820	0.466	1.014	1.018	0.996	1.052	0.977	0.268	0.987	0.930	0.749	0.460	0.858	0.864
Mn	0.000	0.000	0.000	0.001	0.000	0.000	0.000	0.000	0.000	0.384	0.000	0.000	0.011	0.025	0.028	0.002
Mg	0.003	0.001	0.001	0.002	0.000	0.000	0.000	0.000	ND	0.034	ND	ND	ND	ND	ND	ND
Ba	0.000	0.000	0.000	0.004	0.000	0.000	0.000	0.000	0.000	0.033	0.001	0.000	0.018	0.067	0.019	0.000
Sr	0.011	0.013	0.018	0.017	0.020	0.014	0.017	0.017	0.054	0.137	0.036	0.050	0.068	0.206	0.124	0.064
Pb	0.018	0.017	0.010	0.009	0.000	0.000	0.000	0.000	0.003	0.007	0.003	0.005	0.008	0.006	0.001	0.008
Na	0.708	0.743	0.776	0.020	0.776	0.775	0.783	0.768	0.825	0.036	0.846	0.817	0.422	0.007	0.265	0.795
K	0.001	0.001	0.001	0.048	0.000	0.000	0.000	0.000	0.000	0.000	0.000	0.000	0.000	0.000	0.000	0.000
Y	0.004	0.004	0.002	0.002	0.000	0.000	0.000	0.000	0.003	0.001	0.004	0.004	0.003	0.000	0.001	0.005
LREE	0.051	0.061	0.063	0.080	0.035	0.029	0.052	0.018	0.043	0.118	0.027	0.043	0.0415	0.081	0.0975	0.059
U	0.351	0.332	0.253	0.181	0.001	0.025	0.011	0.000	0.002	0.007	0.003	0.003	0.050	0.059	0.012	0.003
Th	0.013	0.013	0.009	0.017	0.029	0.022	0.028	0.031	0.008	0.010	0.009	0.008	0.004	0.009	0.009	0.006
Sum A	2.007	1.996	1.953	0.847	1.875	1.883	1.887	1.886	1.915	0.767	1.916	1.861	1.374	0.920	1.414	1.806
F	0.325	0.339	0.302	0.341	1.015	0.921	0.950	1.007	0.881	0.085	0.831	0.846	0.522	0.054	0.441	0.813

Note. The chemical compositions of minerals belonging to the pyrochlore group were determined using: 1–8 – a CAMEBAX microprobe at the IGM SB RAS (Novosibirsk, analyst V.V. Sharygin); 9–16 – a Cameca-100 microprobe at the IGG, UB RAS (Ekaterinburg, analyst D.V. Zamyatin).

alt – altered; c – core of the crystal, r – rim of the crystal, ND – not detectable. *pyrochlore grain having early generation relics.

1, 2, 3 – U-(Ta)-bearing oxycalcipyrochlore; 4 – U-(Ta)-bearing hydroxyrochlore (sample K-37-95, sövite I, Potanino deposit, Ilmeny-Vishnevogorsky complex); 5–8 – Ta-bearing fluorcalcipyrochlore (sample K-43-62, sövite II, Potanino deposit, Ilmeny-Vishnevogorsky complex); 9–16 – (sample 331, sövite II, Vishnevogorsky deposit, Ilmeny-Vishnevogorsky complex): 9, 11, 12, 16 – Sr-(REE)-bearing fluorcalcipyrochlore; 10 – Sr-(REE)-bearing kenopyrochlore; 13 – relics of U-bearing pyrochlore (grain core 6-1C, sample 331), 14 – U-bearing hydroxyrochlore (middle zone of grain 6-2C, sample 331); 15 – Sr-(REE)-bearing fluorcalcipyrochlore (rim of grain 6-3r, sample 331) (see Fig. 3).

Table 2. Composition and U-Th-Pb isotope system of the pyrochlore-group minerals from the Nb-deposits of Ilmeny-Vishnevogorsky carbonatite-miaskite complex (South Urals)

Sample No.	Host rock	Chemical type of pyrochlore according to [Atencio, 2010]	Composition of pyrochlore (main components, wt %)	Characteristics of the U-Th-Pb system of pyrochlore	U-Pb age of pyrochlore, Ma
Potanino Nb-deposit, Central Alkaline Belt, Ilmeny-Vishnevogorsky carbonatite-miaskite complex					
K37-95*	Sövite I	U-(Ta)-bearing oxycalcipyrochlore	Na ₂ O – 4.6 CaO – 9.1 Nb ₂ O ₅ – 42.5 (PbO + ThO ₂ + UO ₂) – 20	[U]: 130000–240000 Th/U: 0.3–0.9	378.3 ± 4.9 n = 28
K43-62	Sövite II	Ta-bearing fluorcalciopyrochlore	Na ₂ O – 8.4 CaO – 14.6 Nb ₂ O ₅ – 60.7 (PbO + ThO ₂ + UO ₂) – 2	[U]: 300–2800 Th/U: 8.6–92.0 ²⁰⁶ Pb _c : 25–68%	216 ± 5.0 n = 15
Vishnevogorsky Nb-deposit, Ilmeny-Vishnevogorsky carbonatite-miaskite complex					
331	Sövite II	Sr-bearing fluorcalciopyrochlore	Na ₂ O – 8.5 CaO – 13.1 Nb ₂ O ₅ – 65.1 (PbO + ThO ₂ + UO ₂) – 1	[U]: 620–4700 Th/U: 0.7–5.2 ²⁰⁶ Pb _c : 9–39%	230 ± 1.5 n = 40

Note. The U-Pb dating of pyrochlore (less than 2.5 wt % UO₂) was performed through the method of ID-TIMS developed at VSEGEI (St. Petersburg) using a secondary-ion mass spectrometer SHRIMP-II. A detailed description of the technique is given in [Lepekhina et al., 2016].

*The U-Pb dating of U-bearing pyrochlore (more than 2.5 wt % UO₂) was performed using the method of laser ablation and ICP-MS. n – number of analyses, [U] – concentration of U (g/t) calculated relative to the concentration of U (1500 g/t) in the in-house standard (pyrochlore-331); ²⁰⁶Pb_c – relative proportion of non-radiogenic Pb. Detailed chemical composition is given in Table 1.

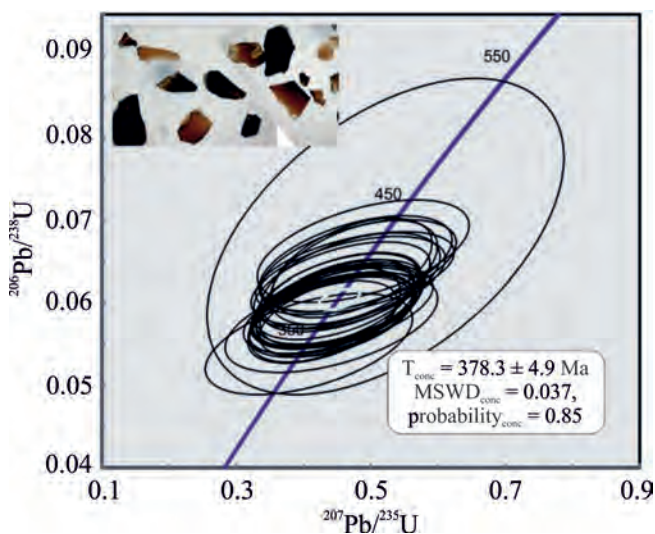


Fig. 5. U-Pb-diagram constructed according to LA-ICP-MS data for sample 37-95 of uranpyrochlore (only concordant analyses are given) from the carbonatites of the Potanino deposit (Ilmeny-Vishnevogorsky complex, South Urals)

The inserted picture shows the external forms of dated grains (incident light). Here and in figures 6 and 7, the error ellipses are at the 2σ level.

collision ore-metasomatic stage in the evolution of the complex 220–250 Ma ago.

As mentioned above, Sr-REE-bearing pyrochlore (sample 331, fluorcalciopyrochlore, sövite II, Vish-

nevogorsky deposit) yielded an age of 230 ± 1.5 Ma (see Fig. 6).

The youngest age (216 ± 5 Ma) was obtained for Ta-bearing fluorcalciopyrochlore from the late carbonatites of the Potanino deposit (sample K-43-62; see Table 2, Fig. 7).

Thus, the U-Pb system of the studied pyrochlore samples indicates the multistep formation of the Nb rare-metal mineralisation in the Ilmeny-Vishnevogorsky complex.

The earliest stage of ore formation (378 ± 4.9 Ma) – possibly associated with the primary crystallisation of the alkaline-carbonatite magmatic system – is determined from the U-Pb isotopic systems of the U-(Ta)-pyrochlores from the Potanino deposit [Krasnobaev et al., 2010a, 2014; Nedosekova et al., 2010, 2014; Ivanov et al., 2010; Nedosekova, 2012]. The U-Pb systems of zircons from the Ilmeny-Vishnevogorsky complex reveal a similar age cluster – 383 ± 14 Ma [Krasnobaev et al., 2010a]. The closest age of 388 ± 50 Ma was yielded by the mineral Sm-Nd isochron obtained for the carbonatites of the richest ore zone of the Vishnevogorsky deposit (ore zone 140, saddle-like miaskite deposit) [Ivanov et al., 2010], which probably reflects the final stages in the functioning of alkaline-carbonatite magmatic system, as well as one of the main stages in the ore formation of the Vishnevogorsky niobium deposit. The following stages of ore formation are widely manifested at the Vishnevogorsky (230 ± 1.5 Ma) and later at the Potanino (217.2 ± 1.9 Ma) deposits. Mineral Rb-Sr isochrons obtained for miaskites show a close age of 245 ± 8 Ma (T₂), which corresponds to the stage

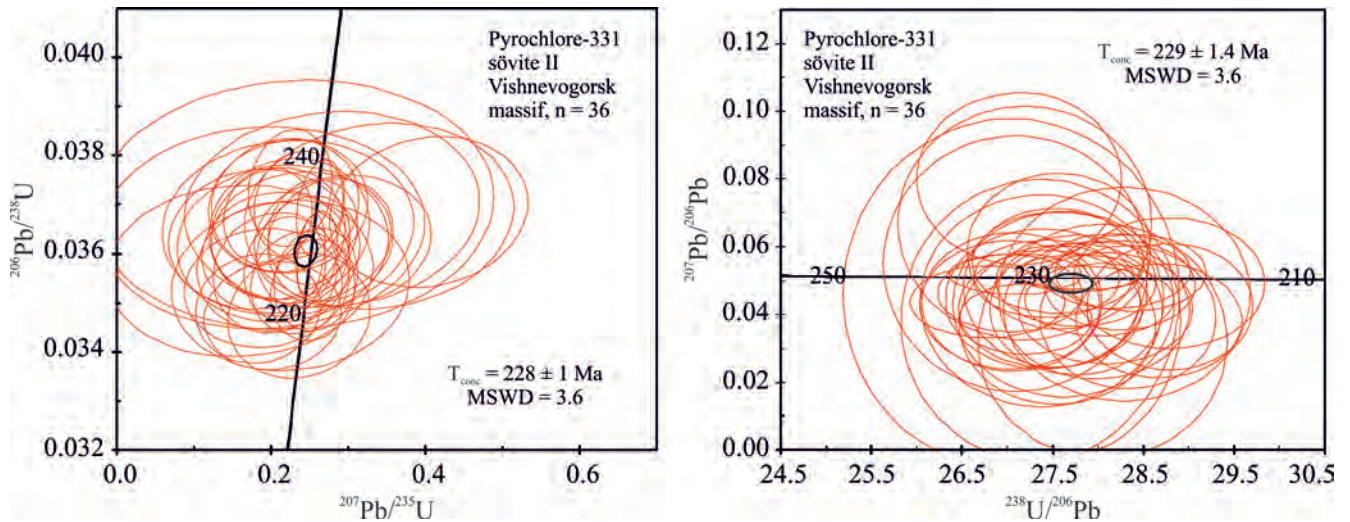


Fig. 6. U-Pb concordia diagram constructed according to SHRIMP-II data for pyrochlore (sample 331) from the late carbonatites of the Vishnevogorsky Nb-ore deposit (Ilmeny-Vishnevogorsky complex, South Urals).

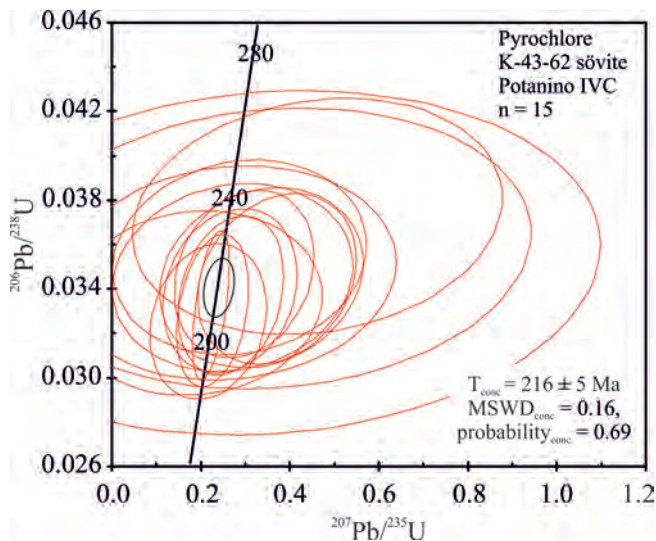


Fig. 7. U-Pb concordia diagram constructed according to SHRIMP-II data for pyrochlore (sample K-43-62) from the carbonatites of the Potanino deposit, Ilmeny-Vishnevogorsky complex.

of metamorphic transformations in the Ilmeny-Vishnevogorsky complex [Kononova et al., 1979; Kramm et al., 1983]. Ages associated with the stage of late-collision metamorphism [Puchkov, 2010] are also yielded by the U-Pb isotopic systems of zircons from the miaskites – 269 ± 6 , 279 ± 10 Ma [Krasnobaev et al., 2010a, 2014] – and zircons from the carbonatites of the Ilmeny-Vishnevogorsky complex – 279 ± 10 Ma [Krasnobaev et al., 2010b], 280 ± 8 (Nedosekova et al., 2014). A considerable number of zircons from miaskite-pegmatites yield an age of 251 ± 6 Ma, which confirms that the formation of pegmatites and rare-metal ores in the pegmatites of the Ilmeny-Vishnevogorsky

complex is associated with the late-collision and post-collision stages in the development of the Ural Orogen.

Thus, the formation of niobium ores occurred both at the final stage in the functioning of the alkaline-carbonatite magmatic system (≈ 380 – 390 Ma ago) and at the post-collision stage (≈ 230 – 250 Ma ago) in the formation of Ural carbonatite complexes. The late stages of ore formation at the Ilmeny-Vishnevogorsky complex are probably associated with the remobilisation and redeposition of alkaline-carbonatite and rare-metal substances. The formation of pyrochlore from the HFSE-enriched fluid is associated with large-scale processes of alkaline metasomatism and pegmatite formation; it included the transformation of rocks from carbonatite complexes at the late-collision and post-collision stages in the formation of the Ural Orogen (≈ 280 – 220 Ma).

CONCLUSION

Studies have revealed that the U-Pb isotopic system of pyrochlore (even in the case of high-uranium varieties of the mineral) can be quite successfully used for dating rare-metal mineralisation, at least in situ version. Moreover, the mineralogical and paragenetic analysis of pyrochlore, which accompanies and precedes U-Pb analytical work, provides the opportunity to adjust the versions of the applied analytical method (laser ablation, secondary-ion microprobe) and interpret obtained geochronological data correctly. Clearly, the rare-metal niobium mineralisation of the Ilmeny-Vishnevogorsky complex was formed over a relatively long time interval (from 380 to 220 Ma), with its development accompanying various formation and transformation stages of magmatic complexes. In addition, the ore potential of mineralisation evolved over time

as well. While high-uranium varieties of pyrochlore, the main ore mineral, were predominantly formed in the early stages, REE-Sr-bearing high-Nb varieties are mainly associated with the late stages of metasomatic recrystallisation.

The work was carried out under the RFBR project No. 17-05-00154 and in line with the state task of the IGG UB RAS No. AAAA-A18-118052590028-9.

REFERENCES

- Atencio D., Andrade M.B., Christy, Giere R., Kartashov P.M. (2010) The pyrochlore supergroup of minerals: nomenclature. *Canad. Miner.*, **48**, 673-698.
- Bagdasarov Yu.A. (2014) On some conditions of formation of carbonatites of the linear fissure type. *Litosfera*, (4), 113-119. (In Russian)
- Braccialli L., Parrish R.R., Horstwood M.S.A., Condon D.J., Najman Y. (2013) U-Pb LA-(MC)-ICP-MS dating of rutile: New reference materials and applications to sedimentary provenance. *Chem. Geol.*, **347**, 82-101.
- Chernyshev I.V., Kononova V.A., Kramm U., Grauert B. (1987) Isotope geochronology of alkaline rocks of the Urals in the light of zircon uranium-lead data. *Geokhimiya*, (3), 323-338. (In Russian)
- Deng X.-D., Li J.-W., Zhao X.-F., Hu H., Selby D., Souza Z.S (2013) U-Pb isotope and trace element analysis of columbite-(Mn) and zircon by laser ablation ICP-MS: implications for geochronology of pegmatite and associated ore deposits. *Chem. Geol.*, **344**, 1-11.
- Efimov A.F., Es'kova E.M., Lebedeva S.I., Levin V.Ya. (1985) Typochemistry of accessory pyrochlore in rocks of the alkaline complex of the Urals. *Geokhimiya*, (2), 202-208.
- Es'kova E.M., Nazarenko I.I. (1960) Pyrochlor of Cherry Mountains, its paragenetic associations and features of the chemical composition. *Voprosy geologii, geokhimi i genezisa mestorozhdenii redkikh elementov* [Questions of geology, geochemistry and genesis of deposits of rare elements]. Proc. IMGRE, **4**, 33-50. (In Russian)
- Es'kova E.M., Zhabin A., Mukhitdinov G. (1964) *Mineralogiya i geokhimiya redkikh elementov Vishnevyykh gor* [Mineralogy and geochemistry of rare elements of the Cherry Mountains]. Moscow, Nauka Publ., 319 p. (In Russian)
- Hogarth D.D. (1977) Classification and nomenclature of the pyrochlore group. *Amer. Mineral.*, **62**, 403-410.
- Ivanov K.S. (2011) About the nature of Ural carbonatites. *Litosfera*, (1), 20-33. (In Russian)
- Ivanov K.S., Valizer P.M., Erokhin Yu.V., Pogromskaya O.E. i dr. (2010) On the genesis of carbonatites of the fold belts (on the example of the Urals). *Dokl. Akad. Nauk*, **435**(2), 218-222. (In Russian)
- Kononova V.A., Dontsova E.I., Kuznetsova L.D. (1979) The isotopic composition of oxygen and strontium of the Ilmen-Vishnevogorsk alkaline complex and the genesis of miaskites. *Geokhimiya*, (12), 1784-1795. (In Russian)
- Kramm U., Blaxland A.B., Kononova V.A., Grauert B. (1983) Origin of the Ilmenogorsk-Vishnevogorsk nepheline syenites, Urals, USSR, and their time of emplacement during the history of the Ural fold belt: a Rb-Sr study. *J. Geol.*, **91**, 427-435.
- Kramm U., Chernyshev I.V., Grauert B., Kononova V.A., Breker V. (1993) Typology and U-Pb systematics of zircons: the study of zircons in the nepheline syenites of the Ilmen mountains, the Urals. *Petrologiya*, **1**(5), 536-549. (In Russian)
- Krasnobaev A.A., Rusin A.I., Busharina S.V., Lepekhi-na E.N., Medvedeva E.V. (2010a) Zirconology of amphibole miaskites of the Ilmenogorsk massif (South Urals). *Dokl. Akad. Nauk*, **430**(2), 227-231. (In Russian)
- Krasnobaev A.A., Rusin A.I., Valizer P.M., Busharina S.V. (2010b) Zirconology of calcite carbonatites of the Vishnevogorsk Massif (Southern Urals). *Dokl. Akad. Nauk*, **431**(3), 1-4. (In Russian)
- Krasnobaev A.A., Valizer P.M., Anfilogov V.N., Nemov A.B., Busharina S.V. (2014) Zirconology of pegmatites of the Ilmensky mountains. *Dokl. Akad. Nauk*, **457**(4), 455. (In Russian)
- Lepekhi-na E.N., Antonov A.V., Belyatskii B.V., Rodionov N.V., Berezhnaya N.G., Shevchenko S.S., Sergeev S.A. (2014) Features of U-Pb pyrochlore dating from the alkaline-ultrabasic polyphase massif Kovdor (North. Karelia): isotope-geochemical characteristics of the evolution of the composition of pyrochlore group minerals. *Region. geologiya i metallogeniya*, (67), 86-94. (In Russian)
- Levin V.Ya., Ronenson B.M., Samkov V.S., Levina I.A., Sergeev N.I., Kiselev A.P. (1997) *Shchelochno-karbonatitovye komplekсы Urala* [Alkali-carbonatite complexes of the Urals]. Ekaterinburg, Uralgeolkom Publ., 274 p. (In Russian)
- Ludwig K.R. (2003) User's manual for Isoplot/Ex. Version 2.49. A geochronological toolkit for Microsoft Excel. Berkeley Geochronology Center, Berkeley, CA, USA. Spec. Publ., **1a**, 75 p.
- Lumpkin G.R., Ewing R.C. (1995) Geochemical alteration of pyrochlore group minerals: pyrochlore subgroup. *Amer. Mineralog.*, **80**, 732-743.
- Millonig L.J., Gerdes A., Groat L.A. (2012) U-Th-Pb geochronology of meta-carbonatites and meta-alkaline rocks in the southern Canadian Cordillera: a geodynamic perspective. *Lithos*, **152**, 202-217.
- Millonig L.J., Gerdes A., Groat L.A. (2013) The effect of amphibolite facies metamorphism on the U-Th-Pb geochronology of accessory minerals from meta-carbonatites and associated meta-alkaline rocks. *Chem. Geol.*, **353**, 199-209. doi: 10.1016/j.chemgeo.2012.10.039
- Mitchell R.H. (2005) Carbonatites and carbonatites and carbonatites. *Canad. Mineral.*, **43**, 2049-2068.
- Nedosekova I.L. (2007) New data on carbonatites of the Ilmeny-Vishnevogorsk complex (the Southern Urals, Russia). *Geol. Rud. Mestorozhd.*, **49**(2), 146-164. (In Russian)
- Nedosekova I.L. (2012) Age and sources of the Ilmeny-Vishnevogorsk alkaline complex (the Southern Urals): geochemical and Rb-Sr, Sm-Nd, U-Pb and Lu-Hf isotopic data. *Litosfera*, (5), 77-95. (In Russian)
- Nedosekova I.L., Belousova E.A., Sharygin V.V. (2010) Sources of the substance of the Ilmeny-Vishnevogorsk alkaline complex according to Lu-Hf isotopic data in zircons. *Dokl. Akad. Nauk*, **435**(2), 234-239. (In Russian)
- Nedosekova I.L., Belousova E.A., Sharygin V.V., Belyatsky B.V., Baynova T.B. (2013) Origin and evolution of the Il'meny-Vishnevogorsk carbonatites (Urals, Russia): insights from trace-elements compositions, Rb-Sr, Sm-

- Nd, U-Pb and Lu-Hf isotope data. *Mineral. Petrol.*, **107**, 101-123.
- Nedosekova I.L., Belousova E.A., Belyatskii B.V. (2014) U-Pb age and Lu-Hf isotopic systems of zircons of the Ilmeny-Vishnevogorsk alkaline carbonatite complex, Southern Urals. *Litosfera*, (5), 19-32. (In Russian)
- Nedosekova I.L., Belyatskii B.V. (2012) Age and sources of the substance of the Ilmeny-Vishnevogorsk alkaline complex (the Southern Ural): Rb-Sr, Sm-Nd, U-Pb and Lu-Hf isotope data. *Dokl. Akad. Nauk*, **446**(1), 71-76. (In Russian)
- Nedosekova I.L., Belyatskii B.V., Belousova E.A. (2016) Rare elements and isotopic composition of hafnium as indicators of the genesis of zircon during the evolution of the alkali-carbonatite magmatic system (Ilmeny-Vishnevogorsk complex, Urals, Russia). *Geol. Geofiz.*, **57**(6), 1135-1154. (In Russian)
- Nedosekova I.L., Vladykin N.V., Pribavkin S.V., Bayanova T.B. (2009) Ilmeny-Vishnevogorsk miaskite-carbonatite complex: origin, ore content, sources of matter (Urals, Russia). *Geol. Rud. Mestorozhd.*, **51**(2), 157-181. (In Russian)
- Nedosekova I.L., Zamyatin D.A., Udoratina O.V. (2017) Ore specialization of carbonatite complexes of the Urals and Timan. *Litosfera*, **17**(2), 60-77. (In Russian)
- Nedosekova I.L., Pribavkin S.V. (2015) Ore niobium mineralization of rare-metal deposits and ore occurrences of Ilmeny-Vishnevogorsk alkaline carbonatite complex (Southern Urals). *Ezhegodnik-2014. Tr. IGG UrO RAN*, **162**, 175-183. (In Russian)
- Pöml P., Menneken M., Stephan T., Niedermeier D.D.R., Geisler T., Putnis A. (2007) Mechanism of hydrothermal alteration of natural self-irradiated and synthetic crystalline titanite-based pyrochlore. *Geochim. Cosmochim. Acta*, **71**, 3311-3322.
- Puchkov V.N. (2010) *Geologiya Urala i Priural'ya (aktual'nye voprosy stratigrafii, tektoniki, geodinamiki i metallogenii)* [Geology of the Urals and Urals (Current problems of stratigraphy, tectonics, geodynamics and metallogeny)]. Ufa, DizainPoligrafServis Publ., 280 p. (In Russian)
- Rass I.T., Abramov S.S., Utenkov U.V. (2006) The role of fluids in the petrogenesis of carbonatites and alkaline rocks: geochemical indicators. *Geokhimiya*, (7), 692-711. (In Russian)
- Rusin A.I., Valizer P.M., Krasnobaev A.A., Baneva N.N., Medvedeva E.V., Dubinina E.V. (2012) Nature of garnet-anorthite-clinopyroxene-amphibole rocks of the Ilmenogorsk complex (South Ural). *Litosfera*, (1), 91-109. (In Russian)
- Stacey J.S., Kramers J.D. (1975) Approximation of terrestrial lead isotope evolution by a two-stage model. *Earth Planet. Sci. Lett.*, **26**, 207-221.
- Wetzel F., Schmitt A.K., Kronz A., Worner G. (2010) In situ ^{238}U - ^{230}Th disequilibrium dating of pyrochlore at sub-millennial precision. *Amer. Mineral.*, **95**, 1353-1356.
- Zoloev K.K., Levin V.Ya., Mormil' S.I., Shardakova G.Yu. (2004) *Minerageniya i mestorozhdeniya redkikh metallov, molibdena, vol'frama Urala* [Minerageny and deposits of rare metals, molybdenum, tungsten of the Urals]. Ekaterinburg, 336 p. (In Russian)

LITHOSPHERE (Russia) Vol. 18 No. 5A

September–October 2018

ISSN 1681-9004 (Print)
ISSN 2500-302X (Online)

Founder

The Federal State Institution of Science
the Zavaritsky Institute of Geology and Geochemistry
Russian Academy of Sciences Ural Branch

Registration certificate PI No. FS77-77043 from October 21, 2019
Ministry of Digital Development, Communications and Mass Media
of the Russian Federation

Technical editor Yevgeniya I. Bogdanova
Translated from the Russian by
Anna V. Kveglis, Natalia G. Popova,
Thomas Alexander Beavitt
Original-layout Nadezhda S. Glushkova
Cover layout Anna Yu. Savelieva

IPD IGG UB RAS № 92A	Signed in print 28.05.2020	Format 60 × 84½	Offset print
Cond. print. sh. 12,75	Found.-publ. sh. 12,75	Circulation 120	Order _____

Institute of Geology and Geochemistry UB RAS 15 Akad. Vonsovsky St., Ekaterinburg, 620016

Printed from the ready-made original layout in typography
OOO Universal Printing House “Alpha Print”
2ж Automation Lane, Ekaterinburg, 620049
Тел.: 8 (800) 300-16-00
www.alfaprint24.ru